

BEHAVIOR OF FRP-STRENGTHENED REINFORCED CONCRETE BEAMS
UNDER FIRE CONDITIONS

By

Aqeel Ahmed

A DISSERTATION

Submitted to
Michigan State University
in partial fulfillment of the requirements
for the degree of

DOCTOR OF PHILOSOPHY

Civil Engineering

2010

ABSTRACT

BEHAVIOR OF FRP-STRENGTHENED REINFORCED CONCRETE BEAMS UNDER FIRE CONDITIONS

by

Aqeel Ahmed

Fiber reinforced polymers (FRP) have emerged as an attractive proposition for retrofitting and strengthening of deteriorating concrete structures due to advantageous properties such as light weight, corrosion resistance and high strength. When FRP is used in strengthening of structural members in buildings, resulting strengthened member has to satisfy relevant fire resistance requirements specified in building codes and standards. Similar to other construction materials, FRP loses its strength and stiffness properties with temperature. However, the degradation in FRP properties is faster as compared to concrete or steel reinforcement due to deterioration of FRP matrix and loss of bond even at modest temperature. To address some of the current knowledge gaps, experimental and numerical studies was carried out with the aim of developing a fundamental understanding on the performance of FRP-strengthened RC beams under realistic fire, loading, and restraint scenarios.

A numerical model was developed for tracing the response of FRP-strengthened RC beams under realistic fire, loading and restraint conditions. The model is based on a macroscopic finite element approach and utilizes time-dependent moment-curvature relationships to trace the response of the beam from pre-fire stage to failure under fire conditions. All of the critical factors, namely; high temperature material properties, fire induced bond degradation and axial restraint force, and different strain components that have significant influence on the fire response of FRP-strengthened RC beams were incorporated in the model.

For validation of the model, four FRP-strengthened RC beams were tested by exposing the beams to fire. The test parameters included different fire scenarios (standard and design fire), type of insulation, effect of anchorage zones and axial restraint conditions. Data generated from fire tests was used to validate the computer model by comparing various response parameters which included cross sectional temperatures, debonding of FRP, mid-span deflection, and fire resistance. The validated model was then applied to conduct a set of parametric studies to quantify the influence of various factors, such as fire scenario, load level, axial restraint, bond degradation, thermal properties and different insulation schemes, on the fire response of FRP-strengthened RC beams. Results from parametric studies shows that fire resistance of FRP-strengthened RC beam is enhanced under most design fire exposures. Provision of optimum insulation schemes, can enhance the fire resistance of FRP-strengthened RC beams. The fire resistance is not improved much by increasing the insulation thickness beyond an optimum thickness level. Higher load levels, lower restraint forces and increased bond degradation at FRP/concrete interface leads to a lower fire resistance in FRP-strengthened RC beams.

Results from parametric studies and fire experiments were utilized to develop guidelines for achieving optimum fire resistance in FRP-strengthened RC beams. These design guidelines, can facilitate wider use of FRP in strengthening of RC beams in buildings where fire safety is one of the key design consideration.

DEDICATION

This research is dedicated to my beloved parents and my wife. Their emotional support and prayers consistently provided me motivation and inspiration to achieve this goal.

ACKNOWLEDGMENT

I wish to express my greatest gratitude to my advisor Dr. Venkatesh Kodur, Professor of Civil Engineering, Michigan State University, for his support, encouragement and guidance received throughout the course of this study. I would like to convey my sincere thanks for his ideas and perseverance which made my graduate studies very educational.

I would also like to thank distinguished faculty members, Prof. Ronald Harichandran, Prof. Parviz Soroushian and Prof. Lawrence T. Drzal, who served on my committee and provided me with their valuable advice and useful guidance and discussions during my stay at Michigan State University.

My appreciations and prayers extended to my friends Monther Dwaikat, and Mahmoud Dwaikat. Also, I would like to thank the lab manager, Mr. Siavosh Ravanbakhsh for his support and help during the experimental program in this research. Obviously, I would like to extend my thanks to Laura Taylor, Mary Mroz, and Margaret Conner for all the help they offered to go smoothly through my study period.

I would like to thank Rustin Fike, Wasim Khaliq, Nikhil Raut, Syed Haider, Syed Hassan, Purushutham Pakala, Nicholas Hatinger and Mahmoud Haq, for their support, particularly in the experimental part of this study.

I would also like to appreciate the support and efforts of my wife who have been taking care of our three lovely children's Zunera Maryam, Abdullah Ahmed and Aisha Sadiqah.

TABLE OF CONTENTS

LIST OF TABLES.....	x
LIST OF FIGURES.....	xi
NOTATIONS.....	xvii
CHAPTER 1 - INTRODUCTION	
1.1 General.....	1
1.2 Performance of FRP under Fire.....	3
1.3 Fire Behavior of FRP-strengthened RC Beams.....	6
1.4 Research Objectives.....	10
1.5 Scope and Outline.....	11
CHAPTER 2 – STATE-OF-THE-ART	
2.1 General.....	13
2.2 Flexural Strengthening of Reinforced Concrete Members.....	14
2.2.1 FRP Products.....	19
2.2.1.1 Fibers.....	19
2.2.1.2 Matrix.....	20
2.2.1.3 FRP Composite.....	23
2.3 FRP Composites for Civil Engineering Applications.....	25
2.3.1 Externally Bonded FRP-strengthening of RC Beams.....	27
2.4 High Temperature Properties.....	28
2.4.1 Reinforcing Steel.....	28
2.4.1.1 Thermal Properties.....	28
2.4.1.2 Mechanical Properties.....	30
2.4.1.3 Deformation Properties.....	31
2.4.2 Concrete.....	32
2.4.2.1 General.....	32
2.4.2.2 Thermal Properties.....	33
2.4.2.3 Deformation Properties.....	38
2.4.2.4 Fire induced Spalling.....	40
2.4.3 Fiber Reinforced Polymers (FRP).....	42
2.4.3.1 General.....	42
2.4.3.2 Fibers.....	43
2.4.3.3 Matrix.....	44
2.4.3.4 FRP Composite – Thermal Properties.....	45
2.4.3.5 FRP Composites – Mechanical Properties.....	47
2.4.3.6 FRP Composites – Deformation Properties.....	48
2.4.3.7 FRP Composite - Bond Properties.....	48

2.4.3.8 Physical Properties – Smoke Generation, Flame Spread and Toxicity	50
2.4.4 Insulation.....	52
2.5 Previous Studies on FRP-strengthened RC Beams.....	56
2.5.1 Experimental Studies	56
2.5.2 Numerical Studies.....	62
2.6 Codes and Standards	64
2.7 Summary	65

CHAPTER 3 – EXPERIMENTAL STUDIES

3.1 General.....	67
3.2 Experimental Program	67
3.2.1 RC Beam Specimens.....	68
3.2.2 FRP Strengthening	73
3.2.2.1 Design and Material.....	73
3.2.2.2 Installation.....	73
3.2.3 Insulation of Beams	75
3.2.3.1 Insulation type.....	75
3.2.3.2 Installation.....	76
3.2.4 Instrumentation	78
3.2.5 Test Apparatus	79
3.2.6 Test Conditions and Procedure	80
3.2.7 Loading	81
3.2.8 Material Testing.....	82
3.2.8.1 Compressive strength of concrete.....	82
3.2.8.2 Steel.....	83
3.2.8.3 Insulation.....	84
3.2.8.4 Glass transition temperature of FRP composite.....	85
3.3 Results and Discussion	87
3.3.1 Test Observations.....	87
3.3.2 Thermal Response.....	91
3.3.2.1 General.....	91
3.3.2.2 Furnace Temperatures.....	92
3.3.2.3 EI-R/Insulation Interface Temperatures	92
3.3.2.4 FRP/Insulation Interface Temperatures	93
3.3.2.5 FRP/Concrete Interface Temperatures.....	94
3.3.2.6 Concrete Temperatures	96
3.3.2.7 Rebar Temperatures	98
3.3.3 Structural Response	99
3.3.3.1 Deflection of Beams	99
3.3.3.2 Axial Restraint Force	104
3.4 Failure Pattern and Fire Resistance.....	105
3.5 Summary	106

CHAPTER 4 – NUMERICAL MODEL

4.1	General.....	108
4.2	Macroscopic Finite Element Model - Methodology	109
4.3	FE Model for FRP-strengthened RC Beams.....	115
4.3.1	Fire Temperatures	115
4.3.2	Thermal Analysis	115
4.3.3	Strength Analysis	119
4.3.3.1	General Analysis Procedure.....	119
4.3.3.2	Evaluating Strain (ε_{slip}) due to Bond Slip	125
4.3.3.3	Fire Induced Axial Restraint Force	130
4.3.4	Generation of Moment-curvature ($M - \kappa$) Relationships.....	132
4.3.5	Beam Analysis	133
4.3.5.1	Stiffness Approach.....	133
4.3.5.2	Failure Limit States	135
4.4	Computer Implementation	137
4.4.1	Computer Program.....	137
4.4.2	Beam Idealization	137
4.4.3	Material Properties.....	138
4.4.3.1	Concrete	138
4.4.3.2	Steel Reinforcement.....	139
4.4.3.3	FRP and Insulation Material	139
4.4.3.4	Input Data.....	140
4.4.3.5	Output Results.....	140
4.5	Summary	140

CHAPTER 5 – MODEL VALIDATION

5.1	General.....	141
5.2	Response of Typical FRP-strengthened Beam	141
5.2.1	Details of Beam.....	141
5.2.2	Thermal Response.....	142
5.2.3	Structural Response	146
5.2.4	Summary	154
5.3	Validation against Test Data.....	154
5.3.1	Blontrock et al. Test Beams	154
5.3.2	William et al. Tested T-Beam.....	159
5.3.3	MSU Test Beams	160
5.4	Summary	169

CHAPTER 6 – PARAMETRIC STUDY AND DESIGN GUIDELINES

6.1	General	171
6.2	Analysis Details	171
6.2.1	Significant Factors	171
6.2.2	Selection of Beam	172
6.2.3	Material Properties	172
6.2.4	Mesh Size	173
6.2.5	Failure Criteria	173
6.3	Results from Parametric Studies	179
6.3.1	Effect of FRP Strengthening	179
6.3.2	Effect of Fire Scenario	182
6.3.3	Effect of Load Level	185
6.3.4	Effect of Axial Restraint	187
6.3.5	Effect of Location of Axial Restraint	190
6.3.6	Effect of Concrete Strength	192
6.3.7	Effect of Concrete Aggregate	193
6.3.8	Effect of Insulation Thickness	194
6.3.9	Effect of Insulation Configuration	198
6.3.10	Effect of Insulation Thermal Conductivity	200
6.3.11	Effect of Bond Degradation	202
6.3.12	Effect of Adhesive Thickness on Bond Degradation	203
6.4	Critical Factors Influencing Fire Performance	205
6.5	Design Guidelines	208
6.5.1	Insulation Scheme	208
6.5.2	Anchorage zone	212
6.5.3	Performance-based Design	213
6.5.4	Rational Fire Resistance Assessment	216
6.6	Summary	217

CHAPTER 7 – CONCLUSIONS AND RECOMMENDATIONS

7.1	General	218
7.2	Key Findings	219
7.3	Recommendations for Future Research	221
7.4	Research Impact	222

Appendices

APPENDIX A	224
APPENDIX B	239
APPENDIX C	248

REFERENCES	250
-------------------------	------------

LIST OF TABLES

Table 2.1: Comparison of widely available resins.....	22
Table 2.2: Qualitative comparison between carbon, aramid and E-glass fibers.....	25
Table 2.3: Thermal conductivities of various unidirectional FRP and building material.....	46
Table 2.4:CTE's of unidirectional FRP composites and building materials	48
Table 3.1: Concrete mix design proportions for beams.....	70
Table 3.2: Summary of test parameters and results	71
Table 3.3: Properties of fibers used for strengthening of test beams.....	73
Table 3.4: Properties of composite laminate.....	73
Table 3.5: Properties of epoxy used in FRP strengthening.....	74
Table 3.6: Compressive strength of concrete.....	82
Table 3.7: Visual Observations for Beams B1 and B2 during Fire Resistance Test	88
Table 3.8: Visual Observations for Beams B3 and B4 during Fire Resistance Test	89
Table 5.1: Summary of properties for beams used in the fire resistance analysis	145
Table 5.2: Material properties for Blontrock beams	155
Table 5.3: Material properties for T-beam.....	159
Table 6.1: Summary of properties for FRP-strengthened RC beams used in the parametric study	176
Table 6.2: Summary of parameters studied in analysis	177
Table 6.3: Summary of the fire resistance values for the analyzed beams	178
Table 6.4: Properties used for design fires.....	182
Table 6.5: Effect of insulation thickness on fire resistance of FRP-strengthened RC beams	197

LIST OF FIGURES

Figure 1.1: Variation of strength in different materials with temperature	5
Figure 2.1: Application of FRP in the field	16
Figure 2.2: RC beams bonded with (a) FRP at beam soffit (b) FRP and U-strip end anchorages (c) Pre-stressed FRP	17
Figure 2.3: Failure modes of FRP-strengthened RC beams (a) FRP rupture (b) crushing of compressive concrete (c) shear failure (d) concrete cover separation (e) plate-end interfacial debonding (f) intermediate flexural crack-induced interfacial debonding (g) intermediate flexural shear crack-induced interfacial debonding	18
Figure 2.4: Tensile strength of typical fibers and metals.....	20
Figure 2.5: Various FRP composite products for strengthening applications	23
Figure 2.6: Stress-strain curves for FRP and mild steel.....	24
Figure 2.7: Typical response (load-deflection curve) of FRP-strengthened and un-strengthened (control) RC beam	28
Figure 2.8: Variation of (a) Thermal conductivity (b) Thermal capacity with temperature for reinforcing steel	29
Figure 2.9: Stress-strain curves for steel (300 MPa yield strength) as function of temperature...	31
Figure 2.10: Variation of (a) Modulus (b) Yield and ultimate strength with temperature for reinforcing steel	31
Figure 2.11: Variation of thermal expansion as function of temperature	32
Figure 2.12: Variations of measured and predicted of thermal conductivity as a function of temperature for normal strength concrete (NSC)	34
Figure 2.13: Variations of measured and predicted of thermal capacity as a function of temperature for normal strength concrete (NSC) mechanical properties	34
Figure 2.14: Variation of elastic modulus of concrete as a function of temperature.....	35
Figure 2.15: Variation of compressive strength as a function of temperature for NSC	37
Figure 2.16: Variation of compressive strength as a function of temperature for HSC	37
Figure 2.17: Variation of residual compressive strength as a function of temperature	38

Figure 2.18: Variations of measured and predicted of thermal expansion for concrete as a function of temperature	39
Figure 2.19: Illustration of spalling of concrete due to pore pressure	41
Figure 2.20: Illustration of thermal dilation mechanism	42
Figure 2.21: Variation in tensile strength of fibers with temperature.....	44
Figure 2.22: Variation in thermal properties with temperature for carbon/epoxy FRP.....	47
Figure 2.23: Variation of bond strength with temperature	50
Figure 2.24: Results of smoke generation tests on various.....	52
Figure 2.25: Normalized thermal conductivity and thermal capacity of VG insulation.....	55
Figure 3.1: Elevation and cross-sectional details of FRP-strengthened RC beams.....	69
Figure 3.2: Fabrication details of tested beams	72
Figure 3.3: Concrete surface preparation by sand blasting.....	74
Figure 3.4: Flexural strengthening and spray-application of insulation on RC beams.....	77
Figure 3.5: RC beams strengthened with CFRP and insulated.....	78
Figure 3.6: Thermocouples and strain gage placement in the beam.....	79
Figure 3.7: Structural fire test furnace and loading setup at MSU Civil and Infrastructure laboratory.....	80
Figure 3.8: Fire time-temperature curves used in fire experiments	81
Figure 3.9: Testing compressive strength of concrete after 28 days and on the day of fire test...	83
Figure 3.10: Testing of reinforcing steel and stress-strain curves	83
Figure 3.11: Test setup and high temperature thermal properties of Tyfo [®] WR AFP system.....	84
Figure 3.12: Variation of T_g as a function of heating rate.....	86
Figure 3.13: Crack development in insulation of FRP-strengthened beam.....	90
Figure 3.14: Formation and widening of cracks in insulation	90

Figure 3.15: A portion of beam B3 exposed to fire after delamination of FRP and insulation	91
Figure 3.16: Time-temperature curve and average furnace temperatures for beam tests	92
Figure 3.17: Exterior layer temperatures in FRP-strengthened RC beams.....	93
Figure 3.18: Measured temperatures at FRP/insulation and FRP/concrete interface	95
Figure 3.19: Formation of temperature plateau at 100°C	95
Figure 3.20: Physical and chemical process during combustion of polymer	96
Figure 3.21: Measured concrete temperatures (TC 9, TC 10 and TC 13) for Beams B2, B4 and control beam B01	98
Figure 3.22: Comparison of reinforcing steel temperatures	99
Figure 3.23: Comparison of mid-span deflections.....	102
Figure 3.24: Unbonded continuous carbon fibers at the beam soffit.....	103
Figure 3.25: Cool anchorage zone of FRP-strengthened RC beam	103
Figure 3.26: Axially restrained FRP-strengthened RC beam (B4)	103
Figure 3.27: Comparison of axial restraint force as function of fire exposure time for beam B4 and beam B02	105
Figure 4.1: Layout of typical FRP-strengthened RC beam, its idealization and discretization for analysis	110
Figure 4.2: Flowchart illustrating the steps associated with fire resistance analysis of FRP-strengthened RC beam.....	112
Figure 4.3: Discretization of beam for analysis and $M - \kappa$ relationship for idealized segment.	128
Figure 4.4: Development of shear stresses and bond-slip in a beam segment.....	129
Figure 4.5: Schematic interfacial shear stress distribution	129
Figure 4.6: Illustration of axial restraint force calculations	132
Figure 4.7: Flow chart illustrating the steps associated of iterative procedure.....	136
Figure 5.1: Beam elevation and cross section details	144
Figure 5.2: Temperatures at various locations in the beam as a function of fire exposure time	144

Figure 5.3: Moment-curvature curves at various times for Beam-I under fire exposure	147
Figure 5.4: Moment capacity and deflection of FRP-RC beam as a function of fire exposure time	148
Figure 5.5: Deflection of FRP-strengthened and RC beam as function of fire exposure time ..	149
Figure 5.6: Ultimate tensile strength (f_T) of CFRP as a function of temperature	150
Figure 5.7: Temperature variation at the interface of FRP-concrete interface as a function of fire exposure time.....	151
Figure 5.8: Moment capacity of FRP-strengthened and RC beam	152
Figure 5.9: Variation of interfacial shear stress as a function of fire exposure time	153
Figure 5.10: Slip distribution for mid span of the beam as a function of fire exposure time	153
Figure 5.11: Elevation and cross section of beams tested by Blontrock et al.....	156
Figure 5.12: Measured and predicted rebar temperatures and mid-span deflection in Beam II	157
Figure 5.13: Measured and predicted temperatures at the interface of FRP/concrete and corner rebar for Beam III.....	158
Figure 5.14: Measured and predicted deflection as a function of fire exposure time for Beam III	158
Figure 5.15: Measured and predicted temperatures at various depths in Beam IV	160
Figure 5.16: Comparison of measured and predicted temperatures in compression and flexural reinforcement and mid-depth of cross section for beams Beam V through Beam VIII	163
Figure 5.17: Comparison of measured and predicted temperatures at FRP/insulation, FRP/concrete interfaces for beams Beam V through Beam VIII.....	165
Figure 5.18: Elevation and cross sectional details of MSU tested FRP-strengthened RC beam	167
Figure 5.19: Measured and predicted deflection of FRP-strengthened RC beams (Beam V through VIII)	168
Figure 5.20: Measured and predicted axial restraint force as a function of time for Beam VIII	169
Figure 6.1: Longitudinal and cross sectional discretization for fire resistance analysis.....	175

Figure 6.2: Time-temperature curves for different fire scenarios.....	175
Figure 6.3: Effect of FRP strengthening on fire response of RC beams.....	181
Figure 6.4: Variation of rebar temperature as a function of fire exposure time in FRP-strengthened RC beam.....	183
Figure 6.5: Variation of temperature at FRP-concrete interface as a function of fire exposure time	184
Figure 6.6: Effect of fire scenarios on mid-span deflections of FRP-strengthened RC beam...	185
Figure 6.7: Effect of load ratio on mid-span deflection of FRP-strengthened RC beam exposed to fire	187
Figure 6.8: Fire induced axial restraint force as a function of time in an FRP-strengthened RC beam	189
Figure 6.9: Effect of axial restraint on mid-span deflection of FRP-strengthened RC exposed to fire.....	189
Figure 6.10: Effect of location of axial restraint force on mid-span deflection of FRP-strengthened RC beam exposed to fire.....	191
Figure 6.11: Effect of axial restraint force location on axial force development	192
Figure 6.12: Effect of compressive strength of concrete on mid-span deflection of FRP-strengthened RC beam exposed to fire.....	193
Figure 6.13: Effect of aggregate type on mid-span deflection of FRP-strengthened RC beam exposed to fire	194
Figure 6.14: Effect of insulation thickness on time to reach T_g	197
Figure 6.15: Corner rebar temperature and yield strength ratio as a function of insulation thickness for 3-hour of fire exposure time.....	198
Figure 6.16: Effect of insulation depth on beam sides on fire response of FRP-strengthened RC beam exposed to fire	200
Figure 6.17: Effect of insulation thermal conductivity on fire resistance of FRP-strengthened RC beam	201
Figure 6.18: Fire induced mid-span deflection in RC beam under different bond configurations	203
Figure 6.19: Bond-slip at FRP concrete interface as a function of fire exposure time.....	203

Figure 6.20: Effect of adhesive thickness on slip at FRP-concrete interface as function of fire exposure time	204
Figure 6.21: Proposed geometric configuration schemes for fire insulation in FRP-strengthened RC beams	210
Figure 6.22: Proposed geometric configuration for insulation in FRP-strengthened RC T-beams	210
Figure 6.23: Proposed optimum thickness for fire insulation in FRP-strengthened RC beams	212
Figure 6.24: Proposed fire insulation layout for FRP-strengthened RC beams.....	213
Figure 6.25: Effect of standard and design (realistic) fire on temperature profile of an insulated FRP-strengthened RC beam.....	214

NOTATIONS

A = area of boundary exposed to fire

A_m = area of each element

A_{frp} = area of FRP

A_s = area of steel reinforcement

b = beam width

b_{frp} = width of FRP reinforcement applied at beam soffit

c_c = clear concrete cover

C_t = total compressive force in the beam cross section

d = effective depth of the beam

E_c = modulus of elasticity of concrete

E_{frp} = modulus of elasticity of FRP

$E_{com,T}$ = elastic modulus of FRP composite, T

F = equivalent nodal heat flux

$f_{c,20}$ = concrete strength at room temperature

$f_{c,T}$ = concrete strength at temperature, T

$f_{com,T}$ = strength of FRP composite, T

f_t = tensile strength of concrete at room temperature

f_{IT} = tensile strength of concrete for temperature, T

f_{fu} = ultimate tensile strength of FRP

f_{fe} = effective stress in FRP

F_v = ventilation factor

f_y = yield strength of steel

F_n and F_{n+l} = equivalent nodal heat flux at the beginning and the end of time step, respectively

h = time step

H = total depth of concrete section

h_f and h_c = heat transfer coefficient of the fire side and the cold side, respectively

h_{rad} and h_{con} = radiative and convective heat transfer coefficient

k = thermal conductivity

k_T = thermal conductivity of concrete

$k_{VG,T}$ = thermal conductivity of insulation (Vermiculite gypsum)

k_i = thermal conductivity of insulation (Promatect calcium silicate boards)

$k_{w,T}$ = thermal conductivity of FRP composite

K = global stiffness matrix

K_g = global stiffness matrix for strength analysis

K_{geo} = geometric stiffness matrix

k_r = axial restraint stiffness

L = length of the beam

l_i = projected length of deformed segment i

L_i = length of segment i in the undeformed beam

LR = load ratio

L_s = length of the beam segment

M = molar mass of water (or global mass matrix)

N = vector of the shape functions

n_y and n_z = components of the vector normal to the boundary in the plane of the cross section

P_f = equivalent nodal load vector due to applied loading

P_i , $\varepsilon_{\theta i}$ and \mathcal{K}_i = the axial force, central total strain, and curvature in segment i

P_s = equivalent nodal load vector due to P - δ effect

q = heat flux

q_{rad} and q_{con} = radiative and convective heat fluxes.

Q = heat source

R = gas constant (or fire resistance)

s = distance along the boundary Γ

s_i = length of deformed segment i

t = time

t^* = fictitious time in Eurocode parametric fire

T = temperature

T_o = initial temperature

T_E = temperature of the environment surrounding the boundary

t_h = time (hours)

T_f = fire temperature

t_s = time at which the area under the heat flux curve is being evaluated

t_t = total duration of fire

T_t = total tensile force in the beam cross section

T_∞ = fire or ambient temperature depending on the boundary

T_{max} = maximum fire temperature

u = variable in finite element analysis for temperature

\dot{u} = the derivative of u with respect to time

u_n and u_{n+1} = values of u at the beginning and the end of time step, respectively

w = applied distributed load

w_{i1}^{n-1} and w_{i2}^{n-1} = deflections at the beginning and the end of the beam segment which were computed in the $(n-1)^{\text{th}}$ time step

w_{i1}^n and w_{i2}^n = deflections at the beginning and the end of the beam segment in the n^{th} time

step

x = depth of neutral axis under service loads

y = the distance from the geometrical centroid of the beam

y_{top} = distance from the top most fibers of the concrete section

Y = location of axial restraint force from the top most fibers of the concrete section

Z = Zener-Hollomon parameter for creep strain

α and β = calibration constants for permeability to be determined from experiment

δ = nodal displacements

Δ = total expansion in the beam length

$\Delta\epsilon_{th}$ = change in thermal strain

$\Delta\epsilon_{tr}$ = change in transient strain

ϵ = emissivity

ϵ_0 = total strain at the geometrical centroid of the beam cross section

ϵ_c = strain at the top most fibers of concrete

ϵ_{bi} = initial strain at beam soffit at the time strengthening

ϵ_{cr} , ϵ_{me} , ϵ_t , ϵ_{th} and ϵ_{tr} = creep strain, mechanical strain, total strain, thermal strain, and transient strain

ϵ_{crs} , ϵ_{mes} , ϵ_{ths} and ϵ_{ts} = creep strain, mechanical strain, thermal strain and total strain in steel.

ε_{i0} = creep strain parameter

ϕ = structural modification factor in evaluating the fire resistance of reinforced concrete beams

Γ = boundary of the beam (or time modification factor)

κ = curvature

θ = temperature-compensated time (or an iterative procedure parameter between 0 and 1)

ρ_s = steel ratio = area of tension steel/effective area of cross section

ρ_{frp} = FRP ratio = area of FRP/effective area of cross section

ρc = heat capacity

$\rho_{c,T}$ = density of concrete as function of temperature

ρ_{VG} = density of Vermiculite Gypsum (VG)

ρ_{cT} = density of concrete as function of temperature

ρ_{wT} = density of FRP composite

ρ_i = density of Promatect calcium-silicate boards

σ = current stress in concrete or steel (or Stevan-Boltzman constant)

σ_m = stress at the center of each element in the cross sectional beam

CHAPTER 1

INTRODUCTION

1.1 General

Reinforced concrete (RC) structures in North America are deteriorating at a rapid pace due to poor maintenance, and corrosion of steel reinforcement, as well as aging related problems. This is because most of the infrastructures were built after the Second World War. Thus, there is an urgent need for the rehabilitation of deteriorating RC structures. In addition, the need for strengthening existing structures due to natural and manmade disasters (earthquake, hurricanes and terrorism) is ever growing. These factors necessitate repairing and strengthening structural members to enhance their performance levels. According to a recent “state-of-infrastructure” report by American Society of Civil Engineers (ASCE), America’s infrastructure is deteriorating at a faster rate and needs immediate fixing (ASCE 2009). Total repair and retrofitting costs for fixing seismic deficient structures, substandard transportation infrastructures (bridges), corroded steel and concrete structures, structurally deficient and functionally obsolete structures run into billions of dollars per year. The total cost of repair, rehabilitation, strengthening, and protection of concrete structures is estimated to be \$18 to \$21 billion a year for US alone. In light of these statistics, there is a need for high performance materials that can offer substantial cost savings (less volume of material), reduced maintenance and longer lifetimes.

Fiber reinforced polymers (FRP) have emerged as an attractive proposition for retrofitting and strengthening concrete structures due to advantages they offer over traditional construction materials such as concrete and steel. Based on their high strength- and stiffness-to-weight ratios, corrosion resistance, environmental durability, and inherent tailorability, FRP composites are increasingly being considered for use in the rehabilitation of existing infrastructure, and for the construction of new structures. Applications of these materials range from strengthening and retrofitting of reinforced and unreinforced masonry walls; seismic retrofitting of bridges and building columns; repair and strengthening of beams, girders, and slabs; and the rehabilitation of structures.

The repaired/strengthened structural systems are designed to satisfy serviceability and safety requirements specified in building codes and standards. One of the major safety requirements in the buildings is the provision for fire safety, since fire represents a major hazard for built environments. The fire safety provisions for structural members are specified in terms of fire resistance ratings. The fire resistance rating requirements depend on the type of structural member, occupancy and other factors. Fire resistance of a structural member is influenced by a number of factors including type of construction material, applied loading, fire characteristics and geometric properties (Kodur 1999). When an RC member is strengthened with FRP, the resulting fire resistance will depend on properties of the original concrete member, as well as the properties of the added FRP. Unlike concrete and steel, FRP is highly susceptible to fire. Therefore, FRP is mainly used in bridges and parking garages where fire hazard is not a major design consideration. However, when used in buildings, FRP-strengthened structural members have to meet stringent fire resistance requirements specified in the building codes and standards.

1.2 Performance of FRP under Fire

Currently, limited knowledge exists about the fire performance of FRP-strengthened concrete structures. This knowledge gap has limited the widespread application of FRP in building applications.

The fire safety of structural members can be achieved by satisfying flame spread, smoke generation and fire resistance ratings. In FRP-strengthened RC members, the overall fire performance of the member depends on high temperature performance of original concrete member, as well as the behavior of FRP. The conventional construction materials such as reinforcing steel and concrete do not combust, and hence do not contribute as fuel or generate smoke. For flexural strengthening of RC structural members, FRP is externally bonded to the tension face of the member. Therefore, performance of FRP is a major concern under fire conditions since FRP is highly vulnerable to elevated temperatures.

FRP materials are highly combustible and burn when subjected to heat flux. These emit combustible gases, ignite, release heat and propagate flame spread when exposed to elevated temperatures (fire). Upon burning, FRP's give off smoke that affects visibility and hinders ability of the occupants to escape and pose difficulties for fire fighters to conduct evacuation operations and suppress the fire. Flammability, which is one of the indicators of fire hazard generally, refers to the tendency of a substance to ignite easily and burn rapidly with a flame. The flame spread and generation of toxic smoke, which are the two major concerns with FRP material, largely depend on the type of FRP formulation (composition). When used in buildings, structural members have to satisfy flame spread, smoke generation and fire resistance ratings prescribed in the building codes. American Society for Testing and Materials (ASTM international) and National Fire Protection Association (NFPA) primarily develop and maintain

fire and flammability test standards. For evaluating flame spread and smoke generation, ASTM recommends three different standard tests. ASTM E84 and NFPA 255 tests specify procedures for relative burning behavior of a building material by measuring flame spread index (FSI) and smoke density index (SDI). ASTM E662 specifies optical density test to measure characteristics of smoke concentration, while ASTM E162 describes test procedures for measuring and comparing surface flammability of different building materials when exposed to radiant heat energy. Testing laboratories such as Under Writer Laboratories have the facilities to conduct flame spread and smoke generation tests on materials. Generally, FRP manufacturers list their products for smoke generation and flame spread classifications in directories after getting specified tests from these specialized testing facilities (laboratories). Thus, for this research, it is assumed that FRP's have met the relevant flame spread and smoke generation rating specified in building codes and standards.

The third requirement of fire safety for a structural system is the fire resistance rating specified in the building codes. A fire resistance rating is the minimum duration that is required for a member to exhibit resistance to fire, and is often rounded off to a nearest hour or half-hour. Fire resistance is the actual duration during which a structural member exhibits resistance with respect to strength, integrity and stability. Fire resistance depends on many factors including structural geometry, constructional material and fire characteristics. Concrete performs reasonably well under fire because of its low thermal conductivity, high thermal capacity and slower loss of strength and stiffness properties. Therefore, concrete structures often satisfy fire resistance ratings without the need for external fire protection. However, when concrete members are strengthened with external FRP system, the response of the whole system can be different under the fire conditions as compared to original concrete member. Thus, fire resistance

of FRP-strengthened RC members is highly influenced by many factors including strength, stiffness and bond properties of FRP in addition to properties of concrete and reinforcing steel.

Similar to other construction materials, FRP loses its strength and stiffness properties with temperature. However, the degradation in FRP properties is faster as compared to concrete or steel since properties of FRP matrix start to deteriorate even at a modest temperature. Figure 1.1 shows degradation of strength with temperature for traditional construction materials including two common types of FRP; namely, carbon based FRP (CFRP) and glass based FRP (GFRP). It can be seen that FRP properties degrade at a faster rate as compared to steel and concrete (Kodur and Baingo 1998). Further, the temperatures in FRP, unlike concrete and steel, rise at a very fast rate since FRP starts to burn when it comes in contact with fire (flame). The loss of FRP strength with temperature is negligible up to 100°C, and thereafter, strength degradation is faster, resulting in 50% strength loss around 250°C.

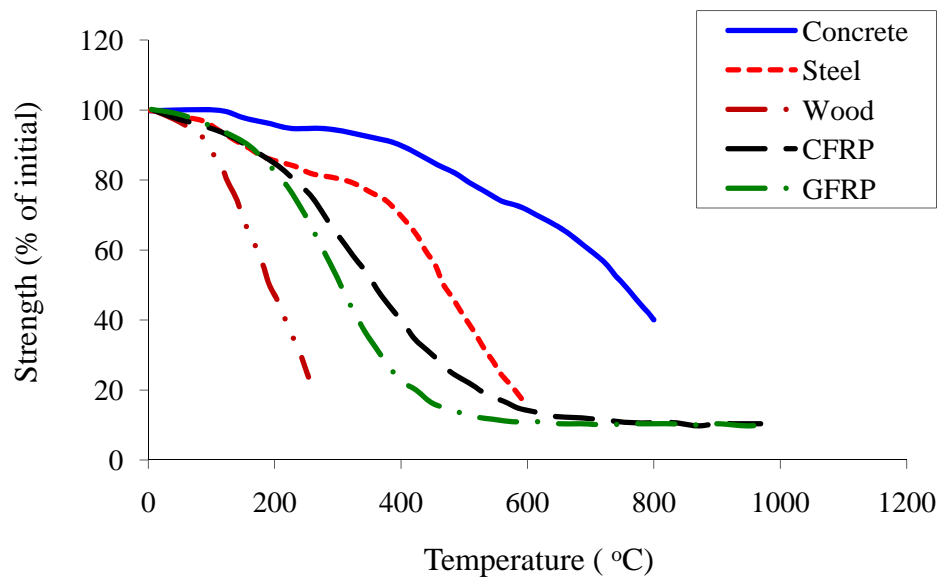


Figure 1.1: Variation of strength in different materials with temperature
(For interpretation of references to color in this and all other figures, the reader is referred to the electronic version of this dissertation)

For flexural strengthening of structural members, FRP is externally bonded to the RC member using an adhesive. Apart from concerns about mechanical properties degradation with temperature, another issue that needs consideration is the loss of bond between FRP and concrete when exposed to elevated temperatures. The performance of FRP depends on the strength of the polymer adhesive used to bond the FRP sheet/laminate to the concrete surface. FRP is susceptible to rapid loss of bond strength and stiffness above glass transition temperature (T_g) (Blontrock et al. 1999). Glass transition temperature refers to the temperature at which an adhesive changes from a relatively stiff material to viscous material leading to a significant drop in strength and stiffness properties. Typically, the glass transition temperature for commonly used polymers (adhesive) varies between 60 to 82°C (ACI 2008).

In FRP-strengthened members, the main load carrying mechanism is through transfer of stresses from concrete substrate to FRP reinforcement. This transfer of forces to FRP reinforcement occurs through development of shear stresses at the interface of FRP and concrete (Denton 2001). However, when the temperature at the interface reaches T_g , the bond properties of the adhesive (shear modulus and bond strength) deteriorate considerably and introduces a slip at the interface (Leone et al. 2009). This slip significantly reduces force transfer from concrete to FRP composite, and subsequently leads to debonding of FRP. Research has indicated that reaching T_g of adhesives is a critical factor governing the fire response of externally bonded FRP-strengthened RC structural members (Camata et al. 2007).

1.3 Fire Behavior of FRP-strengthened RC Beams

Flexural strengthening of RC beams is usually achieved by applying thin layers of FRP sheets on tension face (beam soffit), while shear strengthening is achieved through application of

FRP on the side faces of beam. This technique has wider acceptance as compared to using steel plates or external post-tensioning (surface mounting) techniques due to ease of application. Application of FRP sheets on beam soffit can considerably improve flexural capacity of a retrofitted beam.

When exposed to fire, FRP-strengthened RC beams behave differently from that at ambient temperature since strength and stiffness of the beam (including FRP) degrade with temperature rise. This degradation in strength and stiffness properties leads to decrease in load carrying capacity of a beam. Strength failure occurs in the beam when moments due to applied load exceeds decreasing flexural capacity of the beam. The time to reach this limit state is referred to as fire resistance of the beam. The fire resistance of an FRP-strengthened RC beam depends on a number of factors including type of fire exposure, loading, support conditions, type of insulation and high temperature properties of constitutive materials.

Generally, FRP-strengthened RC beams experience higher stresses as compared to an un-strengthened RC beam since the load level on a strengthened beam is relatively higher. The higher stress level in the beam can lead to early strength failure in the absence of any fire protection since FRP starts to burn in the first 10-15 minutes. Therefore, provision of external insulation is critical to achieving reasonable fire resistance in FRP-strengthened beams (Williams et al. 2006). There is very little information on the required level of insulation under realistic fire, loading, and restraint levels.

Flexural strengthening of beams is bond-critical application in which FRP is bonded to the tension face of the beam using polymer adhesive. At elevated temperatures, bond between FRP and concrete is a critical factor that influences the behavior of FRP-strengthened RC beams. In most previous studies, a perfect bond was assumed at the interface of FRP and concrete up to the

glass transition temperature of the adhesive and thereafter, the bond was assumed to be completely lost. The bond degradation is gradual in early stages of fire exposure (lower temperature increase at interface) and its properties drop significantly in the region of polymers T_g . However, unidirectional FRP continue to be structurally effective (contribute to strength capacity) at temperatures above T_g . Therefore, for a realistic assessment of fire performance of strengthened members, bond degradation with temperature has to be accounted for. Capturing temperature induced bond degradation in full scale fire tests is not easy due to lack of instrumentation (strain gauges) that can survive rapid rising high temperatures. However, numerical models can be effectively used to predict bond degradation, provided bond properties at high temperature are known.

FRP-strengthened RC beams can experience significant thermal expansion under elevated temperatures. When support conditions prevent such free expansion, axial restraint force gets induced in the strengthened beam. This axial restraint force depends on many factors such as type of fire scenario, support conditions, high temperature properties of constitutive materials and loading. During early stages of fire exposure, the fire induced restraining force generates an arch action that helps to counter moments due to applied loading. However, at later stages, when the beam undergoes large deflections due to deterioration of strength and stiffness properties of the beam, the restraining force creates secondary bending moments ($P-\Delta$) that result in an increase in bending moments. Thus, axial restraining force can influence the fire response of a strengthened beam.

Numerous studies have been conducted to trace the response of FRP-RC members at ambient conditions. These studies addressed overall structural response of FRP-strengthened

members (Dortzbach 1999; Grace 2001; Kodur et al. 2006; Mayo et al. 1999; Shahrooz and Boy 2004; Shahrooz et al. 2002; Takeda et al. 1996; Williams et al. 2008), creep and fatigue effects (Scott et al. 1995; Yang and Nanni 2002), and factors contributing to durability enhancement (Green et al. 2000; Green et al. 2003; Neale 2001; Toutanji and Gomez 1997; Waldron et al. 2001). Based on these studies, guidelines have been developed for room temperature design of FRP-strengthened RC members. Such guidelines are available in ACI Committee 440: *Guide for the Design and Construction of Externally Bonded FRP Systems for Strengthening Concrete Structures* (2008), ISIS Design Manual No. 4: *Strengthening Reinforced Concrete Structures with Externally Bonded Fiber Reinforced Polymers* (2001), and Bulletin 14: *Externally bonded FRP Reinforcement for RC Structures* (2001). All these codes and guidelines comment on the susceptibility of FRP materials to elevated temperatures. Even-to-date, no specific fire design guidelines are available for fire design. As an example, ACI 440.2R (2008) assumes no contribution from FRP in the event of fire. Under fire conditions, there have been limited experimental and numerical studies to evaluate fire response of FRP-strengthened RC members. In case of experiments, only standard fire tests have been conducted which aimed at developing proprietary fire resistance ratings. No consideration was given to evaluate response of FRP-strengthened members under realistic fire, loading, restraint and bond conditions. Also, in the case of numerical models, thermal response has been studied under standard fire exposure without giving any due consideration to overall structural response, effect of fire induced bond degradation and axial restraint force. Thus, absence of reliable numerical models, as well as relatively high cost of the tests are the two main reasons for lack of fire design provisions in codes and standards.

To overcome some of the above knowledge gaps, it is proposed to undertake detailed studies on response of FRP-strengthened RC beams exposed to fire. Fire response depends on a number of factors including fire exposure, member type and dimensions, high temperature material properties (concrete, steel, FRP and insulation), load level, geometric properties, restraint and bond etc. The extent of influence of many of these parameters on fire response of FRP-strengthened RC beams is not well established. As part of this research, it is proposed to undertake both fire experiments and numerical studies to develop an understanding of the response of FRP- strengthened RC beams under realistic fire and loading conditions.

1.4 Research Objectives

From the above discussion, it is evident that one of the main impediments for using FRP in buildings is the lack of knowledge about the structural response of FRP-strengthened systems under fire. This experimental and numerical study examines the implications of high temperature thermal susceptibility on currently used FRP materials in civil engineering applications and on structural behavior of FRP-strengthened RC beams. To achieve this objective, extensive literature review followed by development of numerical model, full-scale fire tests and parametric studies on FRP-strengthened RC beams have been conducted. Specific objectives of this research are:

- Conduct detailed state-of-the-art review on fire performance of FRP-strengthened RC beams.
- Develop a macroscopic finite element model (FEM) to trace the response of FRP-strengthened RC beams under realistic loading and fire scenarios. The model will account for non-linear high temperature properties of constitutive materials, fire induced bond degradation and axial restraint effects.

- Conduct fire resistance tests on FRP-strengthened RC beams under standard and design fires for different load levels and insulation schemes.
- Use data generated from fire tests to validate the numerical model.
- Carry out parametric studies to quantify the influence of various critical factors on fire performance of FRP-strengthened RC beams.
- Use data generated from parametric studies and fire tests to develop guidelines for fire design of FRP-strengthened beams.

1.5 Scope and Outline

The work presented in this thesis involves both experimental studies and development and application of a numerical model. As part of experimental program, four full-scale FRP-strengthened RC beams and one control RC beam were fabricated and tested under applied loads to evaluate fire response. The numerical work involved development of macroscopic finite element model to trace the fire response of FRP-strengthened RC beams. The model was validated by using the test data generated from current fire tests and data available in the literature. The validated model was then applied to undertake parametric studies to quantify influence of various factors on fire response of FRP-strengthened RC beams. Results from the fire tests and the parametric studies were utilized to develop guidelines for fire design of FRP-strengthened RC beams.

The thesis is organized into seven chapters. Chapter 2 presents extensive review of the literature related to FRP as material and as a component of a structural member. Detailed discussion on high temperature properties of concrete, steel, FRP and insulation is presented. The chapter also includes summary of experimental and numerical modeling work that has been conducted previously on FRP-strengthened RC beams.

Chapter 3 provides details on the fire resistance tests. Full details on the fabrication of test beams, instrumentation, testing procedure and test results are presented. The discussion focuses on both thermal and structural response of the FRP-strengthened RC beams.

The development of the fire resistance model to trace the response of FRP-strengthened RC beams under fire exposure is presented in Chapter 4. Detailed procedure involved in tracing the fire response of FRP-strengthened RC beams is explained. Chapter 5 deals with model validation, where predictions from the model are compared with the test data from literature, as well as with data obtained from tests conducted as part of this research. Chapter 6 discusses results of parametric studies undertaken to quantify influence of various factors on fire performance of FRP-strengthened RC beams, followed by fire design guidelines. Chapter 7 provides conclusions and recommendations for future research.

A set of appendices is included that provide detailed information not presented in the main body of the text. Appendix A provides high temperature constitutive relationships for material properties which include concrete, reinforcing steel, FRP and insulation. Appendix B summarizes the design and load calculations for FRP-strengthened RC beam according to design codes.

CHAPTER 2

STATE-OF-THE-ART REVIEW

2.1 General

FRP materials were originally developed in early 1960's and 70's by aerospace and defense industries for specific applications such as aircrafts, ships and military hardware's (ACI 2002). Therefore, significant information is available on FRP properties at room temperature (Davies et al. 2004). In the last two decades, FRP's have been extended to civil infrastructure applications and are increasingly used for strengthening and retrofitting of RC structures due to ease of application, cost effectiveness and efficient performance. These strengthening and retrofitting techniques widely utilize externally bonded FRP composites due to unique properties such as strength, light weight, corrosion and chemical resistance (Bakis et al. 2002). The early application of FRP started as flexural strengthening in RC bridge girders and as confinement to RC columns. Today, wide varieties of structural elements are being strengthened using FRP including beams, slabs, columns, shear walls, domes and trusses.

Prior to arrival of FRP, the most popular technique for strengthening RC structures was using steel plates. This technique had many shortcomings like heavy plates (steel), corrosion of steel that deteriorates bond between steel plate and the concrete, and requirement for specialized equipment at site for placement of steel plates. Therefore, FRP sheets have replaced steel plates

in strengthening applications (Teng et al. 2002). These sheets can be tailored to meet specific structural requirements.

Until recently, most strengthening applications of FRP was in bridges and other structures where fire safety is not a major issue (Kodur et al. 2006). For use in buildings, FRP-strengthened RC members have to satisfy fire resistance requirements specified in building codes and standards. Thus, there is a legitimate concern on the performance of such strengthened/reinforced structures under fire conditions.

This chapter presents a state-of-the art review on the fire performance of FRP as material and as a component of structural system. This includes, review of high temperature material properties (concrete, reinforcing steel, FRP and insulation), behavior of FRP strengthened members at elevated temperatures, as well as main findings from previous fire tests and numerical studies on FRP-strengthened beams. Finally, design provisions in different codes and standards for FRP strengthened structural members are reviewed.

2.2 Flexural Strengthening of Reinforced Concrete Members

Flexural strengthening of RC beams through FRP plates was first explored at the Swiss Federal Laboratory for Materials Testing Research (EMPA) in 1994 (Deuring 1994). As part of this research, CFRP plates were applied to the beam soffit for flexural strengthening of RC beams. The key justification for using the FRP technology to strengthen RC beams was the high strength to weight ratio, corrosion resistance, reduce labor cost, ease of handling and durability of FRP (Teng et al. 2002).

Flexural strengthening of RC members is undertaken by applying FRP composite (high strength fibers and matrix) along principle load direction. In beams, the orientation of fibers coincides with the longitudinal axis of the beam. There are several techniques that have been

explored to bond FRP to concrete substrate. Amongst these techniques, externally bonding FRP to tension face of the beam using adhesive (polymer resin) is most conventional technique in civil engineering applications. The FRP sheet is either available as prefabricated (also known as prepeg or pultruded) or constructed on site with a wet lay-up process. In both types, FRP is bonded to the concrete surface using the adhesive. The application of FRP requires special surface preparations to improve bond between FRP and concrete. These surface preparations involve removal of weak smooth surface texture of concrete to expose aggregate which provide a strong bonding surface. Several special techniques are available to externally bond FRP to RC structures, such as (Bakis et al. 2002):

- Prestressed strips
- Automated wrapping and curing
- Fusion-bonded pin-loaded straps
- Placement inside slits
- Prefabricated shapes
- Mechanically fastened FRP strips

There are a number of procedures to strengthen RC beams using FRP composites. The most common method is bonding of FRP to the beam soffit without pre-stressing (unstressed) FRP, as shown in Figure 2.1(a). This application procedure involves adhesive bonding of prefabricated FRP, wet lay-up or resin infusion method (refer to Figure 2.2). To prevent most likely failure mechanism in FRP-strengthened RC beams i.e., debonding of FRP at the terminating ends, installation of mechanical or U shaped anchorage is another technique of strengthening beams. Application of pre-stressed FRP at the beam soffit is another technique adopted at locations where FRP is required to carry some portion of the loading before additional load is applied or

where reduction of existing cracks in concrete is important (Teng et al. 2002). In all these applications, the main concern remains structural performance of the member after adding FRP. A number of failure modes for RC beams bonded with FRP at tension face of the beam have been observed in numerous experimental studies (Arduini and Nanni 1997; Gao et al. 2005; Garden and Hollaway 1998; Pei and Pilakoutas 2003; Ritchie et al. 1991; Saadatmanesh and Ehsani 1991). Figure 2.3 schematically shows the possible failure modes in FRP-strengthened RC beams which include: (a) steel yielding followed by FRP rupture; (b) steel yielding followed by concrete compressive crushing of concrete; (c) shear failure in beam; (d) concrete cover delamination; (e) FRP peel-off initiating at end due to inclined shear cracks in concrete; (f) Peel-off at termination due to high tensile stresses in the adhesive; (g) FRP peel-off at termination/cutoff point due to shear crack in concrete.



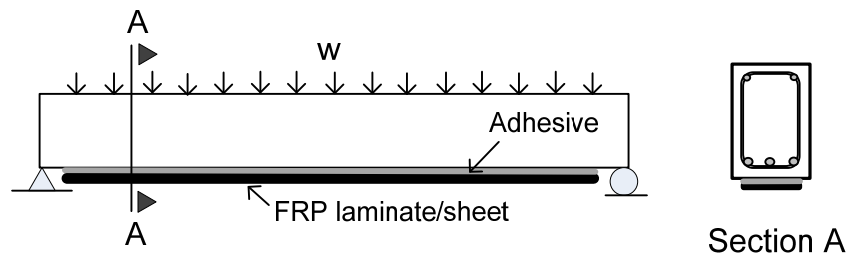
Wet lay-up procedure



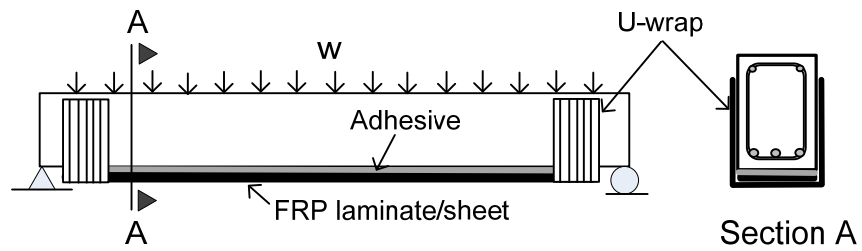
Bonding of pre-fabricated FRP laminate

Figure 2.1: Application of FRP in the field

(a)



(b)



(c)

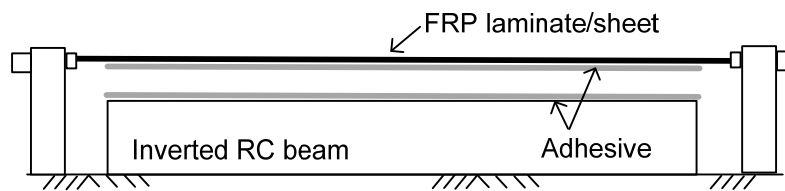


Figure 2.2: RC beams bonded with (a) FRP at beam soffit (b) FRP and U-strip end anchorages (c) Pre-stressed FRP

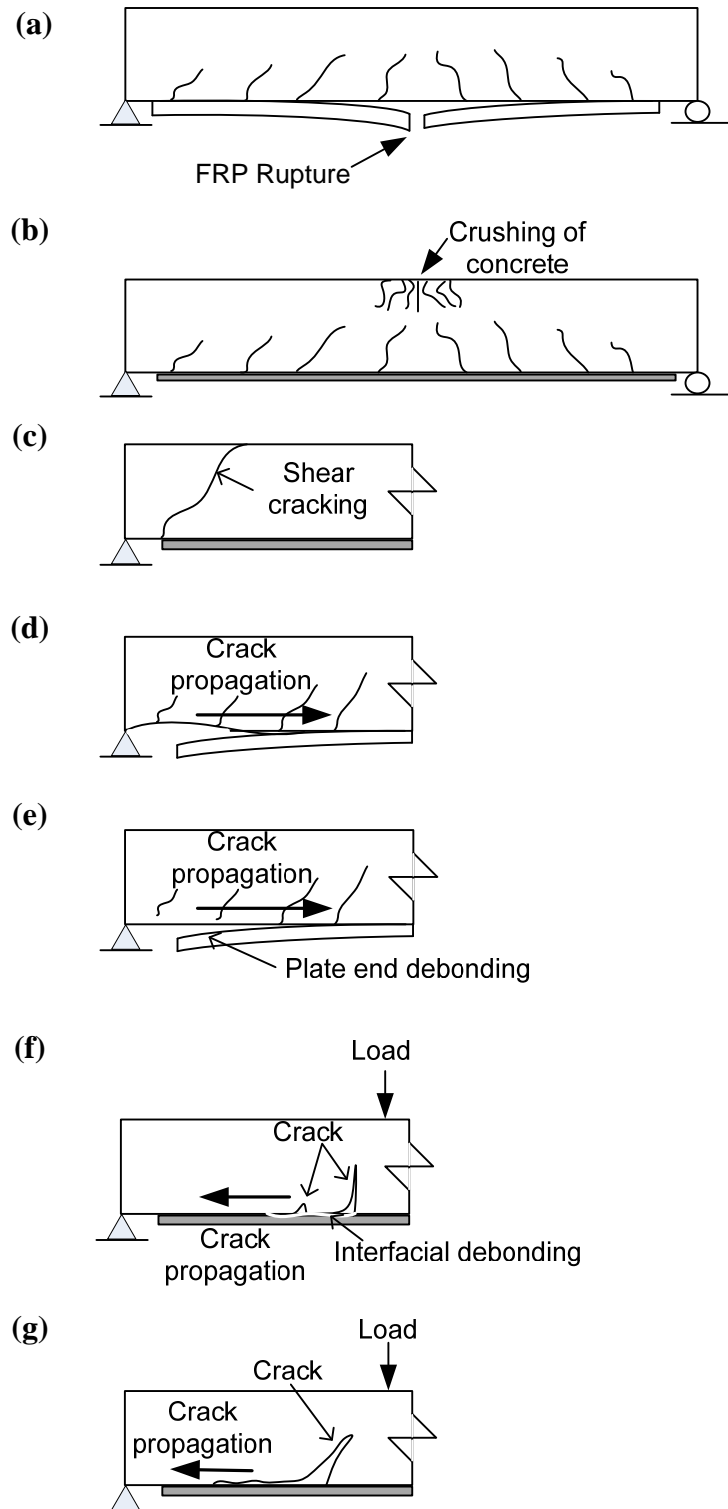


Figure 2.3: Failure modes of FRP-strengthened RC beams (a) FRP rupture (b) crushing of compressive concrete (c) shear failure (d) concrete cover separation (e) plate-end interfacial debonding (f) intermediate flexural crack-induced interfacial debonding (g) intermediate flexural shear crack-induced interfacial debonding

2.2.1 FRP Products

FRP possesses superior properties and is widely usable in numerous forms. With increased use in civil engineering projects, the cost is coming down as the retrofitting market is flourishing over the past decade. The cost of application in civil engineering projects is going down as the industry is flourishing in past decade. FRP composites are formed of continuous fibers embedded in a polymer matrix. Common fibers used are carbon, glass and aramid fibers and accordingly are designated as CFRP, GFRP and AFRP, respectively. Common types of matrix include polyester, vinyl-ester and epoxy. The composite product formed by combining fibers and matrix has superior properties than its original constituent. The volume fraction of fibers in composite varies from 40 to 65%.

2.2.1.1 Fibers

Fibers are main load carrying component in an FRP composite. These are aligned along loading direction of the structural member to utilize high strength and stiffness properties. The performance of FRP composite depends on the type, volume fraction and orientation of fibers. Common types of fibers used are glass, carbon and aramid. Glass fibers are sensitive to moisture and highly susceptible to creep rupture and hence they lose strength and stiffness quickly under sustained loading (Bank et al. 1995). Glass fiber is the most inexpensive amongst the category of high-performing fibers. In structural engineering applications, carbon fibers are widely used for strengthening because of high longitudinal modulus and strength. Moreover, carbon fibers perform satisfactorily in moist environment and under fatigue loading. These fibers are dimensionally very stable with negative or very low coefficient of thermal expansion in longitudinal direction. Carbon fibers provide low impact resistance and insulating capacity. Thus, carbon fibers are preferred choice for use in fire applications. Aramid fibers are the least

commonly used amongst the three high performing fibers due to high cost inspite of superior properties like higher stiffness and excellent impact resistance.

A comparison of tensile strength of common fiber reinforcement, titanium, steel, and aluminum (used in engineering applications) is shown in Figure 2.4. It can be seen that the tensile strength of the carbon, aramid (Kevlar) and glass fibers exceed strength of steel by about two times and from that of aluminum by as much as 400%. The specified strength of all of the fibers surpasses that of the metals by about ten times.

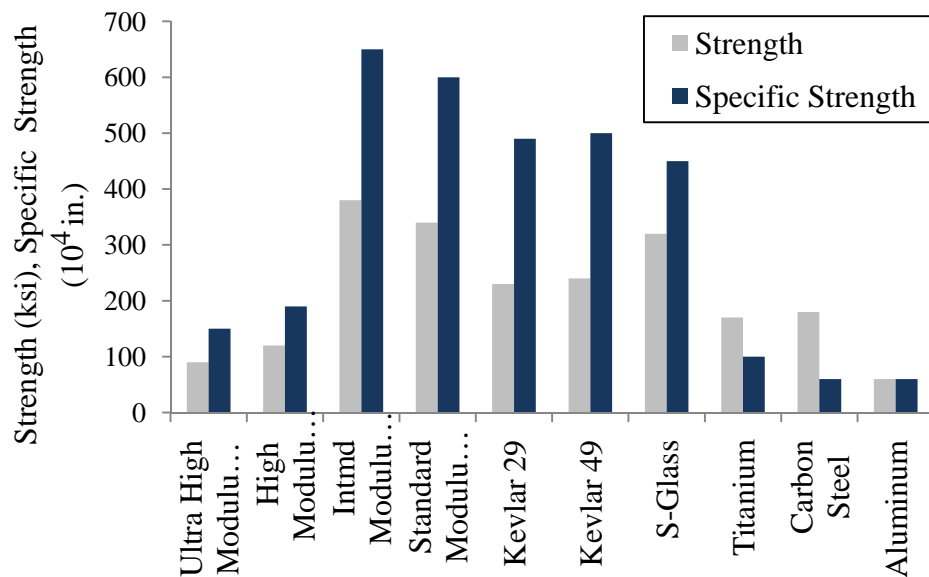


Figure 2.4: Tensile strength of typical fibers and metals (*Source: Composite Tek, 2003*)

2.2.1.2 Matrix

Matrix refers to polymer ingredient of FRP composite that binds the fibers together. Other terms used for its description are resin, polymer and binder. Polymers can be in liquid or solid state, and cured polymer is referred to as *matrix*. Matrixes themselves do not contribute any significant strength to FRP composite since most of the load is shared by the fibers. The matrix provides a medium to transfer stresses between adjoining fibers (load path), a shield against

external environmental effects and protection against mechanical abrasion. In general, the three most common forms of matrices (resins) currently used are polyester, vinyl ester, and epoxy. A brief description of each resin is presented in Table 2.1.

The matrix has poor mechanical and thermal characteristics. There are two broad categories of polymer materials; thermoplastic and thermosetting. Thermosetting polymers are cross-linked by strong covalent bonded atoms. These cannot be heated, softened and reformed into different shapes. While in thermoplastic polymers, the molecular chains are not cross linked, but are held together by weak van der Waals forces. Thermosets are most suitable for structural application due to cross linking property (Blontrock et al. 1999). These are thermally stable at service temperature, have low creep effect and higher chemical resistance as compared to thermoplastics. The advantages of thermoset resins over thermoplastic resins are:

- Better creep resistance
- Improved stress relaxation
- Thermal stability
- Chemical resistance
- Low- T_g polymers such as polypropylene (PP) have lower-weight molecules

and strength

Glass transition temperature (T_g) is a thermal property of polymer (matrix) that is of interest to structural engineers. At T_g mechanical (stiffness) and physical properties of polymer undergo significant changes. When the temperature reaches close to T_g , the polymer changes from glassy (rigid) to rubbery (viscous) state, thus, elastic modulus decreases significantly.

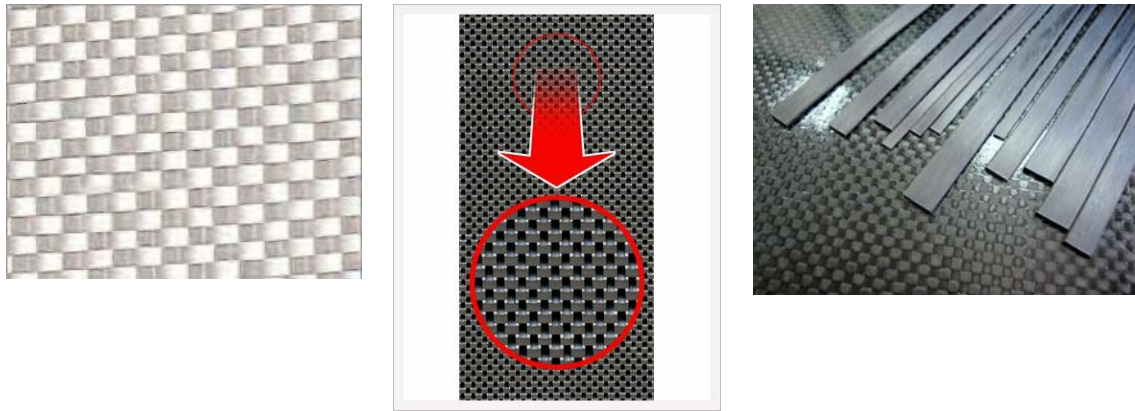
Table 2.1: Comparison of widely available resins

Resin type	Advantages	Disadvantages
Polyesters	Easy to use Lowest cost amongst available resins	Only moderate mechanical properties High styrene emissions in open molds High shrinkage on curing Limited range of working times
Vinyl-esters	Very high chemical/ environmental resistance Higher mechanical properties than polyesters High mechanical and thermal properties	Post-cure generally required for high properties High styrene content Higher cost than polyesters High shrinkage on curing
Epoxies	High water resistance Long working times available Temperature resistance up to 140°C in wet and 220°C in dry conditions Low shrinkage on curing	Low shrinkage on curing More expensive than vinyl esters Corrosive handling Critical mixing

Source: Gurit Composite Technologies, 2008

In wet lay-up process for strengthening applications, epoxy resin is applied to dry unidirectional or multidirectional fiber sheets. This process is commonly referred to "prepeg". These systems are cured in-situ. In such application, the epoxy acts as FRP matrix as well as the binding material (adhesive) between FRP composite and the substrate. FRP strips and laminated sheets are also commercially available in wide variety of shop-manufactured shapes that are known as pre-cured FRP composite systems (refer to Figure 2.5).

Polymer matrix display excellent mechanical properties at ambient temperature and are extremely sensitive to higher temperatures. This sensitivity at higher temperatures weakens overall properties of FRP composite which remains a concern for practitioners. Further discussion of behavior of FRP under fire condition is provided in Section 2.4.3.



(a) Woven glass fiber

(b) Woven carbon fiber

(c) CFRP pultruded sheets

Figure 2.5: Various FRP composite products for strengthening applications

2.2.1.3 FRP Composite

A wide variety of FRP composites (different formulations) are available for RC structures. CFRP and GFRP are most commonly used composites in civil engineering applications. Use of AFRP is rare because of comparatively high cost (Intelligent Sensing for Innovative Structures (ISIS) 2001), sensitivity to creep, durability concerns (moisture absorption) and poor performance at elevated temperatures (Uomoto et al. 2002). The material properties of FRP composite depend on the mechanical properties of matrix, fiber-volume fraction, fiber cross-sectional area, fiber orientation in the matrix, and method of manufacturing (Bisby 2003). The strength and stiffness properties of FRP composite are governed by the fibers. The focus of current work (presented in this section) is on properties of unidirectional FRP composites.

The stress-strain behavior of FRP composite is linear elastic up to brittle failure (in tension). Figure 2.6 give diagrammatic representation of stress-strain curves for CFRP, GFRP and AFRP compared to structural steel. It can be seen that FRP composite exhibit higher tensile strength than steel. Moreover, this material is highly brittle with very less ductility as compared to steel. FRP's do not display yield behavior similar to observed for steel. Therefore, when used for

flexural strengthening RC members, the ductility of member is reduced. However, strength and ductility of structural members (concrete) is enhanced considerably when FRP composite is used for confinement of concrete such as for RC columns. Table 2.2 provides qualitative comparison of available FRP materials with respect to strength, durability and cost criteria.

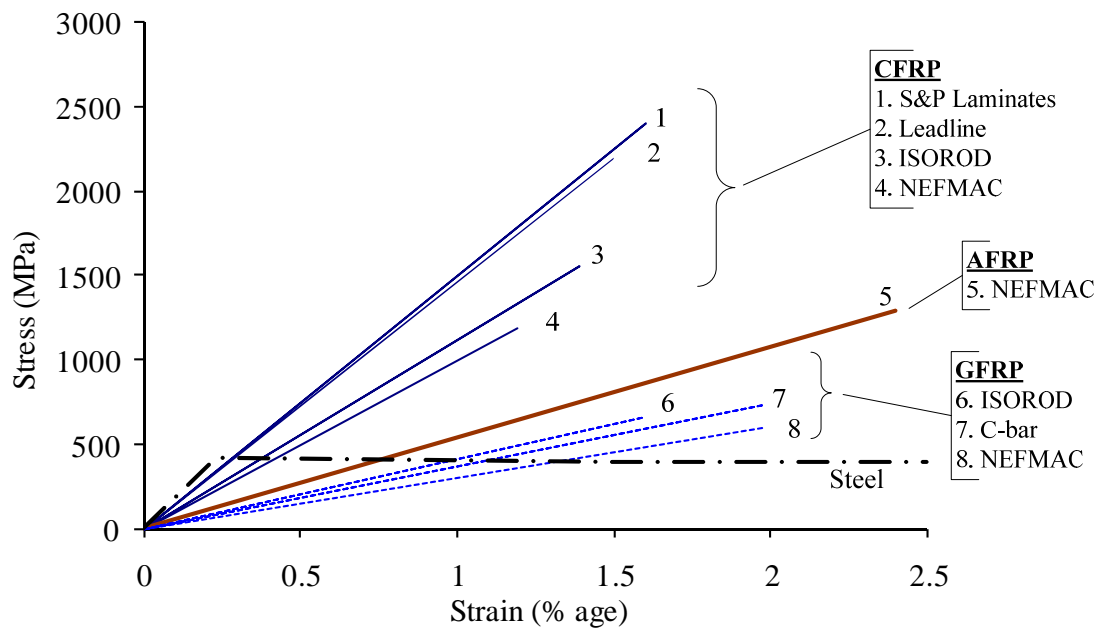


Figure 2.6: Stress-strain curves for FRP and mild steel

Table 2.2: Qualitative comparison between carbon, aramid and E-glass fibers (*Meier 1995*)

<i>Criteria</i>	<i>Carbon</i>	<i>Aramid</i>	<i>E-glass</i>
Tensile Strength	Very good	Very good	Very good
Compressive strength	Very good	Inadequate	Adequate
Modulus of Elasticity	Very good	Good	Adequate
Long term behavior	Very good	Good	Adequate
Fatigue behavior	Excellent	Good	Adequate
Bulk density	Good	Excellent	Adequate
Alkaline resistance	Very good	Good	Inadequate
Price	Adequate	Adequate	Very good

2.3 FRP Composites for Civil Engineering Applications

FRP composite materials are becoming increasingly attractive for retrofitting and strengthening of civil engineering structures. This is because FRP's have strong, durable, light weight and ease of application characteristics and provides cost effective alternative solution for conventional construction materials. For civil engineering application, the required characteristics for a material are high-volume with low cost, extended service and minimum maintenance in its life span. The successful application of FRP composite for strengthening and retrofitting of RC structures is attributed to many advantages such as:

- High strength and stiffness properties
- Enhanced fatigue tolerance
- Resistance to corrosion
- High strength-to-weight ratios

- Controllable mechanical and thermal properties
- Non-magnetic characteristics
- Easy and fast installation in the field resulting in more economical procedures
- Lower life cycle cost
- Reparability
- Design flexibility

Notwithstanding above mentioned advantages, some major disadvantages that are associated with FRP material are:

- High initial material cost
- Lack of ductile behavior
- Long term durability
- Variation in finished product properties
- Environmental effects
- Lack of design guidance
- Uncertain properties at elevated temperatures

In the recent years, considerable research work has been conducted on FRP materials and on FRP reinforced concrete members. This includes overall structural response of FRP-strengthened members (Dortzbach 1999a; Grace 2001; Kodur et al. 2006; Mayo et al. 1999; Shahrooz and Boy 2004; Shahrooz et al. 2002; Takeda et al. 1996; Williams et al. 2008), creep and fatigue effects (Scott et al. 1995; Yang and Nanni 2002), and factors contributing to durability enhancement (Green et al. 2000; Green et al. 2003; Neale 2001; Toutanji and Gomez 1997; Waldron et al. 2001). increasing flexural strength of RC members (Ashour et al. 2004; Dortzbach

1999b; El-Hacha et al. 2001; Grace 2001; Grace et al. 1999), shear capacity enhancement (Chaallal et al. 1998; Chen and Teng 2003; Kachlakev and McCurry 2000; Khalifa et al. 1998; Pellegrino and Modena 2002; Teng et al. 2004; Wang and Hsu 2009; Zhang et al. 2004), repair and rehabilitation of RC columns (Ballinger et al. ; Darwish 2000; Lan et al. 1998; Triantafillou 1998) , retrofitting of columns in earthquake prone areas (Ghobarah 2001). This research has lead to wider spread in use of FRP for strengthening and retrofitting of RC columns, beams and slabs.

2.3.1 Externally Bonded FRP-strengthening of RC Beams

Unidirectional FRP sheets are commonly used to enhance the flexural capacity of RC beams. An increase of up to 160% in beam capacity has been reported in the literature (Meier and Kaiser 1991; Ritchie et al. 1991), however, ductility and serviceability constraints limits the percentage of increase to about 40% (Balaguru et al. 2008). Typical response (load–midspan deflection) of an FRP-strengthened RC beam is compared to that of a control RC beam (un-strengthened) in Figure 2.7. It can be seen that provision of FRP layers increases both the moment capacity and the stiffness of the beam with reduction in deflection at time of failure. In control RC beam, the majority of the load is carried by bottom steel reinforcement. The steel yields at some point and thereafter, the behavior of the beam is ductile till failure. However, in FRP-strengthened RC beam, additional tensile force is carried by the FRP applied at tension face of the beam that results in an increase in load carrying capacity. Thus, strengthening of RC beams with externally bonded FRP is feasible way to increase the load carrying capacity and stiffness characteristics of existing member. However, strengthening significantly reduces the deformability (ductile behavior) of the strengthened member as well as brittle and sudden failure occurs.

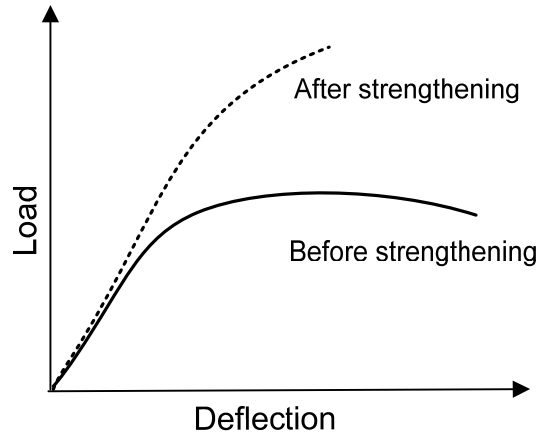


Figure 2.7: Typical response (load-deflection curve) of FRP-strengthened and un-strengthened (control) RC beam

2.4 High Temperature Properties

The fire response of FRP-strengthened RC beams is influenced by the characteristics of concrete, reinforcing steel, FRP and insulation. These include thermal, mechanical and deformation properties at room as well as elevated temperatures. The thermal properties govern the extent of heat transfer, while mechanical properties (strength and stiffness) determine the load carrying capacity and deformation of the structural member. The deformation properties such as thermal expansion and creep determine the extent of deformation in the member. This section provides review on properties of concrete, reinforcing steel, FRP composite (fibers and matrix) and the insulation materials.

2.4.1 Reinforcing Steel

The behavior of reinforcing steel has been extensively studied and a comprehensive review is given by Lie (Lie 1992) and Khoury (Khoury 2000).

2.4.1.1 Thermal Properties

Thermal properties of steel at elevated temperature include thermal conductivity and specific heat (thermal capacity). The steel type and type of fire exposure defines the thermal behavior of

steel reinforcement. The heat transfer through steel is very rapid as compared to concrete due to high conductive characteristics of steel reinforcement. At room temperature, thermal conductivity may vary slightly depending on the chemical composition of steel (Bisby 2003). However, at elevated temperature, thermal properties are more dependent on temperature and are less influenced by the steel composition (Williams 2004a).

Thermal conductivity decreases linearly with increasing temperature up to about 900°C and thereafter remain constant at elevated temperatures (Lie 1992). Figure 2.8(a) shows the variation of thermal conductivity of reinforcing steel with temperature. Specific heat, defined as amount of heat required to raise the temperature of unit mass by unit degree, varies with temperature (see Figure 2.8(b)). The peak in specific heat around 700°C can be attributed to phase transformation. The steel reinforcement area is very small in comparison to overall concrete section and also reinforcing steel is located within the concrete section; therefore, steel has almost no influence on temperature distribution within concrete cross section.

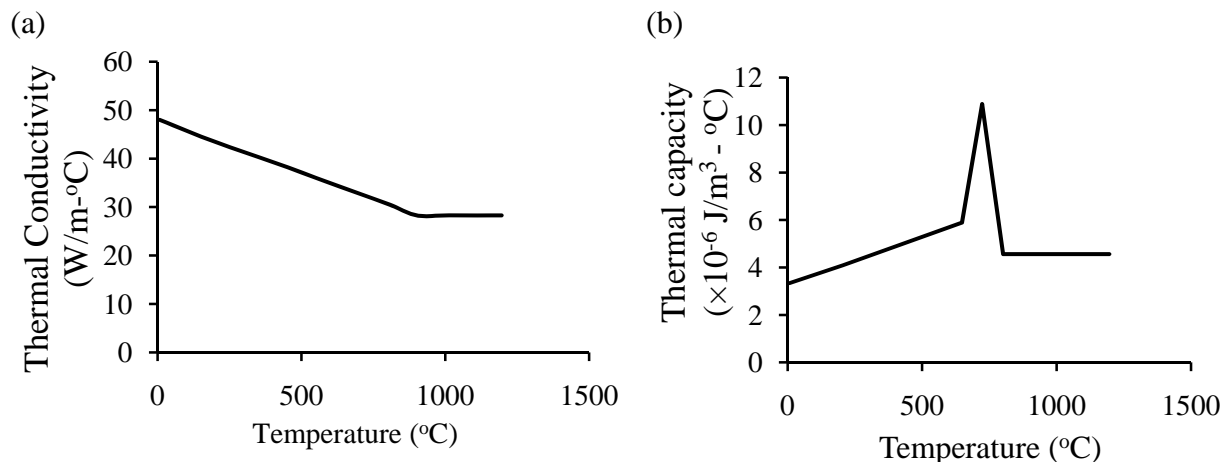


Figure 2.8: Variation of (a) Thermal conductivity (b) Thermal capacity with temperature for reinforcing steel (*reproduced after Lie 1992*)

2.4.1.2 Mechanical Properties

The mechanical properties that influence fire response are yield strength, ultimate strength, elastic modulus and stress-strain relationship. Literature review suggests that there is considerable variation in yield and ultimate strength of steel since these properties depend on steel composition and the definition of yield strength. (Buchanan 2002). Stress-strain curves for mild steel at various temperatures are shown in Figure 2.9. It can be seen that the yield strength decreases with temperature and well defined yield plateau disappears at higher temperatures. Figure 2.10 shows that elastic modulus, yield and ultimate strength of reinforcing steel decreases with temperature. The reinforcing steel recovers nearly all of its original yield strength upon cooling as long as heating temperatures do not exceed 500°C (Neves et al. 1996). Eurocode assumes that reinforcing steel maintain its room temperature strength up to 400°C. Type of fire exposure is an important factor to be considered in evaluating fire resistance of RC members. Concrete and reinforcing steel recover some of its strength and stiffness during decay (cooling) phase of design fires (non standard fire). The amount of recovery depends on the highest temperature recorded in reinforcing steel. Reinforcing steel heated above 500°C experience a gradual decrease in residual strength. Therefore, the behavior of reinforcing steel in the cooling phase is critical for modeling the response of FRP-strengthened RC structural members exposed to real (design) fire scenarios. The details about high-temperature constitutive models for mechanical properties of reinforcing steel are presented in the Appendix A.

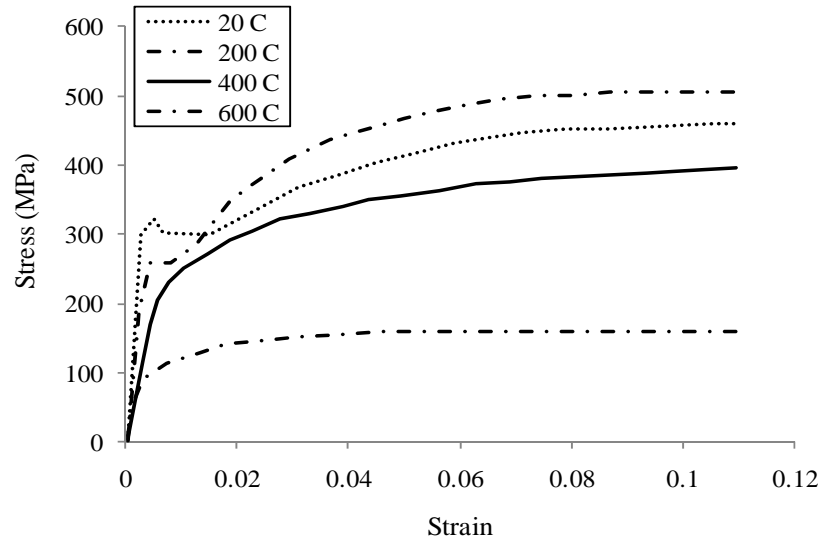


Figure 2.9: Stress-strain curves for steel (300 MPa yield strength) as function of temperature (*reproduced after Lie, 1992*)

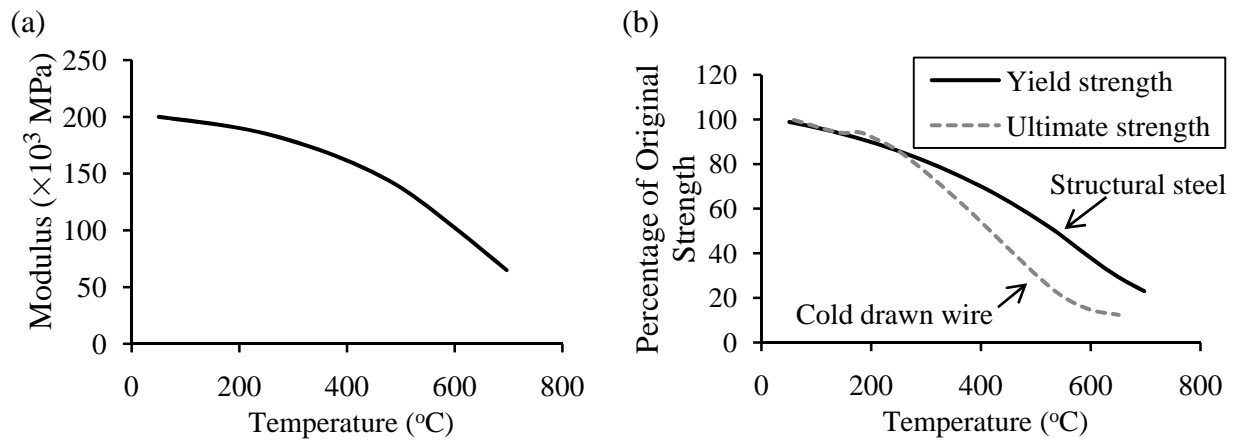


Figure 2.10: Variation of (a) Modulus (b) Yield and ultimate strength with temperature for reinforcing steel (*reproduced after Lie 1992*)

2.4.1.3 Deformation Properties

Thermal elongation and creep strain are the deformation properties of steel. The thermal elongation of steel is quantified through coefficient of thermal expansion (CTE) that indicates thermal strain induced per degree rise of temperature. In general, CTE of reinforcing steel

increases with temperature except between 650 to 815°C where it decreases due to molecular transformation in steel. Thereafter, it increases again as shown in Figure 2.11.

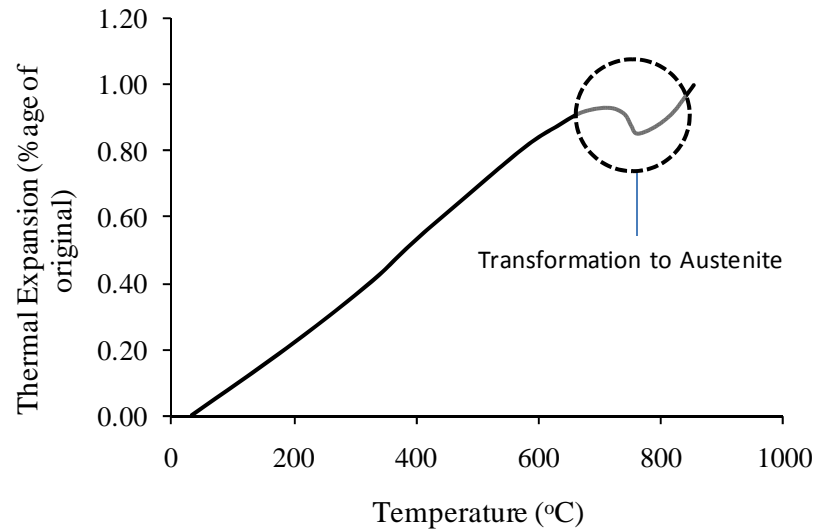


Figure 2.11: Variation of thermal expansion as function of temperature (*reproduced after Lie 1992*)

Creep is time dependant increase in plastic strain under constant stress. This is an important property of reinforcing steel that has significant influence on behavior of RC members under fire conditions (above 450°C). Thus, creep should be included in numerical modeling to evaluate fire performance of structural member (beam). Limited information is available in the literature about creep strain variation with temperature for steel reinforcement. The available creep models, such as the one proposed by Harmathy (Harmathy 1967), are based on Dorn's theory, which relates the creep strain to the temperature, stress, and time. More information on Harmathy's creep model is provided in Chapter 4.

2.4.2 Concrete

2.4.2.1 General

Concrete is a non-combustible construction material that do not contribute readily to heat transfer (good insulating material) (Khoury 2000). Concrete undergoes physiochemical changes

when heated and the influence of temperature is different for sealed and unsealed concrete. Strength loss in concrete depends on type of aggregate and cement blend used in the mix and is negligible up to 300°C. However, this temperature range of deterioration of mechanical properties can be enhanced to 500°C by judicious design of concrete mix (Khoury 2000). Creep strains in concrete gets significant at about 550-600°C, thus, deformations in concrete can be significant above 600°C.

2.4.2.2 Thermal Properties

Thermal conductivity and specific heat (heat capacity) are the two properties that influence thermal response of FRP-strengthened RC beams. In literature, there is available test data on characterizing thermal properties of concrete at elevated temperatures (Kodur and Sultan 2003; Lie and Kodur 1995; Lie and Kodur 1996; Saad et al. 1996; Shin et al. 2002; Van Geem et al. 1997). These properties significantly depend on type of aggregate (siliceous, carbonate or light weight) used in the concrete. Figures 2.12 and 2.13 shows the variation of thermal conductivity and specific heat of normal strength concrete (NSC) as a function of temperature as given in ASCE Manual (1992) and Eurocode 2 (2004) and upper and lower range of values from published test data (shown in solid lines). It can be seen that there is considerable variation in test data which can be attributed to differences in test procedure and measuring techniques. Type of aggregate has considerable influence on thermal properties of concrete. Peaks observed in heat capacity of carbonate aggregate, in the temperature range of 600-800°C is caused by the endothermic reaction as a result of decomposition of dolomite. This reaction consumes large amount of heat energy and this helps to enhance fire resistance. The high temperature constitutive models for thermal properties are presented in Appendix A.

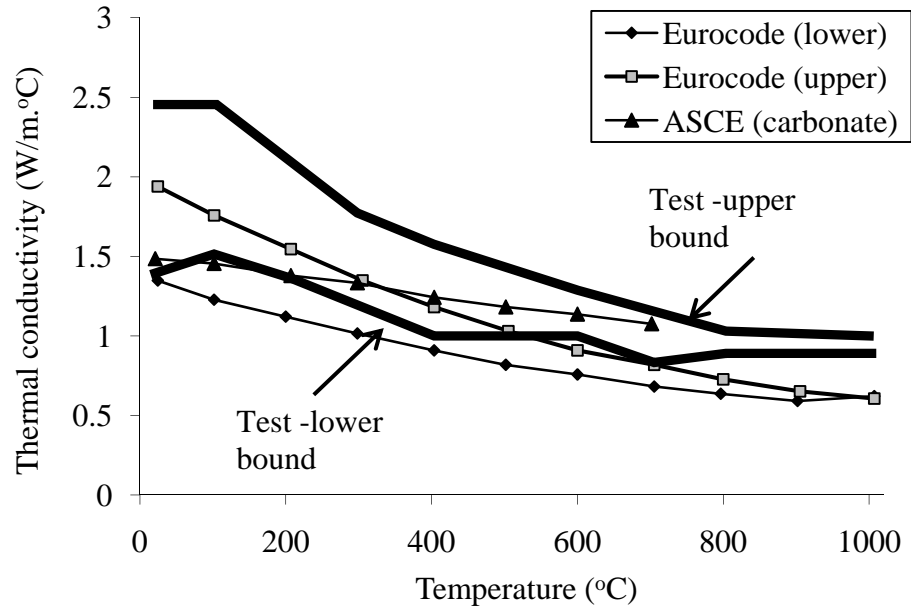


Figure 2.12: Variations of measured and predicted of thermal conductivity as a function of temperature for normal strength concrete (NSC)

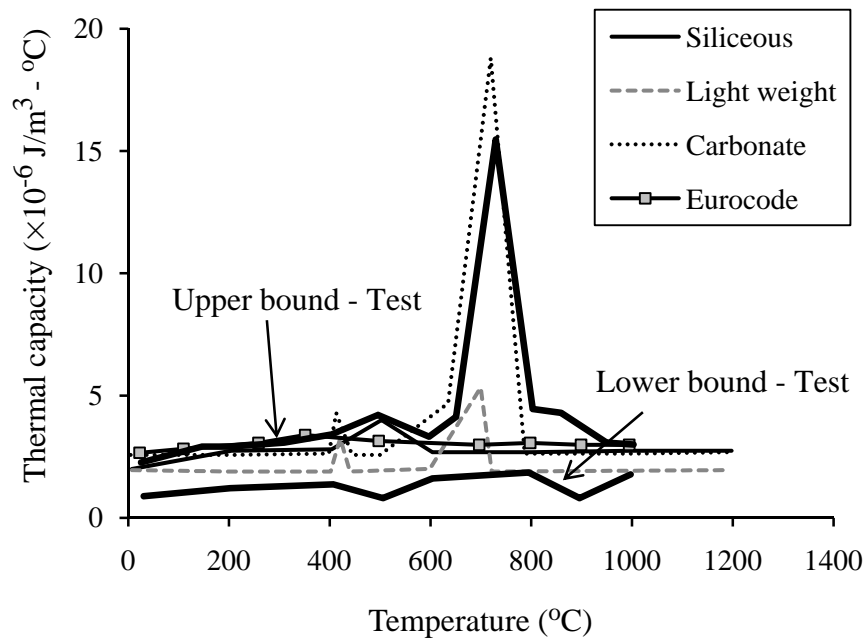


Figure 2.13: Variations of measured and predicted of thermal capacity as a function of temperature for normal strength concrete (NSC) mechanical properties

Mechanical properties include compressive strength, elastic modulus and stress-strain relationship and these vary as a function of temperature. These properties are generally obtained through two test procedures; either measuring the response during specimen is exposed to

elevated temperature or making the measurements when the specimen is cooled to ambient temperature after heated to desired temperature level.

The variation of elastic modulus with temperature for different concrete types is shown in Figure 2.14. In general, the modulus of elasticity of concrete decreases significantly with increase in temperature. Studies have shown that type of aggregate in concrete slightly effect the rate of decrease of elastic modulus. In the tests conducted by Schneider (Schneider 1988), the author reports that factors such as original strength and water-cement ratio do not significantly affect the elastic modulus at elevated temperatures.

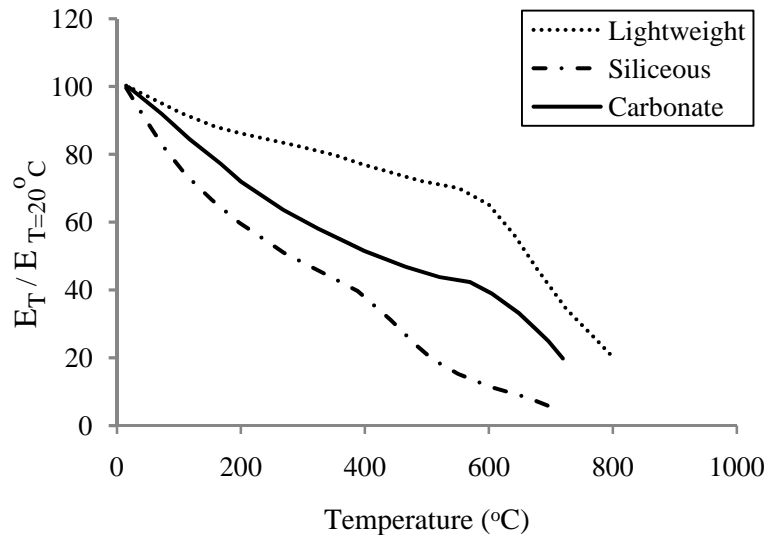


Figure 2.14: Variation of elastic modulus of concrete as a function of temperature

Figures 2.15 and 2.16 show the variation of compressive strength with temperature for normal and high strength concretes, respectively. For normal strength concrete (NSC), there is not much variation in compiled test data. The data for high strength concrete (HSC) shows a large variation especially in the range of 200-500°C. This variation can be attributed to various factors such as occurrence of concrete spalling during testing, variation in testing procedure

(different heating and loading rate), test conditions, limitations of testing apparatus, and measuring techniques. This test data formed the basis of constitutive relationships for high temperature mechanical properties of concrete. These relationships are presented in ASCE Manual, Eurocode 2 and Kodur et al. (Kodur et al. 2004) and included in Appendix A. The compressive strength of concrete computed with these relationships is plotted in Figures 2.15 and 2.16. From the plot, it can be noticed that ASCE model results are close to upper bound test data while Eurocode 2 model follows close to lower bound test results. Kodur et al. showed that using ASCE constitutive model produces better fire resistance predictions as compared to Eurocode constitutive model.

The residual strength of concrete is an important property for modeling structural members exposed to design fire. During cooling phase under design fire, the process of hydration of unhydrated cement components is an ongoing process. These hydrated products have larger volume that introduces cracking in concrete, thus, concrete continues to lose strength and stiffness (Dwaikat 2009). Thus, the residual strength of concrete is less than heated concrete. Data published in literature shows that there is a large variation in residual strength of concrete, as shown in Figure 2.17. This large variation can be attributed to using different heating (or cooling) or loading rate, specimen and test conditions, and the use of admixtures. Codes and standards, such as Eurocode 2 and ASCE manual, do not specify relationships for the residual strength of concrete after fire exposure. However, best fit of the published test data is generally used for evaluating the residual strength of concrete, as shown in Figure 2.17 (Kumar 2003).

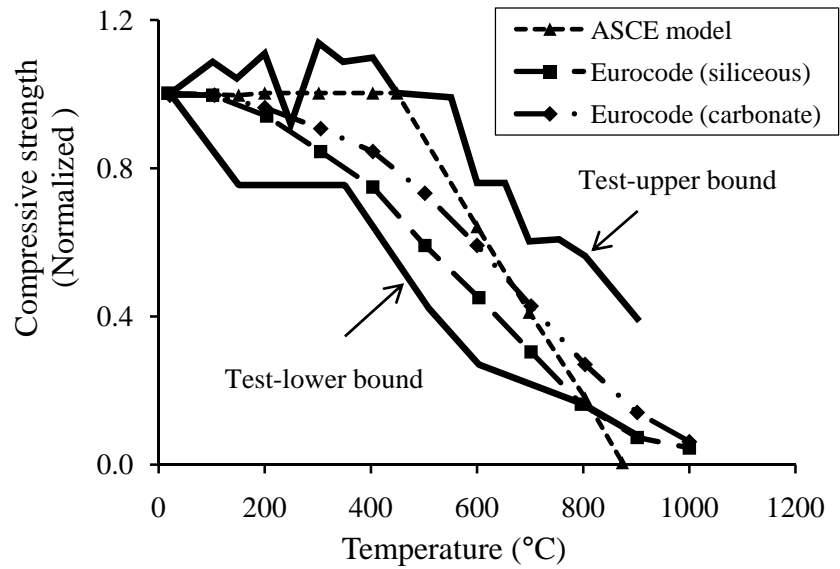


Figure 2.15: Variation of compressive strength as a function of temperature for NSC

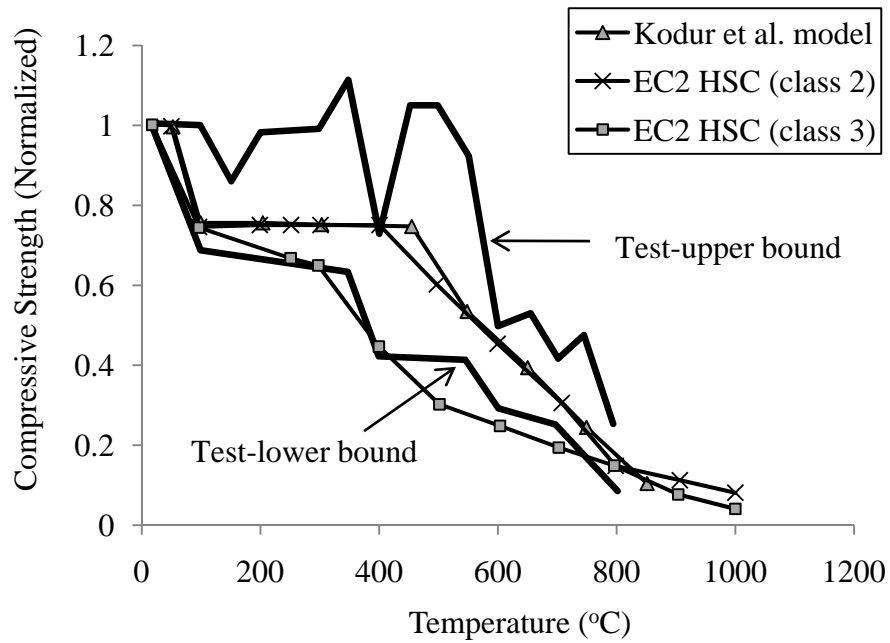


Figure 2.16: Variation of compressive strength as a function of temperature for HSC

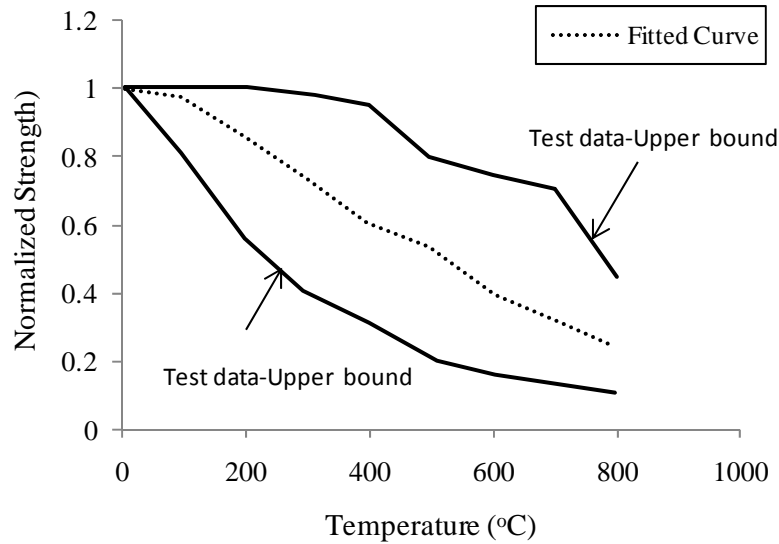


Figure 2.17: Variation of residual compressive strength as a function of temperature
(reproduced after Kumar 2003)

2.4.2.3 Deformation Properties

Deformation properties include thermal expansion, creep and transient strains and these depend on the type of aggregate used, and chemical and physical reactions occurring in cement paste (Schneider 1988).

The coefficient of thermal expansion (CTE), defined by change in length of material per degree rise in temperature, is an important measure to measure thermal stresses as a result of temperature variation (Kodur and Harmathy 2008). CTE of concrete depends on type of aggregate, its composition, and moisture content (Dwaikat 2009). The thermal expansion of concrete with siliceous aggregate is considerably more as compared to concrete with carbonate aggregate. Published data plotted in Figure 2.18 shows that CTE varies for different aggregate types.

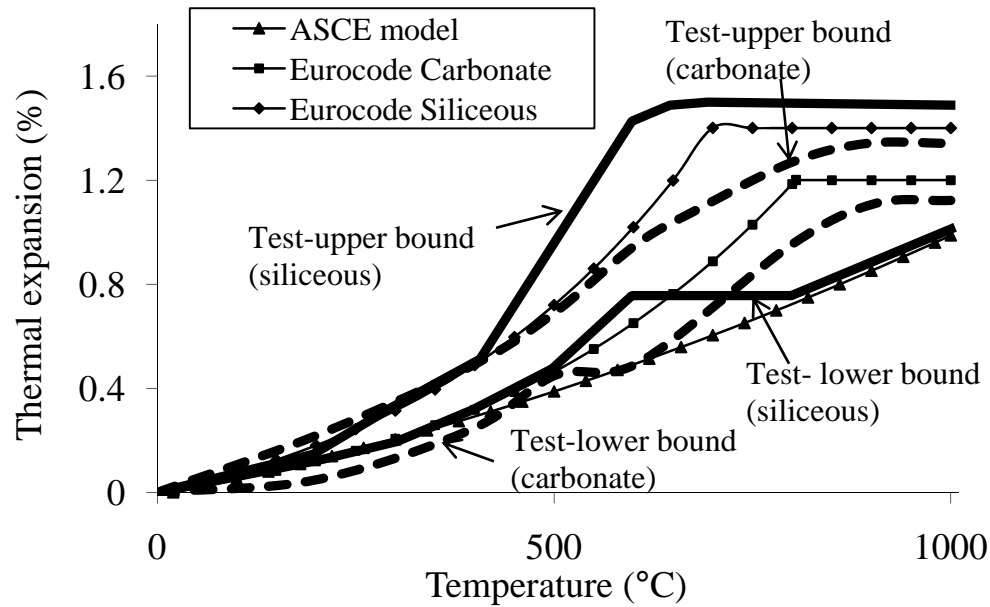


Figure 2.18: Variations of measured and predicted of thermal expansion for concrete as a function of temperature

Creep strain is time-dependent plastic strain under constant stress level. It is associated with the moisture movement inside concrete, therefore, is influenced by the temperature. At elevated temperatures, creep strains are significant since moisture movement occurs more rapidly. Creep strains depends on many factors including temperature, stress levels, time, loading and mix design of concrete (Dwaikat 2009). A review of literature shows that creep strains are significant in low-modulus aggregates. Creep is more pronounced at higher load level and elevated temperatures.

In concrete, transient strain also develops in addition to creep during the first heating under load and is independent of time (Khoury 2000). It is caused by thermal incompatibilities (differential thermal expansion) between aggregate and cement paste (Purkiss 2007). The mismatch in thermal expansion between aggregate and cement paste leads to development of internal stresses and micro-cracking and this results in transient strains to occur in concrete (Schneider 1988). Currently, limited information is available in the literature on high temperature

creep and transient strains (Kodur and Harmathy 2008). Constitutive relationships for high temperature creep and transient strains of concrete have been developed by Anderberg and Thelandersson (Anderberg and Thelandersson 1976) and Harmathy (Harmathy 1993), and is given by these two equations:

$$\varepsilon_{cr} = \beta_1 \frac{\sigma}{f_{c,T}} \sqrt{t} e^{d(T-293)} \quad (\text{Anderberg model}) \quad (2.1)$$

$$\varepsilon_{tr} = k_2 \frac{\sigma}{f_{c,20}} \varepsilon_{th} \quad (\text{Harmathy model}) \quad (2.2)$$

where ε_{cr} = creep strain, ε_{tr} = transient strain, $\beta_1 = 6.28 \times 10^{-6} s^{-0.5}$, $d = 2.658 \times 10^{-3} K^{-1}$, T = concrete temperature (K) at time t (s), $f_{c,T}$ = concrete strength at temperature T , and σ = stress in the concrete at the current temperature, k_2 = a constant ranges between 1.8 and 2.35, ε_{th} = thermal strain, and $f_{c,20}$ = concrete strength at room temperature.

These equations generally produce reasonable estimates for high temperature creep and transient strains in concrete.

2.4.2.4 Fire induced Spalling

Concrete spalling is caused by the exposure of the concrete to high temperatures. Spalling itself is actually the deterioration of the concrete causing chunks of concrete to separate from the concrete structure. Some of the most common concrete spalling causes are fire and high pressure. Most researchers attributed spalling to low permeability of concrete and moisture migration at elevated temperatures. Spalling is believed to be caused by the build-up of pore pressure during heating. High strength concrete (HSC) is believed to be more susceptible to this pressure build-up than NSC because of its low permeability. The extremely high water vapour pressure, generated during exposure to fire, cannot escape due to the high density (and low permeability) of HSC. Spalling in RC member relates to falling off of concrete (in pieces) as a

result of effective pore pressure, which is defined as product of porosity and pore pressure, exceeds tensile strength of concrete (refer to Figure 2.19). This falling off can often be explosive depending on the fire and concrete characteristics. Another possible cause of spalling is related to the restrained thermal dilation close to heated surface. These stresses are compressive in nature and develop parallel to the heated surface as shown in Figure 2.20. These compressive stresses are released by brittle fracture of concrete or in other words concrete spalling. Studies have shown that this phenomenon is more pronounced in HSC as compared to NSC. Moreover, the chances of spalling in RC members with adequate fire protection (insulation) are rare since insulation plays an effective role in limiting the fast rise of temperature in concrete. The limited published data on fire tests conducted on FRP-strengthened RC beams have not reported occurrence of spalling for the entire duration of the tests.

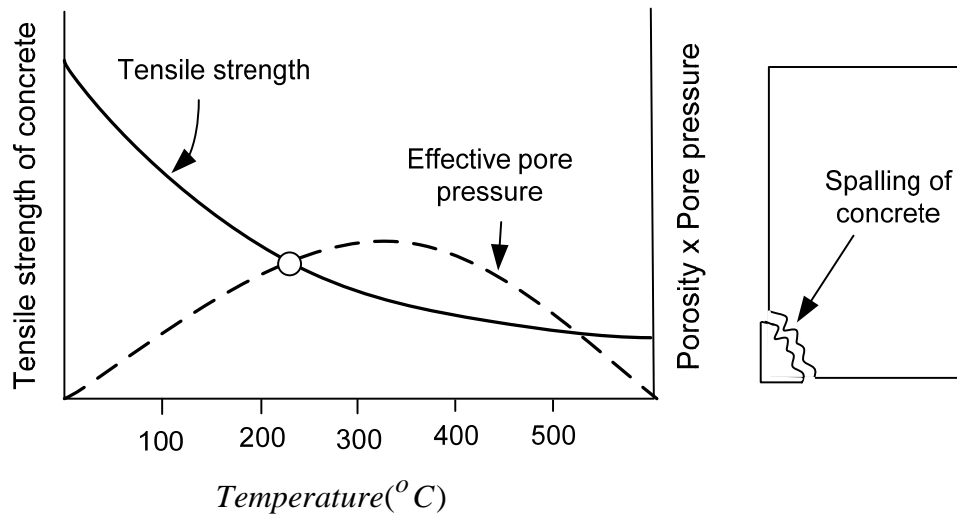


Figure 2.19: Illustration of spalling of concrete due to pore pressure

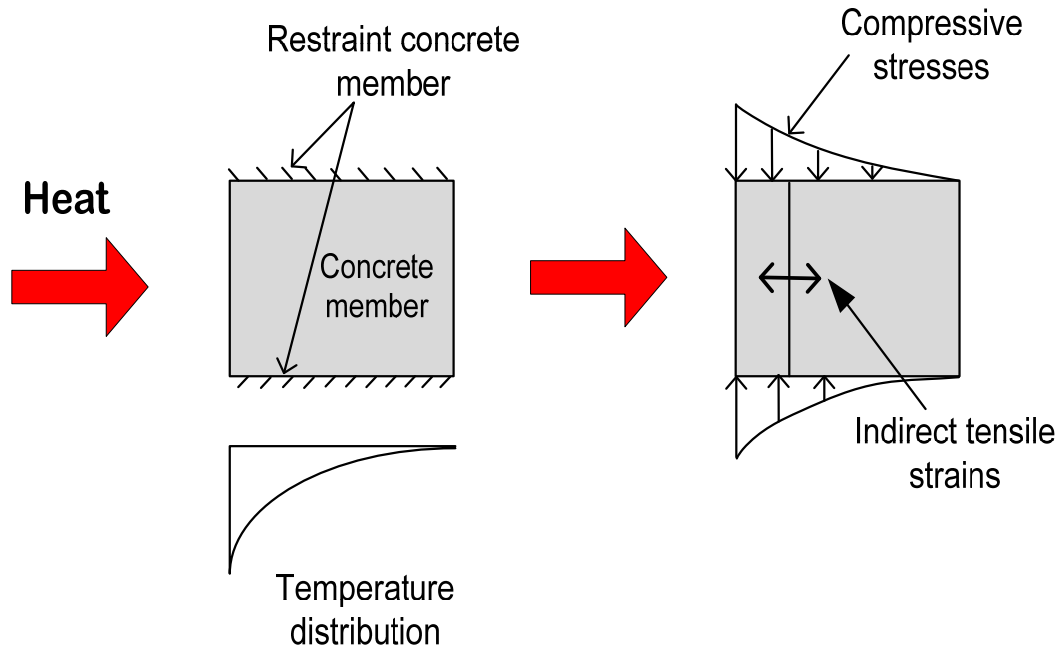


Figure 2.20: Illustration of thermal dilation mechanism

2.4.3 Fiber Reinforced Polymers (FRP)

2.4.3.1 General

A wide range of FRP products are available in the market and any small changes in the composition of FRP (matrix or fiber) might influence the high temperature properties. Unlike RC structural members that perform satisfactorily under fire, many uncertainties are associated with fire performance of FRP-strengthened RC members. These concerns include strength and stiffness degradation, flame spread in FRP, smoke generation in FRP, and loss of bond between FRP and concrete. The complexities are related to the low glass transition temperature (T_g) of FRP. When the temperature reaches close to glass transition temperature of polymer (matrix), it transforms to visco-elastic material (rubbery material) which results in a reduction in strength and stiffness properties (Bakis 1993). Most common polymers (matrix) used in civil engineering application (thermosets) have glass transition temperature in range of 60-82°C. Beyond T_g , the

matrix might ignite, supporting flame spread and toxic smoke generation (Apicella and Imbrogno 1999b). This may result in debonding of FRP due to significant degradation of mechanical properties of the matrix.

In the event of fire, overall behavior of FRP composite is dependent on transverse matrix properties that deteriorate significantly with temperature. Research has indicated that reaching T_g of adhesives is a critical factor governing the fire response of externally bonded FRP-strengthened RC structural members (Camata et al. 2007). Earlier in section 2.2.1, the properties of FRP composite (both fibers and the matrix) at ambient temperature were discussed. Following sections present variations in properties of fibers, matrix and FRP composite at elevated temperatures.

2.4.3.2 *Fibers*

Fibers are more thermally stable than polymer matrix. Glass, carbon and aramid are three types of high performing fibers that are commonly considered for different applications. Amongst these, aramid fibers are non-flammable and form char when exposed to flame. These fibers oxidize around 150°C, thereby limiting their use at higher temperature exposures (Bakis 1993). Glass fibers are relatively more stable with softening point in the range of 650-970°C and tolerance against melting up to 1225-1370°C (Bourbigot and Flambard 2002). Carbon fibers offer the highest modulus of all reinforcing fibers. Among the advantages of carbon fibers are their exceptionally high tensile-strength-to-weight ratios as well as high tensile-modulus-to-weight ratios. In addition, carbon fibers have high fatigue strengths and a very low coefficient of linear thermal expansion and, in some cases, even negative thermal expansion. Carbon fibers have high resistant to higher temperatures with melting temperatures as high as 4000°C and are also considered flame resistance since they burn at very high temperatures (Bourbigot and

Flambard 2002). Carbon fibers are chemically inert and are not susceptible to corrosion or oxidation at temperatures below 400°C. Therefore, these fibers are material of choice for applications at extremely high temperatures.

A survey of strength-temperature data for fibers has been conducted by Bisby (2003) and represented in Figure 2.21. It can be seen that there is significant reduction in tensile strength of aramid fibers above 100°C while carbon fiber showed negligible reduction in strength at higher temperatures. The strength of glass fibers decreases gradually with temperature.

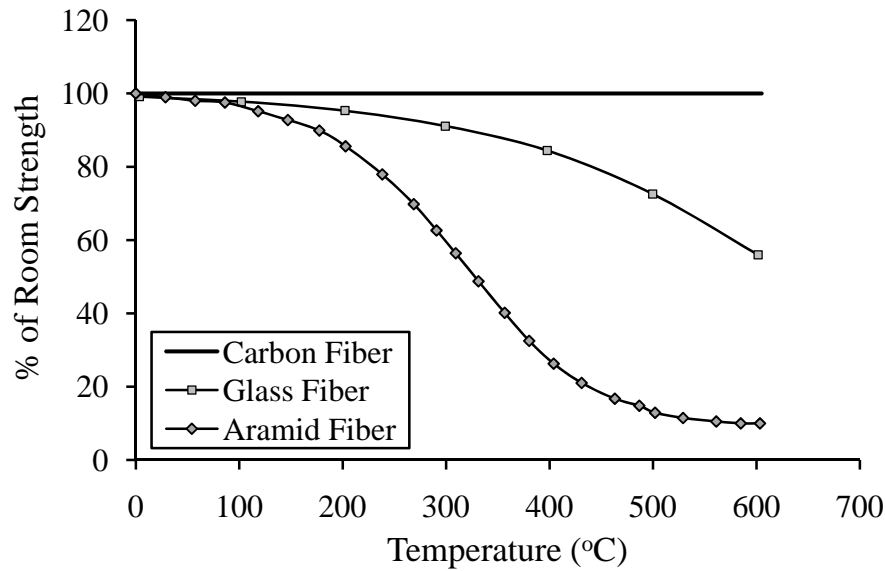


Figure 2.21: Variation in tensile strength of fibers with temperature (*reproduced after Bisby, 2003*)

2.4.3.3 Matrix

The matrix properties degrade with increase in temperature. As the temperature reaches close to glass transition temperature (T_g), defined as the point where matrix softens, most of its elastic as well as the strength properties are lost. This degradation is gradual until the temperature reaches near T_g , and thereafter the stiffness plunges dramatically compared to that at room temperature. The glass transition temperature of polymers (matrix) used in civil

engineering applications is quite low, typically ranges between 60-82°C (ACI 2008). When exposed to higher temperatures (beyond T_g), the polymers decomposes forming a char layer that acts as a thermal barrier and has no flexural stiffness or strength. The decomposition temperature range is a function of cross linking density of the polymer, composition, curing process and type of fiber reinforcement (Mouritz 2002). The polyester resins have shown to decompose around 300-400°C while epoxy resins between 400-600°C based on thermo-gravimetric analysis (Dodds et al. 2000). Also, the time to ignition varies for different type of FRP composites. This depends on the type of reinforcing fibers apart from matrix characteristics. For example, when the matrix resin is same, ignition time for composite with woven glass fibers is longer than composites with chopped glass fibers (Mouritz 2002).

2.4.3.4 FRP Composite – Thermal Properties

Thermal conductivity and specific heat in unidirectional composites are discussed here since these are commonly used in civil engineering applications. In general, polymers (matrix) have low thermal conductivity (Mallik 1988), which is one of the reasons that polymers are used as insulating materials for cables. In case of fibers alone, thermal conductivity depends on the type of fiber used, its orientation and volume fraction. In unidirectional FRP composites, the fibers control the longitudinal thermal conductivity while the matrix controls thermal conductivity in the transverse.. Some of the typical values of thermal conductivities for various FRP materials at ambient temperature are given in Table 2.3. Thermal conductivities of FRP composite are quite low with the exception of CFRP since carbon fibers are highly conductive.

Table 2.3: Thermal conductivities of various unidirectional FRP and building material (*after Mallick, 1988*)

Material	Thermal Conductivity (W/m-°C)	
	Longitudinal	Transverse
Glass/Epoxy	3.46	0.35
Aramid/Epoxy	1.73	0.73
High Modulus Carbon/Epoxy	48.44-60.55	0.87
Ultra High Modulus Carbon/Epoxy	121.1-129.8	0.04
Aluminum	138.4-216.3	
Steel	15.57-46.71	
Epoxy	0.346	

Limited research work has been conducted on thermal properties of FRP composite at elevated temperature. Graffis et al. (1981) conducted tests on graphite epoxy laminate using Laser Irradiation test up to 3000°C. The test results show a significant drop in thermal conductivity with temperature, as shown in Figure 2.22.

Specific heat is the measure of heat transfer through FRP composite and is extremely difficult to determine the variability due to complex nature of chemical reactions taking place in FRP at high temperatures. Griffis et al. (1981) suggested specific heat for carbon/epoxy FRP as shown in Figure 2.22. This variation of specific heat is based on test data where temperature plateau observed between 350-510°C shows consumption of additional heat as a result from thermal degradation of resin (matrix).

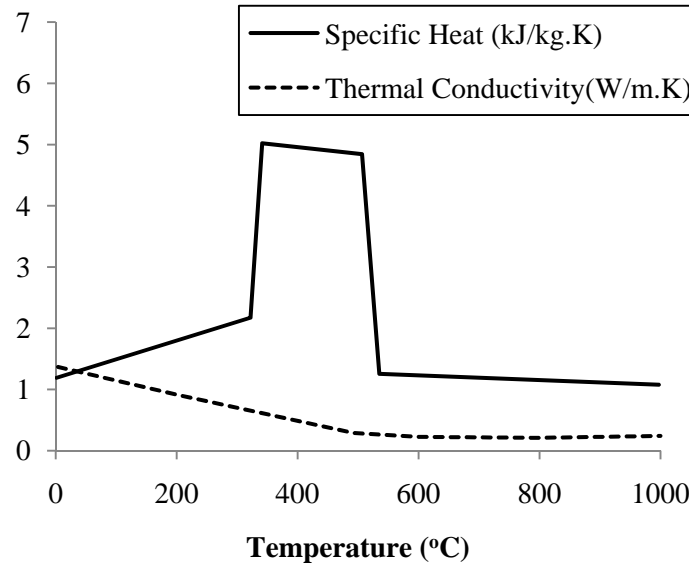


Figure 2.22: Variation in thermal properties with temperature for carbon/epoxy FRP
(reproduced from Griffis et al., 1981)

2.4.3.5 FRP Composites – Mechanical Properties

Mechanical properties of FRP composite deteriorate with increasing temperature. When the temperature reaches close to glass transition temperature, a considerable decrease in strength and stiffness of FRP occurs. As discussed in previous sections, fibers perform well at elevated temperatures, while polymers (matrix) are highly susceptible at high temperatures. Therefore, FRP composites experience significant degradation in mechanical properties as the temperature approaches T_g (Blontrock et al. 1999).

Variation in longitudinal, transverse and shear modulus of carbon/thermoplastic and carbon/bismaleimide thermoset FRP's has been investigated by Gates (Gates 1991) up to 200°C (glass transition temperature of resin is quoted as 220°C) . No significant variation in longitudinal modulus was observed up to 200°C, however, transverse and shear moduli showed degradation. Also, stress-strain behavior showed a strength loss of 40-50% at 125°C and of about

90% at 200°C. These trends conform to the theory that significant loss of strength is observed at temperatures close to T_g .

2.4.3.6 FRP Composites – Deformation Properties

Coefficient of thermal expansion (CTE) is change in length per unit rise in temperature. CTE of polymers is relatively higher than other conventional civil engineering materials (order of 100×10^{-6}). The CTE of thermoset resins is influenced by the degree of cross linkage. CTE's vary considerably with temperature and increase rapidly at temperatures above glass transition temperature. In FRP composite, transverse CTE is higher as compared to that in longitudinal direction since longitudinal properties are dominated by the fibers. CTE's of various common FRP material is tabulated in Table 2.4 (Mallik 1988).

Table 2.4:CTE's of unidirectional FRP composites and building materials

Material	Coefficient of Thermal Expansion ($\times 10^{-6} / ^\circ\text{C}$)	
	Longitudinal	Transverse
Glass/Epoxy	6.3	19.8
Aramid/Epoxy	-3.6	54
High Modulus Carbon/Epoxy	-0.09	27
Ultra-high Modulus Carbon/Epoxy	-1.44	30.6
Boron/Epoxy	4.5	14.4
Steel	10.8-18	
Epoxy	54-90	

2.4.3.7 FRP Composite - Bond Properties

Bond plays a vital role in transfer of loads (forces) from concrete to FRP reinforcement through shear stresses developed in the polymer matrix. As highlighted before, mechanical property of the polymer (matrix) degrades with temperature and is a potential cause for the loss of interaction between FRP and concrete substrate. In literature, there is very limited data on variation of bond strength with temperature. Data compiled from previous tests is plotted in Figure 2.23 in the form of normalized bond strength as a function of temperature (Blontrock et

al. 2002; Di Tommaso et al. 2001; Klammer et al. 2005b; Leone et al. 2009; Wu et al. 2004). The source of this data base includes double-lap shear tests conducted on CFRP laminates bonded to concrete with adhesive. Examining trends in Figure 2.23, it can be seen that there is wide scatter of data and this is because of the variation in mechanical properties of the FRP used in different tests. Results from the experiments conducted by Blontrock et al. (Blontrock et al. 1999) shows an increase in bond strength for specimens tested at 40°C and 55°C and this was attributed to the difference in coefficient of thermal expansion between FRP and concrete, variation of the test specimen sizes and change in failure modes. Klammer et al. (Klammer et al. 2005a) also reported a similar trend in double-lap shear tests performed at three different temperatures. However, Wu et al. (Wu et al. 2004) observed reduction in failure load with increasing temperature which was attributed to lower glass transition temperature of the adhesive.

The degradation of bond at FRP-concrete interface is influenced by many factors such as type of FRP reinforcement (factory produced laminates or hand-layup sheets), glass transition temperature of the adhesive and service temperatures (Leone et al. 2009). Previous studies showed negligible degradation in bond strength at low temperatures. Klammer et al. conducted tests on small scale specimens to evaluate variation of bond strength with temperature (Klammer et al. 2008). In these tests, adhesive used to glue FRP with concrete had glass transition temperature of 62°C. Based on test observations, the authors recommended to disregard the effect of temperature on bond strength in the range of 50°C and below ($T_g - 10^\circ\text{C}$), while, significant reduction in bond strength was observed at temperatures beyond T_g .

Based on the available test data on bond strength, a statistical regression analysis is carried out and following relation was obtained to express variation in bond strength with temperature:

$$f_T = f_{20} \quad (\text{if } T \leq 40^\circ\text{C}) \quad (2.3)$$

$$\frac{f_T}{f_{20}} = 1 - \left(\frac{1}{80} \right) (T - 40) \quad (\text{if } 40^\circ\text{C} < T \leq 120^\circ\text{C}) \quad (2.4)$$

where, f_{20} and f_T are the bond strength at room and higher temperatures respectively, T is the temperature at the interface of FRP and concrete.

The above proposed simplified equations which are based on limited published test data facilitate to estimate of bond degradation with temperature.

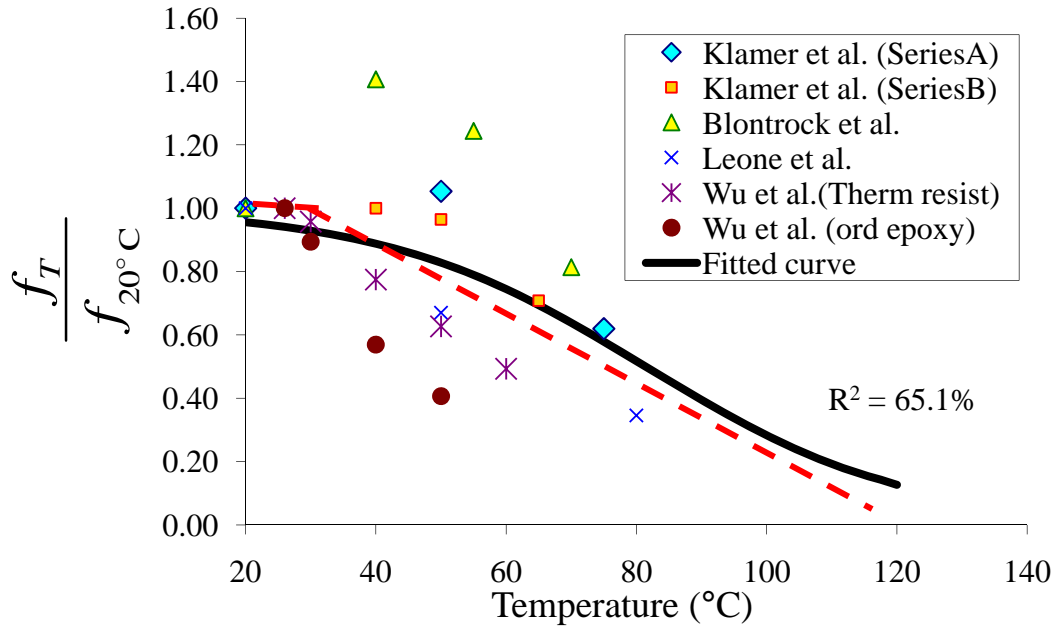


Figure 2.23: Variation of bond strength with temperature

2.4.3.8 Physical Properties – Smoke Generation, Flame Spread and Toxicity

The flame spread, amount of toxicity and smoke generation depends on composition of FRP matrix (Nelson 1995). Fibers are highly stable at elevated temperatures. However, the matrix in FRP composite consisting of polymers (polyester or epoxy resin) ignite quickly that

result in flame spread as well as smoke generation. Mouritz (Mouritz 2002) studied ignition time characteristics of various FRP composites. He reported less than one minute ignition time for glass/epoxy and glass/polyester composites as compared to glass/phenolic that took about 7 minutes. Smoke generation and toxicity characteristics of FRP material used for off shore and marine applications were studied by Sorathia et al (1992). The results shown in Figure 2.24 demonstrate that thermoset resins typically generate unacceptable quantities of smoke and also have relatively poor flame spread characteristics. The limits quoted by the authors for smoke density are 100 within first 300 seconds and 200 at any point during the test. When burnt, thermoset resins generate varying quantities of toxic gases such as carbon monoxide (CO), carbon dioxide (CO₂), hydrogen chloride (HCL), hydrogen sulfide (H₂S), and Hydrogen cyanide (HCN).

For evaluating flame spread and smoke generation, ASTM recommends three different standard tests. ASTM E84 test specifies procedures for relative burning behavior of a building material by measuring flame spread index (FSI) and smoke density index (SDI). ASTM E662 specifies optical density test to measure characteristics of smoke concentration, while ASTM E162 describes test procedure for measuring and comparing surface flammability of different building materials when exposed to radiant heat energy. ASTM E662 allows a maximum allowable smoke index of 100 at 300 seconds. For most of FRP systems, the optical density is less than 100 and ranges from 2 to 96 for glass/epoxy and 1 to 75 for carbon/epoxy composites.

Provision of resin additives is available to reduce flammability of FRP matrix. Flame retardants like phosphorous and alumina trihydrate can be introduced as additives in FRP matrix; however, such chemicals could potentially cause reduction in mechanical properties and degrade into toxic gases during combustion which may be a concern for life safety. Due to the

fact that wide variety of available additives can influence various properties of FRP composites, therefore, any further discussion is not included here.

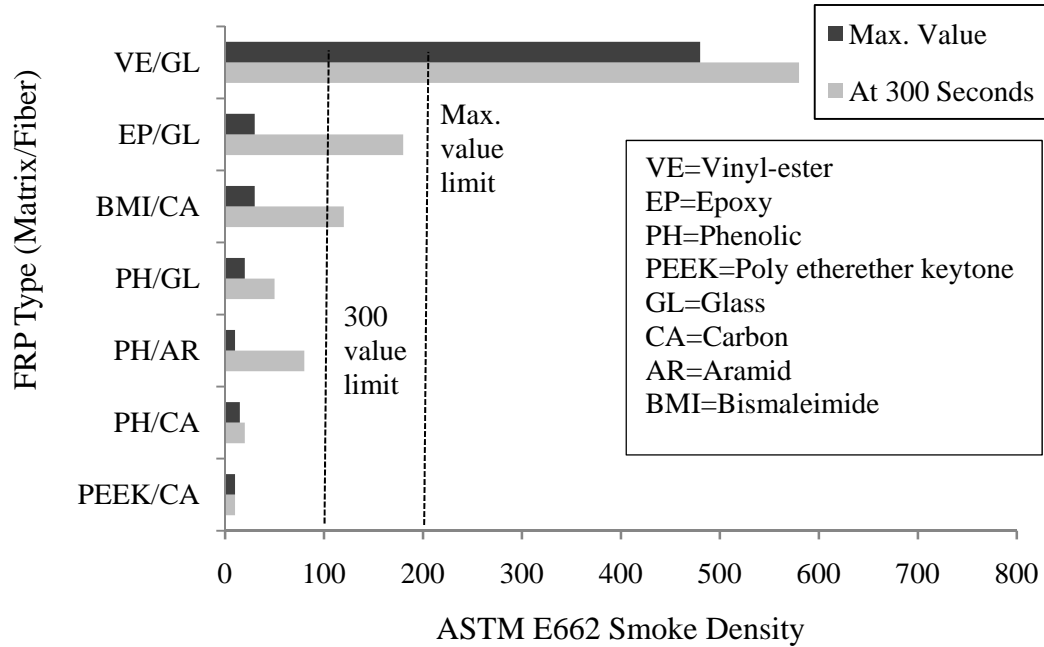


Figure 2.24: Results of smoke generation tests on various FRPs (*reproduced after Sorathia et al. 1992*)

2.4.4 Insulation

Insulation is a material or combination of materials, which retard the rate of heat flow through low thermal conductivity and high heat capacity properties (Al-Homoud and Mohammad 2005). Of various civil engineering materials, concrete has excellent inherent fire resistance properties. On contrary with increasing temperature, most of the FRP composites are susceptible to combustion that results in flame spread and smoke generation. The glass transition temperature threshold of polymers (matrix) ranges as low as 65-82°C. Therefore, in the absence of any fire protection system, FRP's are highly sensitive to modest increase in temperature. At temperatures close to T_g , FRP loses their mechanical and bond properties and indirectly support

flame spread and smoke generation as a result of ignition/ combustion. In literature, a number of studies have been conducted that suggest use of supplemental fire protection system to achieve desired fire resistance in FRP-strengthened structural members. This aspect is more critical in externally bonded FRP reinforcement.

The insulating material is characterized by two main categories (Papadopoulos 2005):

- Inorganic material
 - Foam glass
 - Fibrous
 - Glass- wool
 - Stone-wool
- Organic
 - Foamy
 - Expanded polystyrene
 - Extruded Polystyrene
 - Polyurethan foam
 - Foamy expanded
 - Cork
 - Melamine foam
 - Phenole foam
 - Fibrous
 - Sheep-wool
 - Cotton-wool
 - Coconut fibers

- Cellulose
- Combined material
 - Siliconated calcium
 - Gypsum foam
 - Wood-wool

Insulation boards consisting of calcium silicate, gypsum, and vermiculite are widely used as fire protection systems. These provide protection through low thermal conductivity as well as through evaporation of free and chemically bound water within board. The range of thermal conductivity of calcium and gypsum board is 0.12 to 0.16 W/m-°K (Williams 2004a). Fire proofing systems such as vermiculite mixed with Portland cement or gypsum binder, available in powder form are spray-applied after mixing water to the dry material. These spray applied protection prevent heat transfer through low thermal conductivity (0.043-0.078 W/m-K) and evaporation of entrapped water (during mixing). Tyfo Vermiculite-gypsum (VG) insulation is non-combustible and non-flammable proprietary advance fire protection (AFP) system. This insulation is spray-applied on externally bonded FRP reinforcement to attain up to 4 hours of fire rating of the structural assembly (UL listed, Design No. N790). Bisby (Bisby 2003) performed thermogravimetric analysis and proposed relationships for thermal properties, and relationship are given in Appendix A.

Figure 2.25 show normalized thermal conductivity and thermal capacity for insulation (vermiculite-gypsum) as a function of temperature. It can be seen that thermal conductivity decreases up to 200°C, then remains constant till 500°C, after which it increases with temperature. The peak for thermal capacity at about 100°C and is due to evaporation of trapped water that consumes most of the heat energy.

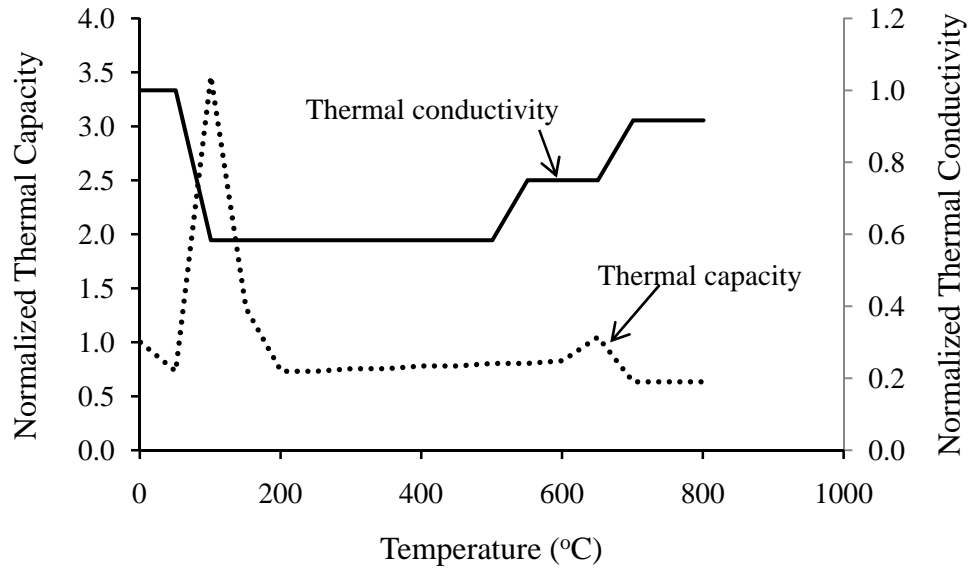


Figure 2.25: Normalized thermal conductivity and thermal capacity of VG insulation

Intumescent coating is another insulating product that is applied in thin layers (0.1-13 mm). An intumescent is a substance which swells as a result of heat exposure, thus increasing in volume, and decreasing in density. Intumescent coatings are typically used for steel structural members. In FRP-strengthened RC members these intumescent coatings are applied as a final coating on spray-applied insulation to provide additional stability against crack formation. Apicella and Imbrogno (Apicella and Imbrogno 1999a) studied performance of intumescent and other coatings applied to CFRP/epoxy laminates for smoke generation and flame spread in accordance with ASTM E84 standards. The unprotected CFRP ignited in 44 seconds, experienced charring and achieved flame spread index of 155 and smoke index of 405. This produced a Class III rating for CFRP which is the lowest according to building code (UBC). The application of intumescent coating increased the ignition time to 58 seconds with flame and smoke index reduces to zero and 20, respectively. Thus, the fire performance was improved to Class I. Sorathia et al. (Sorathia et al. 1992) studied various fire barrier treatments including ceramic coating, intumescent coating, ceramic fabric, silicon foam, and phenolic resin to improve structural

behavior of FRP composites. The ignition time of glass/vinyl ester composite was improved from 22 seconds to 450 seconds using 0.762 mm water based intumescent coating. A layer of phenolic coating increased ignition time of glass/epoxy from 100 to 1000 seconds. Thus, intumescent coating is an effective measure of fire protection.

The insulation products described in this section cover small percentage of what is available in the market. New products are in the process of development and needs further study to keep abreast with fast growing market.

2.5 Previous Studies on FRP-strengthened RC Beams

2.5.1 Experimental Studies

In the last decade, there have been limited studies to investigate the fire behavior of FRP-strengthened concrete members. However, these fire resistance tests were limited in scope and did not consider many of the factors governing fire resistance of FRP. In addition, there have been limited studies to characterize effect of temperature induced bond degradation on fire performance of FRP-strengthened members. Most of these bond tests were performed on small-scale specimens (under double-lap shear test configuration) to understand bond degradation between FRP sheets and concrete. These studies have been reviewed in detail.

Fire Tests

Four experimental programs that focused on studying the behavior of FRP-strengthened beams under fire have been published in the literature. Deuring (1994) conducted standard fire tests on six RC beams strengthened with external carbon fiber reinforced polymer (CFRP) strips and steel plates under ISO 834 standard fire exposure to assess the post-fire residual strength. Four of these beams were strengthened with CFRP sheet; one was strengthened with adhesive

bonded steel plate and the remaining one was an un-strengthened beam. Four of the FRP-strengthened beams were provided with supplemental fire insulation to enhance fire resistance. In the fire tests, a loss of interaction (bond) between concrete and FRP was observed within 20 minutes of fire exposure in the unprotected FRP-strengthened RC beam (without insulation). In protected beams, insulation helped to keep the temperatures low at the interface of FRP and concrete, thus protecting the bond between concrete and FRP. The authors concluded that FRP-strengthened RC beams can achieve required fire resistance ratings provided proper external insulation is applied.

Blontrock et al. (2000) tested two RC beams and six CFRP strengthened RC beams under ISO-834 fire exposure to study the effect of temperature on bond degradation between FRP and concrete. The beams were applied with external fire insulation, Promatect-H and Promatect-100, having a density of 870 kg/m^3 and 875 kg/m^3 respectively. Data from tests indicated that some level of thermal protection is necessary to minimize strength loss in FRP and maintain low deflections in the beam during fire exposure. The authors concluded that external fire insulation is needed to limit the temperatures in adhesive below T_g (about 80-90°C) in order to maintain effective bond between FRP and concrete.

Barnes and Fidell (2006) tested 24 CFRP strengthened RC beams under standard fire conditions (1987) to study the effectiveness of insulation and mechanical bolting of CFRP plate. RC beams of (100×150 mm) size were strengthened with CFRP plate of 100 mm width and 1 mm thickness, and insulated by applying one 15-20 mm thick layer of cementitious (cement/gypsum material based) fire insulation. Beams were exposed to fire for 1 hour without any applied loading and later subjected to four point bending loads till failure occurred in the beams. Test results indicated that no transfer of stresses occurred from concrete to CFRP plate

once the bond between FRP and concrete was lost at temperatures exceeding T_g . It was concluded that applied fire protection (15-20 mm) was not sufficient to keep the temperatures low (below T_g) at the FRP/concrete interface beyond 30-45 minutes. These tests also revealed that the matrix in CFRP plate withstood temperatures up to 310°C, while carbon fibers lasted up to 950°C.

Williams et al. (2006; Williams et al. 2008) conducted four full-scale fire resistance tests on FRP-strengthened RC T-beams protected with varying insulation thicknesses (25 and 38 mm). The beams were tested under service load while exposing to ASTM E119 standard fire (2007). In all the fire tests, T_g of FRP was reached in early stages of fire (about 60 to 90 minutes), but this did not lead to failure of the beams based on strength or critical temperature (rebar temperature) limit state. The beams achieved 4 hours fire resistance rating based on ASTM E119 failure criteria. Williams et al. also developed and validated a thermal model to predict the temperatures in the beam cross-section.

The above review clearly illustrates that there have been only limited tests conducted to evaluate fire performance of FRP-strengthened RC beams. Further, most of these tests have been conducted under standard fire conditions. There have been no tests on fire response of FRP-strengthened RC beams under realistic fire, loading, and restraint scenarios.

Bond Degradation Tests

Bond between FRP and concrete is critical for transferring forces which takes place through development of shear stresses in adhesive. The mechanical properties of bonding material (adhesive) are highly influenced by temperature, and even modest temperature rise leads to loss of interaction between FRP and concrete. A noticeable number of studies, both experimental and

theoretical, have been conducted to understand the behavior of bond between FRP-concrete at ambient temperature. Some of these studies proposed models based on empirical relationships while others utilized fracture mechanics principles to predict bond strength variation (Blaschko et al. 1998; Hiroyuki and Wu 1997; Maeda et al. 1997; Sato et al. 1997; Tanaka 1996; Yuan and Wu 1999; Yuan et al. 2001). However, only limited studies have been reported in the literature on the effect of temperature on bond degradation at FRP-concrete interface.

Tadeu and Branco (Tadeu and Branco 2000) studied the influence of temperature on bond between externally bonded steel plates and concrete by testing concrete specimens of (150×100×100 mm) with a gluing area of 100 mm long and 80 mm wide. The specimens were tested in double-lap shear at five selected temperatures (20, 30, 60, 90 and 120°C). Based on the tests, authors reported a reduction in bond strength with temperature (a 90% reduction at 120°C).

Blontrock et al. (2002) conducted double-lap shear test on CFRP strengthened concrete prisms 150×150×800 mm separated by a thin metal plate. The CFRP sheets were anchored at one end to ensure debonding to occur on opposite side where seven strain gauges recorded strain distribution. The specimens were subjected to direct tensile load at four temperature levels of 20, 40, 55 and 70°C. The tests conducted at 40°C and 50°C showed an increase of failure load by 41% and 24% respectively, however, the failure load decreased by about 19% (compared to maximum load at 20°C) at 70°C (close to T_g).

Klamer et al. (Klamer et al. 2005b) investigated the influence of temperature on debonding behavior of externally bonded CFRP through two different test setups namely: double-lap shear test and small scale three point bending test. For double-lap shear tests (150×250×800 mm), two CFRP laminates (50×1.2×650 mm) were bonded to two faces of concrete prisms, while for three point bending test one CFRP laminate (25×1.2×650 mm) was applied at the soffit of specimen.

Five strain gauges were used on the specimen to measure strains during tests which were performed at five temperatures (-10, 20, 50, 60 and 75°C). Results indicated an increase in failure load by about 10% for specimens tested at 50°C. A further increase in temperature to 75°C resulted in 27% decrease in failure load. This trend of slight increase in failure load before considerable decrease confirmed previously reported test results by Blontrock et al. (2002). However, similar trend was not observed in three point bending test. To investigate influence of temperature on FRP debonding mechanism, Klammer et al. (2008) also tested four full scale FRP-strengthened RC beams at 20, 50 and 70°C. Test results indicated that type of failure and the failure load at room temperature and at 50°C were similar, however, at 70°C failure loads reduced considerably. Therefore, the authors concluded that the contribution of FRP to strength capacity can be ignored when temperature at the FRP-concrete interface reaches T_g .

Leone et al. (2009) conducted double-lap shear tests to study the effect of service temperature (50, 65 and 80°C) on bond strength. The test specimens (150×150×800 mm) consisted of two concrete prisms each of 400 mm in length separated by thin metal plate. Unidirectional CFRP and GFRP hand layup sheets and CFRP laminates ($\pm 45^\circ$) were used to strengthen the specimens. For the test setup, the slip between FRP and concrete was computed from strain measurements on two sides of the prism through strain gauges. The experimental investigation showed a decrease in maximum bond stress for temperatures above T_g of the adhesive. At 80°C, the bond strength in CFRP, GFRP sheet and CFRP laminate was dropped by 54, 72 and 25% respectively. Data from these tests also indicated that magnitude of strain and required bond length increases with increasing temperatures.

Wu et al. (2004) studied the effect of temperature on bond behavior between FRP sheet and concrete. The specimens (100×100×450 mm) were tested at temperatures ranging from 26 to

60°C using ordinary and thermo-resisting epoxies. Based on tests results, the study concluded that close to T_g , debonding fracture energy (G_f) decreases, while requirement of length (L_e) increases to achieve effective bond. It was also observed that the failure load and elastic modulus decreases with temperature.

Gamage et al. (2006) investigated bond characteristics of CFRP plated concrete blocks (130×130×300 mm) at elevated temperatures. The authors conducted two series of shear tests; first series of eleven specimens without any insulation and second series of two specimens with 50 mm thick insulation. The test data showed that the bond strength is independent of bonded length of FRP when exposed to elevated temperatures. The un-insulated test specimens experienced loss of bond after 5-6 minutes into the fire exposure. This indicated that fire protection (insulation) is necessary to maintain effective bond between FRP and concrete at higher temperatures.

Camata et al. (2007) experimentally studied the bond behavior for temperatures ranging from 40 to 80°C using four different types of adhesives that had T_g higher than 85°C. Pultruded laminate and unidirectional woven fabrics were two types of CFRP used in the test. Results from test data and numerical analysis showed no degradation in the bond properties between CFRP and concrete interface up to T_g of adhesive.

Di Tomasso et al. (2001) conducted tests to ascertain the behavior of adhesively bonded CFRP-concrete joints at low and high temperatures. The prismatic concrete specimens (100×100×700 mm) were strengthened with 20 mm wide and 590 mm long CFRP. The adhesive thickness was varied between 1.4 mm and 1.24 mm with corresponding elastic modulus of 300 and 175 GPa, respectively. All specimens were tested to failure at four temperatures (-100, -30,

20, 40°C). The results indicated lower failure loads for specimens tested at 40°C due to softening of the adhesive.

Denton (2001) presented a closed form solution to determine interfacial shear stresses and normal stresses for a prismatic section due to thermal expansion while assuming elastic behavior. The author assumed stresses are purely due to thermal effect and no external loads are applied on the FRP-strengthened beam. The results indicated peak shear stress values near to the end of the FRP plate reducing non-linearly towards the mid-span of the beam. Numerical results also showed that for FRP plates, use of tapered end configuration significantly reduces the peak interfacial shear stress.

The above review clearly illustrates the effect of temperature on bond degradation in FRP-strengthened concrete specimens. Most of these studies were conducted on small scale test specimens. Test data on full scale FRP-strengthened members is limited. The state-of-the-art review also indicates that bond between FRP and concrete is a weakest link at higher temperatures, since concrete and steel properties do not degrade much up to 400°C. Therefore, accounting for deteriorating bond-slip at FRP-concrete interface is critical, to obtain reliable assessment of fire resistance of FRP-strengthened RC beams.

2.5.2 Numerical Studies

Numerical models are attractive tools for evaluating fire response of structural systems, since fire tests are quite expensive and often do not provide reliable data due to severe and unpredictable conditions encountered in fire. Finite element based models have been applied to predict the behavior of FRP-strengthened RC members. Such models are a good source to conduct parametric studies to study influence of various parameters on over all behavior of strengthened members.

Two notable numerical studies specific to FRP-RC members have been reported in the literature on thermal and structural response of FRP-strengthened RC beams. Williams (2004b) developed a 2-D heat transfer model that employs an explicit finite difference formulation and thermal equilibrium equations to determine temperature at each time step. The model is capable of predicting temperature distribution in FRP-strengthened rectangular and T-beam cross sections exposed to standard fire scenarios. The model was validated by comparing predictions with full-scale fire tests on FRP-strengthened T-beams conducted at the National Research Council, Canada. The model predictions for temperature distribution across the beam cross section (concrete and rebars) were reasonably good in comparison to the test data. However, the model under predicts temperature at the interface of FRP and insulation for entire duration of the test.

Hawileh et al (2009) used commercial software, ANSYS, to study the heat transfer and structural response of FRP-strengthened T-beam exposed to standard fire. The model was validated against data from fire tests conducted on the FRP-strengthened T-beams at National Research Council, Canada (Williams 2004b). The model predictions agree reasonably well with the measured temperatures and deflections. However, the model does not take into account several factors such as different high temperature strain components, fire induced bond-slip at FRP-concrete interface, and effect of axial restraint force in the analysis.

The above review illustrates that limited analytical studies were conducted to evaluate fire behavior of FRP-strengthened RC beams. These studies had number of limitations and drawbacks. Specifically, previous numerical studies did not account for important factors such as different fire scenario, different failure criterion, fire induced bond degradation at FRP-concrete interface and effect of axial restraint force.

2.6 Codes and Standards

The codes and standards have been developed since 1980's for FRP materials used in civil structures to control risk in matters of public safety. Without codes and standards, it is unlikely that FRP materials can be used beyond limited research and demonstration projects. These help to minimize the uncertainties in the performance and specifications of FRP materials. For fire design, codes and standards use a prescriptive approach; however, recently there is a shift towards performance-based design. The prescriptive codes are based on the tests conducted on structural assemblies under standard fire conditions with a well defined pass/fail criterion (Purser 2000). Current codes provide little or no opportunity to the designer to adopt a rational approach for provision of fire safety (Buchanan 2002). In performance-based codes, instead of limiting size, height and design, the required level of fire safety is achieved through a creative design.

Various design codes and guidelines currently exist for design of FRP reinforced concrete structures at ambient temperatures (ACI 2006; ACI 2008; CSA 2002; FIB 2001; ISIS 2001). The Canadian standard, CSA S806 (2002), is the first design code that addresses externally bonded FRP reinforcement for concrete. It specifies all possible failure modes (including in FRP) in addition to crushing of concrete. ISIS Design Manual 4 (2001) provides guidelines (including number of design examples) for externally bonded FRP. These guidelines mostly refer to the recommendations of ACI 440.2R-08. In Europe, Bulletin 14 (2001) provides state-of-the-art review and design guidelines for use of FRP in structures. The bulletin specifies the effects when composite action between FRP and concrete (debonding) is lost through a simplified bi-linear bond model. In United Kingdom, the Institute of Structural Engineers has guide on the design of RC structures with FRP reinforcement (ISE 1999). Prestressing and externally bonded

reinforcements are not addressed in this guide. The approaches adopted in this guide closely follow guidelines from Canada, Japan and United States (Bakis et al. 2002).

The above standards do not specify any fire guidelines and assume FRP to be ineffective (lost) in the event of fire. The design documents tend to limit the use of FRP systems for strengthening of concrete members since the information on the fire performance of FRP-reinforced or strengthened concrete is scarce. ACI 440.2R-08 requires that FRP-strengthened members should meet all building and fire code guidelines spelled out for RC structures. Further, ACI 440.2R-08 requires that the FRP-strengthened RC member must be capable of withstanding service loads (1.2 times the dead load and 0.85 times the live load) to prevent collapse that might arise from failure of FRP under fire exposure. In other words, the un-strengthened concrete member should be capable of resisting service dead and live loads under fire conditions.

An overview of current design guidelines in codes of practice indicate that no specific fire design provisions exist for externally bonded FRP structures due to lack of information on fire response of FRP-strengthened members. For structural members that require FRP strengthening, all documents adopt a common approach for fire safety by specifying adequate strength requirements to be met in order to resist loads under fire exposure. The reason for this approach is that in the event of fire, FRP is assumed to be completely ineffective. Therefore, there is a need to develop rational fire design guidelines for use of FRP strengthened RC members in buildings and structures.

2.7 Summary

Based on the information presented in this chapter, it is evident that limited data is available on performance of FRP under fire conditions. FRP loses its strength, stiffness and bond properties with temperature and this degrades the fire resistance of FRP-strengthened RC

members. Limited fire tests conducted did not address critical issues such as realistic loading, fire scenarios, effect of fire induced bond degradation and axial restraint force. Currently available numerical models, do not take into account the effect of fire induced bond degradation and axial restraint force on performance of FRP-RC structural members. There are no specific guidelines in codes and standards for fire design of FRP-strengthened RC beams. Therefore, for widespread application of FRP in civil engineering, there is an urgent need for analytical and experimental studies aimed at developing fire design guidelines.

CHAPTER 3

EXPERIMENTAL STUDIES

3.1 General

The state-of-the-art review indicates that there are very few fire experiments conducted on FRP-strengthened RC beams. Most of these experiments were carried out under standard fire conditions without any consideration for critical factors such as realistic fire exposure, load level, debonding of FRP, fire induced axial restraint force, and effect of anchorages, that influence the fire resistance of FRP-strengthened RC beams. To generate fire test data, FRP-strengthened RC beams were tested under realistic fire, loading and axial restraint conditions. One tested beam was a control RC beam while four other RC beams were strengthened with CFRP. The main purpose of these tests was to study thermal and structural response of FRP-strengthened RC beams under different parameters and to generate test data for validation of numerical models. Full details of the fire experiments, including specimen preparation, instrumentation, test procedures and measured response parameters, together with results are presented in this chapter.

3.2 Experimental Program

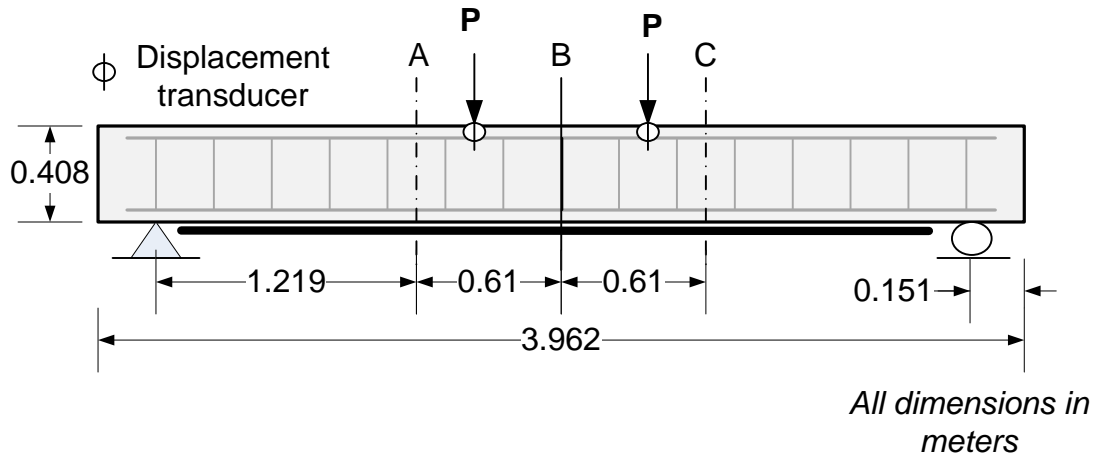
The test program consisted of design and fabrication of five RC beams and testing them under different fire scenarios, insulation system, anchorage configuration and support conditions. Four of the RC beams were strengthened with externally bonded CFRP that was applied at

tension face of the beams, while one beam was tested as control specimen (un-strengthened). The beams were strengthened in flexural without enhancing their shear capacity.

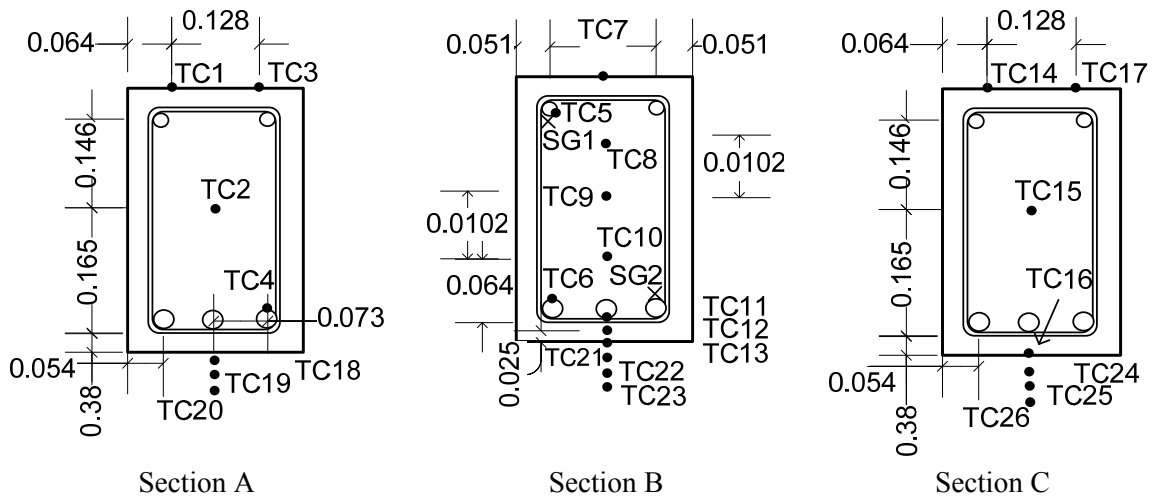
3.2.1 RC Beam Specimens

The specimens for fire resistance tests consisted of five rectangular RC beams (one RC beam, four CFRP strengthened). The beams were designed to be as close to typical building geometries as possible, in order to maximize the usefulness of the test results. The beams were of 254 mm width and 406 mm depth and had 3.96 m span length. The RC beams were designed as per ACI 318 (2008) specifications and were fabricated at the Civil Infrastructure Laboratory (MSU). The RC beams had three 19 mm dia. rebars as flexural reinforcement and two 13 mm rebars as compressive reinforcement. The stirrups used as shear reinforcement were of 6 mm dia. and were spaced at 150 mm over the length of the beam and bent at 135° into the concrete core. The steel used for the main reinforcing bars and stirrups had specified yield strengths of 420 MPa and 280 MPa, respectively. The elevation and cross sectional details of the beams are shown in Figure 3.1.

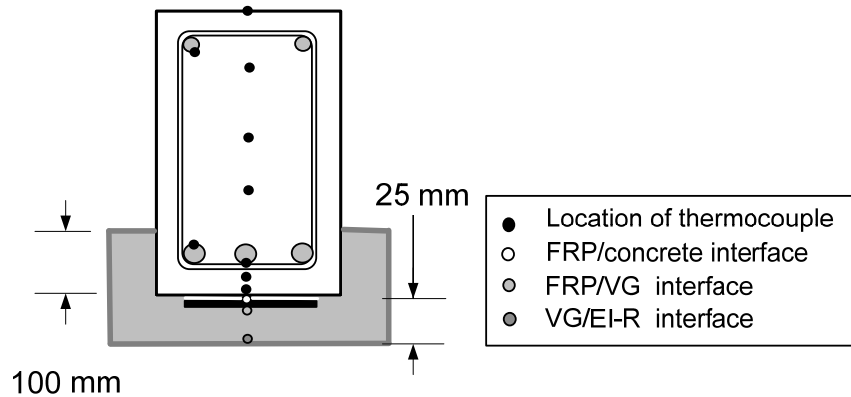
The reinforcement cages were assembled and placed in plywood form which was properly designed and fabricated to have the same internal dimensions as those of the tested beams, as shown in Figures 3.2 (a) and (b). The pre-mixed concrete, ordered from a local contractor to achieve good quality control, was poured from hopper chute (see Figure 3.2(c)). During pouring, concrete was vibrated and finished using concrete trowel to obtain smooth finishing surfaces, as shown in Figure 3.2(d). The concrete mix design (Normal Strength Concrete - NSC) was identical for all the beams with specified 28 days compressive strength of 42 MPa. Mix design details are as given in Table 3.1.



(a): Elevation



(b): Cross-sectional details and location of thermocouples and strain gauges



(c): Mid-span cross section showing location of thermocouples

Figure 3.1: Elevation and cross-sectional details of FRP-strengthened RC beams

Type I Portland cement and carbonate based coarse aggregate was used in concrete. The measured compressive strength of concrete at 28 days was 52 MPa, while on the day of test (at 2 years or later), it was 55 MPa.

The casted beams were sealed within the forms for the first 7 days, as shown in Figure 3.2(e). Thereafter, the beams were lifted out from the forms and stored in the laboratory, at about 25°C (40% relative humidity), for about 18 months before retrofitted with CFRP (refer to Figure 3.2(f)). The details of specimen and testing parameters are provided in Table 3.2.

Table 3.1: Concrete mix design proportions for beams

Ingredients	Quantity
Beams fabricated	B01, B1, B2, B3 and B4
Total cement (kg/m^3)	389.9
Water (kg/m^3)	156.4
Coarse aggregate (kg/m^3)	1036.9
Fine aggregate (kg/m^3)	830.1
Water reducing agent (kg/m^3)	1.9
Slump (mm)	100
Water/cement ratio	0.4
Air content %	1.7
Unit weight (kg/m^3)	2415

Table 3.2: Summary of test parameters and results

Beam designation	CFRP strengthening	Insulation type	Insulation thickness (mm)		Fire scenario	Support condition	Load (kN)	Failure time (min)
			VG	EI-R				
B01	-	-	-	-	ASTM E119	SS	50	180
B1	2 layers of 203 mm wide	Tyfo® WR AFP-Type A	25	0.1	Design fire	SS	70	NF*
B2		Tyfo® WR AFP-Type B	25	0.1	Design fire	SS	70	NF*
B3		Tyfo® WR AFP-Type A	25	0.1	ASTM E119	SS**	70	NF*
B4		Tyfo® WR AFP-Type A	25	0.1	ASTM E119	AR***	70	NF*

* NF – No failure ** Simply supported *** Axially restrained



(a) Reinforcement for the beam



(b) Beams prior to casting



(c) Casting of concrete



(d) Finishing the top surface



(e) Curing of beams



(f) Fabricated RC beams

Figure 3.2: Fabrication details of tested beams

3.2.2 FRP Strengthening

3.2.2.1 Design and Material

The flexural capacity of un-strengthened RC beams, which was 130 kN-m was enhanced by about 50% by flexural strengthening. The resulting moment capacity of FRP-strengthened RC beams was increased to 200 kN-m. To achieve this desired capacity of the beam, two layers of Tyfo[®] SCH-41 composite (203 mm wide) were installed at the beam soffit as per specifications prescribed in ACI 440-2R08 and also by the manufacturer. Tyfo[®] SCH-41 comprises of unidirectional carbon fabric with glass cross fibers to provide additional strength and fabric stability during installation. The carbon fibers are oriented in longitudinal (zero degree) direction. The properties of fibers and the laminate are tabulated in Table 3.3 and 3.4.

Table 3.3: Properties of fibers used for strengthening of test beams

Tensile Strength	3.79 GPa
Tensile Modulus	230 GPa
Ultimate Elongation	1.7%
Density	1740 kg/m ³

Table 3.4: Properties of composite laminate

Property	ASTM Method	Typical Test Value	Design Value
Ultimate tensile strength in primary fiber direction	D-3039	986 MPa	834 MPa
Elongation at break	D-3039	1.0%	0.85%
Tensile modulus	D-3039	95.8 GPa	82 GPa
Nominal laminate thickness	D-1777	1.0 mm	1.0 mm

3.2.2.2 Installation

The concrete surface of the casted beams was fairly smooth due to even surfaced form work. Hence, the concrete surface was roughened by sand blasting to partially expose the aggregate at beam soffit as shown in Figure 3.3. The roughened concrete surface was cleaned using compressed air and brush prior to application of FRP.



Figure 3.3: Concrete surface preparation by sand blasting

First, a thin coat of Tyfo[®] S Epoxy was applied with a roller on the prepared concrete surface as shown in Figure 3.4(a). The resin used to bond fibers was two-component epoxy material with a glass transition temperature (T_g) of 82°C. The mix ratio of the two components is 100 parts of component A to 42 parts of component B, by volume or 100 parts of component A, to 34.5 of component B by weight. Properties of epoxy are tabulated in Table 3.5.

Table 3.5: Properties of epoxy used in FRP strengthening

Property	ASTM Method	Typical Test Value
T_g	D-4065	82° C
Tensile Strength	D-638 Type 1	72.4 MPa
Tensile Modulus	D-638 Type 1	3.18 GPa
Elongation Percent	D-638 Type 1	5.0%
Flexural Strength	D-790	123.4 MPa
Flexural Modulus	D-790	3.12 GPa

Thereafter, a coat of cabosil was applied (in practice applied for overhead installation) to provide stronger adhesion to FRP fabric during installation. Then, two CFRP sheets of 2 mm thick and 203 mm width, saturated in Tyfo[®] S Epoxy were roller-applied at the beam soffit as

flexural strengthening. After placement, the sheets were rolled to remove air bubbles and also to ensure accurate placement, as shown in Figure 3.4(b). The same procedure was followed for applying second CFRP sheet. For beams B1 and B2, CFRP was applied on the entire unsupported length of the beam (3.66 m) terminating at a distance d from the supports. This configuration was adopted to study the influence of anchorages on fire response of FRP-strengthened RC beams. While for beams B3 and B4, central portion of the beam (2.44 m) which is exposed to fire (in the furnace) was retrofitted with CFRP to evaluate the effect of debonding on the response of FRP-RC beams. Unlike in previous tests, no shear strengthening was provided to study failure patterns of the beams under flexural strengthening alone.

3.2.3 Insulation of Beams

3.2.3.1 Insulation type

The fire protection system consisted of a layer of Tyfo[®] WR AFP system with a top coating of Tyfo[®] EI-R. This Tyfo[®] WR AFP system, which is an improved version as compared to previously developed Tyfo[®] AFP system, was spray-applied after the beams were cured for 72 hours. The Tyfo[®] WR AFP system comprises of vermiculite based insulation (VG insulation) and EI-R coating. It is available in two forms, Tyfo[®] WR AFP-Type A and Tyfo[®] WR AFP-Type B. The insulation is non-combustible and non-flammable lightweight material available in a powdered form. Beams B1, B3 and B4 were spray-applied with Tyfo[®] WR AFP-Type A, while Tyfo[®] WR AFP-Type B was used for beam B2. On top of insulation, spray-on EI-R coating was applied of equal thickness. This EI-R coating is a crack resistant surface coating

with excellent adhesion and fire resistance properties and provides additional stability to insulation.

3.2.3.2 Installation

This insulation application comprised of spraying a thin coat of VG primer on a cleaned surface, followed by a dash coat, on the FRP-strengthened beam soffit to enhance FRP/insulation bond (refer to Figure 3.4(c)). Thereafter, insulation material, which is available in powdered form, was mixed with appropriate amount of clear water and spray-applied on the beams using a hopper gun, as shown in Figure 3.4(d). The insulation is spray-applied within 5-6 hours of the dash coat. This was applied in lifts of approximately 8-10 mm thickness to accelerate the drying procedure before next lift is sprayed. Special attention was taken to maintain uniform thickness throughout the beam length. Insulation thickness was measured at several places along the beam length to ensure thickness within a tolerance ($\pm 6\text{ mm}$). The insulation layout comprised of 25 mm at the bottom surface of the beam extending 100 mm on the two sides (refer to Figure 3.1 (c)). The extension of insulation on two sides of the beam was to ensure low temperatures in flexural reinforcement. Insulation material applied is sufficiently low density material that adds negligible dead weight to the beam. This sprayed insulation was cured for 24 hours before final coat of EI-R was spray-applied (refer to Figures 3.4(e) and (f)). The complete insulated beams are shown in Figure 3.5.



(a) Application of epoxy and cabosil



(b) Application of CFRP layer



(c) Spray applying the dash coat



(d) Spray applying insulation in lifts



(e) Insulated beams



(f) Spray applying EIR coating

Figure 3.4: Flexural strengthening and spray-application of insulation on RC beams

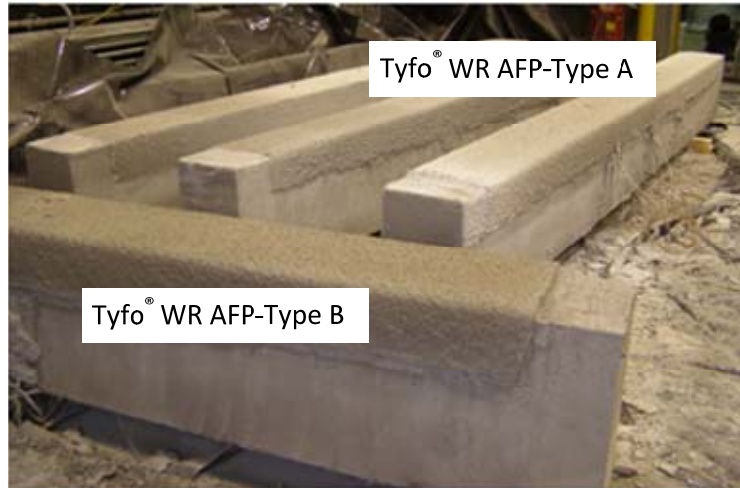


Figure 3.5: RC beams strengthened with CFRP and insulated

3.2.4 Instrumentation

The beams were instrumented to measure the temperature progression across the beam cross section, strains in rebars and deflections. To measure the temperatures, Type-K thermocouples were installed at various depths in concrete, reinforcement, and concrete-FRP and FRP-insulation interfaces at three different sections of the beam, as shown in Figure 3.1(a). A total of 26 thermocouples were installed for each beam. In addition, normal and high temperature strain gauges were placed to record strains in compression and tension rebars respectively, as shown in Figure 3.6. These strain gauges were bonded to flat finished surface of the reinforcing steel rebar and insulated to minimize temperature effects during data recording as well as waterproofing during casting of concrete. The locations and numbering of thermocouples and strain gauges are shown in Figure 3.1. In addition, three “Linear Variable Differential Transducers (LVDT’s)” were installed at unexposed surface (top) along centerline of beam cross section, one at mid-span and two under point loads to measure deflections.

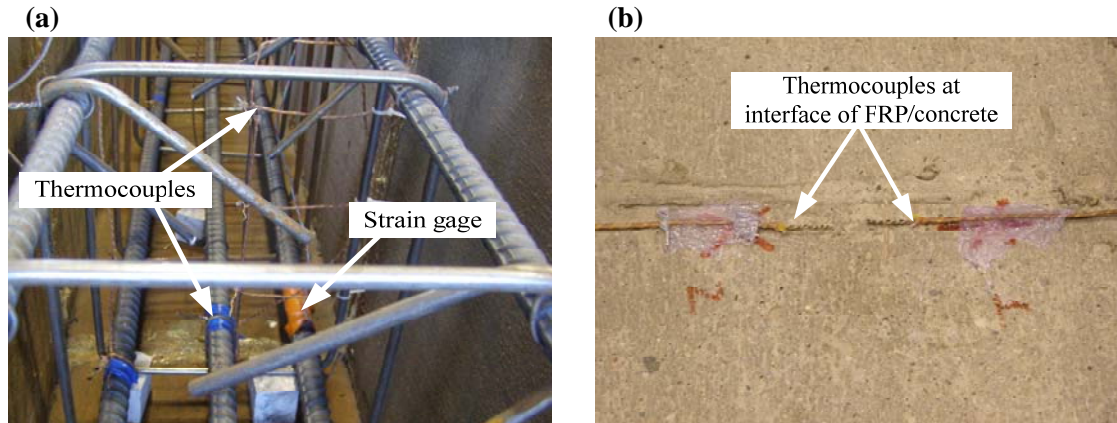


Figure 3.6: Thermocouples and strain gage placement in the beam

3.2.5 Test Apparatus

The fire resistance tests on FRP-strengthened RC beams were conducted at MSU's structural fire testing furnace. The test furnace is specially designed to produce conditions, such as temperature, structural loads and heat transfer, to which a member might be exposed during a fire. The furnace, shown in Figure 3.7, consists of a steel framework supported by four steel columns, with a fire chamber that is 2.44 m wide, 3.05 m long, and 1.68 m high. Six propane burners located within the furnace provide thermal energy, while six thermocouples, distributed throughout the test chamber, monitor the furnace temperature during a fire test. The furnace temperature can be maintained along a desired time-temperature curve as in a standard or design fire. Two small view ports on either side of the furnace wall facilitate visual monitoring of the fire-exposed test specimens during fire tests. The furnace accommodates two beams at a time and different load levels and restrained conditions can be simulated for each beam. One of the two beams can be tested under axial restraint support conditions, while the other beam has to be tested under simply supported end conditions. The axial restraint stiffness of the loading frame and the axial restraint system (axially restraining the beam) is found to be about 13 kN/mm. To minimize damage to the loading frame, the stiffness of the axial restraint system is set to adjust

(automatically) to zero (using relief valve) when the axial restraint force exceeds a value of about 120 kN. Loading is applied using hydraulic system which is driven by pneumatically driven hydraulic pump.

The hydraulic system has the capability to apply loading independently on each tested beam. The data from the test that includes temperatures, displacements, axial force and strains is collected using “Darwin Data DA100/DP120-13” data acquisition system. This data acquisition system can accommodate 70 thermocouple channels, 10 channels for displacement measuring devices (LVDT’s) and 10 channels for measurement of strain-gage channels. All these channels are connected to the data acquisition systems that stores the data in ‘.CSV’ file using “DAQ32” computer program.

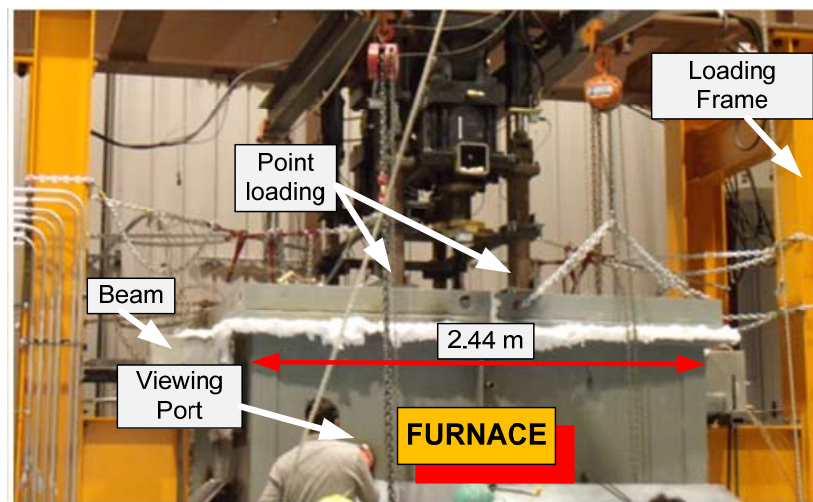


Figure 3.7: Structural fire test furnace and loading setup at MSU Civil and Infrastructure laboratory

3.2.6 Test Conditions and Procedure

During each fire experiment, two FRP-strengthened RC beams were tested simultaneously under loading and fire conditions. The beams were simply supported at the ends with an unsupported length of 3.66 m, of which 2.44 m was exposed to fire in the furnace. To investigate the effect of fire scenario on the fire response of RC beams, the beams were tested under

standard and design fire scenarios. Beams B1 and B2 were tested under design fire while beams B3 and B4 were exposed to ASTM E119 standard fire, as shown in Figure 3.8. The design fire comprised of a rising temperature (growth) phase followed by a cooling phase. In growth phase, the time-temperature curve as that of ASTM E119 standard fire was simulated for the first 180 minutes. Thereafter, a decay phase was introduced at a cooling rate of 10°C/minute. Beam B4 was tested under axially restrained support condition. The axial restraint does not translate into moment fixity at the supports. It has been shown in previous studies that fire endurance of RC beams with axial restraint is higher as compared to similar unrestrained simply supported beams.

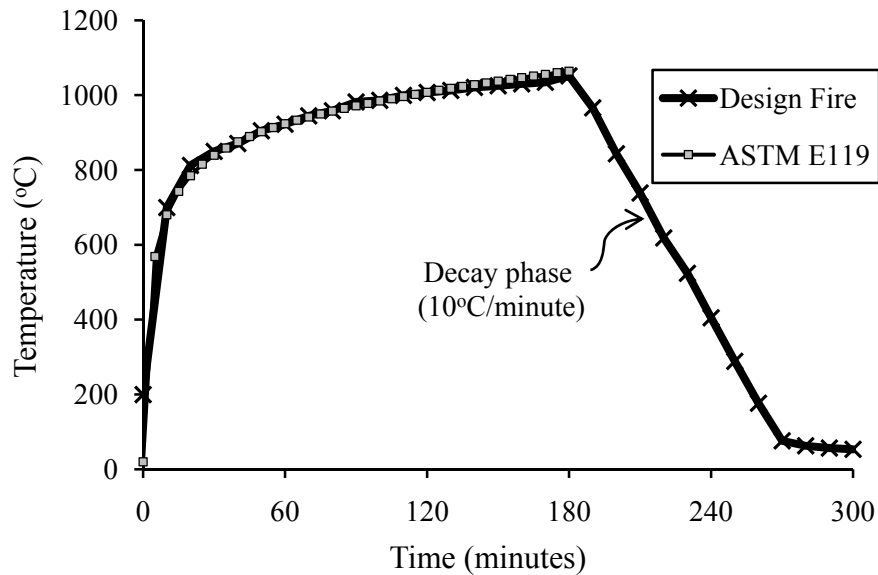


Figure 3.8: Fire time-temperature curves used in fire experiments

3.2.7 Loading

The beams were subjected to two point loads, each of 70 kN, which represents 50% of the strengthened beam nominal capacity at room temperature. The flexural capacity of the strengthened beam was determined according to ACI 440.2R-08 that requires stress in tension steel at service load levels must be less than 80% of f_y to avoid inelastic deformations. Therefore, the moment resistance was computed with this limiting strain to obtain the

superimposed loading. Details of calculations are provided in Appendix B. The point loads were applied at a distance of 1.4 m from the end supports as shown in Figure 3.1(a). The loading was applied approximately 30 minutes before the start of the test until steady condition (no increase in deflection with time) was reached. This was selected as the initial condition for the deflection of the beam.

During the tests, temperatures at various locations of the beam cross section, strains and deflections were recorded at 5-second intervals. Also, visual observations were made through view ports in the furnace to record progression of cracks in the insulation, localized burning of FRP, and delamination of insulation and FRP.

3.2.8 Material Testing

3.2.8.1 Compressive strength of concrete

The concrete cylinders from the batch mix were tested at 7, 28 days and on the day of fire testing of the beams using Forney Compression Testing Machine (refer to Figure 3.9). Split tensile test were also conducted on the cylinders to obtain tensile strength of concrete at 28 days. Average compressive and tensile strength of concrete as determined from cylinder tests, is tabulated in Table 3.6. The design mix compressive strength of the mix was 42 MPa.

Table 3.6: Compressive strength of concrete

Concrete batch	Design compressive strength (MPa)	28-day compressive strength (MPa)	28-day tensile strength (MPa)	Test day compressive strength (MPa)
1	42	52.2 ± 0.6	3.7 ± 0.5	54.8 ± 3.0



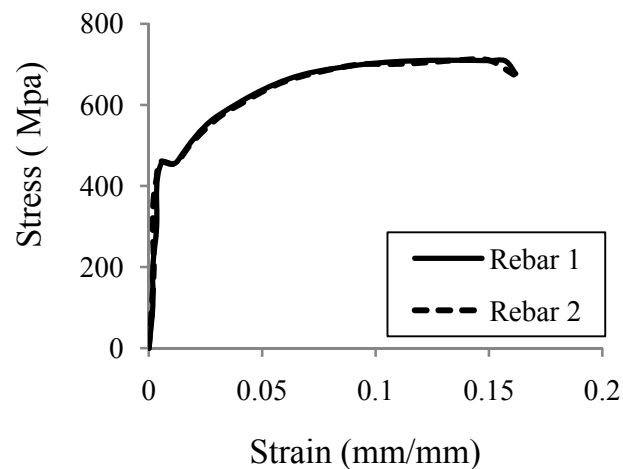
Figure 3.9: Testing compressive strength of concrete after 28 days and on the day of fire test

3.2.8.2 Steel

Tensile tests on reinforcing bars (diameter of 19 mm) used as flexural reinforcement, were performed using 810 Material Testing System (MTS) universal testing machine (refer to Figure 3.10(a)). This MTS machine is provided with hydraulic grips and has the loading capacity (both in tension and compression) up to 245 kN. Yield strength, ultimate strength and failure strain obtained from the test were 450 MPa, 705 MPa and 17%, respectively. The stress-strain curve obtained for the rebars is shown in Figure 3.10(b).



(a) Test setup



(b) Stress-strain curve

Figure 3.10: Testing of reinforcing steel and stress-strain curves

3.2.8.3 Insulation

In current experiments, a newly developed insulation Tyfo® WR AFP system was used as fire protection system. Data on high temperature (HT) thermal properties was not available from the manufacturer. Therefore, HT thermal properties up to 800°C were ascertained and later incorporated in the numerical model (discussed in Chapter 4). The thermal properties were measured using commercially available “Hot Disk TPS 2500S” thermal constant analyzer. Thermal conductivity and specific heat of insulation were measured at thirteen temperature points namely 20, 100, 200, 300, 400, 450, 500, 550, 600, 650, 700, 750, and 800°C. The insulation specimens are exposed to high temperature in a furnace connected to Hot Disk apparatus (see Figure 3.11(a)). The target temperature, sensor resistance and time of measurement are controlled by programmed test set up. In each test the furnace temperature is raised to the target exposure temperature and maintained at that level till the entire test specimen reaches equilibrium conditions (target temperature). At this stage the thermal conductivity and specific heat are recorded by the data acquisition system. Then the temperature in the furnace is increased to next target temperature and this procedure is continued till 800°C. The HT thermal properties (normalized thermal conductivity and thermal capacity) are plotted in Figure 3.11.

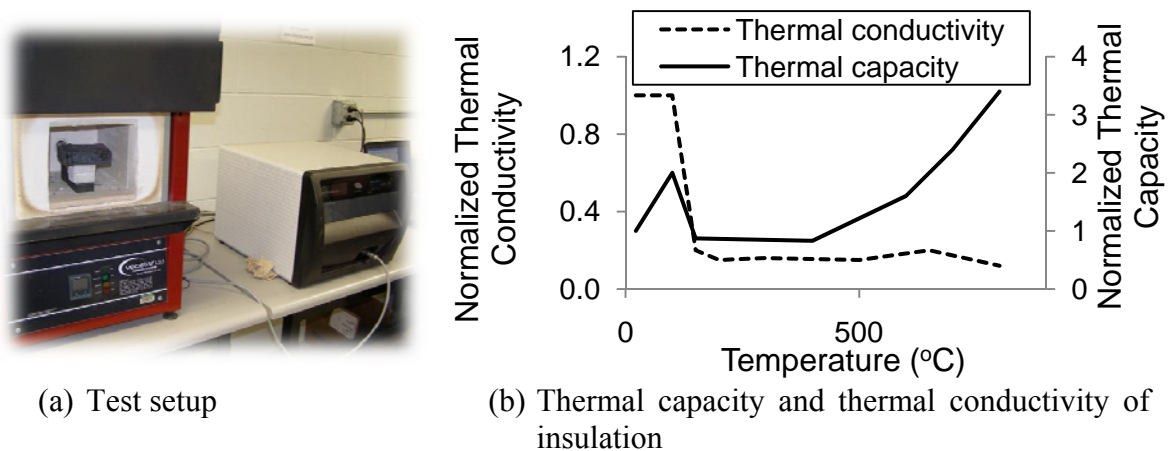


Figure 3.11: Test setup and high temperature thermal properties of Tyfo® WR AFP system

3.2.8.4 Glass transition temperature of FRP composite

A test was conducted using Thermomechanical Analysis (TMA) apparatus to reconfirm the glass transition temperature (T_g) of Tyfo[®] SCH-41 (unidirectional carbon/epoxy composite) specimen used for strengthening of RC beams. The supplier of FRP has reported a T_g value of 82°C based on ASTM D-4065 standard test (DMA).

The glass transition temperature of the specimen was obtained in accordance with the standard test method ASTM E1545-05 (1993)(standard test method for assignment of the glass transition temperature by thermomechanical analysis). With the TMA technique, a number of different probe configurations are offered in order to optimize the test conditions for a specific sample and/or application. These probes include expansion, penetration, compression, flexure, extension and dilatometry. For this experiment, penetration probe was used to ascertain the softening temperature of the material commonly referred to as T_g rather than T_g . The test procedure was repeated for different heating rates (2°C/minute and 10°C/minute) to see the effect on test results. The test results are shown in Figure 3.12.

The increase in deflection at T_g is proportional to the applied force on the probe and the heating rate significantly affected the detection of T_g of the sample. The reduced heating rate increases the measured deflection at T_g , decreases the signal to noise ratio and the transition temperature is shifted downward. This is illustrated in Figure 3.12 where a faster heating rate (10°C/minute) gives a higher value of T_g and the average penetration of the probe drops.

Discussion

The results show a decrease of T_g by about 25% ($T_g = 64^\circ C$) compared to the reported value by the manufacturer ($T_g = 82^\circ C$) which is based on the test performed using DMA. The glass transition temperature determined by DMA is not only heat rate dependant but also depend on the frequency. The manufacturer has not provided any reference for the reported T_g that whether it is based on the damping ratio ($\tan \delta$), or the maximum of E'' or on the onset of E' curve. The T_g based on damping ratio is always higher compared to the TMA results. Secondly, the varying exposure of the material (epoxy) to the atmospheric conditions (air) decreases the glass transition temperature. This is attributed to the moisture present in the air since water content is known to affect T_g (Ferrillo and Achorn 1997). The reduction in T_g of the samples tested can be attributed to the storage of the sample under uncontrolled environments. These effects are not reversible; therefore, the original T_g cannot be restored as reported by the manufacturer.

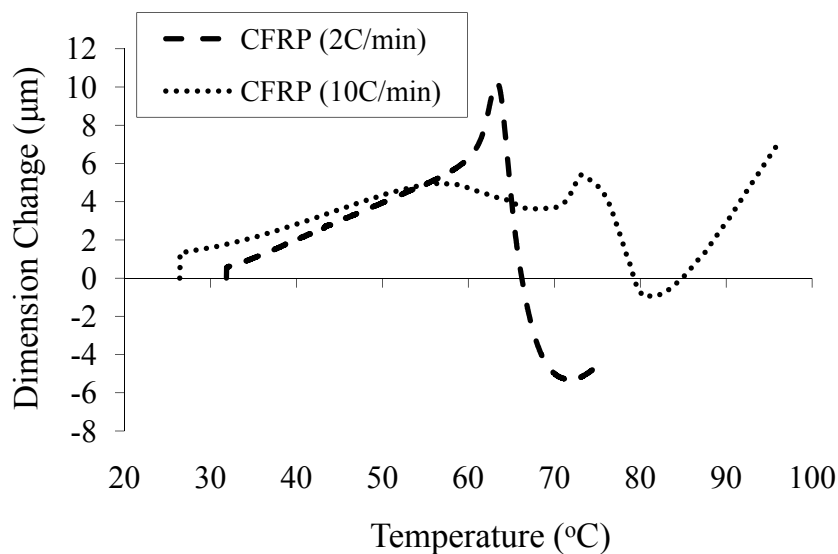


Figure 3.12: Variation of T_g as a function of heating rate

3.3 Results and Discussion

Data generated from above fire tests was used to study thermal and structural response of FRP-strengthened RC beams exposed to fire. The test conditions represented a typical compartment fire in a building. For beams B1 and B2, terminating ends of CFRP near supports (outside fire zones) acted as anchorages. For the other two beams (B3 and B4), central portion of the beam soffit exposed inside furnace was only retrofitted to study the effect of debonding on overall fire performance of FRP-strengthened RC beams. The results from these experiments have also been compared with test results of RC beam (control beam B01) which was tested under ASTM E119 standard fire with applied load ratio of 50% (50 kN).

3.3.1 Test Observations

During the fire tests, visual observations of the specimens were recorded from two viewing ports provided in each opposite side of the furnace wall. These observations were taken for entire duration of the test and backed up by photographs and video recordings at critical moments. Table 3.7 and 3.8 outline the timelines, observation and photograph of each tested beam. Major observation in the test relates to cracking of insulation, burning of epoxy, and delamination of FRP. The performance of EI-R coating was satisfactory during the test with no signs of burning. The VG insulation (Type-A and B) performed very well under fire exposure, and remained intact until test ended except for beam B3, where a part of insulation fell when FRP delaminated. In both types of insulation, cracks appeared in the insulation and widened as the test progressed. It was noticed that cracks formation in Type B insulation was in earlier time as compared to Type A. The crack pattern was parallel to the longitudinal axis of the beam at beam soffit, while cracks extended vertical in insulation applied on the two sides of beam (refer to Figures 3.13 and 3.14). These formation of cracks resulted in localized burning of epoxy in the start and later complete beam soffit got engulfed in fire.

Table 3.7: Visual Observations for Beams B1 and B2 during Fire Resistance Test


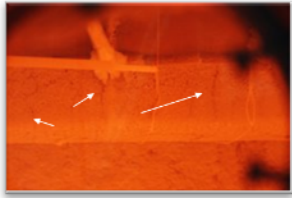
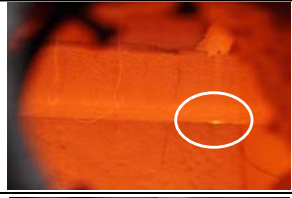

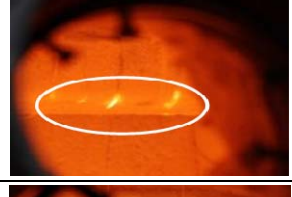
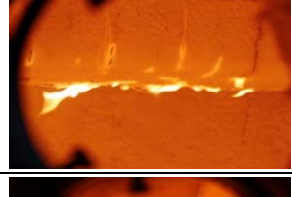
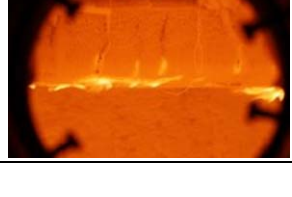

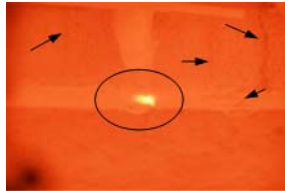
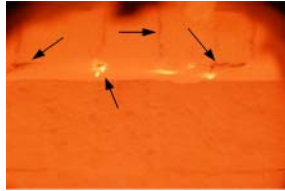
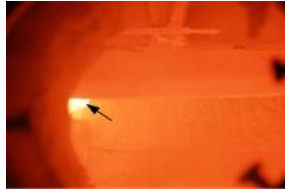

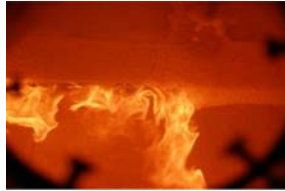

Time (minutes)	Observation	State of the specimen
0	Test started at 2:00 pm	
25-30	Cracks appeared in Tyfo [®] WR AFP-Type B insulation (beam B2)	
32	Localized burning of epoxy in beam B2 spray-applied with Tyfo [®] WR AFP-Type B	
40-45	Cracks wide opened in Tyfo [®] WR AFP-Type B insulation with flaming. Cracks started to appear in Tyfo [®] WR AFP-Type A insulation (beam B1)	
60	Burning of epoxy in Tyfo [®] WR AFP-Type A insulation (B1)	
90	Complete beam soffit of beam B2 engulfed in flames	
200	Burning at beam soffit starting to reduced as result of decay phase in time-temperature curve.	

Table 3.8: Visual Observations for Beams B3 and B4 during Fire Resistance Test

Time (minutes)	Observation	State of the specimen
0	Test started at 3:00pm	
25-30	Visible cracks in insulation (Tyfo [®] WR AFP-Type A) for beam B4.	
38	Localized burning of epoxy in beam B4	
	Flames appeared from one edge of the beam (B3) possibly due to epoxy burning as a result of wide open edge crack in insulation.	
45-48	For beam B4, cracks appeared wide open with visible flame due to burning of epoxy.	
60	Insulation from a portion of beam B3 fell off	
90-120	Wide open cracks in insulation (both the beams) with complete beam soffit engulfed in flames	

In all the beams tests, it was observed that fire performance of Tyfo[®] WR AFP-Type A insulation was better than Tyfo[®] WR AFP-Type B insulation. This observation is based on the appearance and progression of cracks for the duration of the test. In Type-B insulation (spray-applied on beam B2), cracks gradually appeared around 25-30 minutes. Thereafter, widening of cracks progressed rapidly that resulted in burning of complete beam soffit around 60 minutes, as shown in Figure 3.13. The cracks did not appear until 40-45 minutes of fire exposure time in Type-A insulation, therefore, the process involving burning of FRP matrix (epoxy) was delayed considerably. During fire test on beam B3, a portion of insulation fell when FRP delaminated from on edge of the beam at about 30-35 minutes, as shown in Figure 3.15. However, at this stage no cracks could be observed in part of the insulation that remained intact till test terminated. Thus, debonding of FRP may expose part or complete beam soffit to heat flux.

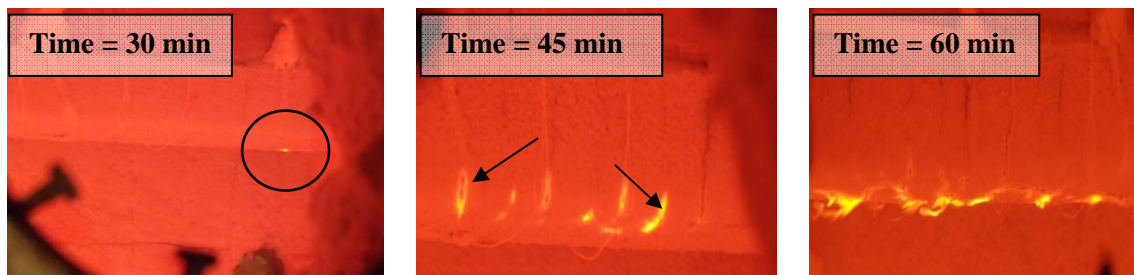


Figure 3.13: Crack development in insulation of FRP-strengthened beam

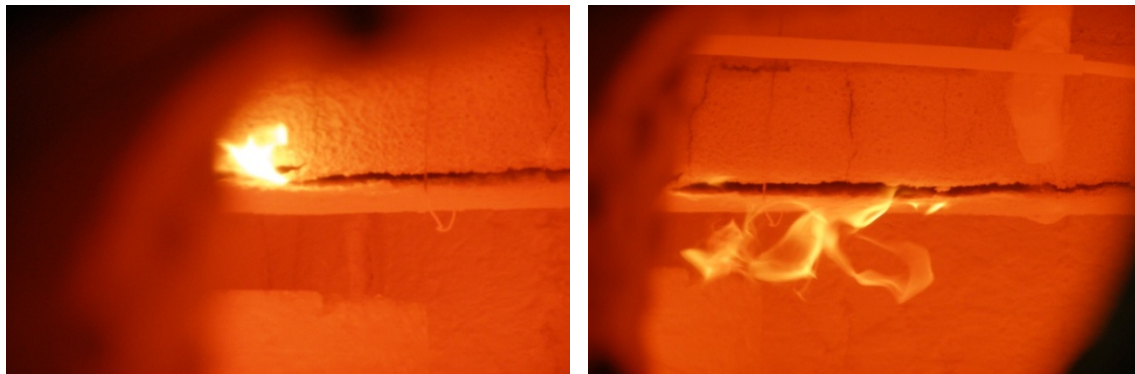


Figure 3.14: Formation and widening of cracks in insulation

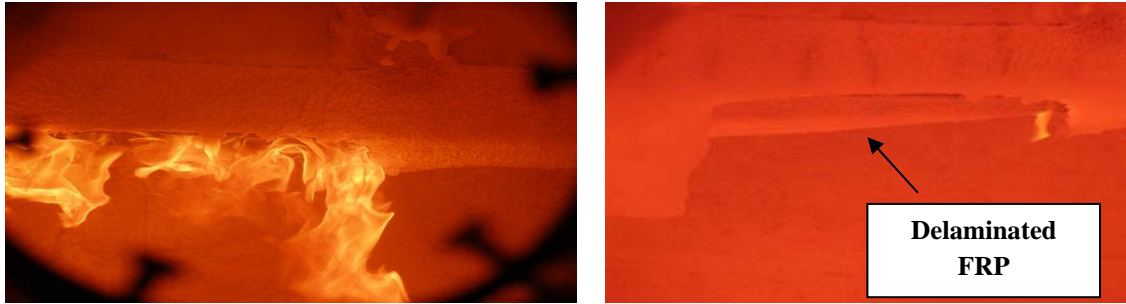


Figure 3.15: A portion of beam B3 exposed to fire after delamination of FRP and insulation

3.3.2 Thermal Response

3.3.2.1 General

Temperatures were monitored through data acquisition system at various locations in beam cross section including at interface of FRP/concrete and FRP/insulation for the duration of fire tests. This section presents and discusses in detail the recorded temperatures at section B and trends that can influence the overall behavior of FRP-strengthened RC beams. Analysis of the data showed similar temperature trends for Section A and C.

Figure 3.17 to 3.22 summarizes temperatures measured in beam B1 through B4 at various locations in the beam cross section. The figures shows average recorded temperatures in insulation and FRP (Figure 3.18), at various concrete depths (Figure 3.21), and in steel reinforcement (Figure 3.22). It can be noticed that temperatures at various levels of beams cross section including in rebar and concrete increases throughout the test duration for beams exposed to standard fire (beams B3 and B4). However, for beams B1 and B2 which were exposed to design fire, the measured temperatures increases to a maximum value and then starts to decrease. This decrease in temperatures can be attributed to the decay (cooling) phase in time-temperature curve of the design fire.

3.3.2.2 Furnace Temperatures

Figure 3.16 compares the measured average furnace temperatures with that of standard ASTM E119 fire curve (2007). Beams B1 and B2 were tested under design fire exposure. In design fire, for first 180 minutes the time-temperature fire curve followed standard fire and thereafter, a decay phase at a rate of $10^{\circ}\text{C}/\text{minute}$ was introduced that depicted an absence of fuel load in the compartment. Beams B3 and B4 were exposed to standard fire for 180 minutes. It can be seen that furnace temperatures were well controlled by the burner control system (operated manually) and this enabled to accurately reproduce furnace temperatures compared to the standard fire time-temperature curve (refer to Figure 3.16).

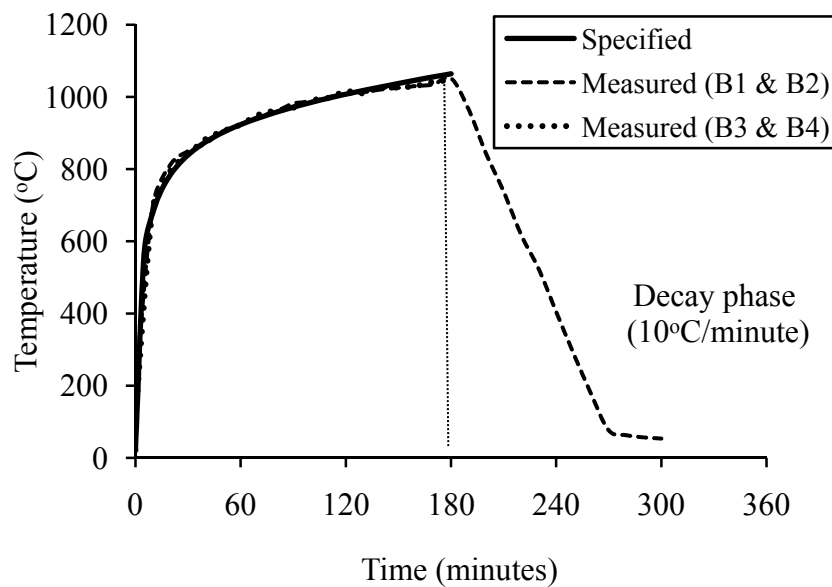


Figure 3.16: Time-temperature curve and average furnace temperatures for beam tests

3.3.2.3 EI-R/Insulation Interface Temperatures

EI-R coating was sprayed-applied as a final surface coat (0.12-0.14 mm thickness) on the insulation. It provides a crack resistant surface and additional stability to insulation when exposed to fire. The temperature measured at interface of EI-R/insulation is shown in Figure 3.17. It can be seen that the trend of measured temperatures at the interface closely follow the average furnace temperatures with a maximum difference of 195°C and less. In fact, the

measured temperatures at this interface should closely follow the average furnace temperature since these thermocouples are located almost at the exposed surface of insulation (EI-R coating is 0.13mm). The possible reasons for lower temperatures recorded in these thermocouples might be due either accumulation of spray applied insulation around these pre-installed thermocouples or due to unintentional embedment of the thermocouples by few millimeters inside the insulation. Never the less, overall measured trends follow the average furnace temperatures.

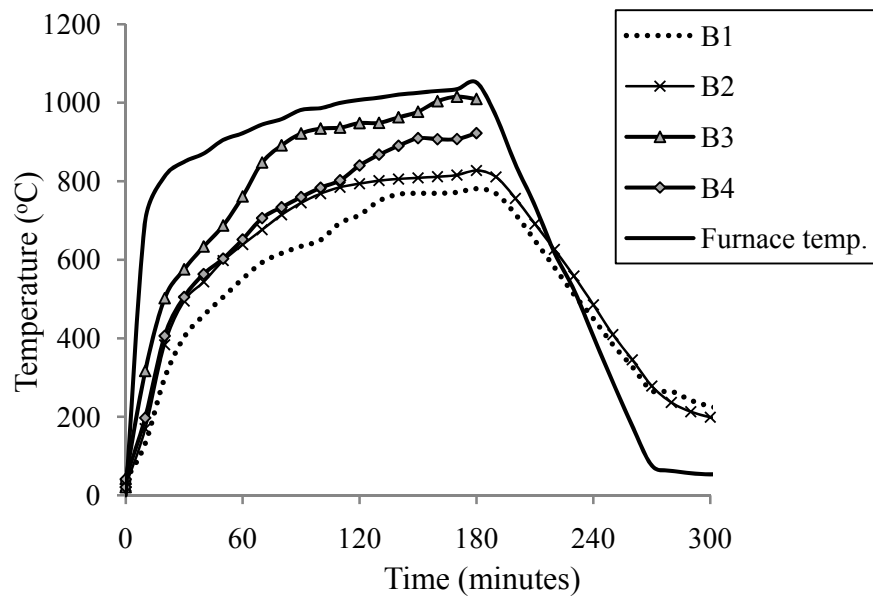


Figure 3.17: Exterior layer temperatures in FRP-strengthened RC beams

3.3.2.4 FRP/Insulation Interface Temperatures

For the duration of the test, VG-EI-R insulation remained intact and provided effective insulation to FRP and concrete substrate. Examining Figure 3.18, it can be seen that the temperature increase recorded in the first 20 minutes is gradual, and this is followed by a temperature plateau around 100°C. This temperature plateau is due to evaporation of free and chemically bonded water in the insulation that consumes significant amount of energy. The insulation, which is spray-applied in the form of slurry, contains free moisture. Most of the free

water in the insulation close to exposed surface, dries-out at room temperature, however, remaining free and chemically bonded water consumed significant energy from fire to evaporate.

Data analysis of the four tested beams showed that all thermocouples located at insulation/FRP interface did not experience temperature plateau for same length of time. Figure 3.19 shows that the time to reach 100°C was almost similar for all the beams. However, temperature plateau lasted for about 20-30 minutes for beams B1 and B4, while the duration of the plateau for beams B2 and B3 was short. This aspect is directly related to crack formation in the insulation. In beam B2, insulated with Type-B insulation, cracks appeared earlier and widening of cracks progressed rapidly that lead to quick evaporation of water with short plateau length. It also depends on the crack size and pattern, and thermocouple location that can result in such variation. The lower thermal conductivity of insulation and higher energy required for evaporation of free as well as chemically bonded water are main contributing factors in maintaining low temperatures in FRP. After crossing temperature plateau, rapid increase in measured temperatures is due to localized burning of matrix (epoxy).

3.3.2.5 FRP/Concrete Interface Temperatures

The temperatures attained at FRP/concrete interface, is an important indicator to assess the fire performance of FRP in situ. Figure 3.18 shows that temperature increase at FRP/concrete interface is similar for all the beams except for beam B3, where FRP debonded from one edge which caused rapid increase in temperatures due to direct exposure of thermocouple to heat flux. As discussed in Section 3.3.2.3, localized burning of epoxy (matrix) resulted in rapid increase in temperature at FRP/insulation interface. A small drop in temperature was expected across a thin layer (2 mm thickness) of CFRP laminate. However, measured test data shows a temperature lag (refer to Figure 3.18). This temperature lag can be attributed to the formation protective char

layer as a result of pyrolysis process in FRP (refer Figure 3.20). This char layer acts as a thermal barrier and insulates the interior interface between FRP and concrete. Thus, the measured temperatures are lower than recorded at FRP/insulation interface.

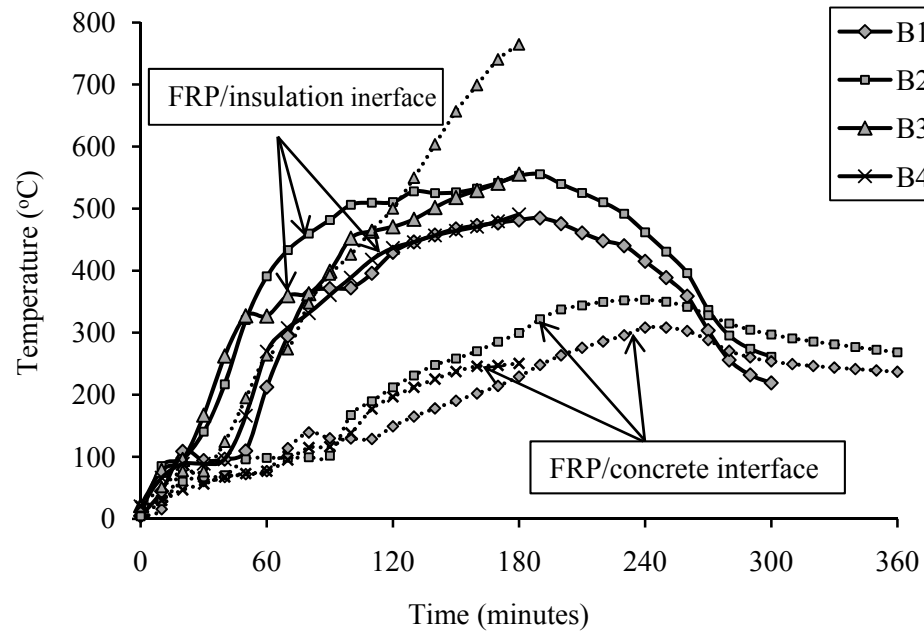


Figure 3.18: Measured temperatures at FRP/insulation and FRP/concrete interface

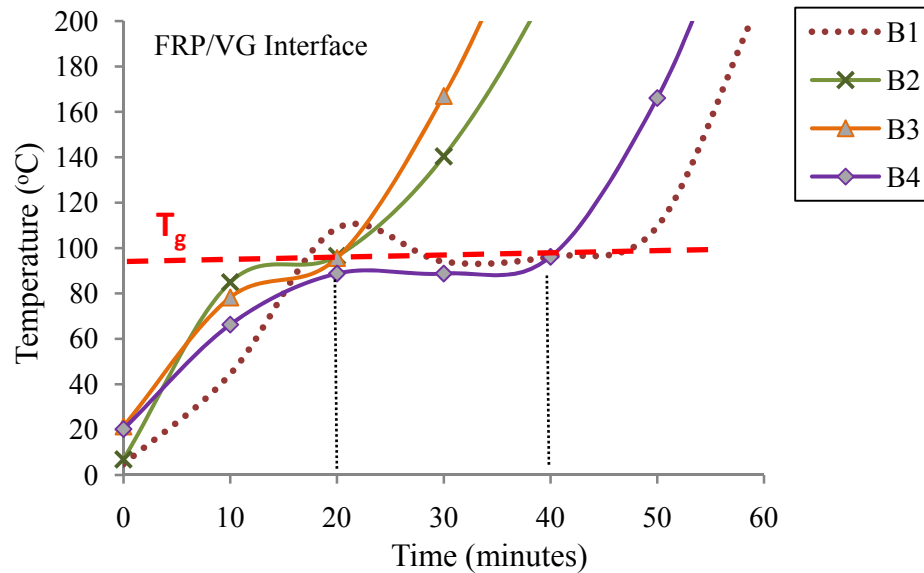


Figure 3.19: Formation of temperature plateau at 100°C

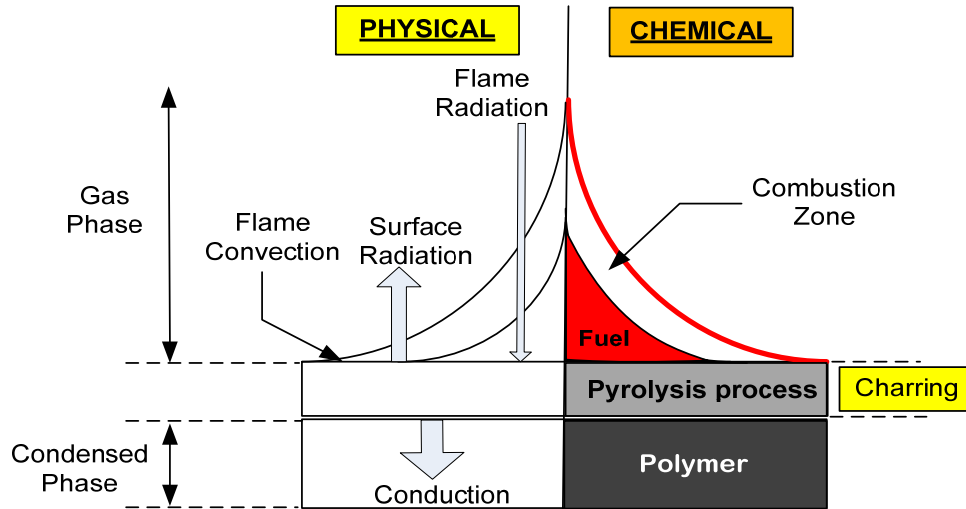


Figure 3.20: Physical and chemical process during combustion of polymer

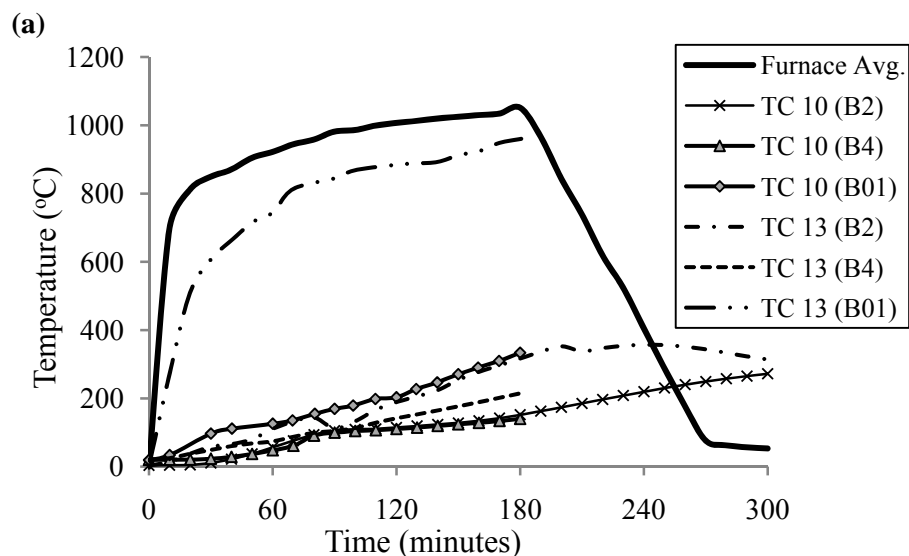
3.3.2.6 Concrete Temperatures

Figure 3.21 shows temperatures within concrete at depths of 203 mm (TC9 at mid-depth of the beam cross section), 300 mm (TC10), and 406 mm (TC13) for FRP-RC beams B2 and B4, and RC beam B01 (control RC beam with no fire proofing). Beam B2 was insulated with Tyfo[®] AFP-Type B insulation while beam B2 was spray-applied with Tyfo[®] AFP-Type A insulation. As expected, Figure 3.21 (a) shows that the temperatures in concrete close to beam soffit remain very low for beams B2 and B4 due to effective protection provided by the insulation as compared to control beam. The measured temperature close to beam soffit (thermocouple TC13) for control beam shows that the temperature increases very rapidly and closely follows average furnace temperatures for entire duration of the test. This is mainly due to absence of any fire protection system.

A close examination of Figure 3.21(a) shows that for the same depth inside concrete (TC10 embedded 106 mm from beam soffit), the difference in measured temperatures is about 120°C after 180 minutes for FRP-strengthened RC beams (B2 and B4) and control beam. This can be

attributed to the beneficial effect of the insulation that helps to limit increase in temperature. After 120 minutes, thermocouple TC13 in beam B2 embedded inside concrete very close to bottom surface, experiences slightly higher temperatures as compared to beam B4. This can be explained based on the visual observations taken during the test where crack formation and widening in the insulation (Tyfo[®] AFP-Type B) started early (at about 25 minutes) followed by the burning of epoxy. Figure 3.21(b) shows there is not much variation in measured temperatures at mid-depth of concrete (TC9) for the three beams. This can be attributed to low thermal conductivity and high thermal capacity of concrete that limit heat flow rate inside concrete.

Analysis of the temperature data indicates that average concrete temperatures in insulated FRP-strengthened RC beams remained below 500°C for the duration of test. Therefore, strength and stiffness of concrete remained unaffected. Temperatures close to exposed surface (TC13) increased to a maximum value and then decreased under design fire exposure. This can be attributed to cooling phase in time-temperature curve. However, this effect is not pronounced for thermocouple TC10 which is located at a farther distance from exposed surface due to time lag in cooling of inner concrete.



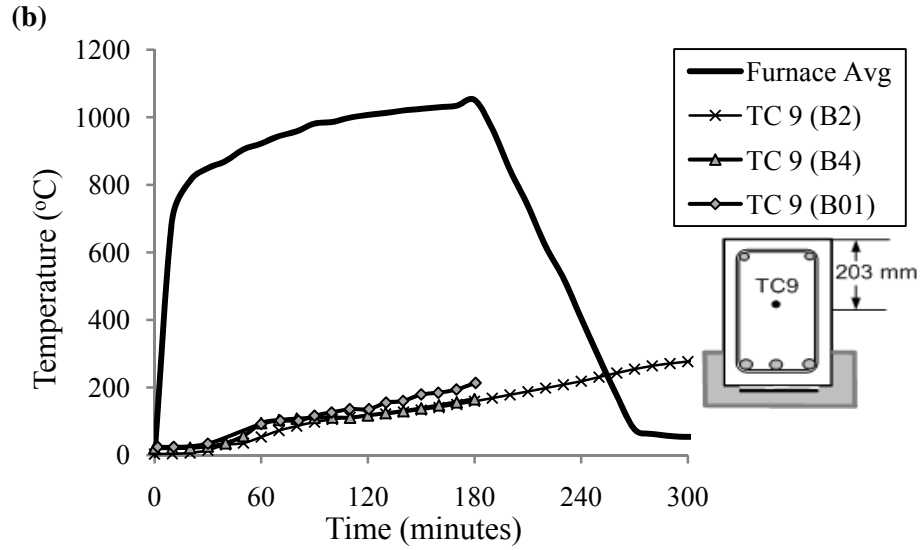


Figure 3.21: Measured concrete temperatures (TC 9, TC 10 and TC 13) for beams B2, B4 and control beam B01

3.3.2.7 Rebar Temperatures

Fire resistance of FRP-strengthened flexural members is mainly influenced by strength and stiffness properties of FRP and steel reinforcement and these properties degrade with temperature. The rate of degradation of strength and stiffness properties of FRP is faster than concrete and reinforcing steel due to low tolerance of the polymer matrix to high temperature. Therefore, FRP contributions to flexural capacity of the beam decreases and rebar temperature becomes an important indicator on the capacity of FRP-RC beams, after early stages of fire exposure. Figure 3.22 shows time-temperature curve for corner rebars (in both compression and flexural reinforcement). Temperature increase in compression reinforcement is higher than that of bottom corner rebar due to presence of insulation in the bottom soffit region. The measured temperatures in compression reinforcement (TC5) for beams (B1, B2 and B4) match closely through entire duration of the fire test. For bottom corner rebar (TC6), temperatures for beams B2 and B4 closely match with slight variation after 120 minutes of fire exposure time. The

possible reason for this variation could be opening of cracks in the insulation and burning of FRP at beam soffit, as explained earlier. In control beam (B01), temperature increase in rebar was very rapid in the absence of supplemental insulation. In this beam, temperature in corner rebar almost reached critical temperature of 593°C by the end of the test (180 minutes). This clearly indicates that insulation significantly contributes in limiting temperature increase in the beam cross section. For entire duration of test, the average rebar temperature measured in FRP-strengthened RC beams was less than 400°C . Since rebar does not lose significant strength up to 400°C , therefore, steel reinforcement maintained full strength capacity for the full test duration.

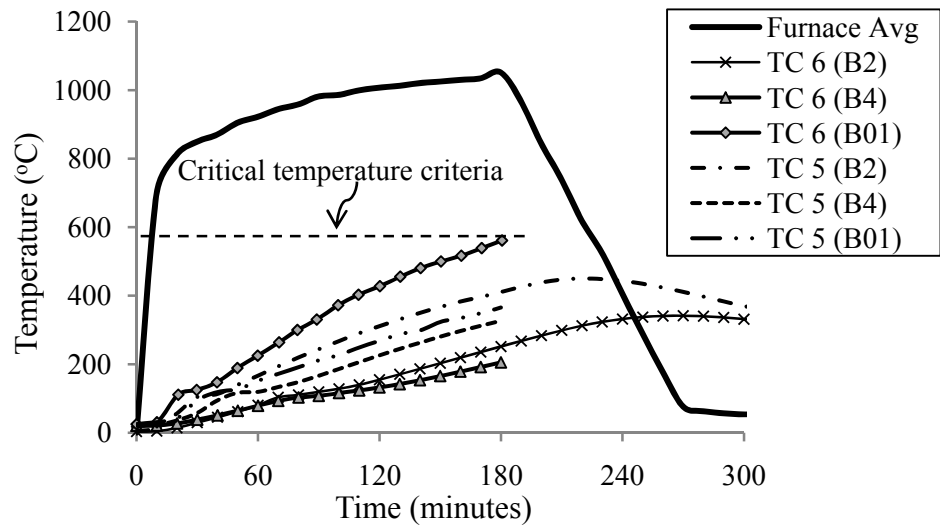


Figure 3.22: Comparison of reinforcing steel temperatures

3.3.3 Structural Response

3.3.3.1 Deflection of Beams

The structural response of the beams can be gauged through deflection progression with fire exposure time. The deflection in each was measured at the mid-span and under two point loads. Figure 3.23 shows variation of mid-span deflection as function of time for the four tested FRP-RC beams and control RC beam (B01). FRP-RC beams (B1 to B4) were applied with two point loads of 70 kN each, while RC beam had a loading of 50 kN. This load represents 50% of the

ultimate capacity of each beam calculated as per ACI 318 (RC beam) and ACI 440.2R-08 provisions (FRP-RC beam). In this section, the structural response (deflection) of FRP-strengthened beams will be discussed first and then deflection response of FRP-RC beams will be compared with that of control RC beam.

A review of the test data indicates that the deflection in all the beams increased steadily until around 20 minutes, at which point beams (B1 to B4) experienced a sudden drop in deflection. This drop is mainly due to the loss of composite action between FRP and concrete substrate (bond). The bond strength properties are highly dependent on the temperature at FRP/concrete interface. At room temperature (start of the test), a perfect bond exists between FRP and concrete. In first 10 minutes of the test, the deflection in the beams is quite small since temperature at FRP/concrete interface does not change much due to insulation. Thereafter, as the temperature at the interface starts to rise, the beam experiences gradual increase in deflections. This gradual increase in deflections (between 10 and 20 minutes) can be attributed to decrease in shear modulus of adhesive (epoxy) with increasing temperature that introduces bond-slip at FRP/concrete interface. Due to this bond-slip, adhesive loses its ability to effectively transfer forces between concrete and FRP and this result in FRP developing only partial tensile stresses as compared to a perfect bond case where full stresses in FRP can effectively be utilized. With increasing slip, the bond deteriorates considerably and ultimately leads to debonding of FRP. After debonding, the structural response of beams B1, B2 and B4 is different as compared to beam B3.

After FRP debonded, the rate of increase in deflection for beam B3 is rapid as compared to measured deflections for beams B1, B2 and B4. This increase in deflections can be explained by first looking into structural response of beam B3 itself and then through a comparison with

other three beams. Similar to other three beams, beam B3 was also loaded with a load level of 50% of the strengthened capacity at the start of the test. After FRP debonded, the beam represented an insulated RC beam (un-strengthened) with a higher load level (almost 80%) compared to the room temperature capacity of RC beam. This resulted in higher deflections in the beam at a given time. However, after this stage the comparative analysis of trends in deflections of un-strengthened and un-insulated RC beam (B01) and insulated un-strengthened beam (B3) showed interesting results. In spite of higher load levels, the measured deflections in beam B3 are lower than beam B01. This is mainly due to beneficial effect of insulation (low thermal conductivity) that slows the temperature rise in steel reinforcement (gradual strength degradation) which mainly contributes to the moment capacity of the beam after FRP is lost. For the control RC beam, the rate of deflection is much higher since mechanical properties of concrete and steel degrade faster in absence of any external fire protection system.

The structural response of beams B1 and B2 is much stiffer as compared to the beam B3. This is due to the 'cable action' behavior (similar to tensile membrane action in slabs) that effectively reduce deflection progression in the beams after debonding of FRP occurs. This "cable action" behavior results from unbonded continuous carbon fibers present at the beam soffit. These carbon fibers are held by the anchorages on either end of the beam, as shown in Figure 3.24. It should be noted that no formal design of anchorages was implemented during strengthening of the beams. These anchorages are referred to the bonded FRP to the beam soffit that lie outside the fire affected area of the beam (refer to Figure 3.25). These cool ends of FRP act as anchorages for the continuous unbonded carbon fibers running under beam soffit. The carbon fibers have high tolerance against thermal decomposition and are less sensitive to temperatures up to 1000°C (Davies et al. 2004). Therefore, in the absence of any complete

delamination of FRP due to cool anchorage zone, the unbonded continuous fibers present at tension face of the beam continue to contribute towards capacity of the beam through "cable" mechanism.

Beams B3 and B4 were tested under similar test conditions except that beam B4 was axially restraint against fire induced thermal expansion (refer to Figure 3.26). The effect of axially restraint force on structural response of FRP-strengthened RC beams can be gauged by comparing the deflections of beams B3 and B4. In both the beams, debonding of FRP occurred around 20 minutes. After this stage, the measured deflections in beam B4 are lower for complete test duration as compared to beam B3. This can be attributed to the counteracting moment developed in the beam as a result of arch action introduced by the axial restraining force. The mechanics of arch action is further explained in Chapter 4.

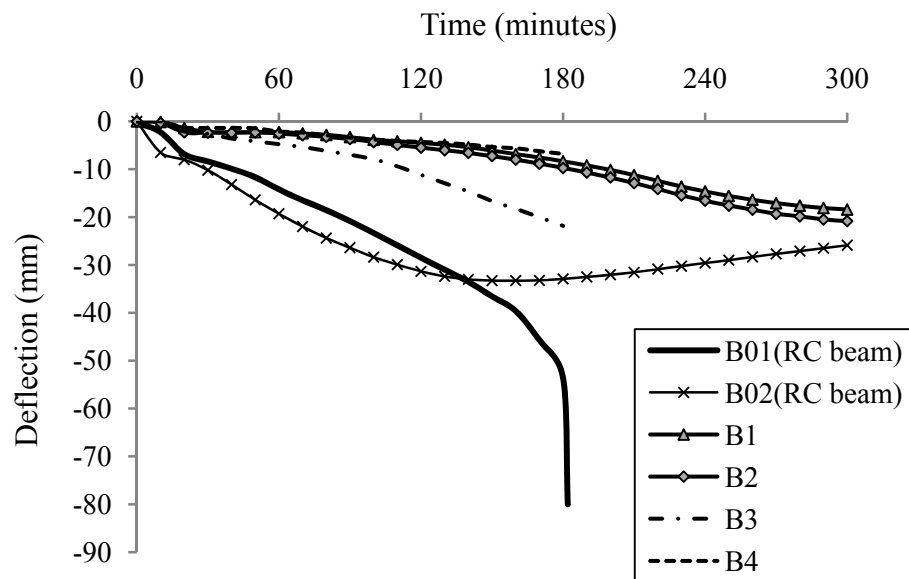


Figure 3.23: Comparison of mid-span deflections



Figure 3.24: Unbonded continuous carbon fibers at the beam soffit

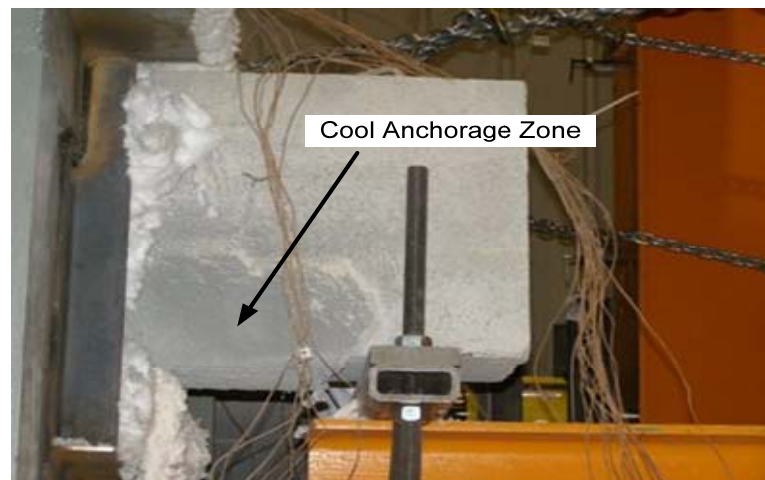


Figure 3.25: Cool anchorage zone of FRP-strengthened RC beam

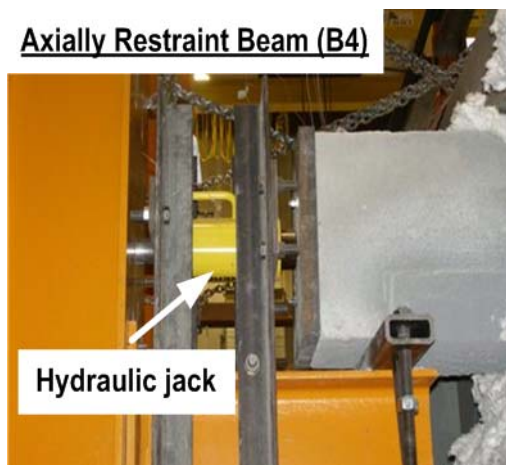


Figure 3.26: Axially restrained FRP-strengthened RC beam (B4)

3.3.3.2 Axial Restraint Force

The measured axial restraint force in axially restrained beam is plotted in Figure 3.27 as a function of fire exposure time. It can be seen that the fire induced axial force in the beam increases with fire exposure time due to restraining of the beam against thermal expansion. Test results of axially restraint RC beam (tested at MSU) referred as beam B02, have also been included in discussion for comparison purpose (Dwaikat 2009). This beam (B02) has similar geometric configuration and dimensions, as FRP-RC beams. The beam was tested under design fire with rapid growth phase followed by gradual cooling phase. The axial restraining force and deflections (plotted in Figure 3.23) are higher in RC beam B02 as compared to insulated FRP-strengthened RC beam B4. This is because RC beam experiences greater thermal expansion and faster degradation in strength and stiffness properties as a result of higher temperature increase in concrete and steel rebars in absence of any fire protection system. Figure 3.23 shows a slight recovery in deflections (beam B02) in later stages of fire exposure due to recovery in strength and stiffness once the beam enters in cooling phase of design fire (Dwaikat 2009).

Figure 3.27 illustrates that the axial force in RC beam is constant after 100 minutes of fire exposure time. This is because relief valve of the restraining system was set to release the pressure to avoid any damage to the test facility or the loading frame, as discussed in Section 3.2.5. In insulated FRP-RC beam, axial restraint force develops gradually since insulation helps in keeping thermal expansion low because temperature increase in beam cross section is slow. Figure 3.23 shows that measured deflections in beam B4 are lower in comparison to beam B3 after debonding of FRP. This can be attributed to development of arch action in the beam due to axial restraining force that counteracts moment due to applied loading. It can be seen from Figure 3.23 that deflections in beam B4 almost match to beams B1 and B2 in which cable action of the continuous carbon fibers effectively contributed in resisting applied loading after

debonding. Therefore, it can be concluded that in absence of any contribution by FRP, the axial restraint force helps to counteract applied gravity loads as by anchored continuous carbon fibers.

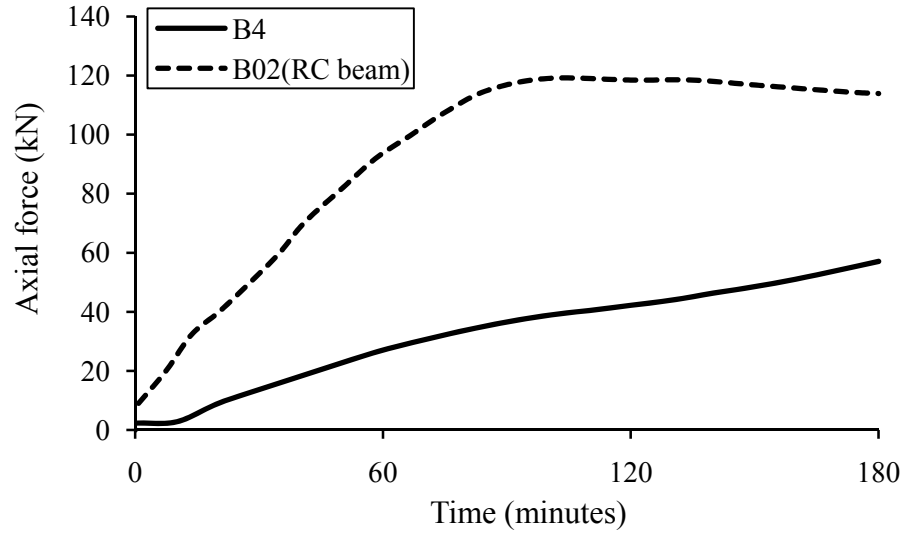


Figure 3.27: Comparison of axial restraint force as function of fire exposure time for beam B4 and beam B02

3.4 Failure Pattern and Fire Resistance

A comparison of fire resistance of five beams is tabulated in Table 3.2. The time to reach failure is defines as the fire resistance of the structural member. Current provisions in design standards specify thermal, strength and deflection limit state as failure criteria for beams (ASTM 2007; BSI 2009). Furthermore, in FRP-strengthened structures the properties of FRP degrade with temperature. Glass transition temperature (T_g) of FRP is often considered as a measure of determining the effectiveness of FRP in beams. All these failure criteria are included in this discussion.

All four FRP-strengthened RC beams met the temperature (critical temperature in rebar defined as 593°C) and strength failure criteria as specified in codes and standards for entire duration of the test. However, the measured fire resistance of beam B01 (control RC beam) was

180 minutes (based on strength limit state) which can be attributed to fast degradation of strength and stiffness properties in absence of any fire protection.

Currently, there are no code provisions that define failure criteria based on FRP, as indicated in Chapter 2. In these test, special attention was given to study effect of FRP behavior on overall structural response of FRP-strengthened RC beams. Analysis of tests data showed that glass transition temperature of FRP exceeded in about 20-25 minutes which resulted in FRP debonding. However, no strength failure occurred in FRP-strengthened beams. For beams B1 and B2, unbonded continuous carbon fibers at tension face of the beams were influential in resisting the applied loading through ‘cable action’ mechanism, while for beam B4, axial restraining force was the key factor that contributed to enhance fire resistance of the beam. Thus, glass transition temperature failure criterion is overly conservative for insulated FRP-strengthened RC beams.

3.5 Summary

Full-scale fire tests were carried out on four FRP-strengthened and insulated RC beams and one RC beam (control beam). Apart from detailed instrumentation, visual observations were made to investigate possible factors influencing fire response of FRP-strengthened beams. The temperature data recorded during tests allowed to evaluate effectiveness of new insulating system, fire induced bond degradation and axial restraint force effect, effect of fire scenario, as well as thickness and geometric configuration effect on fire performance of FRP-strengthened RC beams. Except for the control RC beam (beam B01), all FRP-strengthened RC beams demonstrated fire endurance for more than 3 hours. For entire duration of tests, the average temperature in concrete (inner surfaces) and steel rebars remained less than 400°C. This clearly indicates that both concrete and reinforcing steel retained most of the room temperature strength

for the entire test duration. Results from these fire tests provide better understanding of the response of FRP-strengthened RC beams under realistic fire and loading scenarios and restraint condition. These tests also provide valuable data for validating computer models developed to trace the fire response of FRP-strengthened RC beams.

NUMERICAL MODEL

4.1 General

Fire response of FRP-strengthened RC beams can be modeled through general purpose finite element programs such as ANSYS and ABAQUS. In these microscopic finite element models (FEM), detailed thermal and structural analysis can be carried out, through coupled or uncoupled ways to trace the response of FRP-strengthened concrete members. Analysis using these models is complex, and involves significant computational effort. Further, specific high temperature material models have to be specially provided as input for wide variety of FRP's and insulation materials. Furthermore, modeling in three dimensions has limited application since constitutive relationships are not well established at high temperatures.

In lieu of microscopic based FEM, macroscopic FE models can be used for evaluating fire response of structural systems. Recently, such macroscopic computer models have been successfully applied to trace the response of RC members (Dwaikat 2009; Kodur and Dwaikat 2008). The model has been extended for FRP-strengthened RC beams where it is capable to handle beams of different cross sectional configurations such as rectangle, T or I section FRP-strengthened RC beams and varying insulation thickness and configuration. This new developed

model can account for high temperature material properties of all constitutive materials including FRP and insulation, effect of fire induced bond degradation and axial restraining force, to evaluate fire resistance of FRP-strengthened RC beams. In the model, sectional response generated for various cross sections along the beam length, are utilized to predict over all fire response of FRP-strengthened RC beam. The details of macroscopic FE model are discussed in following sections.

4.2 Macroscopic Finite Element Model - Methodology

A numerical model, initially developed for tracing the fire exposure of RC beams (Kodur and Dwaikat 2008), has been extended to model the response of FRP-strengthened beams. The earlier model developed for RC beams accounts for fire induced spalling, axial restraint effect, high temperature material properties, softening of concrete and various failure criteria. However, the model could not be applied to trace the response of FRP-strengthened RC beams. Current available guidelines for FRP strengthened concrete members assume that the FRP is completely lost during a fire. Therefore, development of a numerical model was challenging due to the lack of available research in this area. A model extension first required a complete understanding of the complex behavior of FRP composites exposed to elevated temperatures. Further, it required incorporation of the mechanics and the effect of degradation of mechanical and bond properties of the FRP, both at ambient and elevated temperatures and possible failure modes. Also, the model needed to be generalized to handle different beam cross sections such as rectangular, T-beams, and various geometric insulation configurations.

A numerical model, based on the macroscopic finite element (FE) approach that uses moment-curvature relationships is developed to trace the response of FRP-strengthened RC beams in the entire range of behavior up to collapse under fire. In the analysis, the fire exposure

time is incremented in steps and the response of the beam is evaluated at each time step. The beam is idealized by dividing it into a number of segments along its length and the mid-section of each segment is assumed to represent the overall behavior of the segment. This mid-section is discretized into a number of elements (see Figure 4.1(c)).

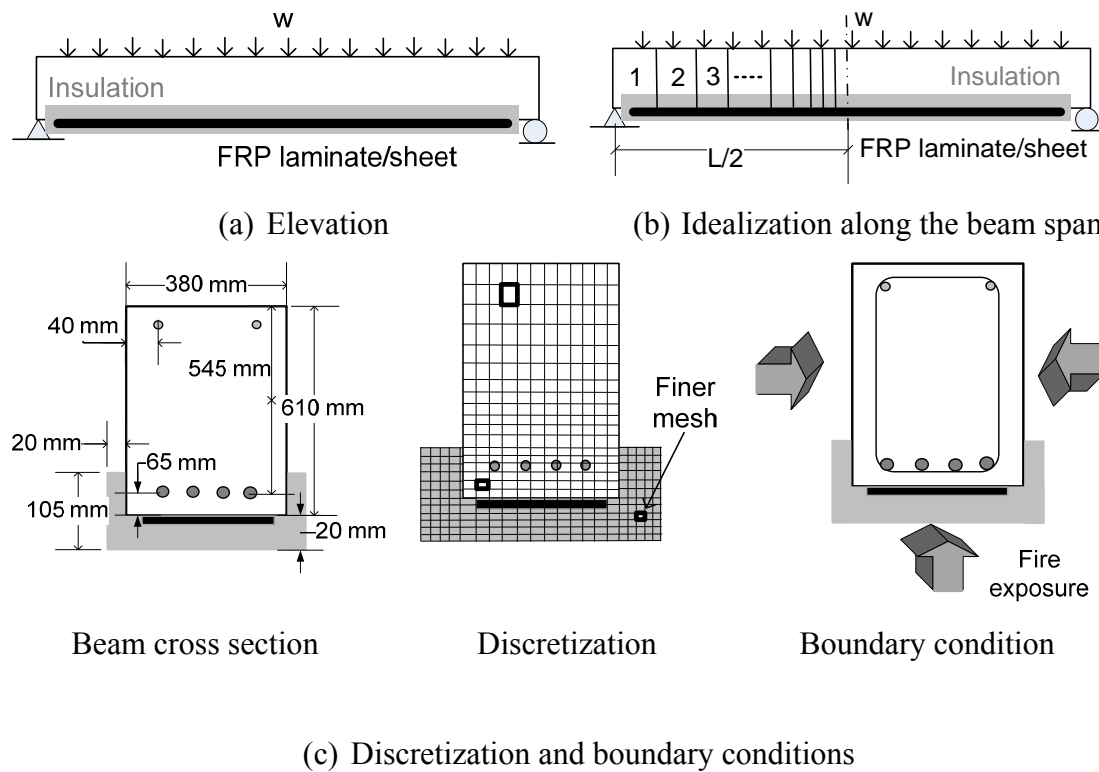


Figure 4.1: Layout of typical FRP-strengthened RC beam, its idealization and discretization for analysis

At each time step, thermal analysis is carried out to determine the temperature distribution within the cross-section of each segment. The computed temperatures are used to generate moment-curvature ($M-\kappa$) relationships for each segment at various time steps. These $M-\kappa$ relationships are in turn used to trace the structural response of the beam under fire conditions. The $M-\kappa$ relationships, at various time steps, are generated using the changing properties of

constituent materials namely concrete, steel reinforcement, FRP and insulation. Thus, the material nonlinearity is automatically accounted for in the generation of $M-\kappa$ relationships.

The load carrying capacity of the beam at a particular time step is evaluated by taking the maximum moment in the $M-\kappa$ relationships. The deflection of the beam at each time step is calculated through the stiffness approach by evaluating average stiffness of the beam. The strength and stiffness of the beam decreases with time and failure is said to occur when one of the failure limit states is reached. A flowchart showing the numerical procedure for fire resistance calculations is illustrated in Figure 4.2.

At each time step, numerical calculations are performed in four steps: namely, calculation of fire temperature to which the beam is exposed, calculation of cross-sectional temperatures in the beam, generation of $M-\kappa$ relationships for each beam segment, and calculation of resulting beam deflection and strength through nonlinear structural analysis. The detailed procedure is outlined in the following sections.

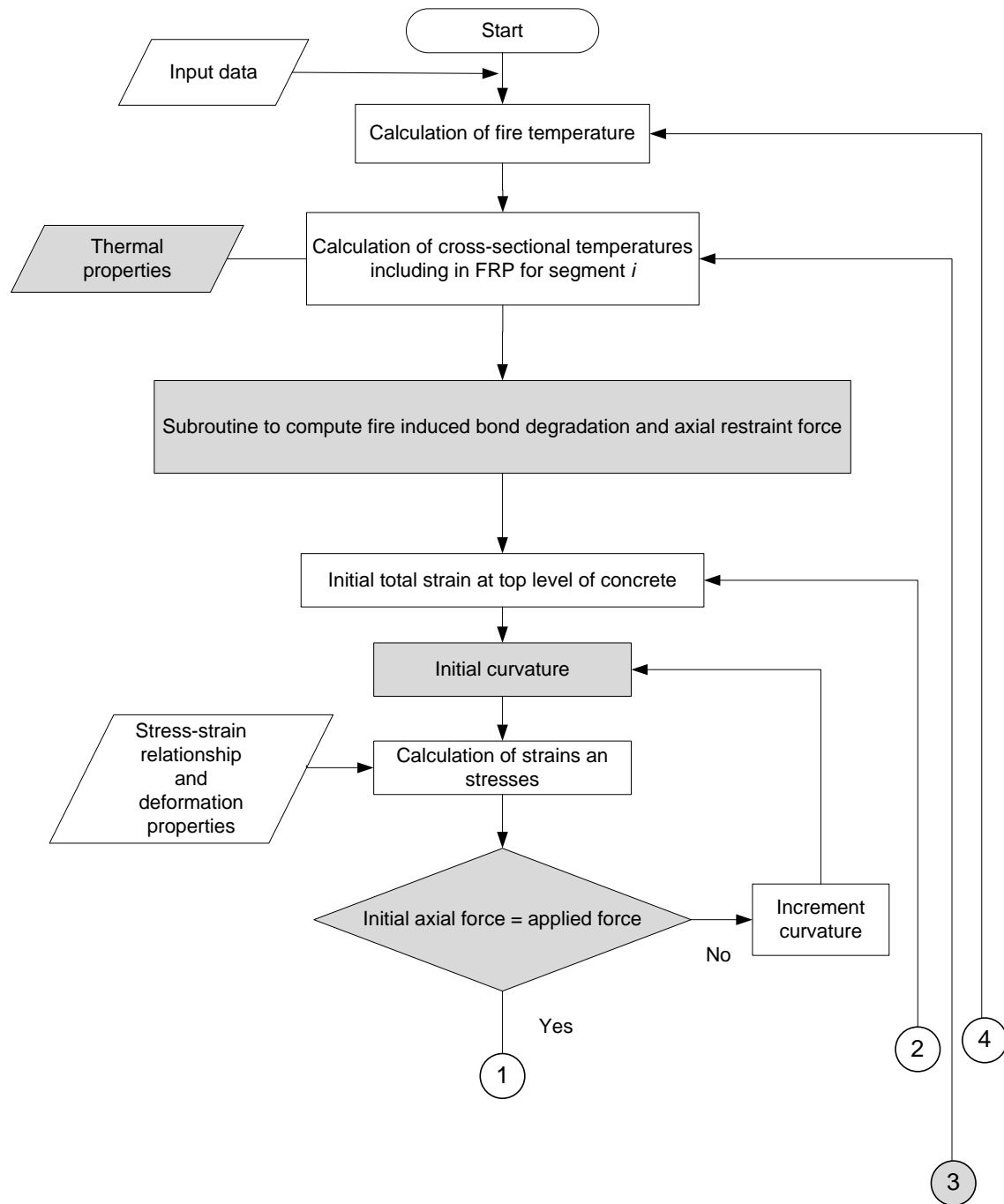


Figure 4.2: Flowchart illustrating the steps associated with fire resistance analysis of FRP-strengthened RC beam

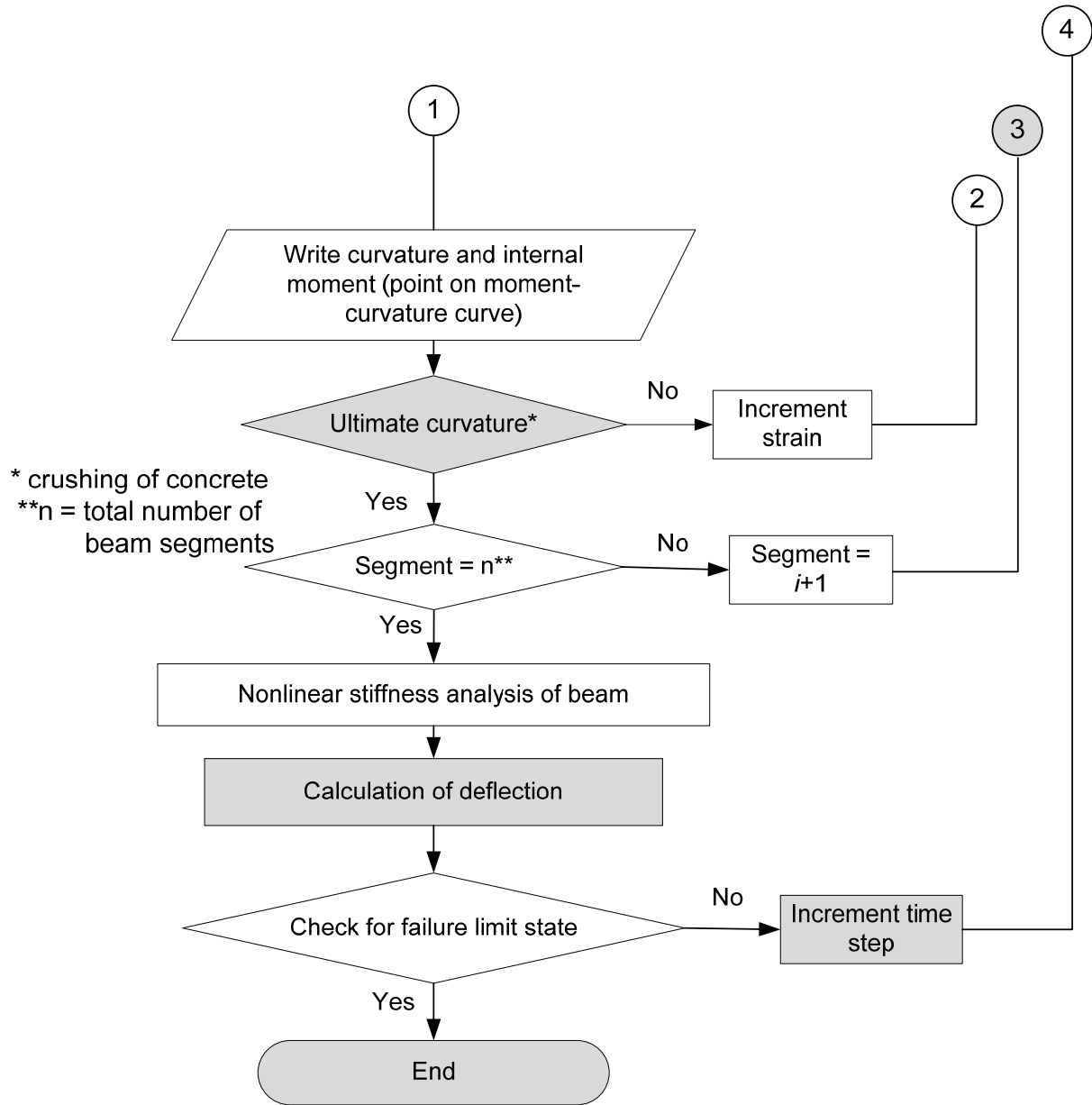


Figure 4.2: (cont'd) Flowchart illustrating the steps associated with fire resistance analysis of FRP-strengthened RC beam

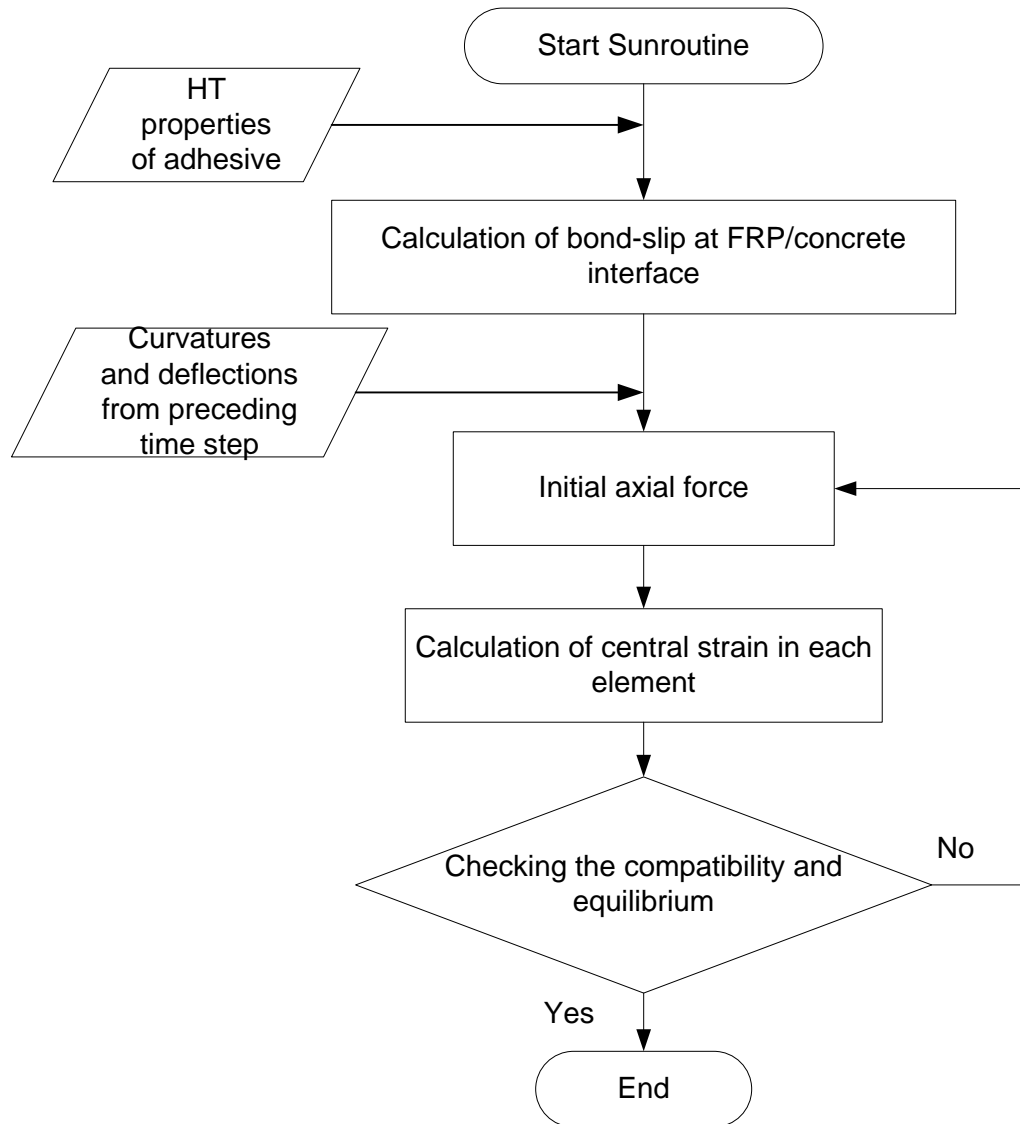


Figure 4.2: (cont'd) Flowchart illustrating the steps associated with fire resistance analysis of FRP-strengthened RC beam

4.3 FE Model for FRP-strengthened RC Beams

4.3.1 Fire Temperatures

In the model, the beam is assumed to be exposed to fire from three sides (sides and bottom surface) while ambient conditions are assumed to prevail on the top side to represent presence of slab. The fire temperatures follow that of a standard fire exposure or any other specified design fire scenario. The time-temperature relationship for the ASTM E119 (2007) and ISO 834 standard fires can be approximated by the following equations:

$$\text{ASTM E119: } T_f = T_o + 750 \left(1 - \exp \left(-3.79553 \sqrt{t/60} \right) \right) + 170.41 \sqrt{t/60} \quad (4.1)$$

$$\text{ISO 834: } T_f = 20 + 345 \log(8t + 1) \quad (4.2)$$

where: t_h = time (minutes), T_o = initial temperature ($^{\circ}\text{C}$), and T_f = fire temperature ($^{\circ}\text{C}$)

Any design fire or standard hydrocarbon fire can be used in the model provided the time-temperature relationships are known.

4.3.2 Thermal Analysis

The temperatures within the beam cross section, including FRP and insulation layer, is calculated through finite element analysis. The beam is divided into number of beam segments (smaller segments towards the mid-span for more accuracy) along its length and the cross section of each segment is further subdivided into elements (see Figure 4.1(c)). For elemental discretization, a finer mesh is used for surfaces (insulation and FRP) in close proximity to fire zone for more accuracy because these are highly sensitive to temperature rise.

In the model, it is assumed that the temperature is uniform along the length of the segment thus allowing the calculations for a unit length of each segment. Temperature distribution in the beam cross section is not significantly influenced if steel reinforcement is not included in

discretization of beam cross-section for thermal analysis (Lie and Irwin 1993). However, in the model, the location of the steel reinforcement is accounted for while discretizing the beam cross-section in to elements for thermal analysis such that more accurate temperature distribution is obtained. The heat transfer from fire to the boundary elements is through convection and radiation. However, from insulation to FRP and FRP to concrete, conduction is the dominant heat transfer mechanism. The governing equation for transient heat conduction within the beam cross-section is given as (Cook et al. 2007):

$$k\nabla^2 T + Q = \rho c \frac{\partial T}{\partial t} \quad (4.3)$$

where: k = thermal conductivity, ρc = heat capacity, T = temperature, t = time, and Q = heat source, ∇^2 = Laplacian operator defined in Cartesian coordinates by $\nabla^2 = \frac{\partial^2}{\partial x^2} + \frac{\partial^2}{\partial y^2} + \frac{\partial^2}{\partial z^2}$

The heat flux on the boundary due to convection and radiation can be given by the following two equations:

$$q_{rad} = h_{rad} (T - T_E) \quad (4.4)$$

$$q_{con} = h_{con} (T - T_E) \quad (4.5)$$

where: q is heat flux and h is heat transfer coefficient. The subscripts *rad* and *conv* represent radiation and convection, respectively.

The radiative heat transfer co-efficient is expressed by:

$$h_{rad} = 4\sigma\epsilon (T^2 + T_E^2)(T + T_E) \quad (4.6)$$

where:

T_E = temperature of the environment surrounding the boundary,

σ = Stefan-Boltzman constant = 5.67×10^{-8} (W/m²·°K⁴), and

ϵ = Emissivity factor

Therefore, total heat flux on the beam boundaries (q_b) can be given by:

$$q_b = (h_{con} + h_{rad})(T - T_E) \quad (4.7)$$

Using Fourier's Law, the governing heat transfer equation on the boundary of the beam can be written as:

$$k \left(\frac{\partial T}{\partial y} n_y + \frac{\partial T}{\partial z} n_z \right) = -h(T - T_f) \quad (4.8)$$

where:

n_y and n_z = components of the vector normal to the boundary in the plane of the cross-section,

and

$$h = h_{con} + h_{rad}$$

Since the beam is exposed to fire from three sides, two types of boundary equations must be considered for thermal analysis, namely:

- Fire exposed boundaries where the heat flux is governed by:

$$k \left(\frac{\partial T}{\partial y} n_y + \frac{\partial T}{\partial z} n_z \right) = -h_f(T - T_f) \quad (4.9)$$

- Unexposed boundary where the heat flux equation is given by:

$$k \left(\frac{\partial T}{\partial y} n_y + \frac{\partial T}{\partial z} n_z \right) = -h_c(T - T_0) \quad (4.10)$$

where:

h_f and h_c = heat transfer coefficient of the fire side and the cold side, respectively, and

T_f and T_0 = fire and cold side temperatures, respectively.

Galerkin finite element method is used to solve Eq. (4.3). In this approach, the material property matrices and the equivalent nodal heat flux (stiffness matrix K_e , mass matrix M_e , and nodal heat flux F_e) are generated for each element. These matrices are given by following equations:

$$K_e = \int_A \left[k \frac{\partial N}{\partial x} \frac{\partial N^T}{\partial x} + k \frac{\partial N}{\partial y} \frac{\partial N^T}{\partial y} \right] dA + \int_{\Gamma} N \alpha N^T ds \quad (4.11)$$

$$M_e = \int_A \rho c N N^T dA \quad (4.12)$$

$$F = \int_A N Q dA + \int_{\Gamma} N \alpha T_{\alpha} ds \quad (4.13)$$

where

N = vector of shape functions

Q = heat source

$\alpha = h_c$ or h_f depending on the boundary condition Γ

s = distance along the boundary and,

T_{α} = fire or ambient temperature dependant on boundary Γ

Once the element matrices are computed, they are assembled into a global system of differential equations and is expressed as:

$$M\dot{T} + KT = F(t) \quad (4.14)$$

where: K = global stiffness matrix, M = global mass matrix, and F = equivalent nodal heat flux and \dot{T} = temperature derivative with respect to time (t).

Eq. (4.14) is solved using finite difference algorithm of trapezoidal family (θ algorithm) in the time domain. This algorithm computes the temperature distribution at any time step using the information available at previous time step, and can be written as (William and Richard 1990):

$$T_{n+1} = T_n(\theta \dot{T}_{n+1} + (1-\theta)\dot{T}_n) \quad (4.15)$$

Multiplying both sides of Eq. (4.15) by M and using Eq. (4.14) at the beginning and the end of the time interval (t_n, t_{n+1}) , the following equation can be obtained:

$$(M + h\theta K)T_{n+1} = (M - h(1-\theta)K)T_n + h(\theta F_{n+1} + (1-\theta)F_n) \quad (4.16)$$

where: h = time step, T_n and T_{n+1} = temperature at the beginning and the end of time step, respectively, F_n and F_{n+1} = equivalent nodal heat flux at the beginning and the end of time step, and θ = a constant between 0 and 1.

For unconditional stability of the numerical calculations, the value of θ has to be greater than or equal to 0.5 (William and Richard 1990). By knowing the temperatures at ambient conditions, Eq. (4.16) can be applied to obtain the temperature-time history at the following time step, and this can be repeated for subsequent time steps. In each time step, an iterative process is required to solve Eq. (4.16) due to the nonlinearity of both material properties and boundary conditions. Details on finite element formation for solving heat and mass transfer equations are provided in Appendix C.

4.3.3 Strength Analysis

4.3.3.1 General Analysis Procedure

The cross-sectional temperatures generated from thermal analysis are used to develop $M-\kappa$ relationships at various time steps. For the generation of $M-\kappa$ relationships, the following assumptions are made:

- Plane sections before bending remain plane after bending
- The FRP has linear stress-strain relationship till failure
- No relative slip occurs between FRP and concrete substrate
- There is no bond-slip between steel reinforcement and concrete

Also, for fire induced bond-slip and axial restraint force calculations, following assumptions are made:

- Shear stresses are invariant across adhesive thickness
- Stress distribution is independent of flexural cracks in concrete
- Curvature at beam soffit and FRP is to be the same
- Axial restraint force is constant along the span of the beam (for each time step)
- The curvatures and displacements from preceding time step are used for computing axial force for current time step

The strength calculations, at elevated temperatures, are carried out using the same mesh as used for thermal analysis. The strength analysis is performed by first estimating fire induced bond-slip at FRP/concrete interface, and axial restraint force in each beam segment. Following this $M - \kappa$ relationship for each segment is generated. Then the generated $M - \kappa$ relationships are used to undertake non-linear stiffness (beam) analysis to trace the response of FRP-strengthened RC beams. At first time step (room temperature), a perfect bond at FRP/concrete interface, with zero axial restraining force is assumed. For subsequent time steps, curvatures distribution obtained from preceding time step are utilized compute bond-slip and axial force. It should be noted that using curvatures from preceding time step has negligible influence on computations if the time increment are small.

The temperatures, deformations and stresses in each element are represented by the corresponding values at the center of the element. The temperature in each element is obtained by averaging the nodal temperatures of rectangular elements. For steel rebars the temperature is assumed to be that at the center of the rebar.

The total strain in a concrete element, at any fire exposure time, is taken as the sum of thermal strain (expansion), mechanical strain, creep strain, and transient strain:-

$$\varepsilon_{tc} = \varepsilon_{thc} + \varepsilon_{mec} + \varepsilon_{crc} + \varepsilon_{trc} \quad (4.17)$$

where: ε_t = total strain, ε_{th} = thermal strain, ε_{me} = mechanical strain, ε_{cr} = creep strain, and ε_{tr} = transient strain. Subscript c for concrete

In the model, thermal strain is calculated by integrating the coefficient of thermal expansion (which depends on the temperature of the concrete) over the temperature domain. Creep strain in concrete is assumed to be a function of time, temperature and stress level, and is computed based on Harmathy's (1993) approach using the following expression:

$$\varepsilon_{cr} = \beta_1 \frac{\sigma}{f_{c,T}} \sqrt{t} e^{d(T-293)} \quad (4.18)$$

where: $\beta_1 = 6.28 \times 10^{-6} \text{ s}^{-0.5}$ (constant), $d = 2.658 \times 10^{-3} \text{ K}^{-1}$ (empirical constant), T = current concrete temperature (K), t = time (s), $f_{c,T}$ = concrete strength at temperature T , and σ = current stress in the concrete.

The transient strain, which is specific to concrete under fire conditions, is computed based on the relationship proposed by Anderberg and Thelandersson (1976). The transient strain is related to thermal strain as follows:

$$\Delta \varepsilon_{tr} = k_2 \frac{\sigma}{f_{c,20}} \Delta \varepsilon_{th} \quad (4.19)$$

where: k_2 = a constant that ranges between 1.8 and 2.35 (a value of 2 will be used in the analysis); $\Delta \varepsilon_{th}$ = change in thermal strain; $\Delta \varepsilon_{tr}$ = change in transient strain and $f_{c,20}$ = concrete strength at room temperature.

At any fire exposure time, the total strain in steel reinforcement is calculated as the sum of three components given in the following equation:

$$\varepsilon_{ts} = \varepsilon_{ths} + \varepsilon_{mes} + \varepsilon_{crs} \quad (4.20)$$

where: ε_{ts} , ε_{ths} , ε_{mes} and ε_{crs} are total strain, thermal strain, mechanical strain and creep strain respectively in the steel reinforcement.

Similar to concrete, thermal strain (expansion) in steel can be calculated. The thermal strain can be computed by knowing the values of coefficient of thermal expansion and temperature of the reinforcing steel. Eurocode 3 (1995) provides a linear coefficient of thermal expansion for use in the design equations. According to Eurocode 3, the thermal strain of reinforcing steel can be approximated as follows:

$$\varepsilon_{ths} = 14 \times 10^{-6} (T - 20) \quad (4.21)$$

where: T=Temperature °C

High temperature creep strain in reinforcing steel is computed based on Dorn's theory and the model proposed by Harmathy (1967) with some modifications to account for varying yield strengths of steel. According to Harmathy's model, creep strain in steel is given as:-

$$\varepsilon_{crs} = \left(3Z\varepsilon_{t0}^2 \right)^{1/3} \theta^{1/3} + Z\theta \quad (4.22)$$

where:

$$Z = \begin{cases} 6.755 \times 10^{19} \left(\frac{\sigma}{f_y} \right)^{4.7} & \frac{\sigma}{f_y} \leq \frac{5}{12} \\ 1.23 \times 10^{16} \left(e^{10.8(\sigma/f_y)} \right) & \frac{\sigma}{f_y} > \frac{5}{12} \end{cases}$$

$\theta = \int e^{-\Delta H/RT} dt, \frac{\Delta H}{R} = 38900 \text{ } ^\circ\text{K}, t = \text{time (hours)}, \varepsilon_{to} = 0.016 \left(\frac{\sigma}{f_y} \right)^{1.75}$, σ = stress in steel as function of temperature, and f_y = yield strength of steel (room temperature).

For FRP, the total strain at any time step can be calculated using the following equation:

$$\varepsilon_{tfrp} = \varepsilon_{thfrp} + \varepsilon_{mefrp} + \varepsilon_{crfrp} - \varepsilon_{bi} - \varepsilon_{slip} \quad (4.23)$$

where: ε_{tfrp} = total strain, ε_{thfrp} = thermal strain, ε_{mefrp} = mechanical strain, ε_{crfrp} = creep strain in FRP, ε_{bi} = initial strain at the soffit of the beam at the time of retrofitting with FRP, and ε_{slip} = slip at the interface of FRP and concrete

At the time of FRP strengthening, RC beam is subjected to dead loads. Consequently the strains in concrete at the level of FRP (ε_{bi}), resulting from dead loads, needs to be considered (deducted) in computing effective strain in FRP. The value coefficient of thermal expansion (CTE) for FRP material in transverse direction is higher as compared to the longitudinal direction. This is because the transverse properties are dominated by the matrix while longitudinal properties for unidirectional FRP are dominated by the fiber properties. From the literature, the CTE of high modulus carbon/epoxy at room temperature in longitudinal direction is $-0.09 \times 10^{-6}/^\circ\text{C}$ while it is $27 \times 10^{-6}/^\circ\text{C}$ in transverse direction (Mallick 1993). Therefore, the coefficient of thermal expansion in the fiber direction, is assumed negligible.

At elevated temperatures, creep strains in FRP are considerable depending on the material used in matrix and the fibers and orientation. The creep effects are minimal both at room and at elevated temperatures if the fibers orientation is parallel to the longitudinal axis of the beam since in such case fiber properties will dominate the overall behavior (Rahman et al. 1993). However, creep strains will be significant if the fiber orientation is off-axis (at 90 degrees). For

the analysis, creep strains in FRP have not been accounted since fiber axis coincides with beam longitudinal axis.

The total strain in a concrete or steel or FRP element, at any fire exposure time can be related to the curvature of the beam by the following expression:

$$\varepsilon_t = \varepsilon_c + \kappa y \quad (4.24)$$

where: ε_t = total strain, ε_c = strain at the top most fiber in concrete , κ = curvature, and y = distance from uppermost fiber in concrete to the center of the element.

At any time step, and for an assumed value of ε_c and κ (curvature), the total strain in each element (concrete, FRP or rebar) can be computed using Eq. (4.24). For known temperatures, other strain components like thermal, transient (for concrete only), ε_{bi} (for FRP only) and creep strains in the concrete and rebars are calculated using appropriate equation given above. Then, the mechanical strain in each element is computed by rearranging Eq. (4.17), (4.20) and (4.23) as follows:-

$$\varepsilon_{mec} = \varepsilon_{tc} - \varepsilon_{thc} - \varepsilon_{crc} - \varepsilon_{trc} \quad (\text{for concrete}) \quad (4.25)$$

$$\varepsilon_{mes} = \varepsilon_{ts} - \varepsilon_{ths} - \varepsilon_{crs} \quad (\text{for steel}) \quad (4.26)$$

$$\varepsilon_{mefrp} = \varepsilon_{tfrp} - \varepsilon_{cfrp} - \varepsilon_{bi} - \varepsilon_{slip} \quad (\text{for FRP}) \quad (4.27)$$

For the estimated mechanical strain, the stresses and subsequently the corresponding forces in each element can be computed using temperature dependent stress strain relationships for concrete, steel, and FRP (Figure 4.3(a)). These forces are used to check force equilibrium for each assumed value of strain and curvature. For an assumed total strain at the top layer of concrete($\varepsilon_{c,T}$), κ is iterated until force equilibrium is satisfied. This iterative procedure is repeated till equilibrium, compatibility and convergence criterion are satisfied. Once these

conditions are satisfied, moment and curvature corresponding to that strain are computed. Through this approach, various points on the moment-curvature curve are generated for each time step.

4.3.3.2 Evaluating Strain (ε_{slip}) due to Bond Slip

In FRP-strengthened RC members, the binding material (adhesive) provides load path for transfer of stresses from concrete substrate to FRP reinforcement. At temperatures beyond T_g , bond properties (shear and bond strength) deteriorate considerably and this introduces a slip at bond interface. Due to this bond-slip, adhesive loses its ability to effectively transfer forces between concrete and FRP and this result in FRP developing only partial tensile stresses as compared to a perfect bond case where full stresses in FRP can effectively be utilized. With increasing slip, the bond deteriorates considerably and ultimately leads to debonding of FRP. Thus, bond degradation with temperature is to be properly accounted for reliable assessment of fire resistance in FRP-strengthened RC members.

In FRP-strengthened members, FRP terminates at a distance from the support. Concentration of shear stresses, which mainly contribute in transfer of forces from concrete to FRP, is substantial near edges of FRP reinforcement. Previous studies have shown that this high shear stress concentration is a major cause of FRP debonding. Figure 4.4 schematically shows development of shear stresses in a beam segment of FRP-strengthened RC beam and related bond-slip at FRP-concrete interface. Thus, variation of these shear stresses with temperature can be used to derive an expression for computing bond-slip at FRP-concrete interface. This expression will account for changing material properties of adhesive (shear stiffness) with temperature. The beam is idealized into a number of segments along its length. For a small

elemental length “ dx ” of the adhesive (see Figure 4.4 (c)), displacement (du) due to slip is given by:

$$du = \frac{\tau}{G} t_g \quad (4.28)$$

where τ is the shear stress, G is the shear modulus and t_g is adhesive thickness.

For each beam segment i , average shear stress τ_i at the FRP-concrete interface can be expressed as (refer Figure 4.4):

$$\tau_i = \frac{P_{frp(i+1)} - P_{frp(i)}}{L_i \times b} \quad (4.29)$$

where $P_{frp(i)}$ is force in FRP reinforcement for segment i , L_i is length of segment i , and b is the width of the beam.

With increasing temperature due to fire, the adhesive softens and experiences a significant reduction in its shear modulus (G). This softening effect results in a relative slip (δ_{slip}) between FRP composite and concrete. Slip in a segment i can be calculated as (refer to Figure 4.4 (c)):

$$\delta_{slip(i)} = \gamma_i \times t_g \quad (4.30)$$

where t_g is adhesive thickness and γ_i is the shear strain in segment i given by:

$$\gamma_i = \frac{\tau_i}{G} \quad (4.31)$$

Substituting γ_i in Eq. (4.30), relative slip (δ_{slip}) in a beam segment can be expressed as:

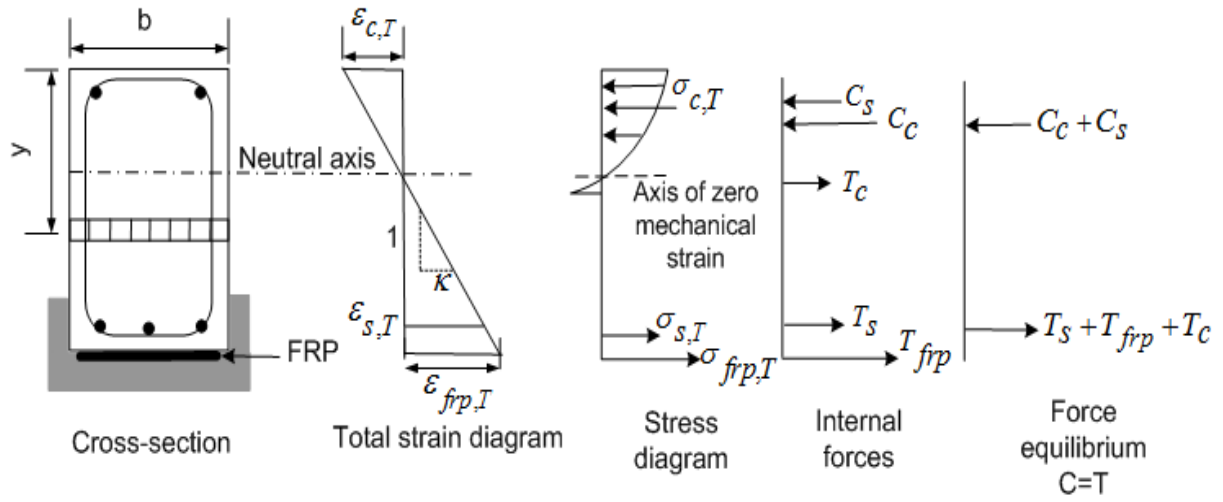
$$\delta_{slip(i)} = \frac{P_{frp(i+1)} - P_{frp(i)}}{L_i \times b} \times \frac{1}{G} \times t_g \quad (4.32)$$

Knowing δ_{slip} , the relative strain due to slip can be established as:

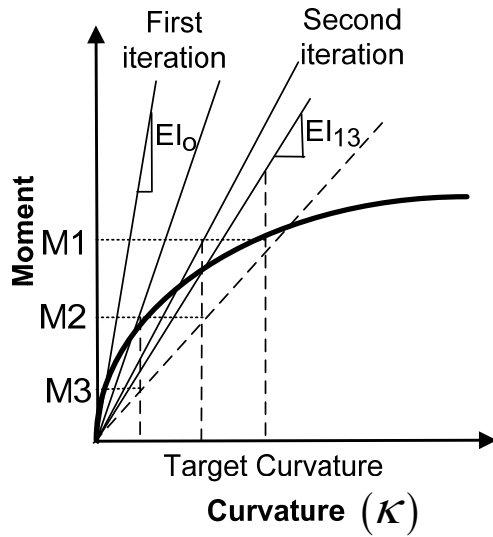
$$\varepsilon_{slip(i)} = \frac{\text{change in length}}{\text{original segment length}} = \frac{\delta_{slip(i)}}{L_i} = \frac{P_{frp(i+1)} - P_{frp(i)}}{L_i^2 \times b} \times \frac{1}{G} \times t_g \quad (4.33)$$

In Eq. (4.33), force in FRP (P_{frp}) is dependent on temperature and strain (ε_{frp}) distribution in FRP reinforcement, while shear modulus decreases with temperature. The bond-slip (ε_{slip}) in each beam segment can be calculated at any fire exposure time using Eq. (4.33). The variation of bond-slip is a function of distance from FRP plate ends. As schematically shown in Figure 4.5, peak bond-slip occurs near FRP plate end and varies exponentially towards center of the beam. The beam segment with peak bond-slip represents critical segment of the FRP-strengthened beam since delamination of FRP initiates at this segment. For simplification, bond-slip evaluated in critical segment can be assumed consistent in all beam segments, for a given time step.

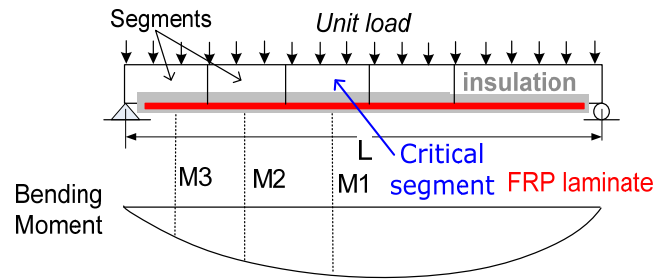
Under fire conditions, FRP only develops partial tensile strength due to bond-slip. Therefore, in computing effective mechanical strain in FRP, strain due to bond-slip (ε_{slip}) is to be subtracted from the total strain. This effective mechanical strain, which takes into consideration bond degradation, can be used to calculate stress and tensile force in FRP. The effect of temperature induced bond-slip is significant when the temperature at FRP-concrete interface exceeds T_g .



(a) Variation of strains, stresses and internal forces in a beam cross section exposed to fire



(b) $M - \kappa$ of typical beam segment



(c) Segments in idealized beam and bending moment diagram

Figure 4.3: Discretization of beam for analysis and $M - \kappa$ relationship for idealized segment

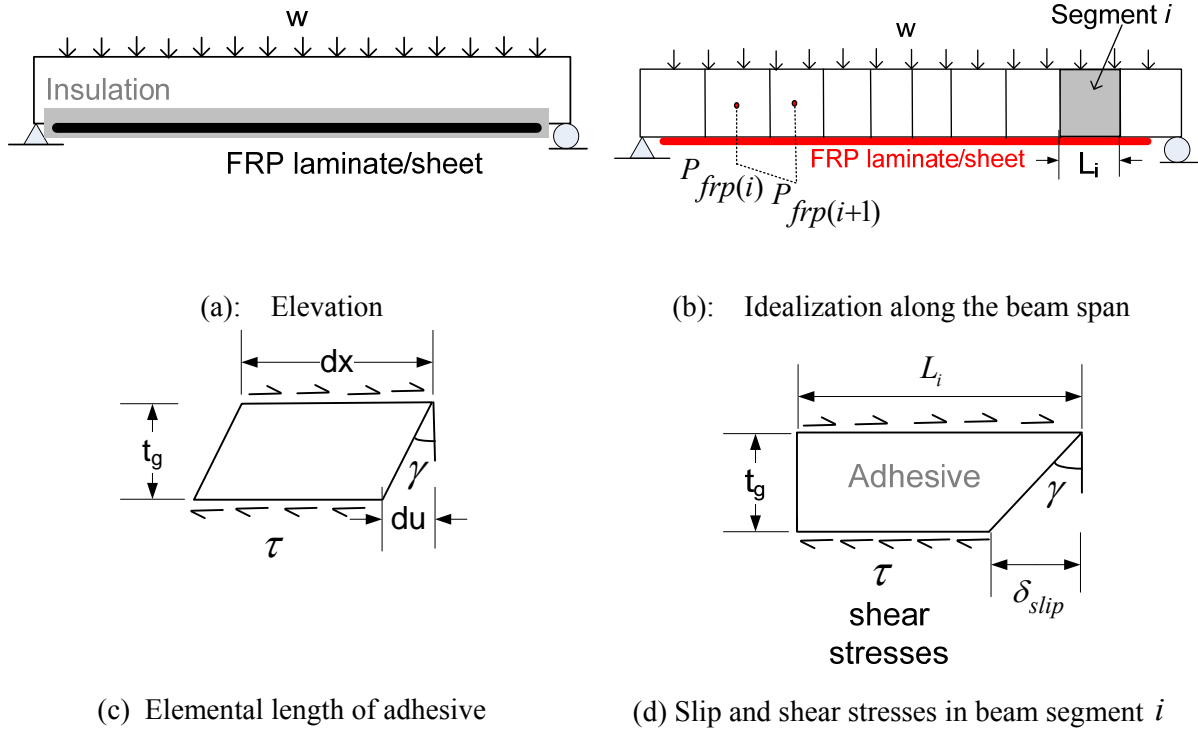


Figure 4.4: Development of shear stresses and bond-slip in a beam segment

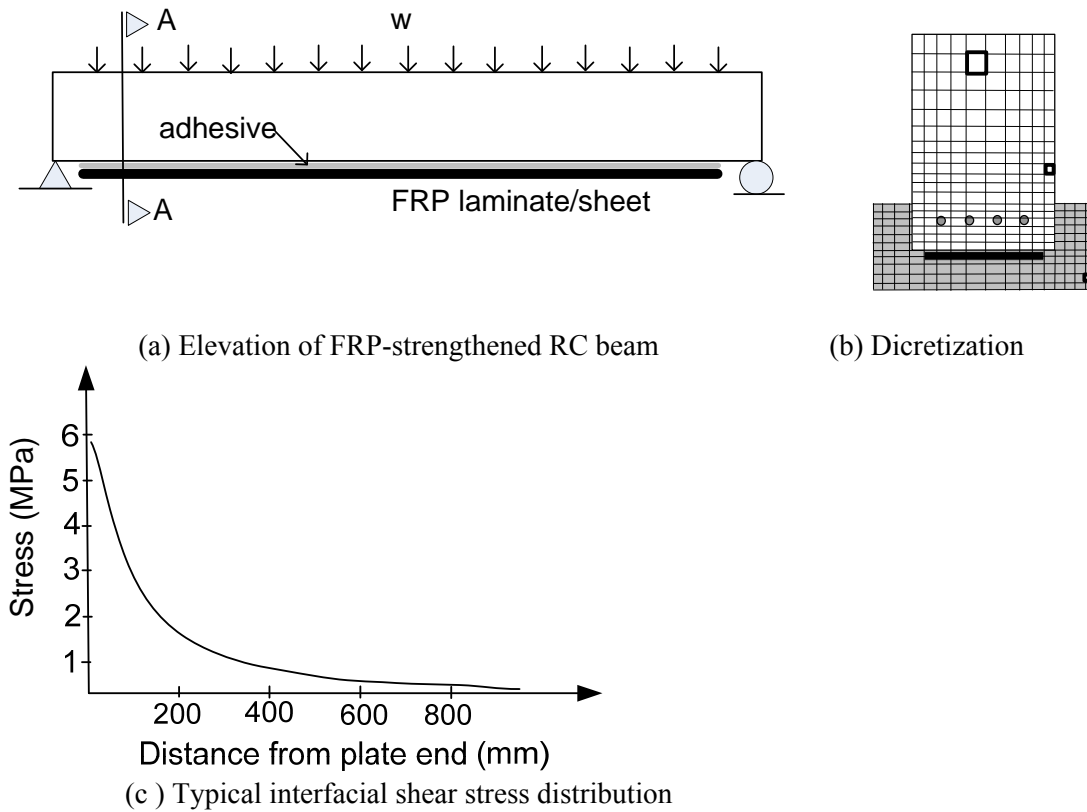


Figure 4.5: Schematic interfacial shear stress distribution

4.3.3.3 Fire Induced Axial Restraint Force

In addition to bond slip, the effect of fire induced axial restraint force can significantly influence fire resistance of FRP-strengthened RC beam. This is because FRP-strengthened RC beam can experience considerable expansion when exposed to high temperature. If the beam is restrained from expanding, a significant axial restraint force develops at the supports. This restraint axial force, which can be computed in a similar manner to that for a RC beam (Dwaikat and Kodur 2008), can have a positive effect on fire resistance. The total axial restraint force (P) induced in the beam can be calculated from summation of compressive and tensile forces in each element of the beam cross section. Thus, the total axial force (P) in the beam is:

$$P = C + T = \sum \sigma_e A_e \quad (4.34)$$

where σ_e is stress and A_e is area of each element in beam cross section.

In the calculations, it is assumed that axial restraint force in all the beam segments remains constant (is equal) at a given time step. Also, as a starting point, it is assumed that the curvature (κ) in beam segment i , at n th time step is equal to the curvature computed in the previous time step ($n-1$). It should be noted that for a small increment in time step, this difference in curvature will be negligibly small. With these assumptions, Eq. (4.34) can be expressed in terms of central total strain (ε_o) and curvature (κ) for each beam segment i as:

$$P = \phi(\varepsilon_{oi} \kappa_i^n) \approx \phi(\varepsilon_{oi} \kappa_i^{n-1}) \quad (4.35)$$

After establishing total axial restraint force P , compatibility along the beam length (L) needs to be satisfied which is given by Dwaikat and Kodur (2008):

$$\sum l_i - L - \Delta = 0 \quad (4.36)$$

$$\sum \sqrt{(1 + \varepsilon_{oi}) L_i^2 - (w_{i2}^{n-1} - w_{i1}^{n-1})^2} - L - \Delta = 0 \quad (4.37)$$

where ε_{oi} = total central strain for segment i , l_i = length of beam segment i , w_{i1} and w_{i2} are deflection of the two nodes of beam segment i computed for $(n-1)$ and n th time step, as shown in Figure 4.6.

An iterative procedure is applied to evaluate axial restraint force (P) in FRP-strengthened RC beam and this involve following steps:

- Assume a value of ' P ' (axial restraint force) for known value of curvature (κ_i^{n-1}) from previous time step $(n-1)$. For first time step (at room temperature), $P = 0$.
- Compute central total strain (ε_{oi}) for each beam segment i .
- Calculate ' Δ ' for a known value of spring stiffness (k).
- Check compatibility using Eq. (4.37)
- Iterate ' P ' until Eq. (4.37) is satisfied within a pre-determined tolerance value.

At the support, boundary conditions are represented by a spring with stiffness(κ). The stiffness(κ) can be assigned any value depending on the degree of restraint experienced in practical applications. Once the axial restraint force is computed through iterative procedure explained above, $M-\kappa$ relationships are generated through similar approach described for previous numerical model (Kodur et al. 2009). Therefore, accounting for axial restraint force allows a more realistic analysis of the strengthened beams while taking into account primary (due to loading) as well as secondary moments due to $P-\delta$ effect.

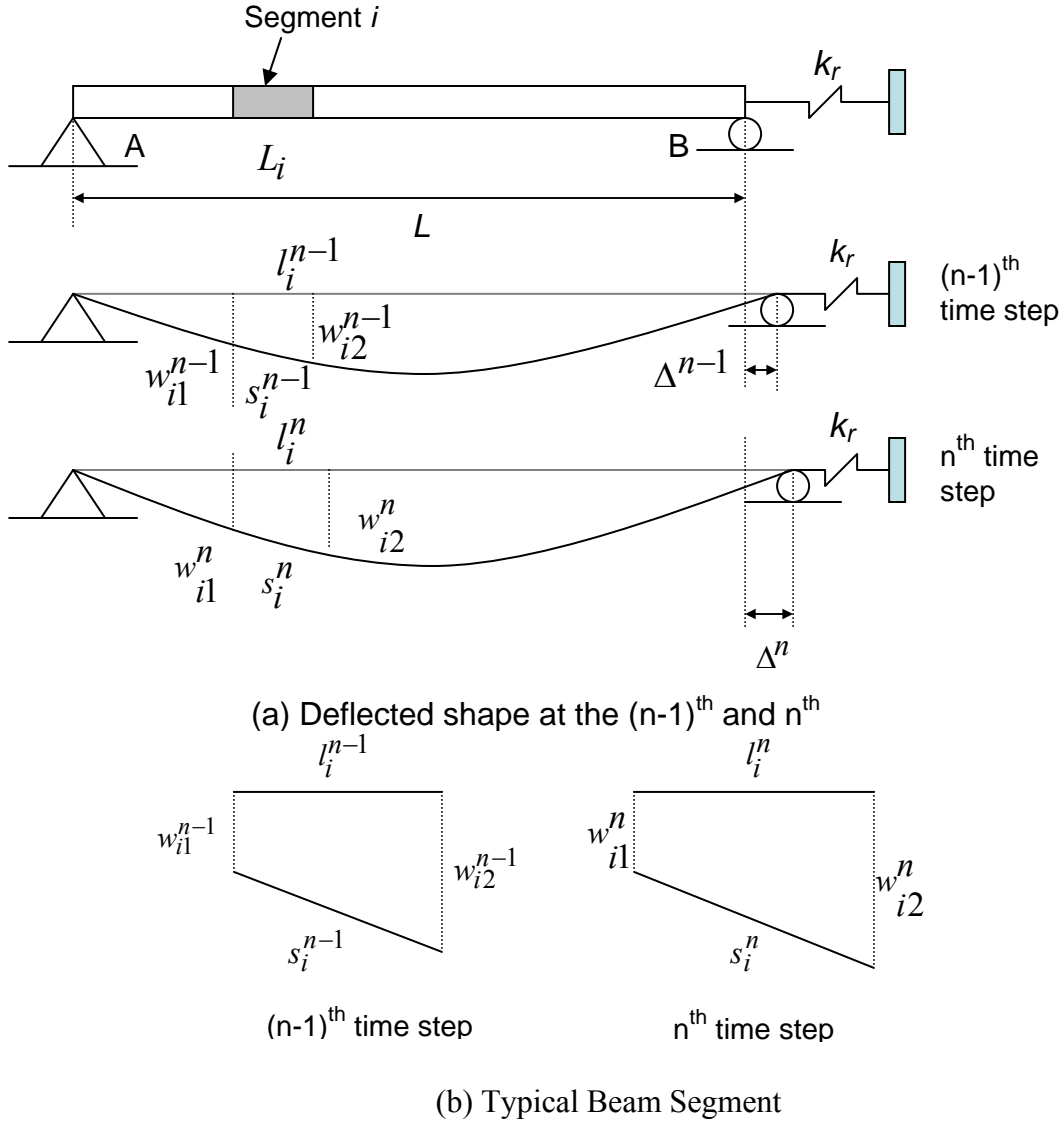


Figure 4.6: Illustration of axial restraint force calculations

4.3.4 Generation of Moment-curvature ($M - \kappa$) Relationships

The $M - \kappa$ generation, at elevated temperatures, is carried out using the same rectangular network described above and shown in Figure 4.1 (c). Once the bond-slip and axial restraint force in the beam is computed, the $M - \kappa$ relationships are generated through an approach analogous to the method used for the analysis of prestressed concrete beams. In this approach, $M - \kappa$ relationships are established by iterating the total top strain ($\varepsilon_{c,T}$) and the curvature (κ).

At the beginning of the analysis, values for curvature and total top strain (in concrete) are assumed, as shown in Figure 4.3(a). Then, the total strain in each of the concrete elements, steel reinforcement and FRP is computed from the assumed strain and curvature. Constitutive laws of materials are used to determine stresses in concrete, steel reinforcement and FRP. Once the stresses are known, then the forces in concrete, steel and FRP are computed. The curvature is then iterated until equilibrium of forces is satisfied (internal force equal to the fire induced axial restraint force). Once the equilibrium is satisfied, the moment and the corresponding curvature are calculated. Thus, the values of moment and curvature are stored to represent a point on the $M-\kappa$ curve.

The value of the total top strain is incremented to generate subsequent points on the moment curvature curve. This procedure is repeated for each time step of fire exposure. The generated $M-\kappa$ curves are used for tracing the behavior of the FRP-strengthened RC beam through nonlinear structural analysis. The generation of $M-\kappa$ relationships is an important part of the numerical model since these relationships form the basis for the fire resistance analysis of the beam.

4.3.5 Beam Analysis

4.3.5.1 Stiffness Approach

The moment curvature relationships generated for various segments are used to trace the response of the beam exposed to fire. At each time step, the beam analysis is carried out by utilizing updated secant stiffness of various segments. The secant stiffness for each segment is determined from the moment-curvature relationships, based on the moment level reached in that particular segment.

Following the generation of $M-\kappa$ relationships, an iterative procedure described by Cambell and Kodur (1990) is employed to evaluate deflections of the beam at each time step.

The beam analysis starts under a unit applied load using initial rigidity (EI_o) and the moment and corresponding curvature in each beam segment is determined. The segment that has the maximum moment is selected as the critical (key) segment of the beam. Then, a target curvature in the key beam segment is selected on pre-generated $M - \kappa$ curve. Utilizing unit load analysis, a scaling factor is evaluated by dividing the target curvature with unit load curvature in the key segment. The unit load curvatures in all beam segments are scaled by multiplying them with the by this scaling factor. An iterative procedure, illustrated in Figure 4.3(b) and (c), is employed till convergence of secant rigidity within a certain tolerance is achieved. Once tolerance is achieved, the above procedure is repeated for next assumed target curvature (Dwaikat 2009). After each iteration procedure, load required to attain target curvature (key segment) is computed and stored. To compute the actual curvatures and deflections in the beam, applied load is interpolated between these stored values. The flow chart explaining the procedure is shown in Figure 4.7.

In the above procedure, stiffness matrix and the loading vector are computed for each longitudinal segment and assembled in the form of a nonlinear global stiffness equation, and solved to compute deflections at that time step:

$$[K_g] [\delta] = [P] \quad (4.38)$$

where: K_g = global stiffness matrix, δ = nodal displacements, $P = P_f + P_s$ where P_f = equivalent load vector due to applied loading and P_s = equivalent nodal vector due to $P - \delta$ effect.

The effect of the second order moments, developed due to the axial restraint force, is calculated using the following equation:

$$[P_s] = -[K_{geo}] [\delta] \quad (4.39)$$

where: $[K_{geo}]$ = geometric stiffness matrix, $[\delta]$ = nodal displacements, and $[P_s]$ = equivalent nodal load vector due to $P - \delta$ effect.

4.3.5.2 Failure Limit States

In the analysis, various parameters, including cross sectional temperatures, stresses, deflections, and moment capacity are generated at each time step. These parameters are used to evaluate failure of the beam. ASTM E119 specifies thermal and strength limit state as failure criteria for beams. In addition, British Standard BS 476-10 (BSI 2009) specifies deflection criterion as failure limiting state. Furthermore, in FRP-strengthened structures the properties of FRP degrade with temperature. Glass transition temperature of FRP is often considered as a measure of determining the effectiveness of FRP in beams. Therefore, in the model the temperature of FRP (T_g) can be used as a possible failure limit state. The following limiting criteria have been incorporated in the model to determine the failure of the FRP-strengthened RC beam:-

In the model, any or all of the following limiting criteria can be applied to evaluate failure of the FRP-strengthened RC beam:-

- The moment due to applied load exceeds the strength capacity of the beam.
- The temperature in reinforcing steel (tension reinforcement) exceeds 593°C .

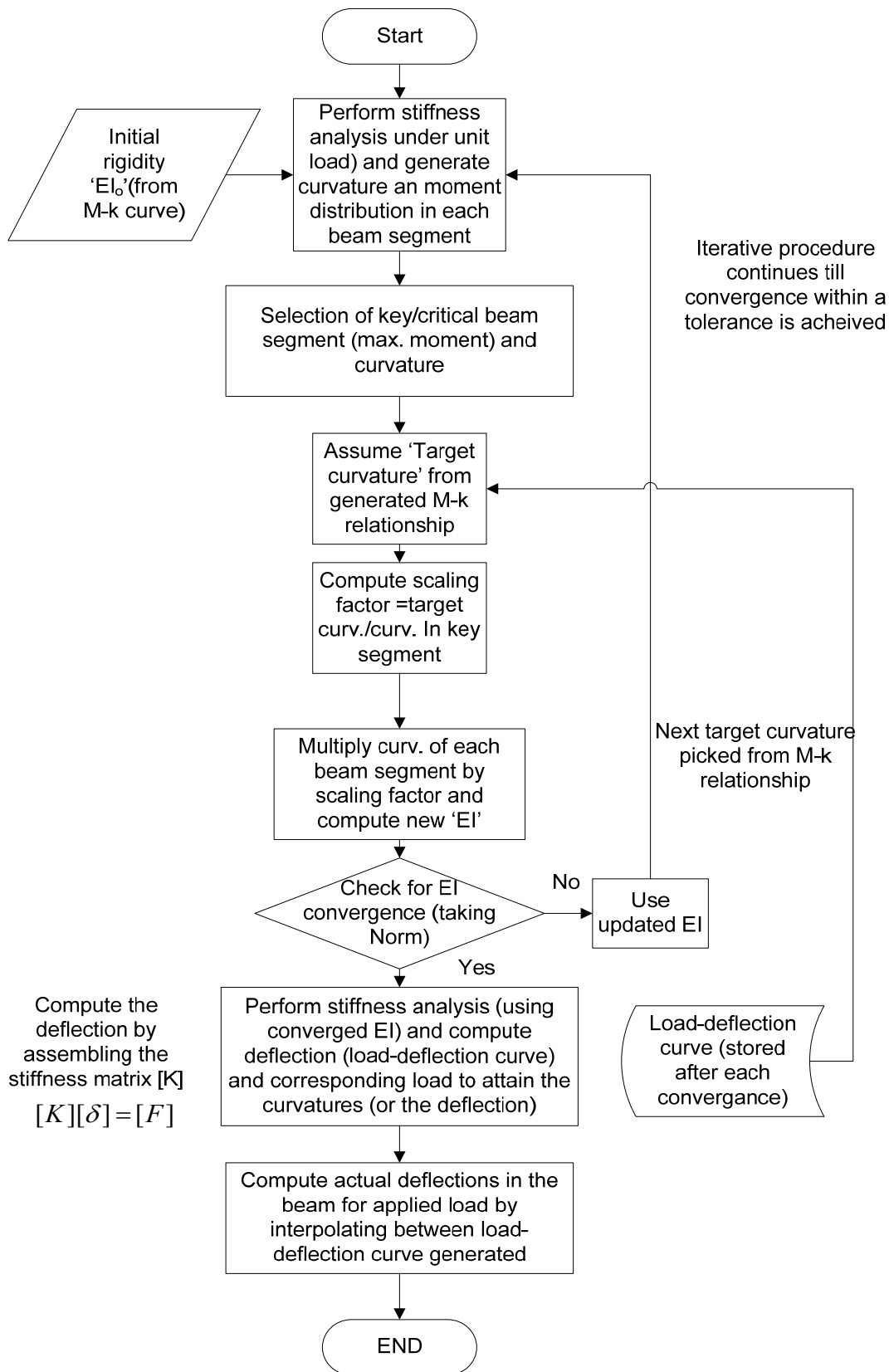


Figure 4.7: Flow chart illustrating the steps associated of iterative procedure

- The deflection of the beam exceeds $L / 20$, where L is the length of the beam, at any fire exposure time.
- The rate of deflection exceeds the limit $L^2 / 9000d$ (mm/min) where L is the length of the beam (mm); and d , effective depth of the beam (mm).
- The temperature in FRP layer exceeds glass transition temperature (T_g) of FRP.

It should be noted that the user has the option to specify any (or all) of the five limit states to define failure.

4.4 Computer Implementation

4.4.1 Computer Program

To facilitate large computations involved in numerical procedure described in Section 4.3 and 4.4, computer program has been developed using FORTRAN language. This program takes into account the iterative approach required for computations. The flow chart explaining this numerical procedure is shown in Figure 4.2.

4.4.2 Beam Idealization

The numerical procedure involves idealization of FRP-strengthened RC beam in longitudinal beam segments. For hydro-thermal and mechanical analysis, the cross-section of the beam is idealized as a mesh of elements as shown in Figure 4.1(b). The number of longitudinal segments and the number of elements and the grid size in each direction must be specified in the input file. The program allows for non-uniform grid size in the cross-sectional mesh. The program determines the element size based on the specified number of elements. The program also allows for any rebar configuration. However, the section must be symmetrical around the vertical centroidal axis, since the model cannot account for the development of torsional forces due to non-symmetrical geometry.

4.4.3 Material Properties

For modeling the response of FRP-strengthened beams, high temperature properties of concrete, steel, FRP and insulation are required. These properties include thermal, mechanical and deformation properties which vary as a function of temperature. There is reliable data on high temperature properties of concrete and steel. However, only limited knowledge of high temperature properties of FRP and insulation exists. In the following sections, the constitutive models that have been inbuilt into the numerical model for thermal and structural analyses are presented. A detailed discussion on mechanical and thermal properties of each constitutive material has been included in Chapter 2 and 3. The selection of the constitutive models that will be used in the analysis (as presented in Chapter 5) is based on the material type used for fabrication (like aggregate type with moisture content measure at time of testing) and mechanical and thermal properties of specific material used for strengthening and insulating beams.

4.4.3.1 Concrete

Three sets of concrete properties suggested by Eurocode 2 (2004), the ASCE Manual (Lie 1992), and Kodur et al. (2004), as discussed in Chapter 2 (Section 2.4.2), have been incorporated into the program. In addition, the program allows for general material properties read from other input files where the material properties should be presented in a tabular format as a function of temperature. The user can specify any of the material models in the input file. The user also has the option of selecting either siliceous aggregate concrete or carbonate aggregate concrete. Relevant formulae for both mechanical and thermal properties of concrete as a function of temperature are built into the program. In the input file the user has to specify the 28-day compressive strength of concrete, initial moisture content, initial concrete permeability, tensile strength of concrete, concrete model (Eurocode, ASCE, or Kodur), and the type of aggregate in the concrete.

4.4.3.2 Steel Reinforcement

The mechanical properties of reinforcing steel (stress-strain-temperature relationships) given in the ASCE Manual (Lie 1992) and in Eurocode-2 (2004) have been incorporated into the program. In addition, the program also allows for general stress strain relationships as a function of temperature, which can be input into the program in a tabulated form. For a selected ASCE or Eurocode model, yield strength of steel is provided as input parameter to the program that uses the built-in stress-strain-temperature relationships.

4.4.3.3 FRP and Insulation Material

As previously illustrated in the literature review (Chapter 2), very limited data on high temperature material properties of FRP and insulation are available. In the current model, high temperature material properties of FRP's (carbon-, glass-, and aramid-, fiber reinforced polymers) and insulations (Tyfo Vermiculite-Gypsum (VG), Promatect calcium silicate boards and Tyfo WR AFP system) have been incorporated in the model. For VG insulation and calcium silicate boards, constitutive relationships which are based on semi-empirical relationships suggested by Bisby (2003) and accounts for variation of strength and stiffness as a function of temperature for unidirectional FRP composites, have been included in the model. Thermal properties of new insulation system (Tyfo WR AFP system) used for fire protection of the test beams were obtained from high temperature material testing at MSU. The details are discussed in Chapter 3. It should be noted that the model cannot account for mechanical properties (bond strength) of the insulation which are required to predict its delamination (falling off) since there is lack of data availability at room as well as at elevated temperatures. In addition, the model can be easily extended to account for other types of FRP and insulation materials provided thermal property data are available at room as well as elevated temperatures.

4.4.3.4 Input Data

The basic input for the program consists of cross-sectional properties, material properties, and general data such as the number of time increments. The sequential order of the input data must be followed. Consistent units must be used throughout.

4.4.3.5 Output Results

The output from the program includes the results from the hydro-thermal and structural analyses. At each incremental time step, the temperature at each elemental node is computed. The output results also include the $M-\kappa$ curves. In addition, the deflection of the beam and the rate of deflection are also recorded for each time step.

4.5 Summary

A numerical model was developed for tracing the response of FRP-strengthened RC beams exposed to fire. The three stages associated with the fire resistance analysis, namely; fire growth, thermal, and structural analysis, are explained. Equations governing the hydro-thermal and mechanical analyses are derived. The proposed macroscopic FE model accounts for high temperature material properties, various fire scenarios, fire induced bond degradation in FRP, axial restraint effect, geometrical nonlinearity, and different high temperature strain components. In the nonlinear beam analysis, the model uses a curvature controlled iterative procedure in which the softening of the beam is accounted for. This numerical procedure was incorporated into a computer program and the program is capable of tracing the response of rectangular, T or I RC beams strengthened with FRP. The validity of the computer model will be established in the following chapter.

CHAPTER 5

MODEL VALIDATION

5.1 General

In this chapter, the validity of the computer model, presented in Chapter 4, is established by comparing predictions from the model with data from fire tests. The validation process covered response parameters from both thermal and structural analysis. The validation was carried out using data from the fire tests on FRP-strengthened RC beams that are published in the literature, as well as from fire tests conducted as part of the current research. The response parameters covered in validation include cross sectional temperatures in FRP, rebars, insulation and concrete, mid-span deflections, debonding of FRP and fire resistance. In addition to validation, an FRP-strengthened RC beam designated as Beam I, has been analyzed to illustrate the usefulness of the program and to discuss various trends, in tracing the fire response of a typical FRP-strengthened RC beam in the entire range of loading up to collapse under fire exposure.

5.2 Typical Response of FRP-strengthened Beam

5.2.1 Details of the Beam

A beam was analyzed using the computer program to illustrate the behavior of fire exposed FRP-strengthened RC beam. The details of the beam, including geometric and material

properties are summarized in Figure 5.1 and Table 5.1. The RC beam is strengthened with 2 mm thick CFRP laminate and has 20 mm thick insulation at the beam soffit extending on two sides of the beam up to 105 mm height (measured from the soffit insulation thickness), as shown in Figure 5.1. The beam has a uniformly distributed load of 60 kN/m which represents a load level of 52% of its strengthened capacity. The load ratio is defined as the ratio of the applied loading during the time of fire to the capacity at room temperature. The high temperature material properties for concrete and steel are assumed to follow that specified in ASCE manual (Lie 1992) while for FRP and insulation, the properties suggested by Bisby (2003) have been utilized. For hydro-thermo-mechanical analysis, the beam is idealized into a number of longitudinal segments along its span length. Each segment is further idealized into a mesh of elements (see Figure 5.1(c) and (d)). The beam is exposed to ASTM E119 standard fire (2007) and fire resistance analysis is carried out by incrementing exposure time at every 5 minutes. Results from the analysis are used to illustrate the response of a typical FRP-strengthened RC beam (refer to Figures 5.2 through 5.10).

5.2.2 Thermal Response

Figure 5.2 shows temperatures at various cross-sectional locations of the beam as a function of fire exposure time. As expected, the predicted temperatures in FRP, rebars and concrete decreases with increasing distance from the fire-exposed side. The low thermal conductivity and high heat capacity of insulation keeps the temperatures in FRP and steel rebars quite low. The analysis shows that the concrete temperature at mid-depth of the section remains relatively low throughout the fire exposure. This is due to the low thermal conductivity and high thermal capacity of concrete. Figure 5.2 shows that the temperature in the corner rebar is higher than that in the inner (central) rebar throughout fire exposure time. This trend can be attributed to

the fact that the corner rebar is exposed to fire from two faces, the bottom and the side faces of the beam cross section, while the inner rebars experience heat transfer only from the bottom face.

Externally bonded FRP-strengthened RC members are bond-critical applications and the bond strength is particularly important for evaluating the structural fire response. The temperature rise at FRP/concrete interface serves as an indicator for potential loss of bond between FRP and concrete. The bond properties are sensitive to even a modest increase in temperature and bond strength degrades significantly when the temperature exceeds the glass transition temperature of the adhesive (matrix). The temperature rise at the interface depends on the thermal properties of insulation (thermal conductivity) and the insulation thickness. Figure 5.2 shows that the temperature at FRP/concrete interface reaches the glass transition temperature at about 40 minutes ($T_g = 81^\circ\text{C}$)

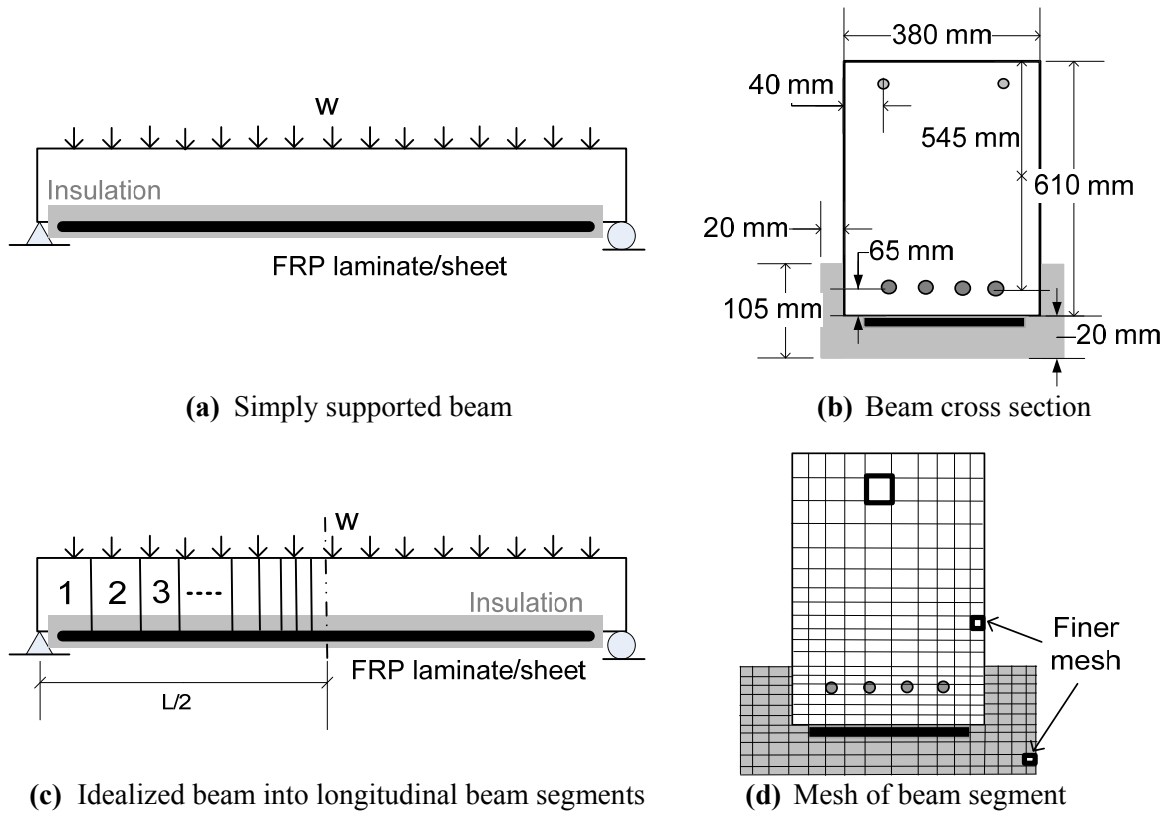


Figure 5.1: Beam elevation and cross section details

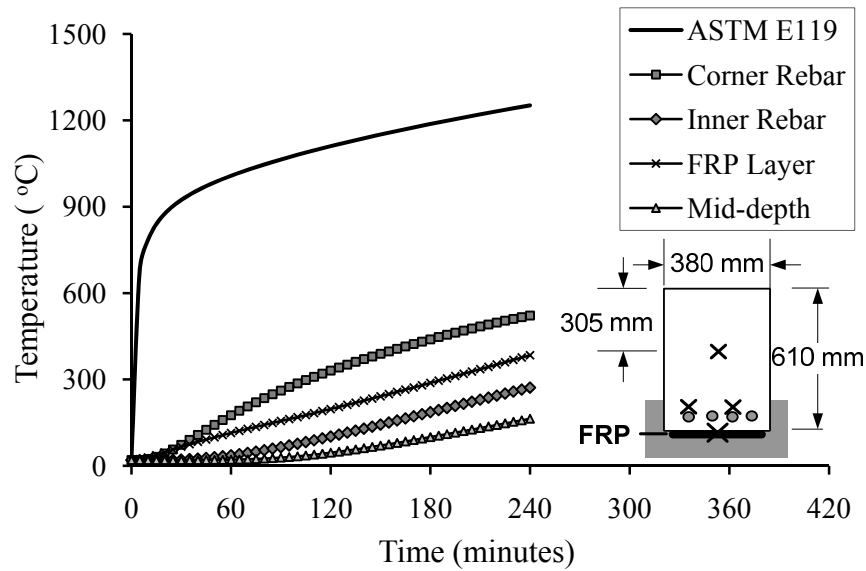


Figure 5.2: Temperatures at various locations in the beam as a function of fire exposure time

Table 5.1: Summary of properties for beams used in the fire resistance analysis

Property		Beam I	Beam II & III	Beam IV	Beam V to VIII
Description		Typical FRP-RC beam	Tested by Blontrock et al. (2000)	Tested by Williams et al. (2008)	Tested at MSU
Cross Section (mm)		380×610	200×300	Flange: 1220×150 Web: 300×250	254×406
Length (m)		6.7	3	3.9	3.96
Reinforcement	Top	$2 \times 15.8 \text{ mm}$	2 bars $\phi 10 \text{ mm}$	-	$2 \times 12.7 \text{ mm}$ (#4 bar)
	Bottom	$4 \times 25 \text{ mm}$	2 bars $\phi 16 \text{ mm}$	$2 \times 20 \text{ mm}$	$3 \times 19.05 \text{ mm}$ (#6 bar)
$f'_c \text{ (N/mm}^2\text{)}$		38	57.5	41	58.2
$f_y \text{ (N/mm}^2\text{)}$		414	591		413
Applied loading		60	$2 \times 40.6 \text{ (kN)}$	34 (kN/m)	$2 \times 70 \text{ (kN)}$
Concrete cover thickness (mm)		40	25	40	53.6
Aggregate type		Carbonate	Siliceous	Carbonate	Carbonate
Structural discretization (number of segments)		40	20	-	40
FRP type		CFRP	Sika carbodur S1012	SCH-41 (CFRP)	CFRP
FRP thickness (mm)		3	1.2	1.0	2
FRP ultimate tensile strength (kN/mm ²)		0.65	2.8	0.74	3.76
FRP Modulus of Elasticity (kN/mm ²)		38.6	165	72.4	230
Rupture strain (mm/mm)		1.7%	1.7%	1.2%	1.7%

Table 5.1 (cont'd)

Insulation thickness (mm)	20	25	38	25
Insulation type	VG-EI-R	Promatect - H	Vermiculite-gypsum (VG)	Vermiculite-gypsum (VG)
*Insulation thermal conductivity (W/m-°K)	0.0815	0.175	0.0815	0.0815

* at room temperature

5.2.3 Structural Response

5.2.3.1 *Moment-curvature Relationships*

For beam, the structural response can be gauged by looking at the moment-curvature relationships as a function of fire exposure time. The moment-curvature curves, generated at various time steps for a representative segment in FRP-strengthened RC beam, are shown in Figure 5.3. At early stages of fire exposure (up to about 30 minutes), the bending moment increases with curvature till certain a curvature and thereafter, the moment drops, and this is mainly due to the rupture of FRP. At ambient temperature, this moment drop is not captured since the concrete crushes prior to the rupture of FRP. The percentage drop in the moment capacity after rupture of FRP decreases with increasing fire exposure time. This can be attributed to the rapid loss of strength and stiffness of FRP at elevated temperatures which reduce its contribution towards the moment capacity of the beam. The ultimate curvature of the beam increases with temperature due to the higher deterioration in the strength and stiffness properties of the constituent materials. The beam behaves as un-strengthened RC beam after FRP loses all its strength and does not contribute towards the moment capacity. It should be noted that the moment capacity of the strengthened beam at room temperature (735 kN-m) is slightly higher (12%) than the calculated capacity based on ACI 440.2R-08 (2008) provisions (without taking

into account the additional reduction factor $\psi = 0.85$ for bending strength contribution by FRP). This can be attributed to strain hardening effect of the steel reinforcement which is accounted for in the model (Dwaikat 2009). This effect is not taken in to account in ACI design equations.

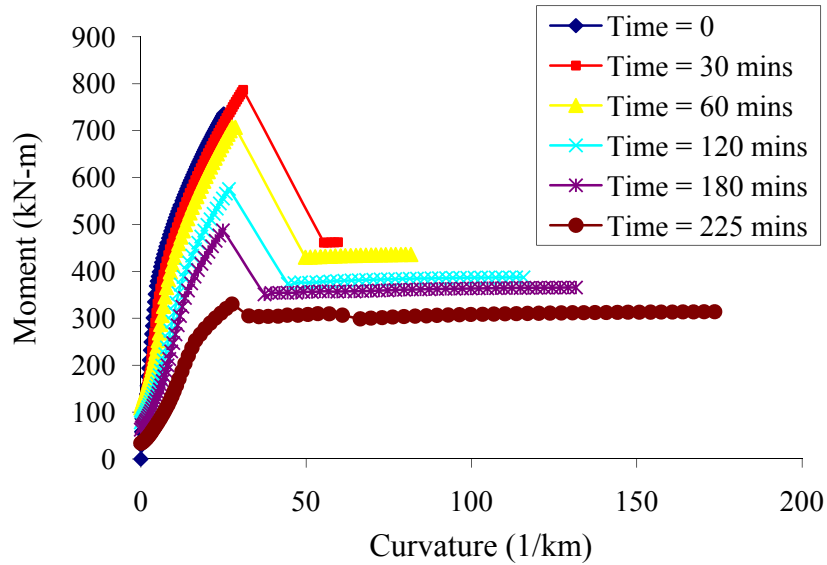


Figure 5.3: Moment-curvature curves at various times for Beam-I under fire exposure

5.2.3.2 Moment Capacity and Deflections

The variation of mid-span deflection and moment capacity are plotted as a function of fire exposure time in Figure 5.4. The trends in Figure 5.4 indicate that there is a slight increase in moment capacity for early stages of fire exposure followed by its degradation. This slight increase in the moment capacity results from full utilization of the bonded length of FRP at the beam soffit. The cross sectional temperatures of the beam increase with fire exposure time, particularly in the upper part of the beam cross section since the two surfaces of the beam are exposed to direct heat flux in absence of any fire protection. This results in a rapid loss of concrete strength and stiffness properties. Correspondingly, the beam curvature increases with the fire exposure time under a constant applied load. This increase in curvature introduces an even distribution of strain in FRP. This uniform strain distribution results in an increase in the

tensile force in FRP which leads to a slight increase in the moment capacity. However, strength and stiffness properties of constituent materials (FRP, concrete and reinforcing steel) degrade significantly with the increasing temperature, and this results in a reduction in the moment capacity of the beam with an increase in the mid-span deflection, as shown in Figure 5.4.

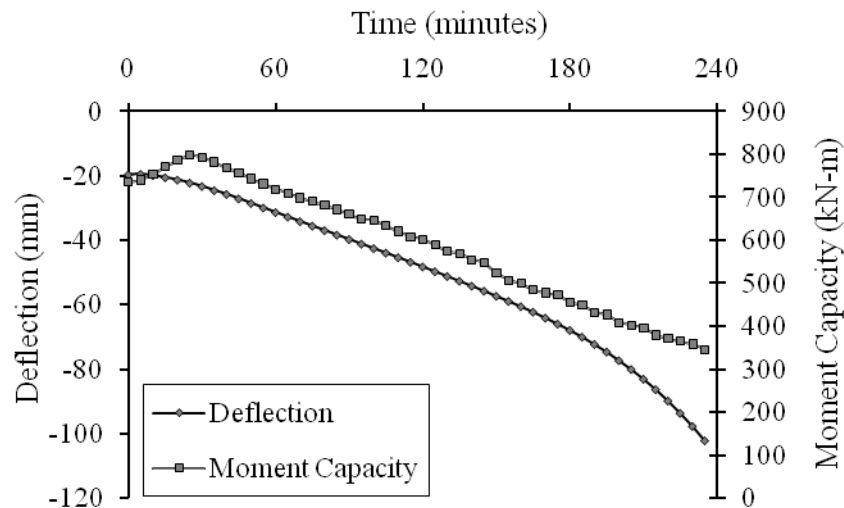


Figure 5.4: Moment capacity and deflection of FRP-RC beam as a function of fire exposure time

The fire resistance of the beam is evaluated by applying five failure criteria as discussed in Chapter 4, Section 4.6.2. The predicted fire resistance based on the critical temperature in the steel (corner) rebar is 315 minutes. However, based on the strength limit state, the failure occurs in 225 minutes. The deflection failure limit state did not govern since the insulation delays the degradation of strength and stiffness of reinforcing steel and FRP, and this result in a relatively lower deflection.

5.2.3.3 Bond Degradation

To illustrate the effect of bond degradation at FRP-concrete interface on fire response, Beam I was analyzed under three cases of possible bond namely; with perfect bond, with temperature induced bond degradation and with a plain RC beam. Figure 5.5 show a comparison

of time-deflection response for two cases of FRP-strengthened RC beams, namely; with perfect bond, with temperature induced bond-slip, and the case of an un-strengthened RC beam with no externally applied fire protection. It can be seen that the response of both strengthened beams (with and without accounting for bond degradation) is stiffer as compared to the un-strengthened RC beam, and this is due to high strength and stiffness properties provided by FRP composite. For the un-strengthened RC beam, the rate of deflection is much higher because the mechanical properties of concrete and steel degrade faster in the absence of any external fire protection. For the strengthened beam with a perfect bond, the response primarily depends on the high temperature properties of FRP. The strength properties of FRP, used for flexural strengthening of the analyzed beam (Beam I), only degrade when the temperature is above the range of 250-300°C, as shown in Figure 5.6. The externally applied insulation limits the rise in temperature of FRP. Therefore, the contribution of FRP towards the capacity of the strengthened beam is for longer time which results in lower mid-span deflections.

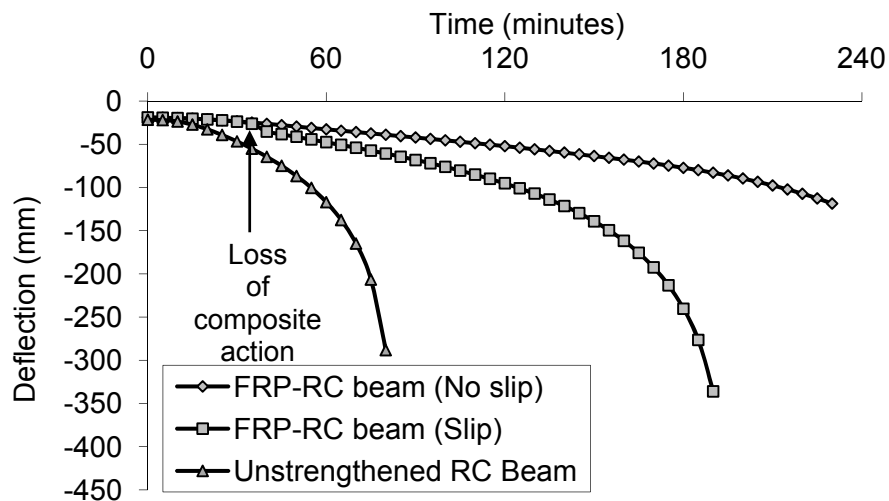


Figure 5.5: Deflection of FRP-strengthened and RC beam as function of fire exposure time

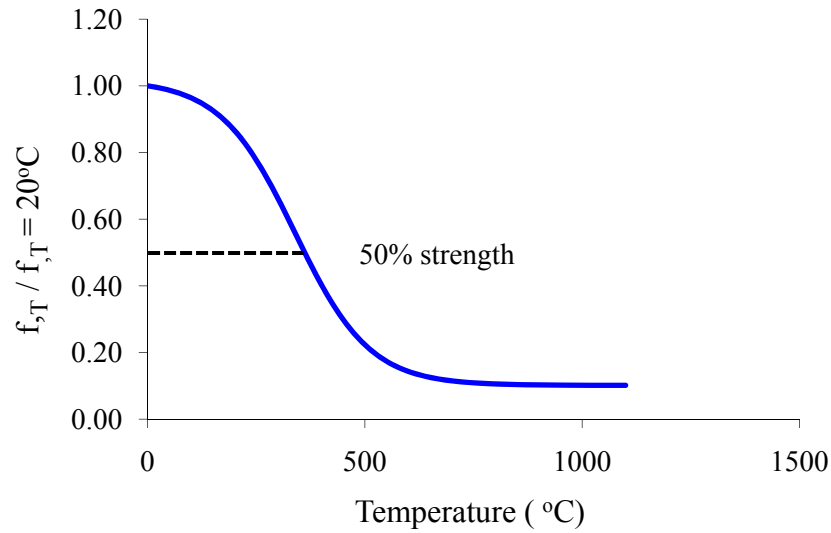


Figure 5.6: Ultimate tensile strength (f_T) of CFRP as a function of temperature

Analysis of similar a beam, with accounting for bond degradation at FRP/concrete interface, shows that the FRP debonded at around 40 minutes when the temperature at bond interface exceeded the glass transition temperature of the adhesive (T_g of adhesive is 81°C), as shown in Figure 5.7. The bond properties of the adhesive degrade with increasing temperature, and this result in a relative slip between FRP and concrete. Due to this bond-slip, the force transfer from concrete to FRP reduces as compared to a perfect bond case. Figure 5.5 illustrates that this effect of bond-slip appears at about 25 minutes, when the temperature at bond interface is 46°C , and full debonding of FRP occurs at 40 minutes. At this stage, stiffness of the beam decreases significantly and the beam behaves as an insulated and un-strengthened RC beam since the contribution of FRP to the beam capacity is zero. This results in an increase in rate of deflection of the beam. However, this increase in deflection is smaller when compared to an un-strengthened and un-insulated RC beam. This is mainly due to the beneficial effect of the insulation which slows the temperature rise in steel reinforcement, which mainly contributes to

resist the applied load on the beam after the FRP is lost. Therefore, strength and stiffness degradation in steel reinforcement is gradual and this leads to a lower deflection, at a given time.

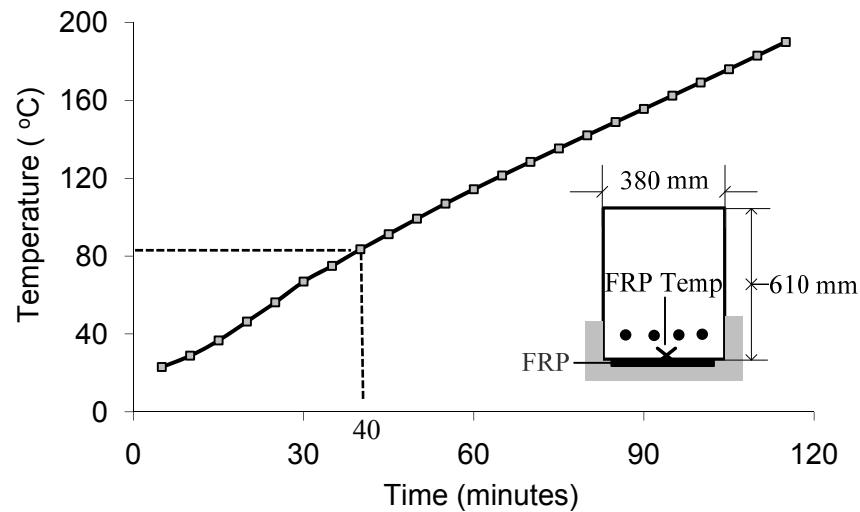


Figure 5.7: Temperature variation at the interface of FRP-concrete interface as a function of fire exposure time

Effect of bond-slip on the strength of FRP-strengthened RC beams is further illustrated in Figure 5.8 where the variation of moment capacity is plotted as a function of time for two cases of bond. In both of the cases, the behavior of the beams is identical in the early stages of fire exposure (up to 30 minutes) when there is an abrupt decrease in the moment capacity of FRP-strengthened beam that accounts for bond degradation. This sudden drop represents the debonding of FRP. In case of the FRP-strengthened RC beam with a perfect bond, the moment capacity decreases almost linearly since strength and stiffness of FRP degrade gradually with temperature.

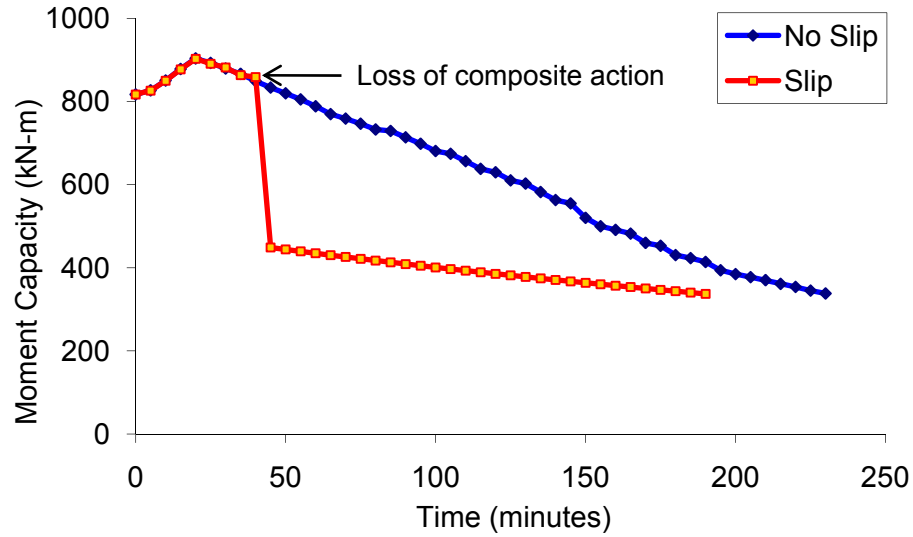


Figure 5.8: Moment capacity of FRP-strengthened and RC beam as function of fire exposure time

The variation of interfacial shear stress and strain (bond-slip) distribution over half the span of the beam for various fire exposure times is presented in Figures 5.9 and 5.10. It can be noticed that the peak interfacial shear stress and strain (ϵ_{slip}) occur in the vicinity of FRP termination zone (edges) and are relatively more uniformly distributed far from FRP ends (towards mid-span of the beam). As expected, shear stresses predicted at the FRP end are zero and match the free surface stress condition. As the temperature at the interface increases with fire exposure time, the maximum interfacial shear stress and corresponding strain (ϵ_{slip}) also increase towards the FRP end. These increasing shear stresses contribute to debonding of FRP when its magnitude exceeds decreasing shear capacity of the adhesive with temperature. Also, with increase in temperature, strain distribution along the bonded length of FRP becomes more uniform which can be attributed to the reduction in stiffness of the adhesive with temperature. As the temperature in FRP exceeds the glass transition temperature, the strain in FRP increases significantly ultimately leading to debonding of FRP (refer to Figure 5.9).

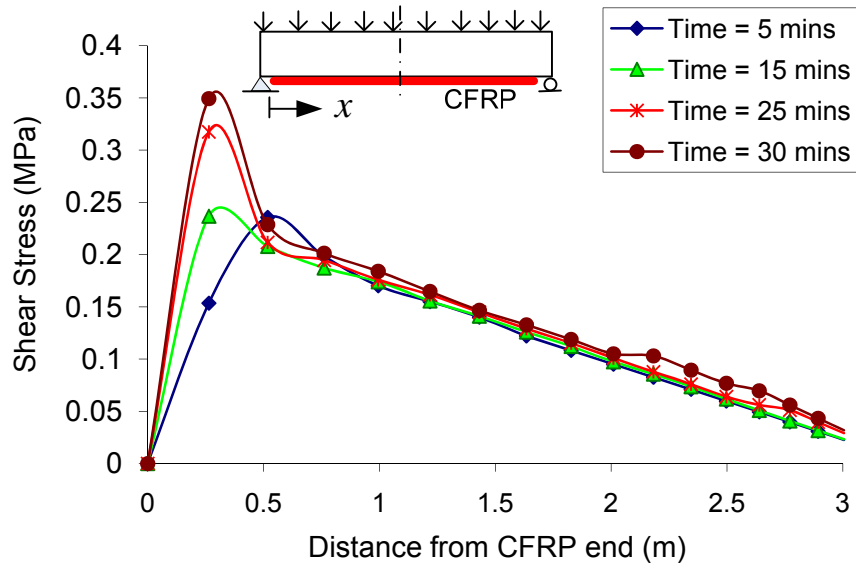


Figure 5.9: Variation of interfacial shear stress as a function of fire exposure time

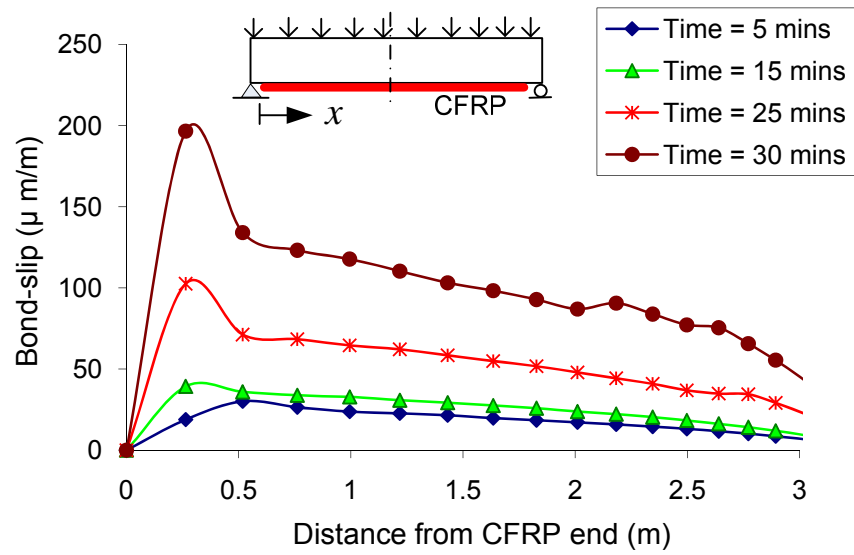


Figure 5.10: Slip distribution for mid span of the beam as a function of fire exposure time

5.2.4 Summary

FRP-strengthened RC beams experience significant degradation in moment capacity and stiffness when the temperature at FRP-concrete interface exceeds glass transition temperature. FRP-strengthened RC beam protected with insulation, attains lower deflection under fire conditions as compared to an un-strengthened RC beam, due to the beneficial effect of external insulation which slows the temperature rise and strength loss in steel reinforcement. The adhesive loses its strength and stiffness with temperature, and composite action between FRP and concrete is lost when the temperature approaches glass transition temperature. At this point, results show an abrupt decrease in the moment capacity of FRP-strengthened beam that accounts for bond degradation. However, for FRP-strengthened beam with a perfect bond, the moment capacity of the beam decreases almost linearly since strength and stiffness of FRP degrade with temperature.

5.3 Validation Against the Test Data

The validity of the numerical model is established by comparing predictions from the model with test results published in the literature and against results from fire tests conducted as part of the current research. From the literature, two beams that were selected for the validation are rectangular FRP-strengthened RC beams tested by Blontrock et al. (2000) while the third beam is a T-beam tested by Williams et al. (2008). The remaining four beams are the specimens tested as part of this study.

5.3.1 Blontrock et al. Test Beams

The two beams, designated as Beam II and III, were simply supported (not axially restrained) and tested under ISO 834 standard fire exposure. Both of the beams had a cross section of 200×300 mm and a span length of 3 m, as shown in Figure 5.11. The beams had two

10 mm and 16 mm diameter rebars as top and bottom reinforcement respectively. Both beams were strengthened with CFRP (1.2 mm thick and 100 mm width) at the beam soffit and were insulated with Promatect-H type insulation. Beam II and III had 25 mm of insulation thickness at bottom of the beam, while for Beam III an additional 12 mm thickness of insulation was provided on the two sides of the beam that extended up to a height of 105 mm, as shown in Figure 5.11. The geometric and material properties of these beams are tabulated in Tables 5.1 and 5.2. Predicted results from analysis are compared with measured values in Figures 5.12 to 5.14. The length of the beam was idealized into 40 beam segments (keeping finer segment length near mid-span) and fire resistance of the beams is computed based on four failure criteria as discussed in Chapter 4.

Table 5.2: Material properties for Blontrock beams

Material	Property
Concrete	$f'_c = 58 \text{ N/mm}^2$; E_c (elastic modulus) = $34,825 \text{ N/mm}^2$
Steel	$f_y = 591 \text{ N/mm}^2$; E_s (elastic modulus) = $20,5000 \text{ N/mm}^2$ ϵ_u (ultimate strain) = 6.7%
Sika Carbodur S1012 (CFRP)	$f_u = 2800 \text{ N/mm}^2$; E_{frp} (elastic modulus) = $16,5000 \text{ N/mm}^2$ ϵ_u (ultimate strain) = 1.7%

For Beam II, Blontrock et al. have measured the corner rebar temperature and mid span deflection only, while for Beam III, temperature increase at FRP-concrete interface has also been reported. During the test on Beam II, the insulation had fallen off after 7 minutes of fire exposure, and thereafter, the interaction between FRP and concrete was lost. This effect was simulated in the analysis.

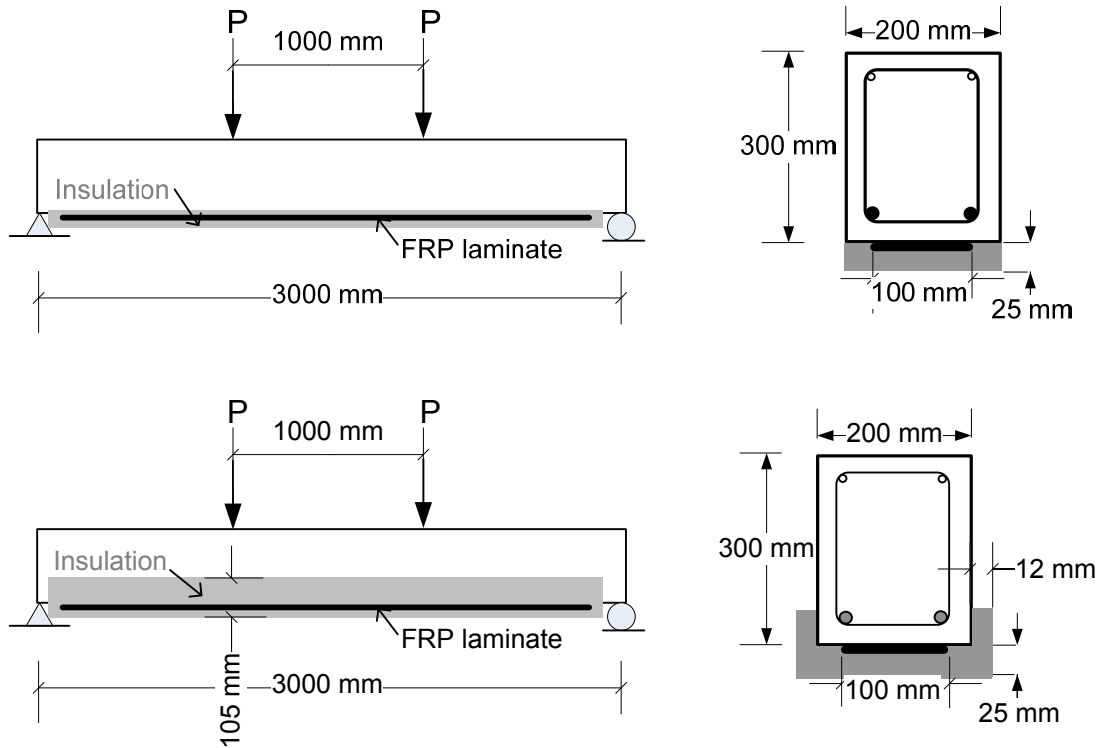


Figure 5.11: Elevation and cross section of beams tested by Blontrock et al.

Figure 5.12 shows a comparison between the predicted and the temperatures measured in steel reinforcement and mid-span deflection as a function of exposure time for Beam II. There is a good agreement between the predicted and the measured temperatures of steel reinforcement for the entire range of the test. In the test, deflections could not be recorded beyond 75 minutes of fire exposure time due to increase in rate of deflection just prior to the failure. For most part, the deflections computed by the model are in good agreement with measured values. The model predicts strength failure in the beam at about 85 minutes.

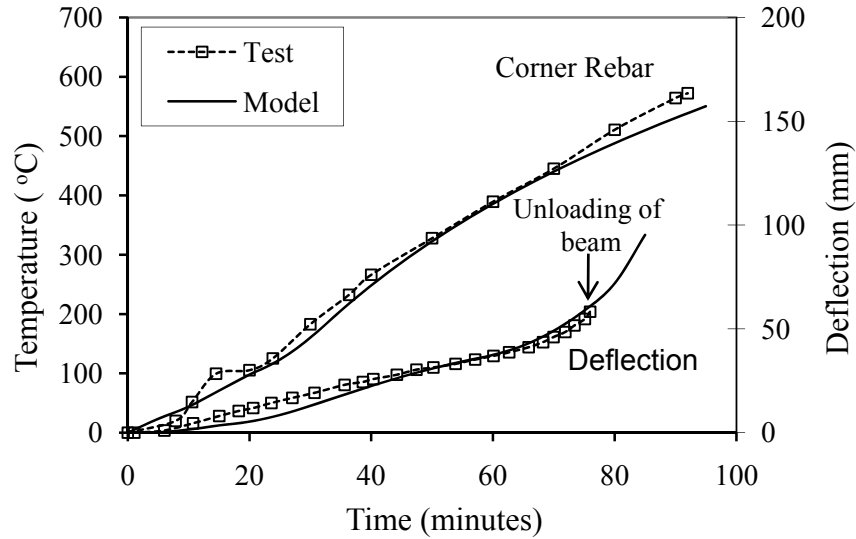


Figure 5.12: Measured and predicted rebar temperatures and mid-span deflection in Beam II

Results from the fire resistance analysis for Beam III have been compared with measured test data in Figures 5.13 and 5.14. Blontrock et al. (2000) reported loss of interaction between FRP and concrete after 26 minutes of fire exposure time while analyzing the test data. Figure 5.13 shows the comparison of the predicted and the measured temperature in steel reinforcement and at the interface of FRP/concrete, respectively. There is a good agreement between the predicted and measured values in the entire range of fire exposure. Predicted deflections are compared with the measured deflections in Figure 5.14. Analysis of the results indicates that debonding of FRP occurred at 30 minute of fire exposure time, and that is slightly higher than that reported by Blontrock et al. (26 minutes when the temperature at the interface was 52.1°C i.e., less than measured $T_g = 62^{\circ}\text{C}$). This can be attributed to a variation in bond properties used in the analysis as compared to actual properties. Nevertheless, over all model prediction of the beam deflection up to and beyond debonding point of the FRP, matches the measured test data closely.

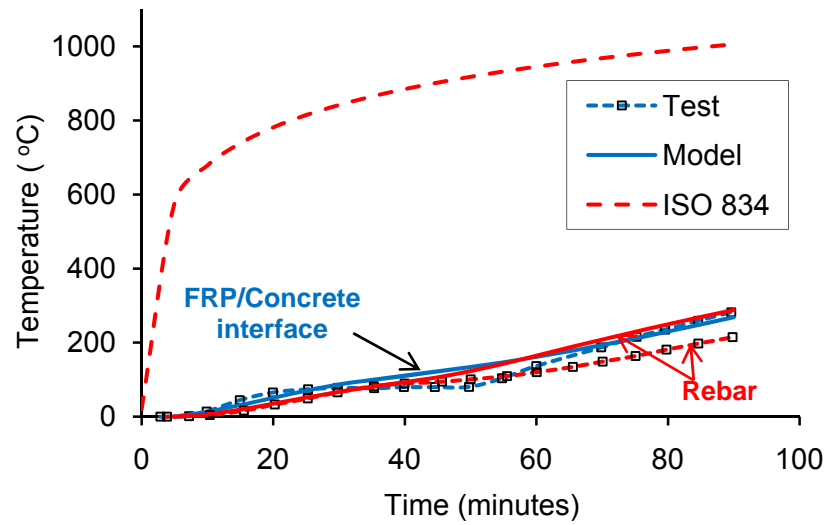


Figure 5.13: Measured and predicted temperatures at the interface of FRP/concrete and corner rebar for Beam III

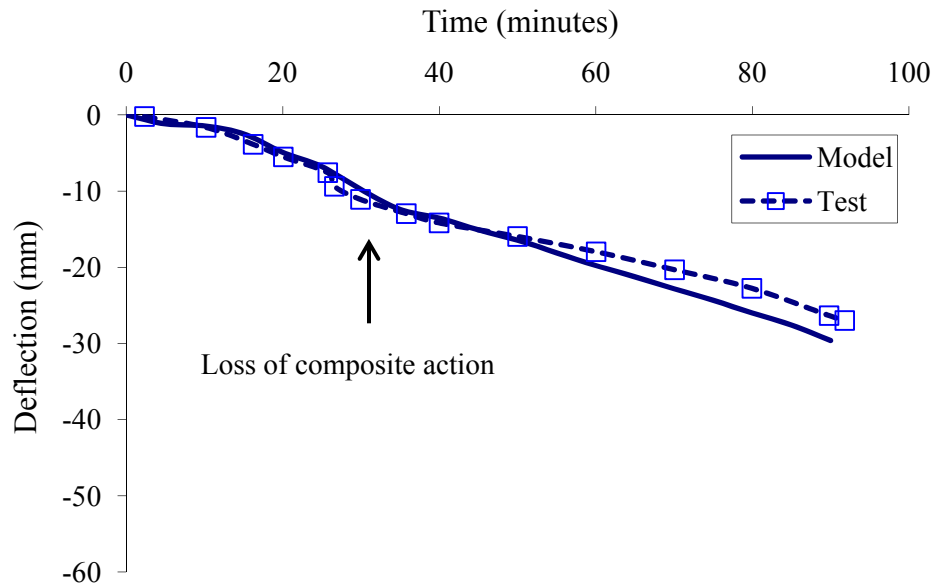


Figure 5.14: Measured and predicted deflection as a function of fire exposure time for Beam III

The above comparison indicates that the model is capable of tracing overall thermal and structural response of FRP-strengthened beams, including the effect of fire induced bond.

5.3.2 William et al. Tested T-Beam

The T-beam was tested in accordance with the ASTM E119 standard fire testing procedure under sustained service load. The overall length of the insulated T-beam was 3900 mm and 400 mm in depth. The flange width and web depth were 1220 mm and 300 mm, respectively. Two 20 mm diameter rebars were used as flexural reinforcement. The beams were strengthened with 100 mm wide CFRP layer. The beam was fire protected with 25 mm of VG insulation on the bottom as well as both sides of the web. The VG insulation extended to a distance of 125 mm under flanges as shown in Figure 5.15. The material properties, taken from the test data reported by Blontrock et al. and used in the analysis, are presented in Table 5.3.

Table 5.3: Material properties for T-beam

Material	Property
Concrete	$f'_c = 41 \text{ N/mm}^2$; E_c (elastic modulus) = $30,414 \text{ N/mm}^2$
Steel	$f_y = 450 \text{ N/mm}^2$; E_s (elastic modulus) = $20,0000 \text{ N/mm}^2$ ϵ_u (ultimate strain) = 0.2%
SCH-41 (CFRP)	$f_u = 745 \text{ N/mm}^2$; E_{frp} (elastic modulus) = $72,400 \text{ N/mm}^2$ ϵ_u (ultimate strain) = 1.2%

The measured and predicted temperatures at steel rebar, interface of FRP/concrete and unexposed top surface for the T-beam are shown in Figure 5.15. In addition, Figure 5.15 provides a comparison of temperatures measured in steel against temperature predicted by the model. Overall there is a good agreement between the predicted and measured values in the

entire range of fire exposure time. The model could not be validated against measured deflections in this test since the applied loading was lost during the test.

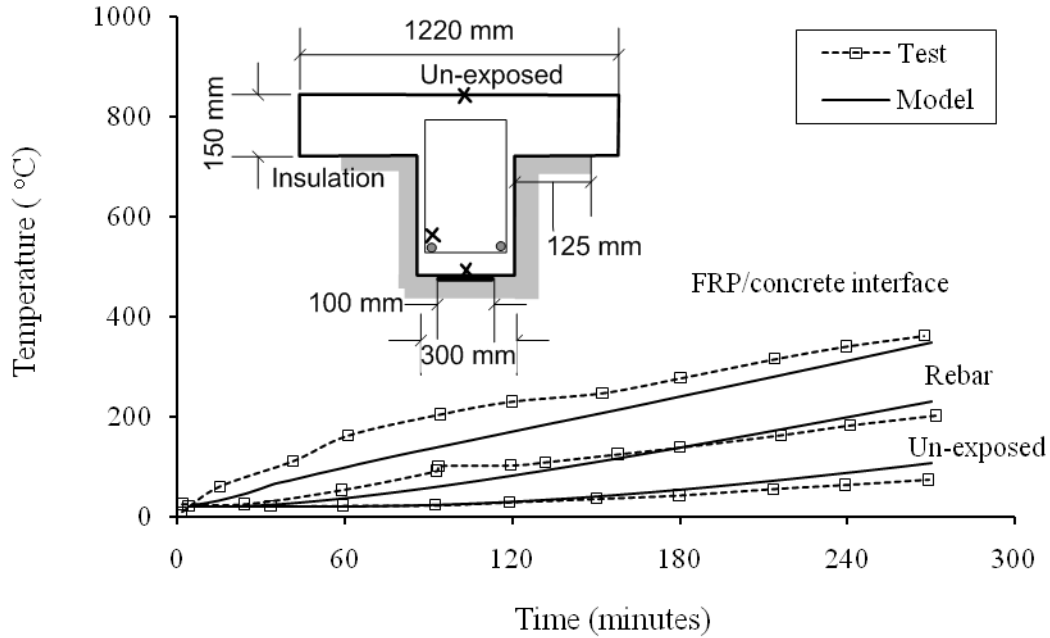


Figure 5.15: Measured and predicted temperatures at various locations in Beam IV

5.3.3 MSU Test Beams

Further validation of the numerical model was undertaken by comparing measured temperatures, deflections and axial restraint force in the fire tests conducted as part of the current research, with the model predictions. Two beams (Beams V and VI) were tested under design fire (with well defined decay phase), while the other two beams (Beams VII and VIII) under ASTM E119 standard fire exposure. The details about the beams characteristics and the fire scenarios is given in Chapter 3 and tabulated in Table 5.1. Each beam is analyzed under the corresponding fire scenario and end support conditions and the results are presented in Figures 5.16 through 5.20.

5.3.3.1 Thermal Response

Figure 5.16 and 5.17 provides a comparison of temperatures at FRP/concrete and FRP/insulation interfaces, and at three different locations (TC5, TC6 and TC9) in the beam cross section. TC5 represent the temperature in compression reinforcement, TC6 represent corner rebar temperature (flexural reinforcement) while TC9 is at the mid depth of beam cross section (203 mm), as shown in Figure 5.18. It can be seen in Figures 5.16 (a) to (d) that the measured and predicted temperatures are in a good agreement throughout the fire duration for all of the four beams.

Figures 5.17 (a) to (d) provides a comparison between predicted and measured temperatures at FRP/concrete and FRP/insulation interfaces. These temperatures are critical indicators of the performance of FRP under elevated temperatures. The model predicts temperature fairly well up to 40 minutes of fire exposure time. The model could not capture 100°C plateau observed in the test data. This plateau is most likely due to migration of the moisture present in the insulation towards the FRP/insulation interface (away from fire). This accumulated water consumes heat energy in evaporation and this effect was captured by thermocouple at FRP/insulation interface.

Beyond this point, the model under predicts temperature at FRP/insulation interface and over predicts FRP/concrete interface temperatures for all FRP-RC beams. This could be attributed to the fact that measured temperature at FRP/insulation interface increase rapidly after 40 minutes due to the localized burning of the epoxy as a result of cracks propagation in insulation. Due to this localized burning, measured temperatures are higher as compared to those predicted by the model. On the contrary, increase in temperatures recorded at FRP/concrete interface is slightly lower than those predicted by the model. This is because of formation of a

solid char layer as a result of thermal degradation of epoxy (pyrolysis process) that acts as a thermal barrier and restricts the heat flow. Model predictions for beam Beam VII does not match with the measured temperatures since a portion of insulation fell off when FRP delaminated around 38 minutes and the model could not account for falling-off of insulation. In beams Beam V and VI, the temperature rises to a maximum value and starts to drop. This drop is due to the cooling phase in time-temperature curve of the fire. Also, it is interesting to note that temperature rises moderately at mid-depth of concrete (TC9) as compared to TC5 (compression reinforcement) which is closer to the exposed side of the beam cross section. This can be attributed to low thermal conductivity of concrete. Similarly, temperature decreases slowly during the cooling phase since it takes longer time to dissipate heat energy from the inner portions (away from exposed surface) of the beam cross section. Overall, the model predicts temperature progression reasonably well. Compared to the measured time of FRP debonding which was around 20 minutes, the model predicts it to be about 25 minutes. This variation can be attributed to the discrepancy between measured and predicted temperatures at interface of FRP as discussed above. Overall, the model provides reasonable estimates of temperature at different locations of beam cross section.

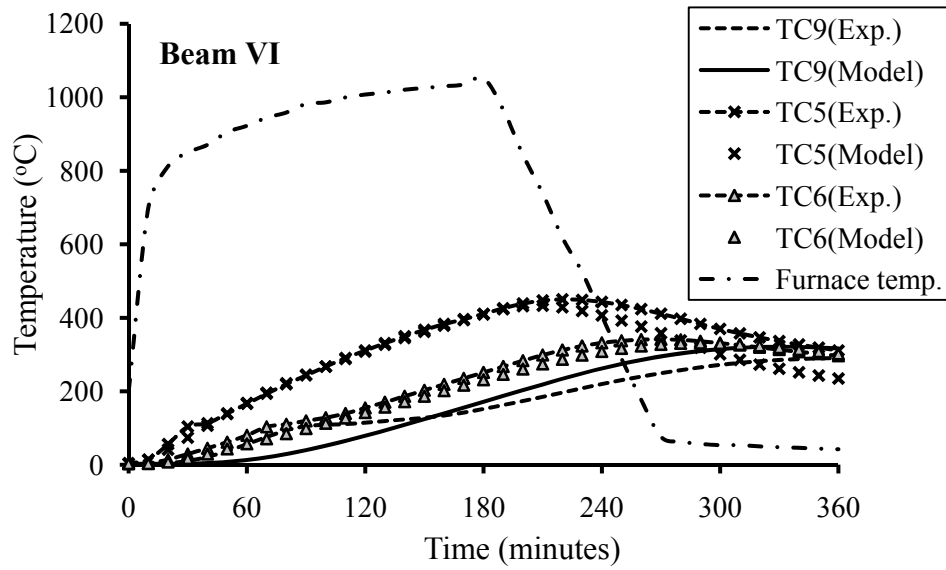
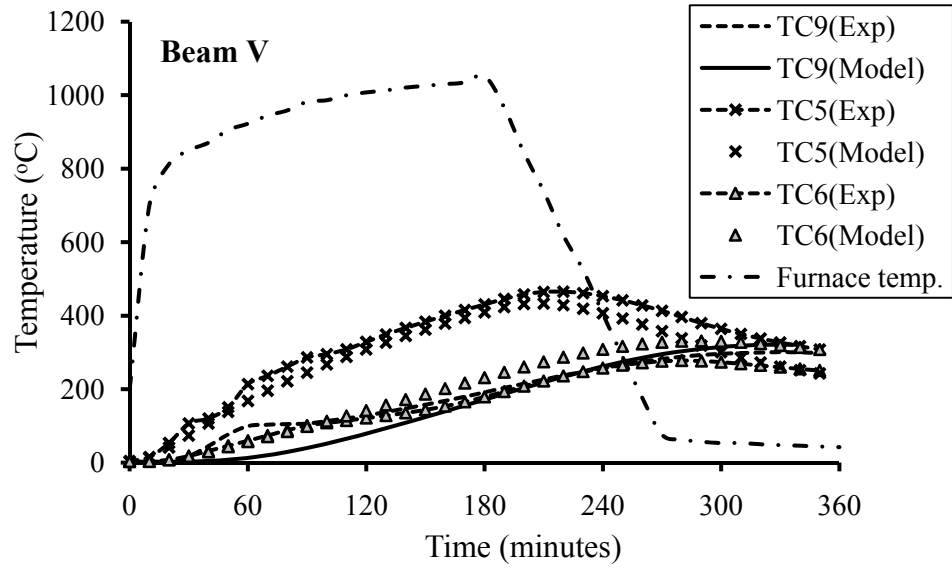


Figure 5.16: Comparison of measured and predicted temperatures in compression and flexural reinforcement and mid-depth of cross section for beams Beam V through Beam VIII

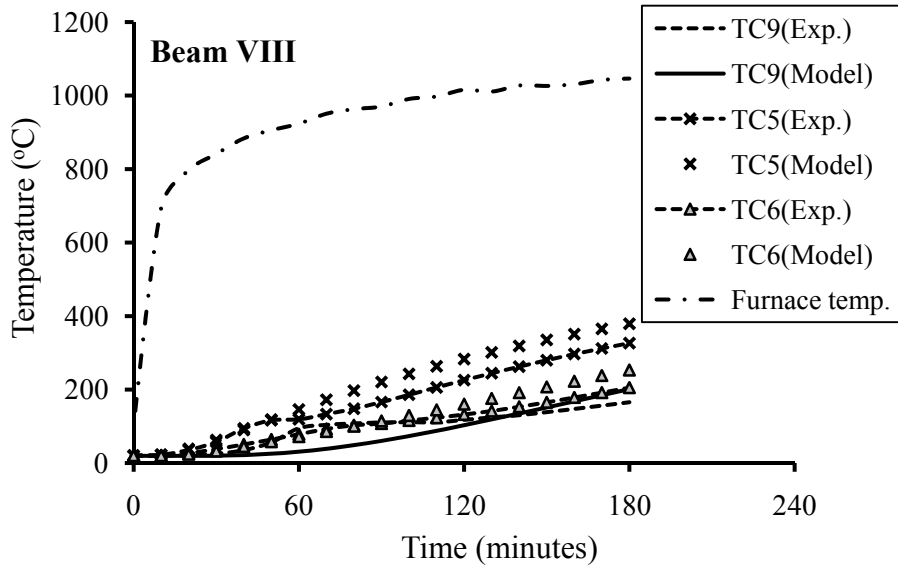
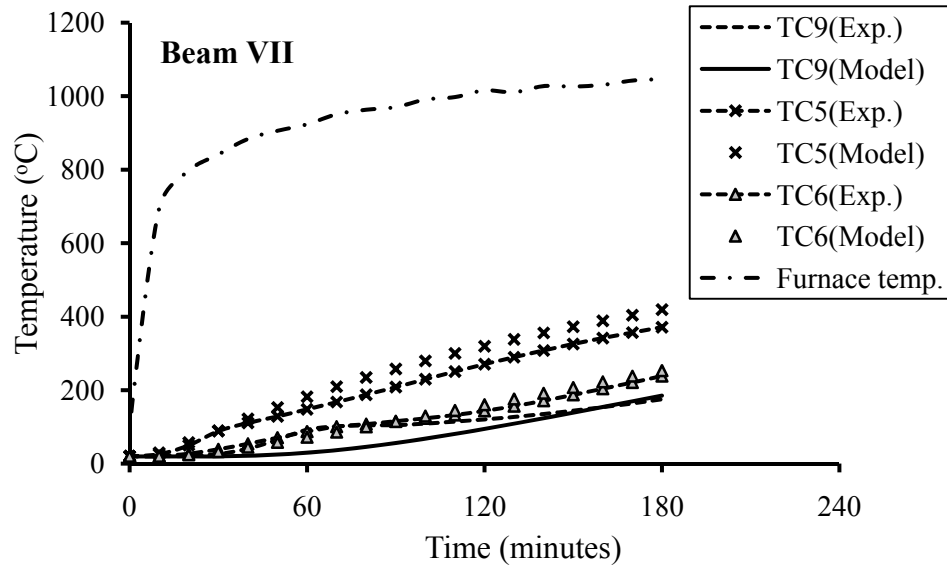


Figure 5.16 (cont'd): Comparison of measured and predicted temperatures in compression and flexural reinforcement and mid-depth of cross section for beams Beam V through Beam VIII

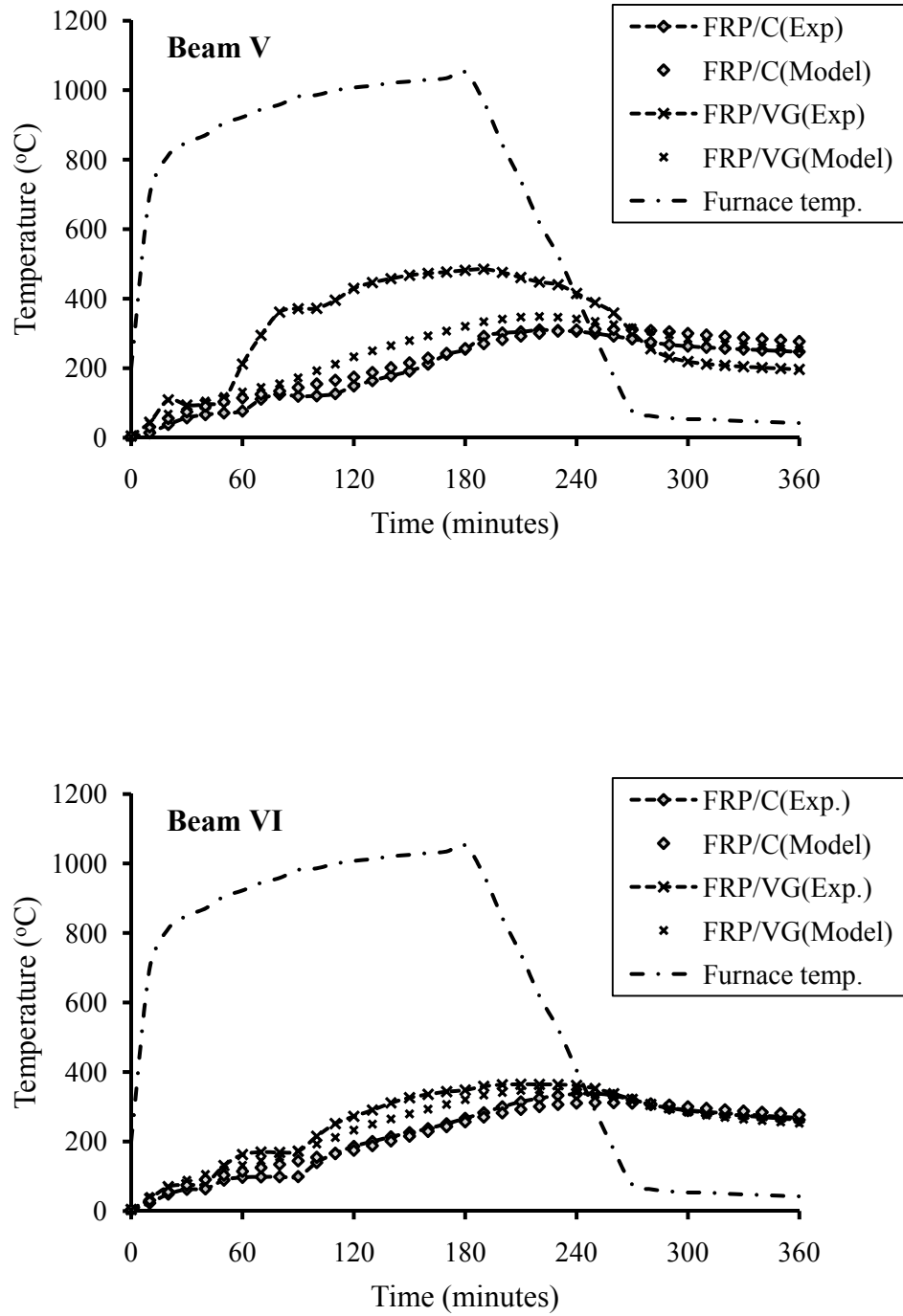


Figure 5.17: Comparison of measured and predicted temperatures at FRP/insulation, FRP/concrete interfaces for beams Beam V through Beam VIII

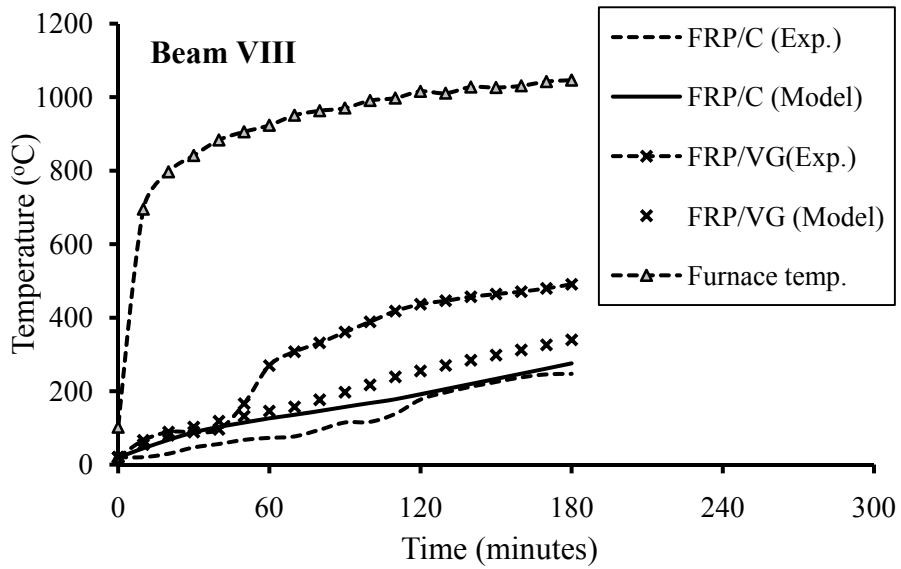
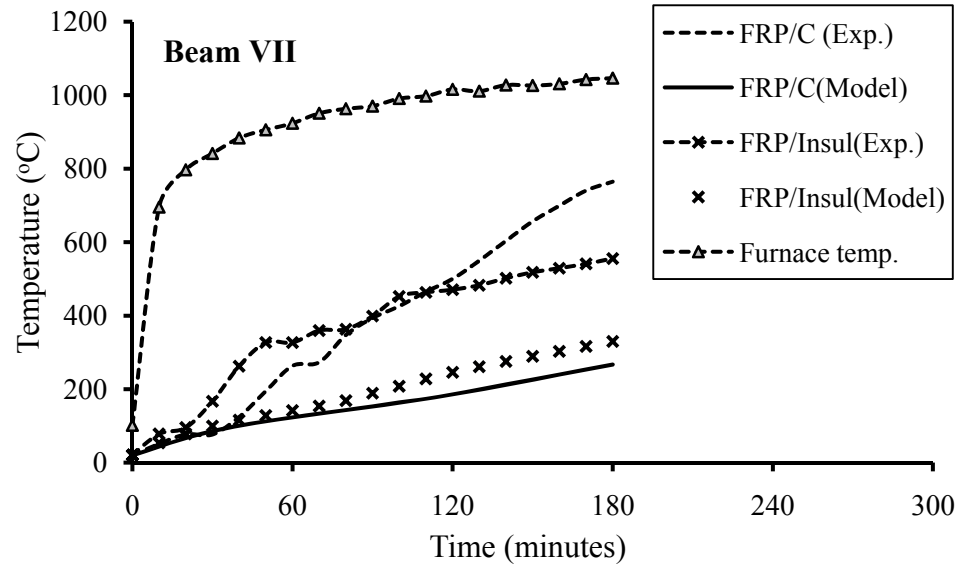


Figure 5.17 (cont'd): Comparison of measured and predicted temperatures at FRP/insulation, FRP/concrete interfaces for beams Beam V through Beam VIII

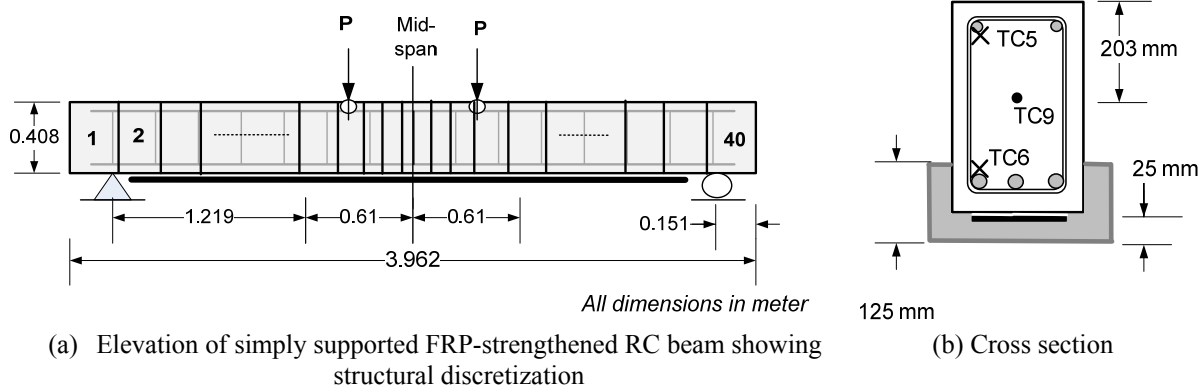


Figure 5.18: Elevation and cross sectional details of MSU tested FRP-strengthened RC beam

5.3.3.2 Structural Response

The predicted and the measured increase in mid-span deflection for the tested FRP-strengthened RC beams are compared in Figure 5.19. There is a good agreement between the measured and predicted deflections for all of the four FRP-RC beams. Under fire, the deflection increased gradually and around 20 minutes, beams experienced a sudden increase in deflections due to loss of bond at FRP/concrete interface. The model predicts debonding of FRP at about 25-30 minutes. This discrepancy can be due to differences in measured and predicted temperatures at the interface due to formation of cracks in the insulation as well as burning of epoxy (matrix) as discussed earlier.

After debonding, the rate of deflection in Beam VII increases as compared to the measured rate of deflections of Beam V, VI and VIII. This is because Beam VII, which was initially was loaded with load ratio 50% of strengthened capacity, experienced higher load ratio (as compared to capacity of RC beam at room temperature) after FRP contribution to the capacity of the beam was lost. This leads to higher deflection in the beam as illustrated in Figure 5.19. However, after debonding of FRP in beam Beam VIII, fire induced axial restraint force contributed to limit

deflections due to the development of arch action in the beam that helps resisting the applied loading.

In Beams V and VI, the factor that contributes towards lower deflections after debonding of FRP is due to ‘cable action’ (similar to tensile membrane action in slabs) provided by anchored continuous carbon fibers. The composite action between FRP and beam soffit (concrete) was lost in the heated portion of the beams (2.44 m). However, delamination of FRP did not occur due to the location of the anchorages outside the fire zone. Thus, the unbonded continuous fibers at the beam soffit continued to contribute towards the strength of the beam through ‘cable’ mechanism. The model predicted no strength failure in Beams V through VIII, same as measured in the test.

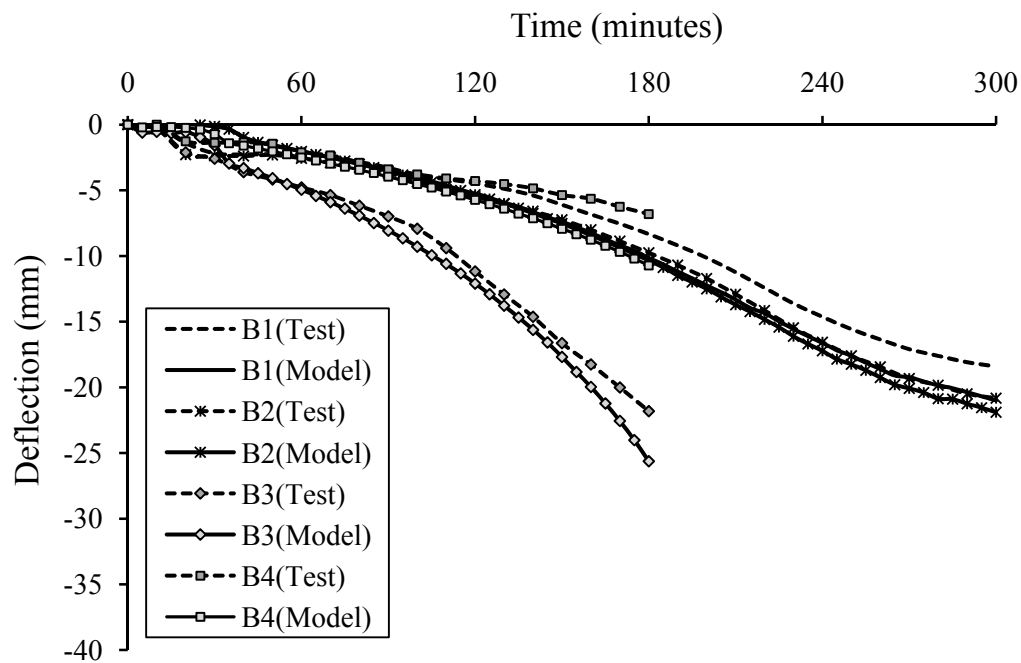


Figure 5.19: Measured and predicted deflection of FRP-strengthened RC beams (Beam V through VIII)

The predicted and measured axial restraint forces are compared in Figure 5.20 for axially restrained Beam VIII. The figures show that there is a good agreement between measured and predicted axial restraint forces for entire duration of test.

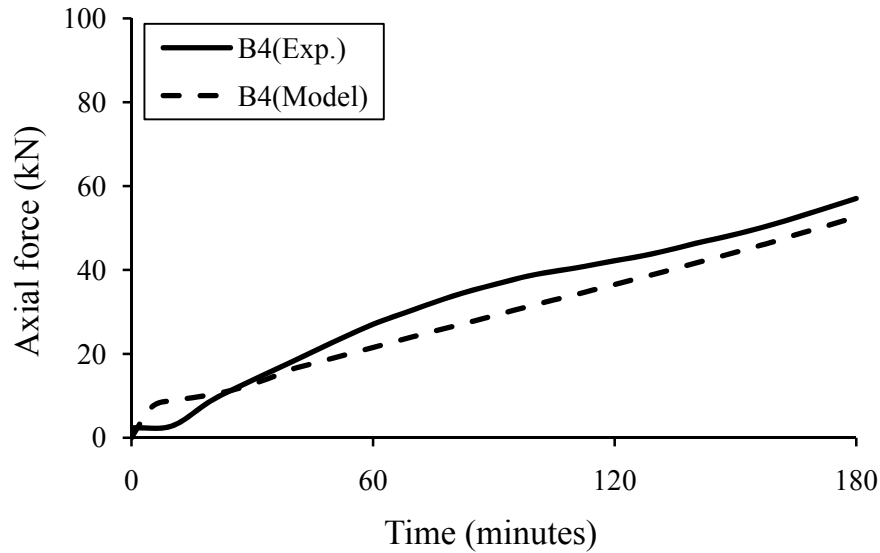


Figure 5.20: Measured and predicted axial restraint force as a function of time for Beam VIII

5.4 Summary

The validity of the computer model, developed as part of the current study, is established in this chapter. The thermal and structural response produced by the model is compared with the data generated from fire resistance tests. During the validation process, the influence of material constitutive models, effect of bond degradation and axial restraint force on the fire resistance of FRP-strengthened RC beams, on the model predictions is carefully examined.

The model accounts for the high temperature material properties of the constituent materials (including FRP and insulation), various fire scenarios, fire induced bond degradation and axial restraint effects, geometric nonlinearity, and various high temperature strain components. The model validation results are in good agreement with the results from the tests.

This indicates that the developed macroscopic finite element model is capable of predicting the fire response of FRP-strengthened RC beams under realistic fire, loading and restraint scenarios. In the next chapter, this validated model will be applied to conduct parametric studies to investigate and quantify the influence of various parameters on the fire resistance of FRP-strengthened RC beams.

CHAPTER 6

PARAMETRIC STUDY AND DESIGN GUIDELINES

6.1 General

The experimental studies presented in Chapter 3 indicated that tracing the thermal and mechanical response of FRP-strengthened RC beams is complex and a number of parameters have to be accounted for in the analysis. The valuable data and observations from fire experiments were utilized to validate the numerical model for tracing the fire response of FRP-strengthened RC beams. This validated model was then applied to study and quantify the effect of various parameters on the fire response of FRP-strengthened RC beams. The varying parameters included: load level, bond strength, insulation material, axial restraint force and its location, aggregate type, concrete strength, and fire scenario.

6.2 Analysis Details

6.2.1 Significant Factors

The literature review together with fire tests and numerical studies presented in Chapter 2 to 5 clearly indicated that the fire resistance performance of FRP-strengthened beams is influenced by a number of factors and many of these factors are interdependent. It was shown through

qualitative parametric studies (Ahmed and Kodur 2010) that the main factors influencing the fire response of FRP-strengthened RC beams are:

- Load level,
- Fire scenario,
- Axial restraint stiffness and its location,
- Concrete strength,
- Aggregate type in concrete,
- Insulation thermal properties, its thickness and geometric configuration
- Bond strength and adhesive thickness

To generate data on the effect of these factors, fire resistance analysis was carried out by varying above parameters in the practical range.

6.2.2 Selection of Beam

A simply supported (SS) FRP-strengthened RC beam was selected for the fire resistance analysis. The beam is 6.7 m in length with a cross section of 380×610 mm (refer to Figure 6.1). The beam is strengthened in flexure by providing three layers of unidirectional CFRP at tension face of the beam. These CFRP layers are applied at full width (380 mm) of the beam cross section. For fire protection, Tyfo[®] VG insulation is applied at the bottom of the beam that extends 105 mm on two sides of the beam cross section, as shown in Figure 6.1. The thickness of insulation is kept 20 mm (constant) except when specified. The details of geometric properties are tabulated in Table 6.1.

6.2.3 Material Properties

The beam has normal strength concrete (NSC) with a compressive strength of 38 MPa and carbonate aggregate. The beam has four 25 mm reinforcing rebars at the bottom (flexural reinforcement) with yield strength of 414 MPa and 2% yield strain. The CFRP composite has

ultimate tensile strength of 650 MPa, an elastic modulus of 3860 MPa and rupture strain of 1.7%. For analysis, thermal and mechanical properties as suggested by Lie 1992 are used for concrete and reinforcing steel whereas for FRP and insulation these properties are obtained from semi-empirical relationships proposed by Bisby [3]. It is assumed that the insulation does not crack and remain intact for the duration of fire test. It has no strength contribution towards capacity of the beam. Unless specified, the insulation thickness is assumed to be 20 mm. The high temperature material properties used in the analysis are given in Table 6.1 and Appendix A.

6.2.4 Mesh Size

For analysis, the beam length is discretized into 40 segments, as shown in Figure 6.1. The length of beam segments is so arranged that it decreases (gets finer) towards the mid-span (critical regimes of the beam) in order to improve the accuracy of predicted response. The beam cross section is idealized into elements such that aspect ratio, defined as ratio of length to depth, of the mesh is small (refined mesh) close to fire exposed boundary. It is important to note that in general, the accuracy of the finite element solution is improved by refining the discretization of the structure. Based on the study by Dwaikat (Dwaikat 2009) on effect of longitudinal and cross sectional discretization, an optimum mesh size is adopted for parametric analysis. Three cross sectional discretization patterns are used in analysis, namely; 10×20 mm and 5×6 mm elements in concrete and 3×3 mm in FRP and insulation, as schematically shown in Figure 6.1.

6.2.5 Failure Criteria

The fire resistance for analyzed beam is computed according to three failure criteria, namely strength, deflection, rate of deflection, and temperature in steel reinforcement. The glass transition temperature failure criterion has not been considered to define failure in FRP-strengthened RC beam since literature review and analysis of the test data, presented in Chapter

2 and 3 respectively, showed that the beams do not fail at the time when temperature at FRP/concrete interface reaches T_g . However, this criteria has been included while discussing about improving fire resistance of FRP-strengthened and insulated beam. Also, deflection and rate of deflection failure criteria do not govern failure in FRP-strengthened and insulated beams. Moreover, rebar temperature failure criteria is not effected by load ratio, support conditions (axial restraint), and mechanical properties of constitutive materials.

6.2.5.1 Range of Parameters

The parameters varied in the analysis include five load ratios (30, 40, 50, 60 and 70%), two aggregate types (carbonate and siliceous aggregate), four degrees of axial restraint stiffness (5, 50, 100 and 200 kN/mm) and five restraint force locations (Y/H) (0.3, 0.4, 0.5, 0.6 and 0.7), three types of beams, namely; un-strengthened RC beam, un-strengthened and insulated RC beam and FRP-RC beam with applied insulation. The analysis includes fire behavior of FRP-strengthened beam with a perfect bond and also while accounting for bond degradation with temperature. The location of axial restraint is measured from the top most fiber of the beam cross-section as a ratio of the total depth of the beam. To investigate the effect of fire scenarios, FRP-RC beams were analyzed under two standard fire exposures (ASTM E119 (2007) standard fire and ASTM E1529 (1993) hydrocarbon fire) and three design fire exposures (Fire I, Fire II and Fire III). The time temperature curves for the five fire scenarios are given in Figure 6.2. The fire resistance of this beam was evaluated based on thermal, strength, and deflection failure criteria. A summary of parameters studied and fire resistance results are presented in Table 6.2 and 6.3, respectively.

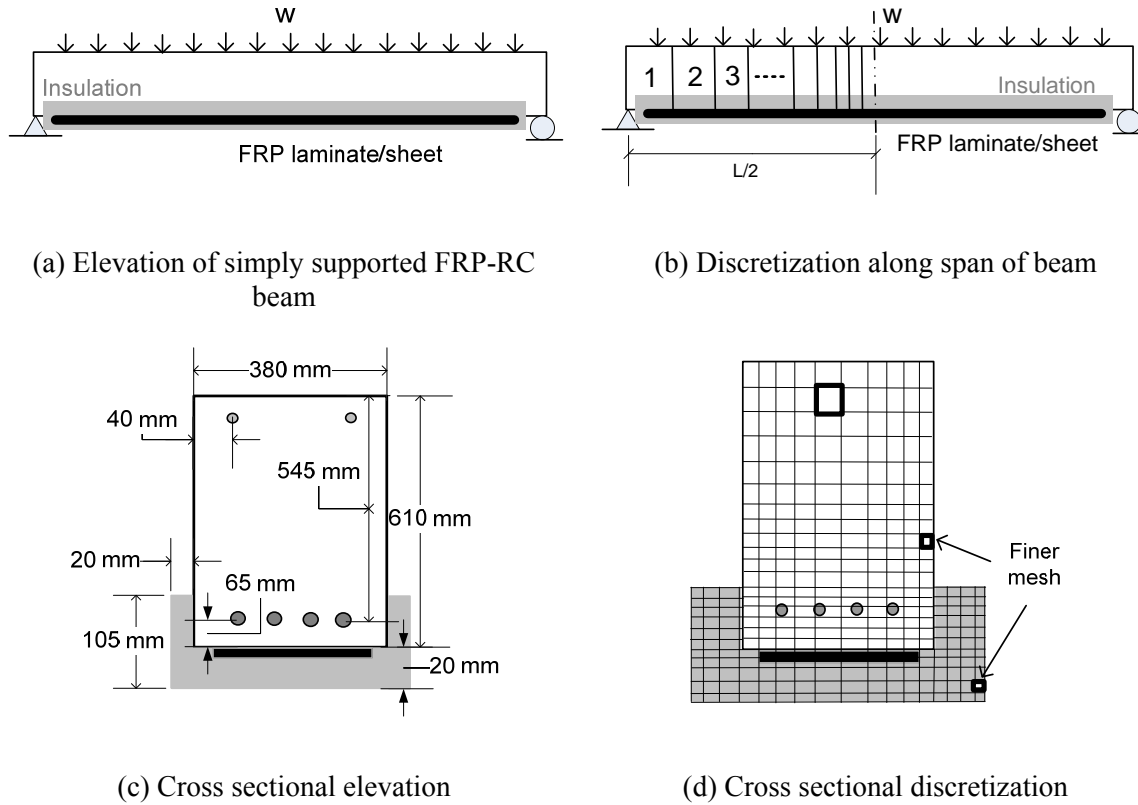


Figure 6.1: Longitudinal and cross sectional discretization for fire resistance analysis

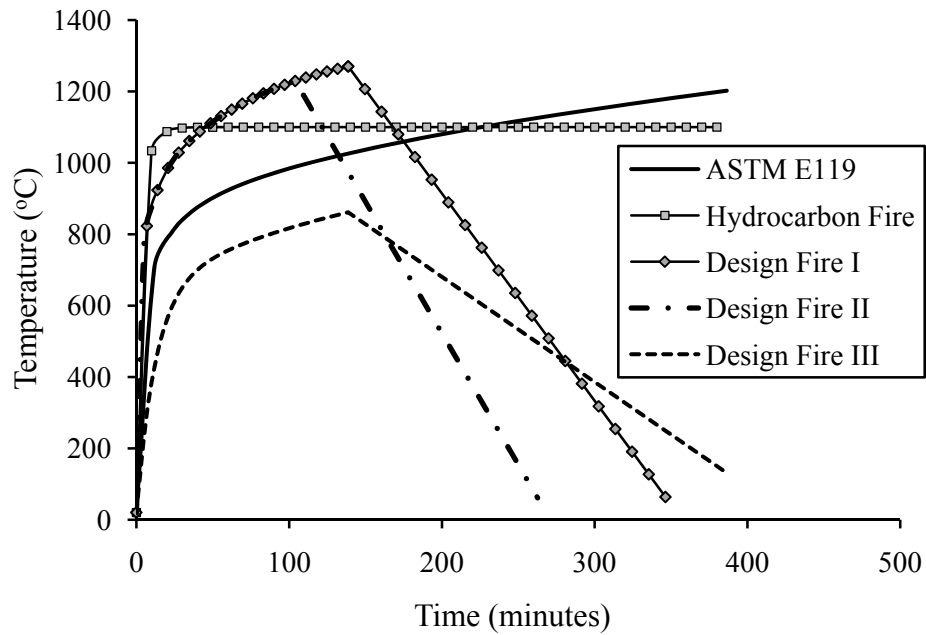


Figure 6.2: Time-temperature curves for different fire scenarios

Table 6.1: Summary of properties for FRP-strengthened RC beams used in the parametric study

Property		Nomenclature/dimension
Cross section (mm)		380×610
Length (m)		6.7
Reinforcement	top bars	$2 \times 15.8 \text{ mm}$
	bottom bars	$4 \times 25 \text{ mm}$
$f'_c \text{ (N/mm}^2\text{)}$		38
$f_y \text{ (N/mm}^2\text{)}$		414
Applied total load (kN/m)		60
Concrete cover thickness (mm)		40
Aggregate type in concrete		Carbonate
FRP type		CFRP
FRP thickness (mm)		3
FRP ultimate tensile strength (kN/mm ²)		0.65
Modulus of elasticity FRP (kN/mm ²)		38.6
Rupture strain of FRP (mm/mm)		1.7%
Insulation thickness (mm)		20
Insulation type		VG-EI-R

Table 6.2: Summary of parameters studied in analysis

Factors	Range	Relevant Figures
Section type	<ul style="list-style-type: none"> • RC beam (Plain) • Un-strengthened RC beam with insulation • FRP-RC beam with insulation 	Figure 6.3
Fire scenario	ASTM E119, ASTM E1529, and three design fires (Fire I, II and III)	Figure 6.4, 6.5, and 6.6
Load ratio	30,40,50,60 and 70 %	Figure 6.7
Axial restraint stiffness	0, 5, 50, 100 and 200 kN/m	Figure 6.8, and 6.9
Location of axial restraint force (Y/H)	0.3, 0.4, 0.5, 0.6 and 0.7	Figure 6.10 and 6.11
Concrete strength	40, 50 and 60 MPa	Figure 6.12
Type of aggregate	Carbonate and siliceous	Figure 6.13
Insulation thickness	0, 15, 25, 40 and 50 mm	Figure 6.14 and 6.15
Insulation depth on sides of the beam	20, 50, 100, 150 and 200 mm	Figure 6.16
Thermal property of insulation (thermal conductivity)	0.1, 0.2, 0.3, 0.4, 0.5, 0.6, 0.8, 1.0, 2.0, 3.0, 4.0 W/m-°K	Figure 6.17
Bond degradation	<ul style="list-style-type: none"> • Bond degradation with temperature • Perfect bond 	Figure 6.18 and 6.19
Adhesive thickness	1, 2, 3 and 4 mm	Figure 6.20

Table 6.3: Summary of the fire resistance values for the analyzed beams

Studied Parameter	Designation	Load Ratio (%)	Y/H ratio	Axial Restraint k (kN/mm)	Fire resistance based on failure criteria (minutes)		
					Strength	Deflection	Rate of deflection
Section Type	RC Beam	50	0	0	80	NF	NF
	Insulated RC beam	50	0	0	190	190	NF
	FRP-RC beam (bond degradation)	50	0	0	190	190	NF
	FRP-RC beam (perfect bond)	50	0	0	230	NF	NF
Load Ratio	FRP-RC beam	30	0	0	440	NF	NF
	FRP-RC beam	40	0	0	345	NF	NF
	FRP-RC beam	50	0	0	235	NF	NF
	RC Beam	50	0	0	210	190	NF
	FRP-RC beam	60	0	0	190	NF	NF
	FRP-RC beam	70	0	0	165	NF	NF
Fire Scenario	ASTM E119	50	0	0	225	NF	NF
	Hydrocarbon	50	0	0	180	NF	NF
	Design Fire-I	50	0	0	165	NF	NF
	Design Fire-II	50	0	0	NF	NF	NF
	Design Fire-III	50	0	0	NF	NF	NF
Axial Restraint	FRP-RC Beam	50	0.5	0	225	NF	NF
	FRP-RC Beam	50	0.5	5	235	NF	NF
	FRP-RC Beam	50	0.5	50	300	NF	NF
	FRP-RC Beam	50	0.5	100	310	NF	NF
	FRP-RC Beam	50	0.5	200	305	NF	NF
Location of Axial Restraint	FRP-RC Beam	50	0.3	200	140	NF	NF
	FRP-RC Beam	50	0.4	200	185	NF	NF
	FRP-RC Beam	50	0.5	200	280	NF	NF
	FRP-RC Beam	50	0.6	200	480	NF	NF
	FRP-RC Beam	50	0.7	200	600	NF	NF
Aggregate Type	Siliceous	50	0	0	180	NF	NF
	Carbonate	50	0	0	190	NF	NF
Concrete Strength	$f'_c = 40$ MPa	50	0	0	190	NF	NF
	$f'_c = 50$ MPa	50	0	0	195	NF	NF
	$f'_c = 60$ MPa	50	0	0	200	NF	NF

Table 6.3 (cont'd)

Thermal Conductivity	$k=0.1 \text{ W/m-}^{\circ}\text{K}$	50	0	0	190	NF	NF
	$k=0.2 \text{ W/m-}^{\circ}\text{K}$	50	0	0	155	NF	NF
	$k=0.3 \text{ W/m-}^{\circ}\text{K}$	50	0	0	135	NF	NF
	$k=0.4 \text{ W/m-}^{\circ}\text{K}$	50	0	0	125	NF	NF
	$k=0.5 \text{ W/m-}^{\circ}\text{K}$	50	0	0	115	NF	NF
	$k=0.8 \text{ W/m-}^{\circ}\text{K}$	50	0	0	105	NF	NF
	$k=1.0 \text{ W/m-}^{\circ}\text{K}$	50	0	0	100	NF	NF
	$k=2.0 \text{ W/m-}^{\circ}\text{K}$	50	0	0	95	NF	NF
	$k=3.0 \text{ W/m-}^{\circ}\text{K}$	50	0	0	90	NF	NF
	$k=4.0 \text{ W/m-}^{\circ}\text{K}$	50	0	0	90	NF	NF
Insulation depth	H = 0 mm	50	0	0	80	NF	NF
	H = 20 mm	50	0	0	140	NF	NF
	H = 50 mm	50	0	0	160	NF	NF
	H = 100 mm	50	0	0	185	NF	NF
	H = 200 mm	50	0	0	265	NF	NF

6.3 Results from Parametric Studies

Results from the parametric studies are presented in Table 6.3 and 6.5 and Figures 6.3 through 6.20 where progression of deflection with time is plotted. The effect of the studied parameters on structural response of FRP-strengthened RC beam (time-deflection curves) is included in the discussion. The thermal response of the beam (rebar and concrete temperatures) is not presented here explicitly except for the parameter of fire scenario because many of these parameters such as load ratio, axial restraint do not influence the thermal response of the analyzed beams especially when the FRP-strengthened beam is provided with insulation. The effect of each of the parameters on the fire response of the beam is discussed below.

6.3.1 Effect of FRP Strengthening

The effect of different section types on fire response can be gauged from Figure 6.3 that shows a comparison of deflection-time response for two cases of FRP-strengthened RC beams, namely; with a perfect bond, with temperature induced bond-slip, and two cases of un-strengthened RC beams, namely with and without externally applied fire protection. For

comparison purposes, all beams were analyzed under similar load level. In early stages of fire exposure, the response of both strengthened beams (with and without accounting for bond degradation) is stiffer as compared to un-strengthened RC beam due to high strength and stiffness properties provided by FRP composite. For the un-strengthened RC beam, the rate of deflection is much higher since mechanical properties of concrete and steel degrade faster in the absence of any external fire protection. For strengthened beam with a perfect bond, the response of the beam is stiffer for entire duration of fire exposure as compared to the FRP-RC beam that accounts for bond degradation. This is because overall behavior of the beam (deflection) primarily depends on high temperature properties of FRP (degrades beyond 300-400°C) and strength and stiffness properties of FRP are not much affected since insulation works efficiently in keeping FRP temperatures sufficiently low. This results in relatively low deflections in FRP-RC beam with a perfect bond.

For the case of FRP-strengthened beam, where slip is accounted for in the analysis, it can be noticed from Figure 6.3 that debonding of FRP occurred at around 40 minutes. This can be attributed to the loss of bond when the temperature reaches glass transition temperature of the adhesive (T_g of adhesive is 81°C). However, rate of increase in deflection in this FRP-strengthened RC beam and un-strengthened insulated RC beam is much slower than that in RC beam (no insulation) which is mainly due to beneficial effect of insulation that slows the temperature rise in steel reinforcement leading to a slower stiffness degradation. For initial 20-30 minutes of fire exposure, the behavior of un-strengthened insulated RC beam is similar to that of RC beam with no external fire protection. This is because in absence of any strengthening in these beams, flexural steel reinforcement that mainly contribute to moment capacity, maintains its full strength due to slower rebar temperature increase resulting from effective protection

provided by the concrete cover. In later stages with increasing temperatures, fire insulation continues to protect the un-strengthened insulated RC beam, while non-insulated RC beam loses much of its strength and stiffness in the absence of externally applied fire protection. This leads to rapid increase in deflections in un-insulated RC beam, as shown in Figure 6.3. This behavior concludes that in absence of any fire protection, FRP will debond in first 5-6 minutes of fire exposure (Gamage et al. 2006) and thereafter, the beam will fail in strength (before reaching critical temperature limit state) due to higher load ratio (compared to capacity of RC beam). In RC beam (loaded with 50% load ratio), critical temperature (593°C) in steel rebar mostly governs the failure criteria (Kodur and Ahmed 2010). It can also be noticed that after FRP fully debonds, the deflections in FRP-strengthened RC beam and insulated un-strengthened RC beam closely match. This is because, after debonding, FRP does not contribute towards capacity of the beam and the steel rebars are the one that carry tensile forces. Thus, FRP-strengthened RC beam behaves similar to un-strengthened insulated RC beam. This comparison highlights the importance of fire protection system for fire endurance of FRP-strengthened RC beams.

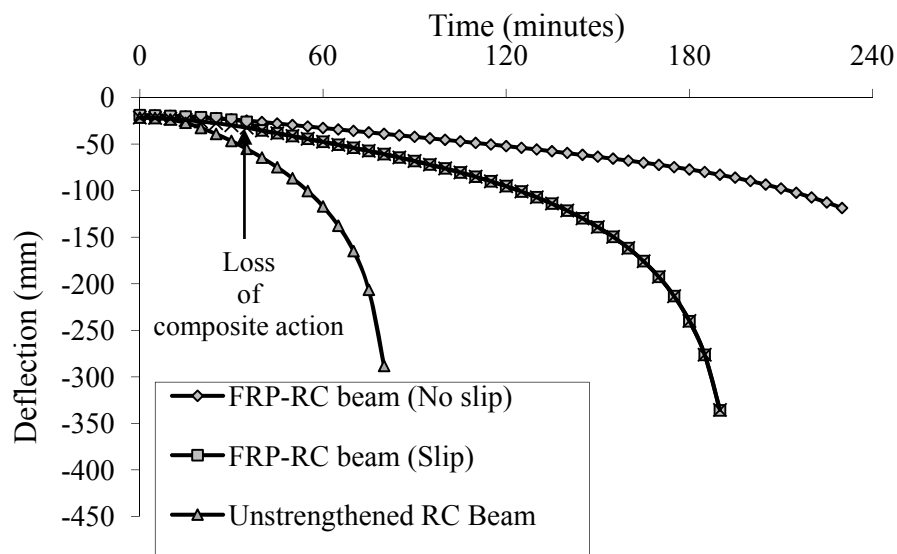


Figure 6.3: Effect of FRP strengthening on fire response of RC beams

6.3.2 Effect of Fire Scenario

To study the effect of fire scenario on fire resistance, FRP-strengthened RC was analyzed under five different fire exposures. Figure 6.4 shows the time-temperature curve of two standard (ASTM E119 and ASTM E1525 (hydrocarbon)) and three design (realistic) fire scenarios namely; Fire I, Fire II and Fire III. There is no decay phase in the time temperature curves of the standard fire scenario. However, the design fires takes into account compartment characteristic such as fuel load, lining material and ventilation and therefore, have a well-defined decay phase.

Three design fires, taken from Eurocode 1 (2002), are selected to represent wide range of compartment characteristics including fuel load and ventilation. Design fires are assumed to occur in a room with dimensions of 8×4×3 m and other assumed properties are tabulated in Table 6.4. Design Fire I represents severe fire in a library or a storage area with sufficient ventilation and large amount of combustible material. The peak temperature of about 1250°C is attained in about 150 minutes, while the decay phase lasts for about 200 minutes representing slow burn out fire. Design Fire II is also a sever fire, however, it burns out quickly compared to Fire I. Design Fire III represents a typical fire in a residential compartment.

Table 6.4: Properties used for design fires

Fire Scenario	Lining material	Thermal Capacity of lining material ($Ws^{0.5} / m^2 \text{ } ^\circ K$)	Ventilation Factor (\sqrt{m})	Fuel Load (MJ/m^2 of floor area)
Fire I	Gypsum board	488	0.02	1600
Fire II	Gypsum board	488	0.02	1200
Fire III	Concrete	1900	0.02	1600

The variation of temperature at corner rebar and at the interface of FRP-concrete is plotted in Figures 6.4 and 6.5. As expected in the first 120 minutes, temperatures in rebar and at interface of FRP-concrete increases for standard, as well as design fire exposure. The rate of increase in temperature is high for Hydrocarbon, and Fire I and II exposures since there is steep increase in fire temperature at early stages of fire exposure. However, for all design fires, the temperature starts to decrease after attaining the peak temperature. This can be attributed to presence of decay phase in design fires wherein fire temperature starts to cool down. It can also be noticed in Figure 6.4 that critical (failure) temperature in rebars (593°C) is not attained under design Fire I and II inspite of fire temperatures exceed 1200°C . This can be attributed to low thermal conductivity of the insulation that keeps the temperatures low till fire temperatures starts to cool down in the decay phase.

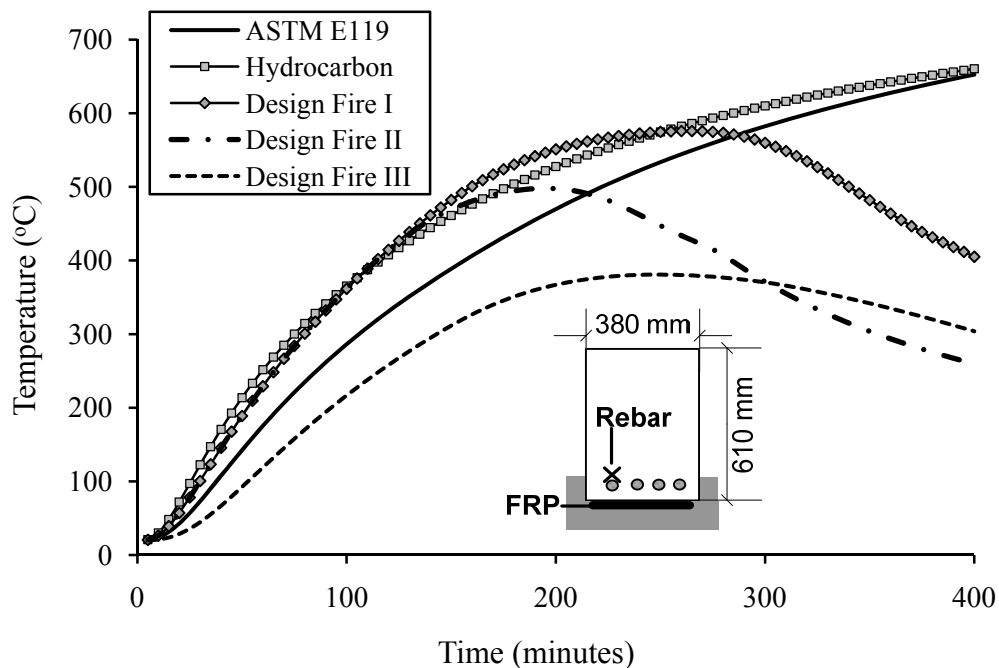


Figure 6.4: Variation of rebar temperature as a function of fire exposure time in FRP-strengthened RC beam

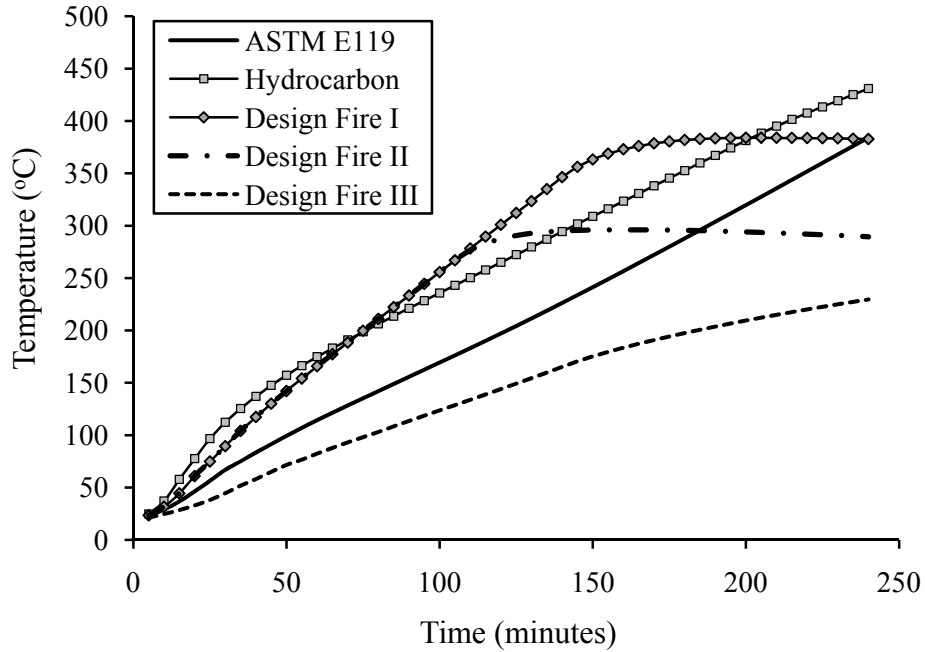


Figure 6.5: Variation of temperature at FRP-concrete interface as a function of fire exposure time

Figure 6.6 compares deflections of FRP-RC beam under five fire scenarios. Under Hydrocarbon and Fire I and II scenarios, the cross sectional temperature increases faster in early stages of fire exposure and thus leads to relatively large deflections resulting from high thermal strains. The deflections under Fire II exposure starts to decrease in later stages which can be attributed to strength and stiffness recovery in concrete and rebars during cooling phase of fire. Under design Fire I, deflection increase is considerable after 120 minutes into the fire. This can be attributed to high temperature creep strains. During decay phase under design Fire I, recovery in strength and deflection is not noticed since the beam fails under strength limit state.

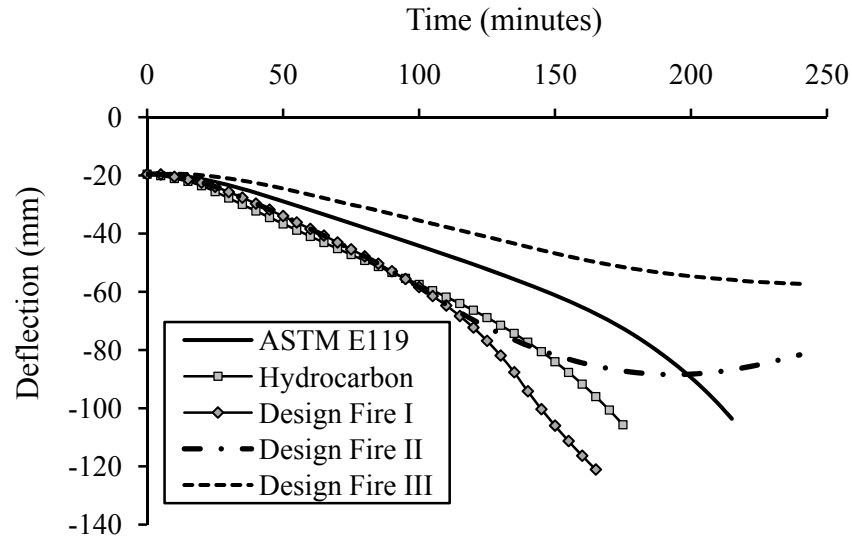


Figure 6.6: Effect of fire scenarios on mid-span deflections of FRP-strengthened RC beam

The computed fire resistance under different fire scenarios is presented in Table 6.3. Results show that strength limit state governs failure in all the cases. Lowest fire resistance is achieved under design Fire I as compared to hydrocarbon and ASTM E119 standard fires. This can be attributed to faster degradation in mechanical properties of constitutive materials in first 120 minutes due to a higher rate of increase in fire temperatures. By examining Table 6.3, it can be noticed that failure is not attained in FRP-RC beam under design Fire II despite temperatures attained during growth phase are higher as compared to standard fires. Therefore, it can be inferred that FRP-strengthened RC beams have higher fire resistance under most design fires that have a well defined decay phase.

6.3.3 Effect of Load Level

To study the influence of load level, analysis was carried out on FRP-strengthened RC beam under 30, 40, 50, 60 and 70% load ratios. The load ratio is calculated as the ratio of applied load

present under fire condition to the room temperature nominal capacity of the beam. The effect of load ratio on the fire response of FRP-RC beam is illustrated in Figures 6.7 and Table 6.3.

Results from the analysis show that load ratio does not affect failure evaluated based on limiting temperature (593°C) since rebar properties are independent of applied loading. However, load ratio significantly influences fire resistance of FRP-strengthened RC beam computed based on strength criteria. It can be seen from results listed in Table 6.3 that the fire resistance decreases with increasing load ratio. This is mainly due to the fact that at higher loads, the strength and stiffness properties of constitutive materials degrade significantly with temperature and beam will experience higher stresses and moments leading to early strength failure. The results from analysis also shows that the beam with higher load ratios (more than 50%) experience lower deflections just prior to failure (refer Figure 6.7). This can be attributed to external insulation that keep the temperature relatively cool at the bottom face of the beam that introduces reverse thermal gradient leading to lower thermal and creep strains in steel reinforcement. After FRP ruptures at ultimate strain value, the beam behaves as RC beam that has higher load levels as compared to capacity of RC beam. This leads to an early strength failure before deflections are pronounced at later stages of fire due to increased ductility as shown in Figure 6.7.

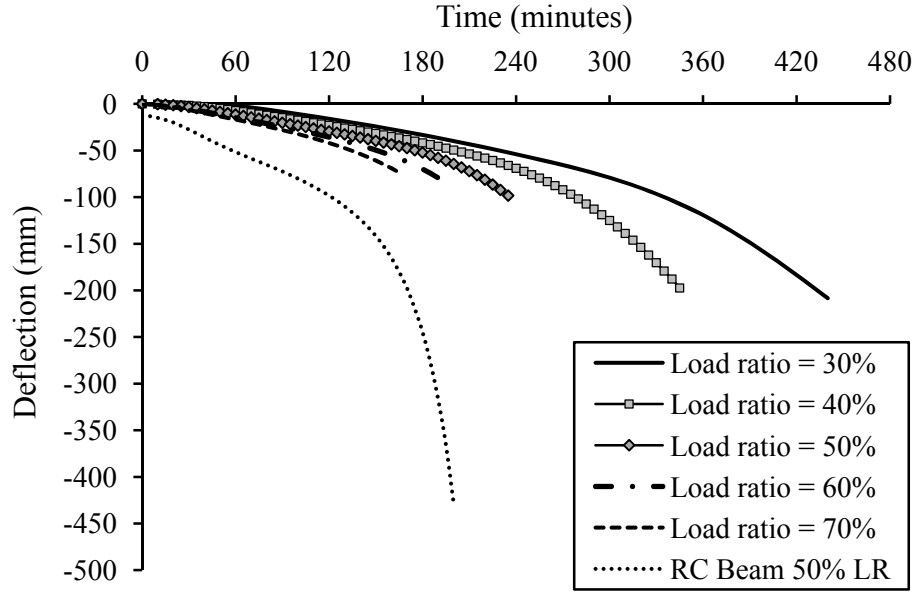


Figure 6.7: Effect of load ratio on mid-span deflection of FRP-strengthened RC beam exposed to fire

6.3.4 Effect of Axial Restraint

Figures 6.8 and 6.9 show the effect of axial restraint on fire resistance of FRP-strengthened RC beam. To represent different boundary conditions encountered in practical applications, axial stiffness (k) of spring is varied between zero and 200 kN/mm . As an example, stiffness of $k = 200 \text{ kN/mm}$ represent the boundary condition offered by a shear wall, while a stiffness of 5 kN/mm represents a typical beam column connection in a building. The beams are exposed to ASTM E119 standard fire and loaded with 52% of load ratio (60 kN/m).

Figure 6.8 shows the variation of axial restraint force as function of fire exposure time for different stiffnesses. It can be seen that the magnitude of axial restraint force increases with stiffness for a given fire exposure. This can be attributed to the fact that with temperature increase, thermal expansion (Δ) of the beam will be high towards the supports. Therefore, for beam with stiffer (higher k) end conditions, a higher magnitude of axial restraint force will

develop. The location of axial restraint force is generally below the geometric centroid (neutral axis) of the beams (Dwaikat and Kodur 2008). Thus, axial force developed at the support introduces an arch action in the beam that helps in resisting the applied loading and reduces mid-span deflection. Axially restraint FRP-strengthened RC beam with stiffness of 50 kN/mm experiences a 75 minutes increase in fire resistance as compared to a simply supported beam. This increase in fire resistance can be attributed to arch action developed in the beam due to restraint effect at the supports.

Figure 6.9 shows the variation of deflection with axial stiffness as a function of fire exposure time. FRP-strengthened RC beam behaves stiffer (less deflections) as compared to un-strengthened beam due to high strength and stiffness properties of CFRP. Moreover, results indicate that at early stages of fire exposure, the deflection in axially restrained FRP-strengthened beam is less as compared to an un-restrained beam. This is due to arch action generated in the beam as a result of fire induced restraint force. However, for beams with higher stiffness, large deflections are observed prior the failure. This can be attributed to $P-\delta$ effect that creates an additional moment at the critical section of the beam thereby increasing deflections.

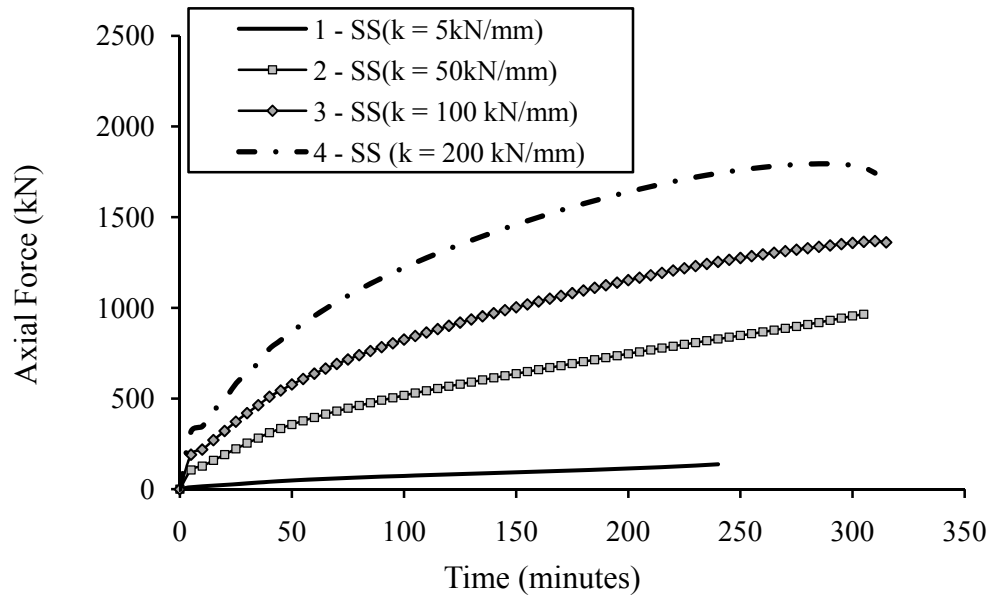


Figure 6.8: Fire induced axial restraint force as a function of time in an FRP-strengthened RC beam

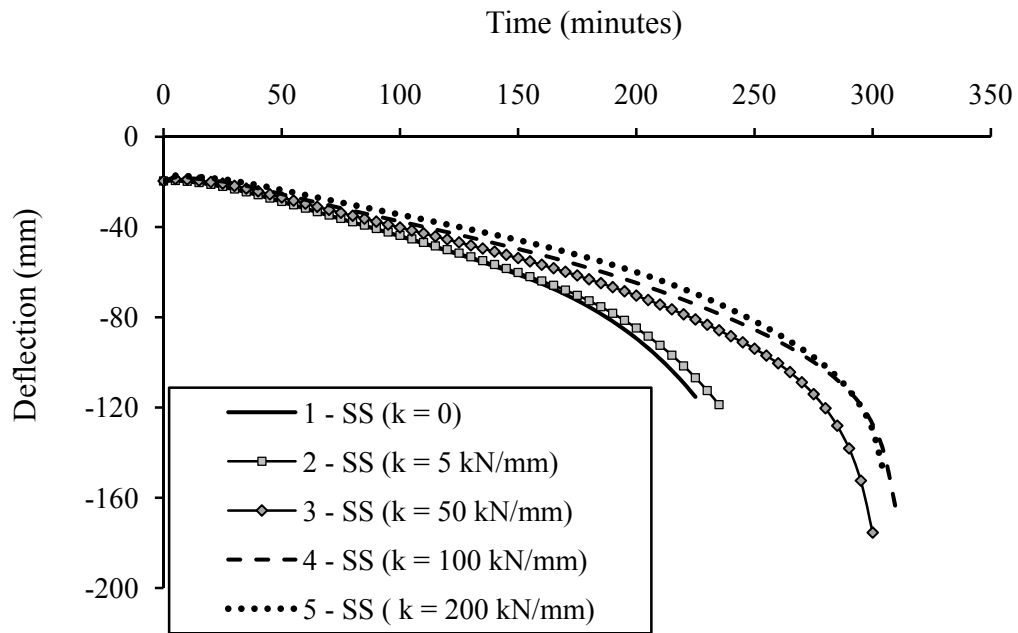


Figure 6.9: Effect of axial restraint on mid-span deflection of FRP-strengthened RC exposed to fire

6.3.5 Effect of Location of Axial Restraint

The effect of location of axial restraint location is illustrated in Figure 6.10. For this study, the value of spring constant is assumed to be 200 kN/mm , and fire induced bond degradation is accounted for. Five positions of axial restraint (Y/H), namely; 0.3, 0.4, 0.5, 0.6, and 0.7 were used in the analysis. The definition of Y and H is illustrated in Figure 6.10. The bond-slip is accounted for this analysis and beam is exposed to ASTM E119 standard fire.

Figure 6.10 show variation of deflection for FRP-RC beam for different axial restraint locations. The analysis results show that location of axial restraint has significant influence on response of FRP-strengthened RC beams. The deflection of the beam reduces by shifting the location of axial restraint downward (increasing Y/H). For Y/H ratio greater than 0.5, it can be seen the beam deflections are considerably lower at any stage of fire exposure. This is because of arch action developed in the beam that contributes in resisting applied loading and its effect is more pronounced when the location is shifted downward. For the values of Y/H ratio equal to 0.5 and lower, the FRP-RC beam experience maximum deflections and time to failure. This is attributed to $P - \Delta$ effect as a result of axial restraint force. At early stages of fire exposure, fire induced axial force (P) and the beam deflections are small, therefore, the effect of $P - \Delta$ is small. However, at later stages, this increasing axial restraint force induces secondary moments in the beam that causes flexural buckling. Thus, for $Y/H < 0.5$, the development of axial force is not beneficial for FRP-RC beam.

The variation of fire induced axial restraint force with its location (Y/H) is shown in Figure 6.11. It can be seen that with increasing Y/H ratio, magnitude of axial restraint increases and is maximum for $Y/H = 0.6$. This is because for lower Y/H ratios (less than 0.5), time to failure of the beam is minimum that result in lower axial restraint force. While for higher Y/H ratios

(greater than 0.5) the response of the beam is predominantly controlled by arch action that reduces the deflection and increase time to failure. Thus, larger axial restraining force is developed. Figure 6.11 shows that axial force starts to reduce after reaching maximum value for $Y/H = 0.7$. This can be attributed to increase in beam deflections due to degradation of strength and stiffness properties at later stages of fire exposure.

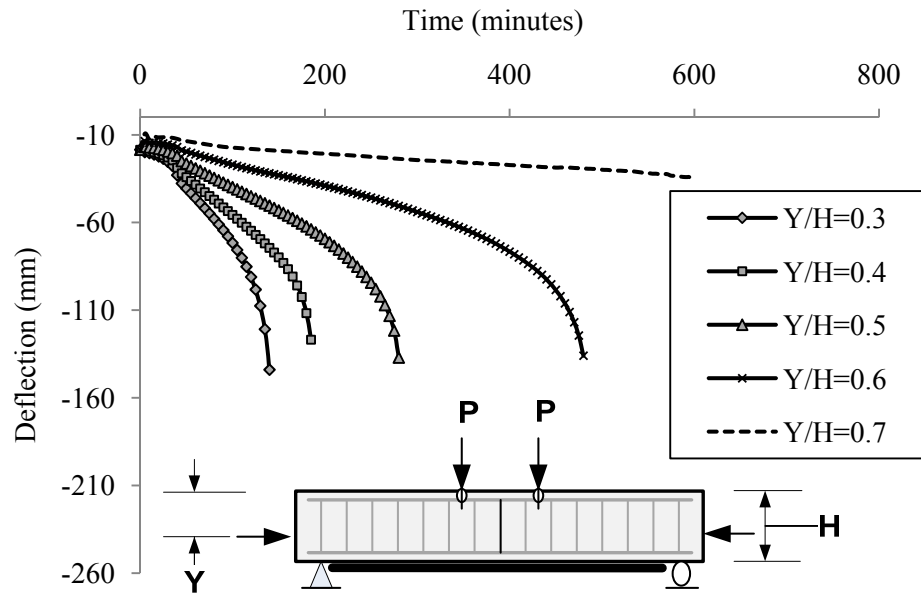


Figure 6.10: Effect of location of axial restraint force on mid-span deflection of FRP-strengthened RC beam exposed to fire

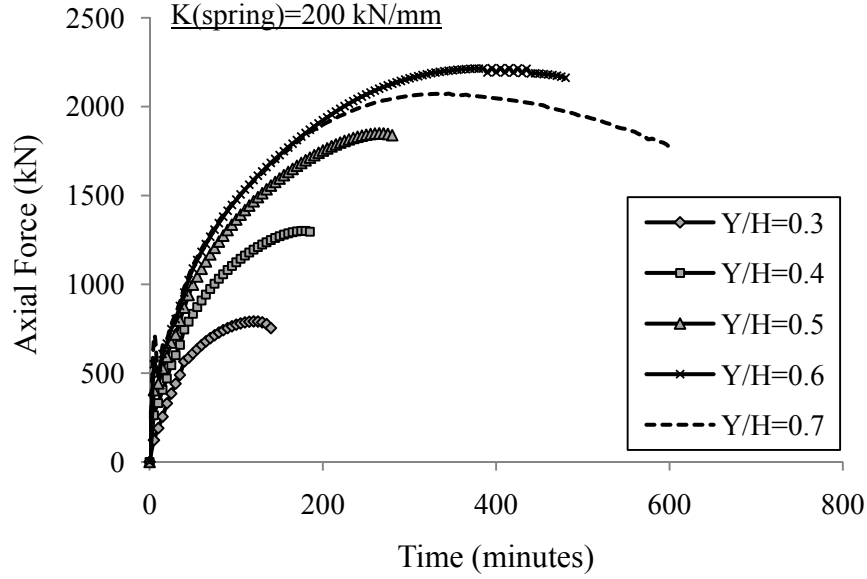


Figure 6.11: Effect of axial restraint force location on axial force development

6.3.6 Effect of Concrete Strength

Figure 6.12 shows the effect of compressive strength of concrete (f'_c) on fire resistance of FRP-strengthened RC beams. Three different strengths of concrete ($f'_c = 30, 40$ and 50 MPa) were analyzed and results are plotted in Figure 6.12. It can be seen that concrete strength does not influence fire response of FRP-strengthened RC beam. In general, it is accepted that a dense concrete with low permeability is produced by increasing concrete strength. However, insulation plays a vital role in influencing overall response of such beams. The insulation limits increase in temperature in the beam cross section including in flexural reinforcement. Therefore, no fire induced spalling occurs in concrete and this has been verified in fire tests presented in Chapter 3. Secondly, after FRP debonds, flexural steel reinforcement mainly contributes in moment capacity of the beam. Thus, in presence of externally applied fire protection, rebars maintain much of its room temperature strength due to low increase in temperature. Moreover,

temperature in tension rebars is not significantly influenced by concrete strength. Under fire conditions, reduction in moment capacity and increase in deflection of the beam is mainly attributed to strength degradation of rebars which is directly related to rebar temperature. Therefore, effect of concrete strength on fire resistance of FRP-strengthened and an insulated beam is minor.

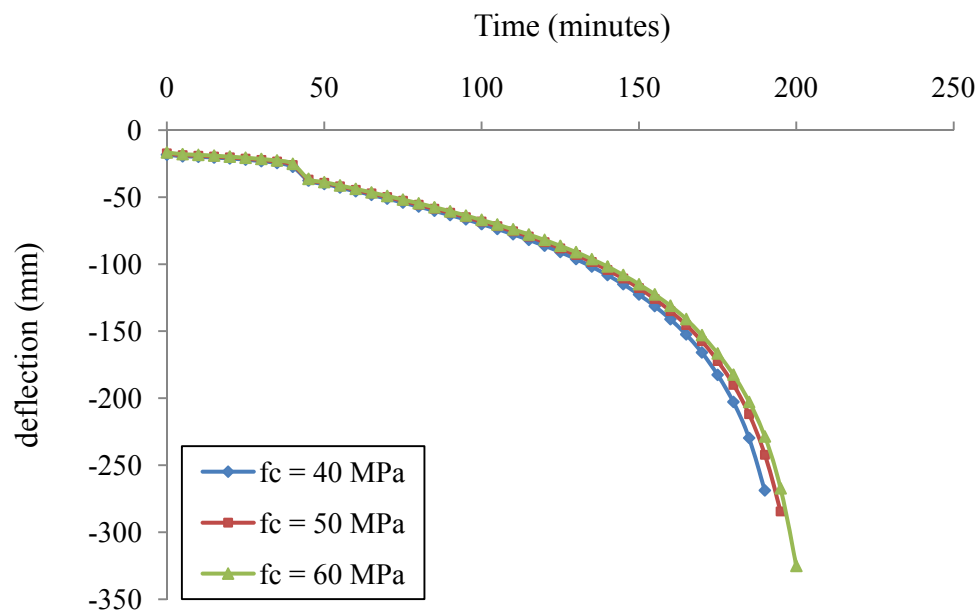


Figure 6.12: Effect of compressive strength of concrete on mid-span deflection of FRP-strengthened RC beam exposed to fire

6.3.7 Effect of Concrete Aggregate

Two types of concrete aggregate are considered in this parametric study, namely; carbonate and siliceous. In literature, previous studies have shown that the type of aggregate in concrete influences the high temperature concrete properties and thus the fire resistance of FRP-RC members. Figure 6.13 illustrates that the beam with carbonate aggregate concrete attains lower deflection at a given time as compared to siliceous aggregate. This is mainly because of high thermal capacity and low thermal conductivity of carbonate aggregate that result in lower rise in

temperature, and thus lower deflections. The endothermic reaction that occurs in temperature range of 600-700°C as a result of dislocation of dolomite consumes huge amount of energy. This endothermic reaction increases specific heat of carbonate aggregate by about 10 times as compared to siliceous aggregate. The difference in response of the beam with two types of aggregate concrete is not very significant for FRP-RC beams since insulation effectively protect rise of temperature in concrete. However, for RC beams with no insulation, resistance of beams made with carbonate aggregate concrete is about 20% to 30% higher than that for beams made of siliceous aggregate concrete (Dwaikat 2009). In general, type of aggregate concretes (carbonate and siliceous) for insulated FRP-strengthened RC beams has minor influence on fire response.

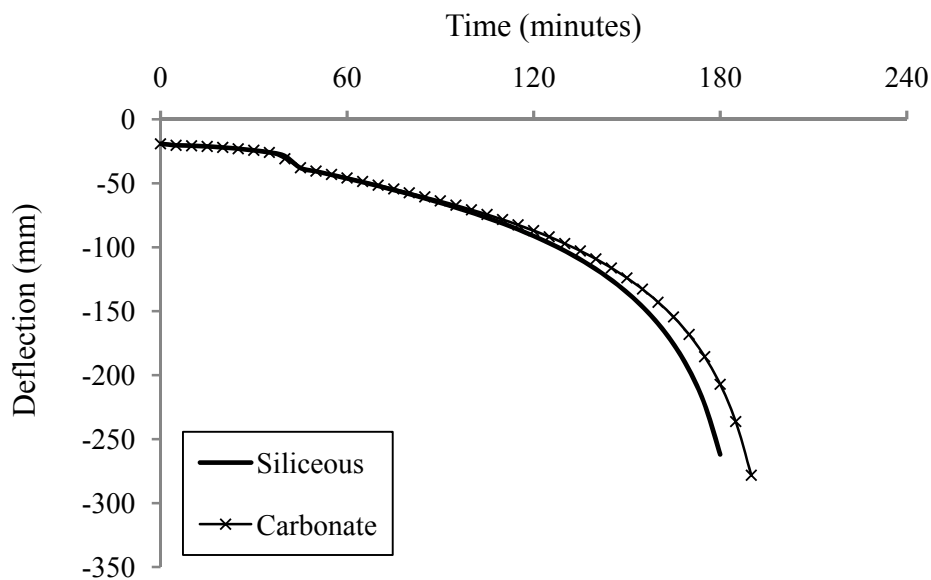


Figure 6.13: Effect of aggregate type on mid-span deflection of FRP-strengthened RC beam exposed to fire

6.3.8 Effect of Insulation Thickness

To investigate the effect of insulation schemes on fire resistance of FRP-strengthened RC beams, six beams designated RC1, FRP-RC1, FRP-RC2, FRP-RC3, FRP-RC4 and FRP-RC5

have been analyzed. The dimensions and material properties of all the beams are similar (Table 6.4). Beam RC1 is un-strengthened RC beam, Beam FRP-RC1 is FRP- strengthened RC beam with no insulation applied, while the remaining four beams have been strengthened with FRP and provided with supplement insulation of varying thicknesses and configuration schemes. On the sides of the beam, the insulation thickness (20 mm) and application depth (105 mm) is kept consistent. However, insulation thickness at the beam soffit has been varied to be 15, 25, 40, and 50 mm for beams FRP-RC2, FRP-RC3, FRP-RC4 and FRP-RC5, respectively. The analysis was carried out by exposing the beams to the standard ASTM E119 fire from three sides with applied load ratio of 52%.

Results presented in Table 6.4 can be used to gauge the influence of insulation thickness on the fire resistance of beams. The failure of the beam is computed based on strength, rebar critical temperature and deflection limit states. No failure occurred in any of the insulated FRP-strengthened beams under deflection or rate of deflection limit states. Previous experimental studies and test results presented in Chapter 3, illustrated that reaching glass transition temperature of FRP does not indicate failure of FRP-strengthened RC beams. Therefore, failure based on this failure criterion has not been included in the Table 6.4. However, provision of insulation is a requirement for externally bonded FRP systems to protect FRP from direct fire exposure since it is highly combustible material. Externally bonded FRP strengthening is bond critical application and its effectiveness depend on the glass transition temperature of the adhesive. Figure 6.14 shows effect of insulation thickness on time to reach glass transition temperature of the adhesive. As expected, time to reach T_g decreases with increasing insulation thickness. An increase in insulation thickness from 15 to 40 mm enhances time to reach T_g by about 70 minutes. This can be attributed to the low thermal conductivity of the fire insulation

that helps to keep temperatures low at the FRP-concrete interface. Therefore, for FRP-strengthened structural members, where reaching T_g is critical for structural performance, provision of external fire protection of appropriate thickness is necessary.

The numerical analysis shows that for all the FRP-strengthened beams, strength limit state governs the failure, but for un-strengthened beam (RC1), critical temperature in the corner rebar governs failure. Closer examination of results in Table 6.4 indicates that increasing insulation beyond an optimum thickness, does not contribute much to fire resistance. This can be attributed to the fact that the strength (moment capacity) of the beam, under fire conditions, is controlled by the tension forces in the FRP (up to certain fire exposure time) and steel reinforcement. Increase in insulation thickness helps to reduce temperature in rebars and this in turn helps to achieve higher moment capacity at a given fire exposure time. However, beyond optimum insulation thickness, at which rebar temperatures reaches about 400°C, any further reduction in rebar temperatures does not result in higher tension force or capacity of the beam. This is because the strength loss in rebars occur only after 400°C and any decrease in temperature below 400°C (Eurocode 2 2004), through increased insulation thickness, does not contribute to increase tension force. This is illustrated in Figure 6.15, where rebars temperature and corresponding yield strength ratio ($f_{y,T}/f_{y,20}$), obtained from parametric studies, is plotted as a function of insulation thickness for 3 hours of fire exposure time. It can be seen that increasing insulation thickness from 0 to 15 mm has maximum benefit and beyond this thickness, the beneficial effect gradually decreases. Beyond optimum insulation thickness of 40 mm, there is no distinct advantage of increasing the insulation thickness. This study clearly illustrates usefulness of the model in developing optimum insulation scheme for FRP-strengthened RC beams for a specified fire resistance.

Table 6.5: Effect of insulation thickness on fire resistance of FRP-strengthened RC beams

Beam designation	Insulation thickness (mm)		Fire resistance based on failure criteria (minutes)		
	Beam soffit	Side face	Rebar temp	Strength	Deflection
RC1*	0	0	155	200	180
FRP-RC1 [#]	0	0	155	80	**
FRP-RC2	15	20	295	205	**
FRP-RC3	25	20	330	235	**
FRP-RC4	40	20	355	280	**
FRP-RC5	50	20	370	300	**

* RC beam , ** No failure, # FRP-strengthened RC beam with no insulation

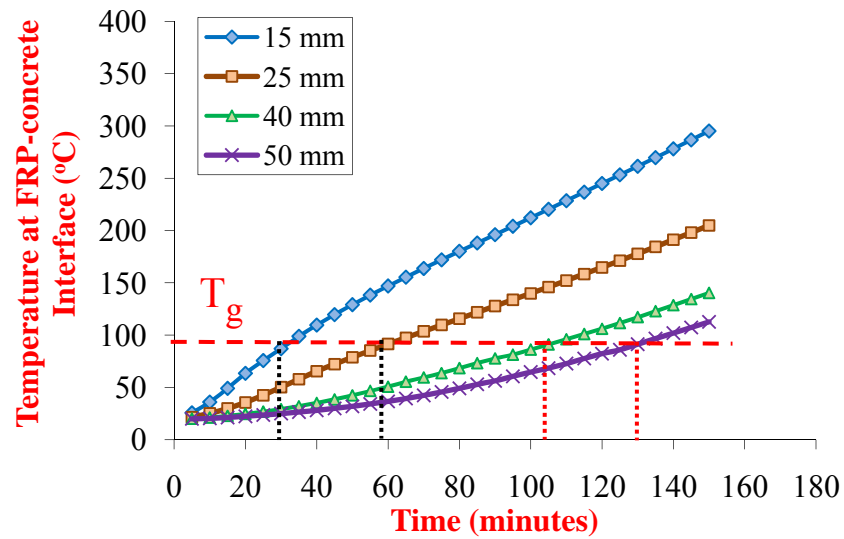


Figure 6.14: Effect of insulation thickness on time to reach T_g

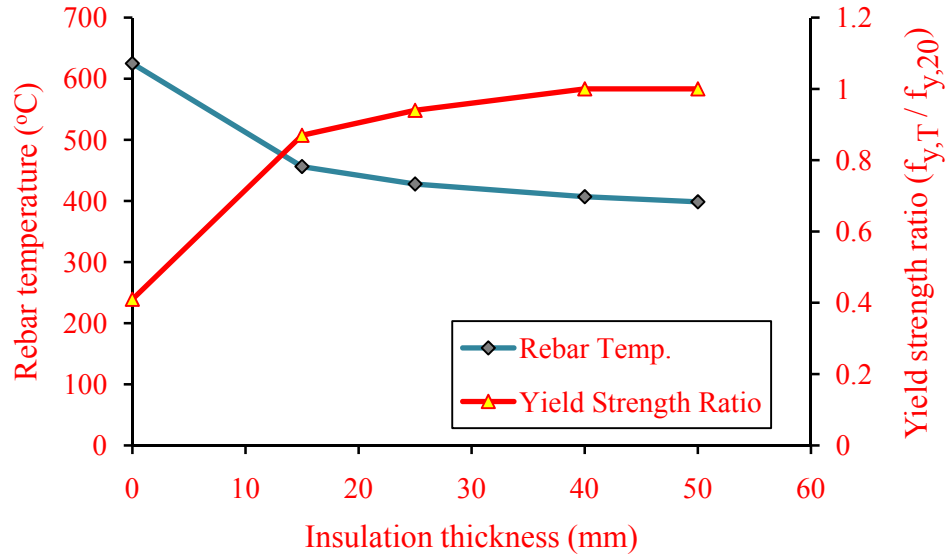


Figure 6.15: Corner rebar temperature and yield strength ratio as a function of insulation thickness for 3-hour of fire exposure time

6.3.9 Effect of Insulation Configuration

For externally bonded FRP-strengthened RC beams, supplemental fire protection system is necessary to achieve desired fire resistance. The parametric study results presented in Section 6.3.8 showed that an optimum insulation thickness is required to achieve required fire resistance. The study was extended to quantify the effect of geometric configuration of insulation on fire performance of FRP-RC beam. For this study, the thickness of insulation is kept constant (20 mm), while insulation depth "H" (refer to Figure 6.16) has been varied. The bond degradation is accounted for in this analysis and beam is exposed to standard fire exposure from three sides.

Figure 6.16 shows the effect of insulation depth "H" on mid-span deflection of the beam as a function of fire exposure time. It can be seen that the beam strengthened with FRP without providing any fire protection experience large deflections and fails in 80 minutes. This is because in absence of any insulation, FRP is lost in first 5-10 minutes and strength and stiffness degradation in steel reinforcement and concrete is at a faster rate. Examining the Figure 6.16, it

can also be seen that the time to reach debonding of FRP is independent of insulation depth provided on the two side of the beam cross section since it depends on insulation thickness provided at beam soffit which is assumed to be constant for this study. Results indicate that increasing insulation depth improves fire resistance of FRP-strengthened RC beam. This is mainly attributed to the low thermal conductivity of insulation that helps to limit rise of temperature in beam cross section. Increasing insulation depth from 20 mm to 200 mm (100%) enhances the fire resistance by about 120 minutes. This indicates that by increasing the insulation depth, the degradation of strength and stiffness properties is slower and this enhances the fire resistance of FRP-strengthened RC beams. Figure 6.16 also shows that before and after debonding of FRP occurs, the response of the beam with insulation depth of $H=200$ mm is stiffer as compared to the case of $H=20$ mm. The more ductile behavior of FRP-strengthened RC beam with smaller insulation depth of $H=20$ mm is attributes to rapid loss of strength and stiffness of the beam due to more exposed surface area. After debonding, tension rebars mainly contribute in moment capacity of the beam. Due to low insulation depth, its contribution is not very effective to limit increase of temperature in rebars and this result in rapid reduction in strength and stiffness properties leading to more deflections in the beam. Therefore, insulation configurations significantly affect fire resistance of FRP-strengthened RC beams.

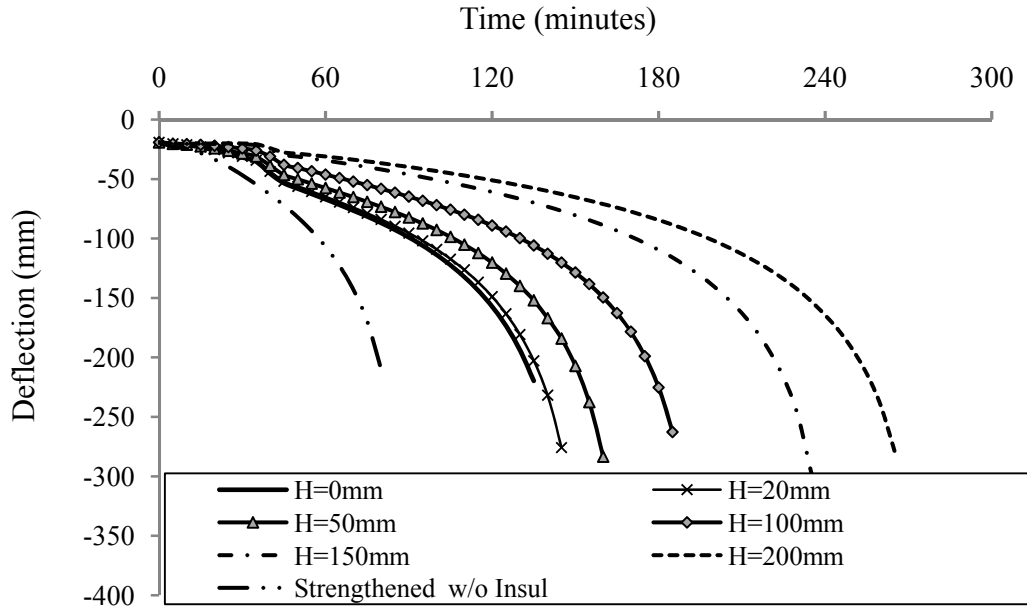


Figure 6.16: Effect of insulation depth on beam sides on fire response of FRP-strengthened RC beam exposed to fire

6.3.10 Effect of Insulation Thermal Conductivity

Thermal conductivity of insulation has significant influence on temperature distribution in beam cross section. Typically, thermal conductivity of insulation varies with temperature. However, for this parametric study it is assumed to be constant with temperature for each case study. Currently, data on variation of thermal conductivity with temperature is proprietary in nature and mostly is not provided by the manufacturers. Therefore, it is essential to study influence of this parameter on fire performance of FRP-strengthened and insulated beams. Thermal conductivity of VG insulation (Tyfo® WR AFP system) $0.12 \text{ W/m}^\circ\text{K}$ is taken as a reference and correspondingly, its value is increased up to a maximum of $4 \text{ W/m}^\circ\text{K}$. For analysis, the beam is externally applied with 25 mm of insulation, the effect of bond degradation is accounted for and the beam is exposed to standard fire from three sides.

Figure 6.17 illustrates effect of thermal conductivity on time-deflection of FRP-RC beam. The results indicate that with reducing thermal conductivity, the gain in fire endurance of the FRP-RC beam increases. This gain is negligibly small for thermal conductivities in the range of 1-4 W/m-°K. However, maximum beneficial effect is obtained by reducing the value from 0.8 to 0.1 W/m-°K, where fire resistance of the beam is increased by about 70 minutes. Therefore, for practical applications, insulation material with thermal conductivity higher than 1 W/m-°K may not be considered since above this threshold, thermal conductivity produces negligible variation in fire endurance. This study illustrates that low thermal conductivity of insulation is an important factor to enhance fire resistance of FRP-strengthened structural members in accordance with building codes and standards.

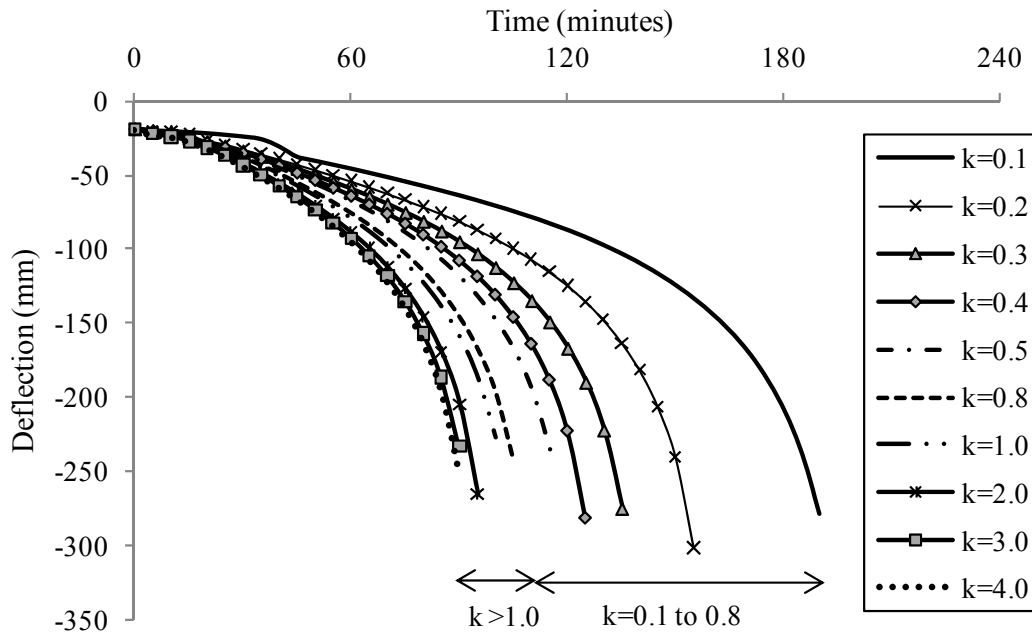


Figure 6.17: Effect of insulation thermal conductivity on fire resistance of FRP-strengthened RC beam

6.3.11 Effect of Bond Degradation

To illustrate the effect of bond-slip at FRP-concrete interface, the beam was analyzed under three scenarios, namely un-strengthened (RC beam), FRP-strengthened RC beam assuming a perfect bond and bond degradation. The beam was strengthened with CFRP which is bonded to concrete substrate using 2 mm thickness of adhesive layer. The beam was analyzed under ASTM E119 standard fire exposure with applied load of 60 KN/m (load ratio=0.52).

Figure 6.18 shows comparison of deflections for three different cases as function of fire exposure time. Results indicate a stiff response (lower deflections) for CFRP strengthened beam as compared to un-strengthened beam and this can be attributed to high strength and stiffness properties of CFRP. For the beam with perfect bond, FRP contributes to moment capacity till its strength degrades with temperature and its effect diminishes beyond certain temperature range. Results from analysis of the strengthened beam showed that debonding of FRP occurred in 40 minutes. This can be attributed to degradation of mechanical properties of adhesive close to glass transition temperature ($T_g = 81^\circ C$). Figure 6.19 shows that at FRP-concrete interface, bond-slip occurs after about 20 minutes of fire exposure and then increases exponentially beyond 35 minutes indicating debonding of FRP. Also, it can be seen that after FRP debonds, the deflections are not high as compared to RC beam. This can be attributed to presence of insulation that keeps the temperatures low in rebars thereby delaying the loss of strength and stiffness properties. For the RC beam with no insulation, the rate of deflection is higher due to faster degradation in mechanical properties of concrete and steel with rise in temperature.

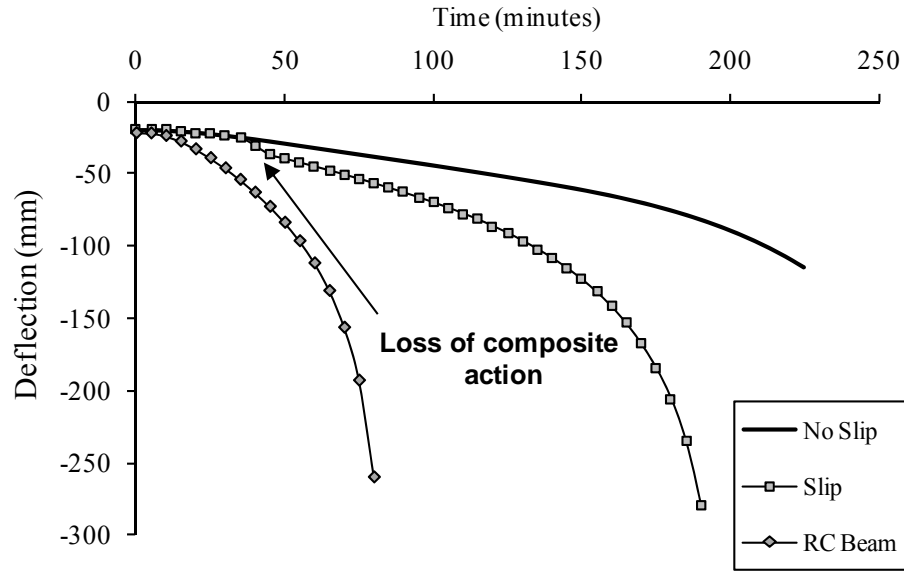


Figure 6.18: Fire induced mid-span deflection in RC beam under different bond configurations

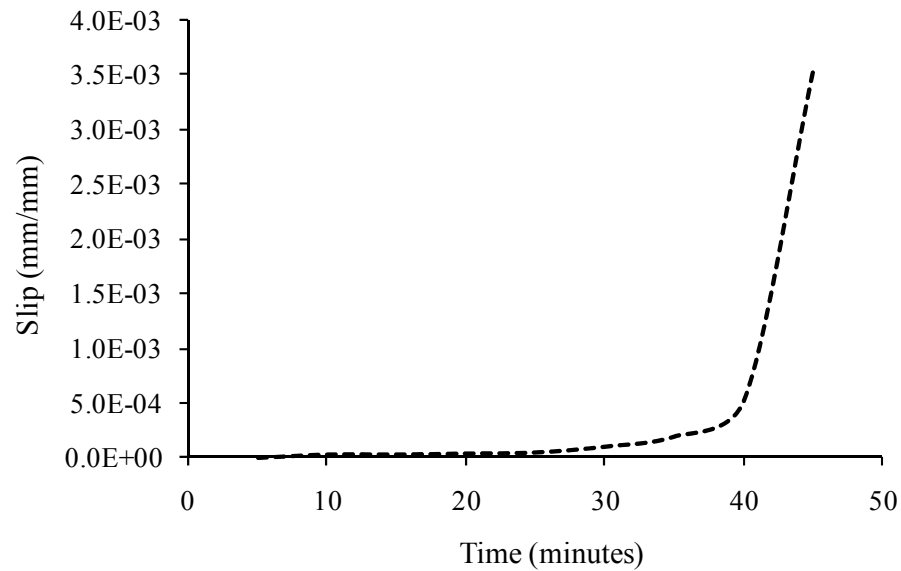


Figure 6.19: Bond-slip at FRP concrete interface as a function of fire exposure time

6.3.12 Effect of Adhesive Thickness on Bond Degradation

To study the effect of adhesive thickness on temperature induced debonding of FRP, an FRP-strengthened RC beam was analyzed for varying thickness of adhesive from 1 to 4 mm.

Figure 6.20 shows the deflection-time curves for the four cases of insulation thicknesses and for the case of fully bonded FRP beam. Results from the analysis indicate that up to first 20 minutes of fire exposure, there is no noticeable effect of adhesive thickness on time-deflection response. Beyond 20 minutes when debonding starts to occur, insulation thickness has minor influence on the deflections. For an increased adhesive thickness, bond-slip starts to occur in an earlier fire exposure time and as a consequence, the beam deforms slightly more. However, irrespective of adhesive thickness, beam experiences similar deflection after debonding of FRP. Therefore, adhesive layer thickness does not have significant effect on bond degradation and fire resistance of FRP-strengthened RC beam.

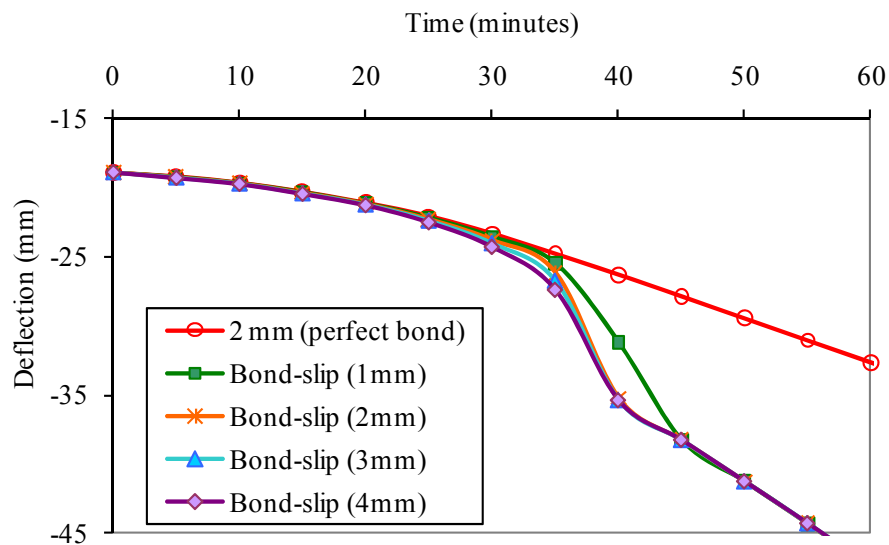


Figure 6.20: Effect of adhesive thickness on slip at FRP-concrete interface as function of fire exposure time

6.4 Critical Factors Influencing Fire Performance

The above parametric studies indicate that fire scenario, insulation scheme, anchorages, bond degradation, axial restraint force and load level, have significant influence on the fire response of FRP-strengthened RC beams. The concrete strength, aggregate type (carbonate and siliceous), and adhesive thickness at FRP/concrete interface does not influence fire resistance significantly. Based on the parameters studied, the critical factors that have to be considered in fire design of FRP-strengthened RC beams are further discussed below.

Design Fire

In practical situations, when fire occurs there always exists a growth phase and a decay (cooling) phase. These fires are generally referred to as design fires in codes and standards. Under such fires, the fire performance of FRP-strengthened RC beams is generally better. Results from parametric studies show that in the cooling phase of the design fire, the beam recovers parts of its strength and stiffness in concrete and reinforcing steel and this enhances the fire resistance of the beam. Hence, fire resistance values computed based on standard fire scenario are conservative if the resulting fires have a decay phase. Therefore, type of fire exposure plays an important role and should be taken into account in evaluating fire resistance of FRP-strengthened RC beams.

Anchorage

For flexural strengthening of RC beams, FRP strengthening is often applied at the critical (higher) moment zones. It is well established that for achieving desired fire resistance, FRP reinforcement along the beam length is to be insulated. Results from both experimental and parametric studies show that provision of adequate fire protection in the anchorage zones (terminating ends of FRP) is critical in achieving good fire resistance in FRP-strengthened RC

beams. Such insulation schemes help to keep the temperature of FRP, particularly in anchorage zones, relatively low. The lower temperatures in FRP fibers within anchorage zone help to maintain the bond between FRP and concrete to be effective for longer duration. The effectiveness of bond at anchorages ensures unbonded continuous fibers to act as cables and facilitate in load transfer through *cable mechanism*. This cable mechanism helps the member to carry the applied loads for longer duration. Therefore, ensuring adequate fire protection to the anchorage zone is critical to enhance the fire resistance of the FRP-strengthened RC beams.

Insulation Schemes

Provision of supplemental fire insulation in FRP-strengthened RC beams not only protects FRP, but also limits temperature rise in concrete and reinforcing steel. In externally bonded FRP strengthened RC beams, fire resistance depends on the rate of bond degradation at FRP and concrete interface with temperature. At certain stage, when bond (and FRP contribution) is lost, concrete and steel reinforcement carry the applied moments. Hence, after debonding of FRP, the overall fire response of the beam depends on the strength and stiffness properties of concrete and steel reinforcement. An optimum fire protection scheme (both thickness and geometric configuration) for the whole FRP-strengthened RC beam (that includes concrete, steel rebars and FRP) is required for achieving good fire resistance rating.

Load Level

In evaluating fire resistance of FRP-strengthened RC beams, the strength failure criterion is the one that often governs failure. Under this failure criterion, the load level influences the fire resistance significantly. Since higher the load, lower will be the fire resistance. However, in many fire tests, temperature limit in FRP or steel rebars is often used to determine the failure. This is not a realistic failure limit state and using this failure criterion may not account for effect

of load level on fire resistance since the resulting temperatures in FRP or steel rebars are independent of the applied loading. Higher load level cause an early softening and weakening of the constitutive materials which already experience degradation in strength and stiffness properties with increasing temperature. This results in higher stresses and moments and ultimately leads to early strength failure. Therefore, strength limit state is to be applied to evaluate fire resistance of FRP-strengthened RC beams.

Axial Restraint Force

Flexural members can experience considerable expansion when exposed to high temperatures and when the beam is restrained from expanding, a significant axial restraint force develops at the supports. The magnitude of fire induced axial restraint force and its location influences the fire resistance of FRP-strengthened RC beams. This axial force introduces an arch action in the beam that contributes to load carrying mechanism in later stages of fire exposure. The fire response of FRP-strengthened RC beam improves when the axial restraint force is located below the geometric centroid of the beam. By shifting the location towards top of the beam significantly reduces the fire resistance due to development of secondary moments in the beam which causes flexural buckling. Therefore, it is important to consider the stiffness of the structural members surrounding the FRP-strengthened RC beam for realistic fire resistance analysis.

Bond Strength

Results from fire tests and parametric studies show that in FRP-strengthened RC beams, temperature induced bond deterioration degrade the fire response of the beam. The bond between FRP and substrate concrete is lost when the temperature at the interface exceeds glass transition

temperature (T_g) of FRP since shear stresses in the adhesive (polymer resin) remain sufficiently low above T_g . It is often assumed that after debonding, the FRP does not contribute to the moment capacity. However, an insulated FRP-strengthened RC beam exhibits better fire performance (higher strength capacity with lower deflections) due to lower temperatures in concrete and steel rebars. Therefore, the beam continues to resist applied service loads and reaching T_g cannot be taken as failure of the FRP-strengthened RC beam.

6.5 Design Guidelines

The research presented in this study clearly emphasizes that there are a number of critical factors apart from insulation, that influence the response of FRP-strengthened RC beams under fire conditions. The current guidance for fire design of FRP-strengthened RC beams, which is based on standard fire tests, specifies that fire insulation as a means to achieve desired fire resistance. Provisions in current codes and standards recommend treating FRP to be ineffective in the event of fire. There are very few specifications that take into consideration the critical factors discussed above. Based on test results and parametric studies, the following guidelines are recommended for enhancing fire response of FRP-strengthened RC beams.

6.5.1 Insulation Scheme

It is well established that an FRP-strengthened RC beam is to be provided with adequate insulation to achieve code specified fire resisting ratings. However, there is lack of guidance with respect to optimum insulation thickness and its geometric configuration to achieve desired fire resistance.

Insulation Layout

In FRP-strengthened RC members, in addition to insulation thickness, the layout of insulation should be an important consideration for achieving fire resistance. The insulation helps to keep overall beam cross sectional temperatures (concrete steel rebars and FRP) low. Therefore, proper detailing of insulation can help to keep the temperatures low not only in FRP but also in tension steel reinforcement and assist in arriving at optimum insulation levels. An optimum geometric insulation configuration can be developed to achieve good fire resistance in FRP-strengthened RC beams.

The five insulation schemes that can be adopted for FRP-strengthened RC beam with rectangular beam cross section are shown in Figure 6.21. It has been established that externally bonded FRP without fire protection is not appropriate for FRP-strengthened RC beams (Gamage et al. 2006). Therefore, FRP without supplemental insulation is not recommended (refer to Figure 6.21(a)). The two insulation schemes shown in Figure 6.21(b) and (c) do not lead to optimum protection since these insulation schemes do not help in keeping temperatures low in bottom rebars for sufficient time to yield good fire resistance. From the parametric studies and fire tests, it was found that extending the insulation to a depth of " $2c_c$ " from bottom of the beam cross section (on either side) is required to achieve optimum fire resistance. Based on this results, the two recommended insulation configurations are shown in Figure 6.21 (d) and (e). Both these insulation configurations can provide effective fire protection to overall beam cross section. However, the insulation scheme shown in Figure 6.21(d) is preferred option as compared to the one shown in Figure 6.21(e) since applying insulation along complete exposed surfaces of the beam cross section is not practical and is a very expensive proposition. Similar insulation schemes can also be utilized for FRP-strengthened T-beams. Based on the results from

parametric studies conducted as part this research and test results on T-beams (Williams et al. 2006), the recommended insulation schemes for FRP-strengthened RC T-beams are shown in Figure 6.22 (a) to (e).

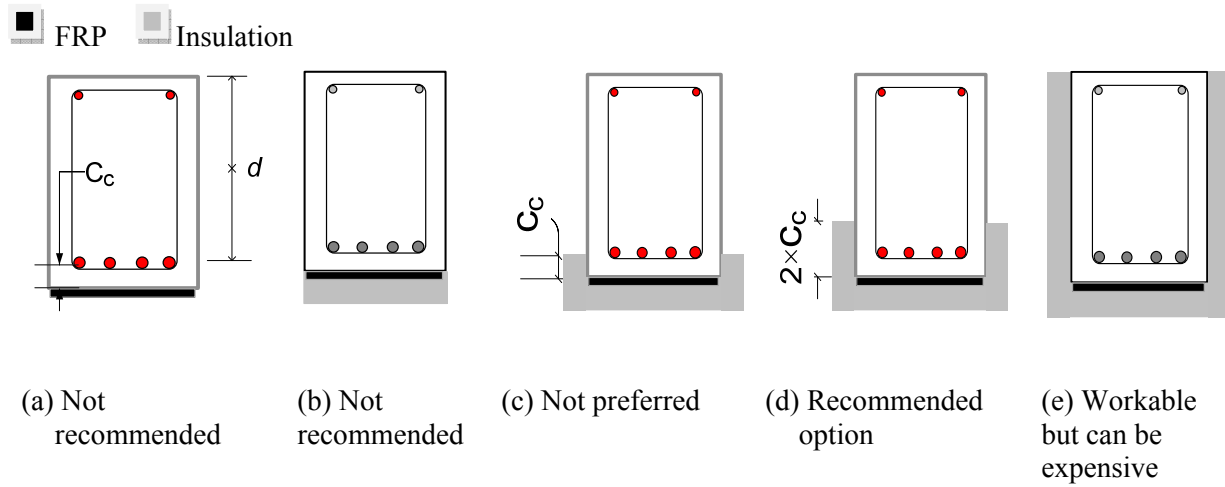


Figure 6.21: Proposed geometric configuration schemes for fire insulation in FRP-strengthened RC beams

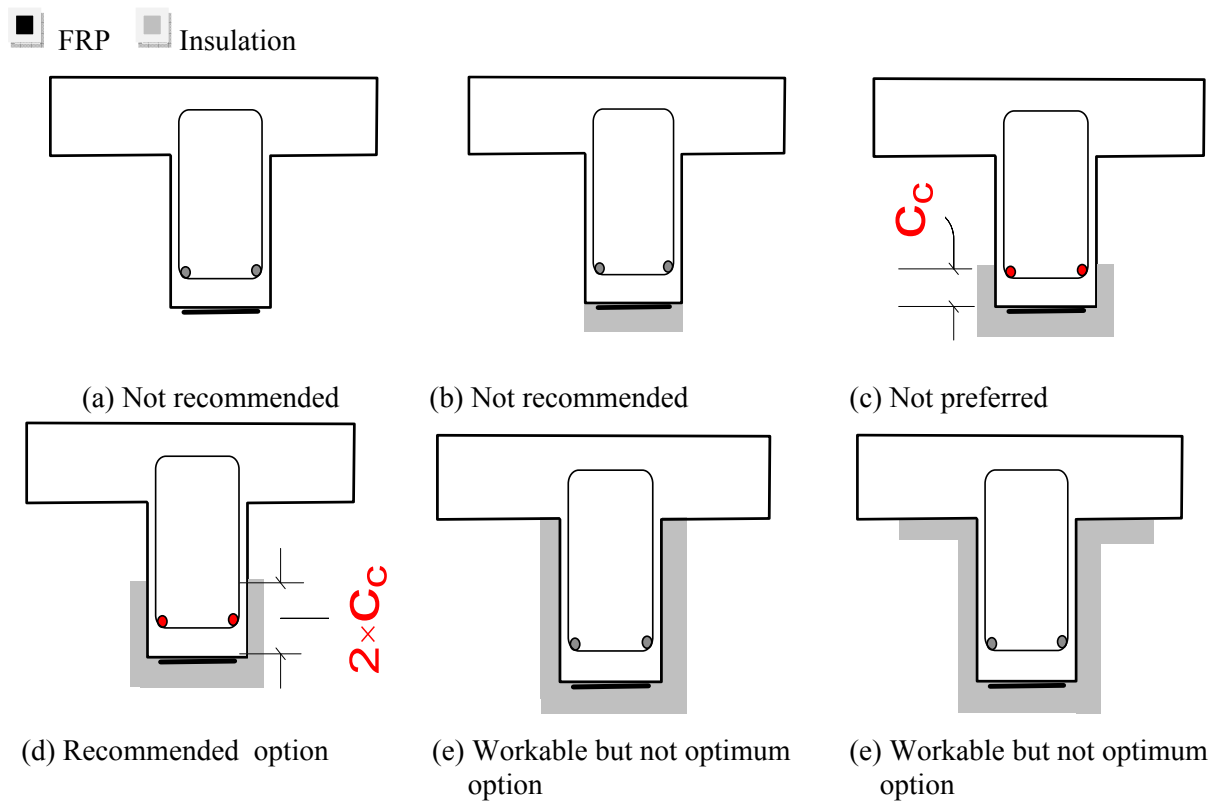
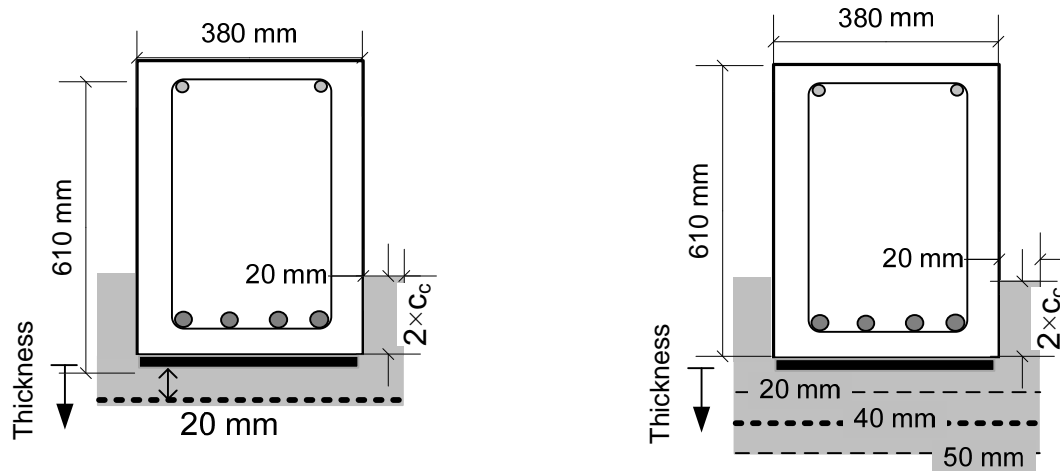


Figure 6.22: Proposed geometric configuration for insulation in FRP-strengthened RC T-beams

Insulation thickness

Apart from the geometric configuration, insulation thickness is another key factor that governs fire resistance of FRP-strengthened RC beams. The effectiveness of insulation on fire resistance mainly depends on the thickness, specific heat and thermal conductivity properties of fire insulation. The available fire insulation in the market has thermal conductivity in the range of 0.12 to 0.5 W/m-°K. The fire resistance of FRP-strengthened RC beams increases with insulation thickness. However, there is a certain level of thickness beyond which any further increase in the thickness is not beneficial. This level of insulation thickness is referred to as "*optimum insulation thickness*".

For flexural members such as beams, it is not desirable to have insulation thickness beyond an optimum value since it adds weight and accelerate insulation fall off under its dead weight, especially when beam deflections increases under fire conditions. The insulation also limits the temperature rise in steel reinforcement and this in turn helps to achieve higher moment capacity at a given fire exposure time. However, beyond optimum insulation thickness, at which steel rebar temperatures reaches about 400°C, any further reduction in steel reinforcement temperature does not result in higher tension force or capacity of the beam (Eurocode 2 2004). Figure 6.22 (a) and (b) shows the optimum insulation thicknesses required for FRP-strengthened RC beam derived from parametric studies for insulation that has thermal conductivity of 0.12 W/m-°K. An optimum insulation thickness of 40 mm is required to achieve 3 hours of fire resistance while a minimum of 20 mm thickness is needed to acquire fire resistance up to 2 hours.



Insulation thickness for 2 hours of fire resistance

Insulation thickness for 3 hours of fire resistance

Figure 6.23: Proposed optimum thickness for fire insulation in FRP-strengthened RC beams

6.5.2 Anchorage zone

Externally bonded FRP systems are provided with supplemental insulation and a possible configuration is shown in Figure 6.24(a). As explained earlier in Section 6.5.1, insulation keep the temperatures low in overall beam cross section (concrete, steel rebars and FRP) and this helps in achieving good fire resistance. When the bond between FRP and concrete is lost, the insulation continues to limit the temperature rise in the tension reinforcement which enhances the fire resistance of FRP-strengthened RC beams as a result of slow degradation of strength and stiffness properties of steel reinforcement. However, if the anchorage zones are kept cooler such that the glass transition temperature in FRP near the anchorage zone is not exceeded, this will provide an additional benefit in enhancing the fire resistance of the strengthened beam. To achieve this benefit, which is possible in most of the practical applications, provision of adequate insulation length and thickness near the anchorage zone is critical, as shown in Figure 6.24 (b). Based on the test results presented as part of this research work, it is recommended that insulation should extend atleast equal to the depth of the beam cross section (h) beyond the terminating end of FRP making a total anchorage zone length equal to $2h$. Moreover, it should be

provided with an adequate insulation thickness to keep temperatures at FRP/concrete interface (bond face) lower than glass transition temperature (T_g) of FRP for desired length of time. For instance, an insulation thickness of 50 mm is required to keep the temperature at FRP/concrete interface within anchorage zone below T_g for more than 2 hours.

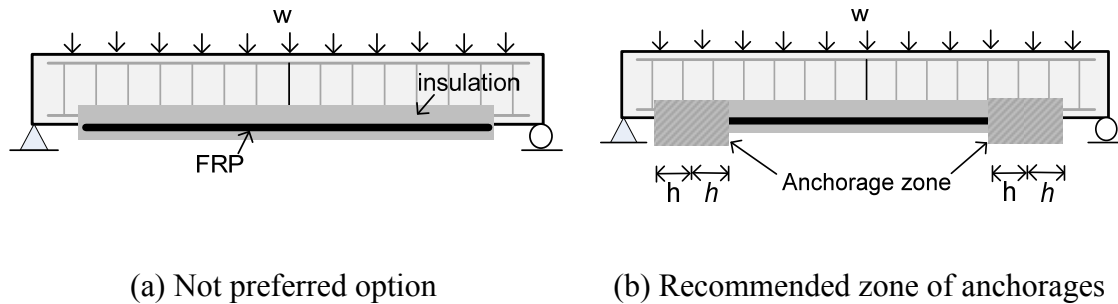


Figure 6.24: Proposed fire insulation layout for FRP-strengthened RC beams

6.5.3 Performance-based Design

FRP-strengthened RC beams have higher inherent fire resistance under realistic (design) fire scenarios, loading conditions and failure criteria. This higher fire resistance in FRP-strengthened RC beams can be realized by accounting for these critical factors:

- Realistic (design) fire scenario
- Axial restraint force
- Failure criteria
- Load level

Design fire

In prescriptive approach, the fire resistance is mostly evaluated under standard fire exposure (ASTM E119 fire or ISO 834 fire). In these fires, temperature increases with time throughout the

fire duration, and there is no decay phase, as shown in Figure 6.25. Therefore, such standard fires do not represent often less heating environments encountered in real fires. In real fires a cooling phase starts after flash over since the fire progression is characterized by availability of fuel load and ventilation factor of the fire compartment. In the decay phase of the fire, the cross section of the beam enters the cooling phase, in which the steel reinforcement and the concrete recovers parts of its strength and stiffness (assuming that FRP has debonded in early stages of fire exposure), and this enhances the fire resistance of the beam. In general, FRP-strengthened RC members have higher fire resistance under most design (realistic) fires that have well defined decay phase.

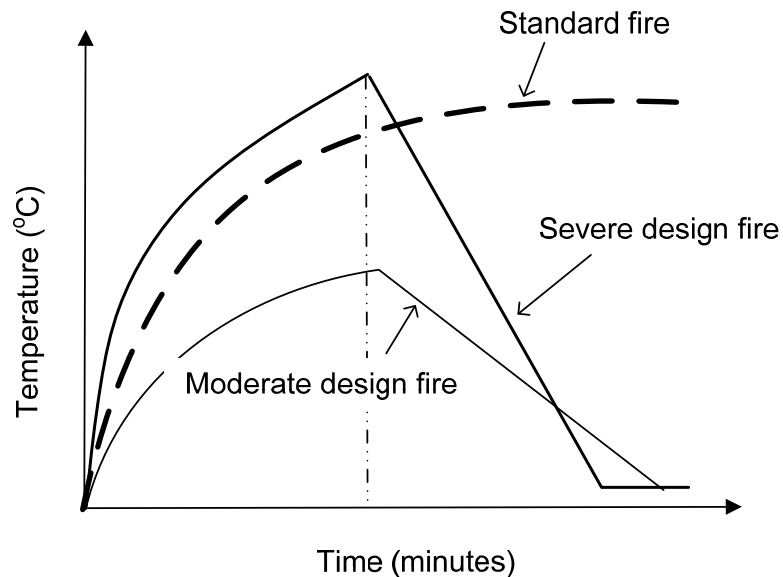


Figure 6.25:Effect of standard and design (realistic) fire on temperature profile of an insulated FRP-strengthened RC beam

Axial Restraint

The effect of axial restraints on the fire resistance of FRP-strengthened RC beams depends on the vertical location of the restraint force. The location of axial restraint force below the

geometric centroid of beam improves the fire resistance of the FRP-strengthened RC beam through the arch action associated with axial restraint force, which increases the load carrying capacity of the beam under fire exposure. For realistic fire resistance assessment of fire resistance, relevant axial restraint scenario should be accounted for.

Failure Criteria

The conventional approach of evaluating fire resistance is based on thermal and strength failure criteria as specified in ASTM E119. For FRP-strengthened RC beams, in addition to strength and deflection limit states, glass transition temperature (T_g) limit is also considered as one of the failure criteria. This T_g criterion is overly conservative from fire resistance point of view since a number of fire tests indicated no strength failure of FRP-strengthened RC beams even though T_g exceeded in early stages of the fire exposure. Therefore, in reality fire resistance of FRP-strengthened RC beams will be governed by strength or deflection limit state. These criteria should be applied for evaluating failure in FRP-strengthened RC beams under fire conditions.

Load Factors and Load Level

Generally RC beams are strengthened to increase the moment capacity by up to 50% of original room temperature capacity. Generally in fire design, the expected loads on the structures are often taken to be about 50% of the ultimate capacity of the beam or equal to the service load levels (Buchanan 2002). ACI 440.2R-08 requires that the FRP-strengthened RC member must be capable of withstanding service loads (1.2 times the dead load (DL) and 0.85 times the live load (LL)) under fire exposure. This is expressed by following equation:

$$\phi R_n^{original} = 1.2SD_{new} + 0.85SL_{new}$$

where: SD and SL is dead load and live load effect, respectively.

However for evaluating fire resistance, recent edition of ASCE 7-05 recommends a further reduction in load levels by lowering live load factor from 0.85 to 0.5, but maintain 1.2 factor for dead load. Such lower load levels are consistent with limit state design approaches used in Europe. For fire resistance evaluation, Ellingwood and Corotis (1991) have proposed to use load factors of 1.0 and 0.5 for dead and live loads, respectively. Under such lower load levels, an FRP-strengthened beam will have higher fire resistance since the beam can sustain the loads for a longer duration under lower load levels. Therefore, accounting for relevant and realistic load factors through rational fire resistance calculations can yield higher fire resistance. Thus, this factor should be considered for realistic fire safety assessment of FRP-strengthened RC beams.

6.5.4 Rational Fire Resistance Assessment

Once the above relevant factors are established, then a fire resistance analysis can be carried out using a computer model, such as the one presented in this research. The analysis can be performed as explained in Chapter 4. In such analysis, the main steps involved are:

- Identifying appropriate realistic (design) fire scenario, load level, and axial restraint conditions.
- Carryout detailed thermal and structural analysis of FRP-strengthened RC beam.
- Applying realistic limit state (strength or deflection, not T_g criterion) to evaluate failure.

The application of above rational approach for fire resistance assessment can be facilitated under recently introduced performance-based codes.

6.6 Summary

A parametric study was performed to illustrate the sensitivity of various factors on fire resistance of FRP-strengthened RC beams. Results of parametric studies indicate that fire scenario, load level, bond degradation, axial restraint and its location, thermal properties, thickness and geometric configuration of insulation has significant influence on fire resistance of FRP-strengthened RC beams. The parameters that have moderate influence are: concrete strength, aggregate type (carbonate and siliceous), and adhesive thickness. Data from parametric studies and fire resistance tests was utilized to recommend fire design guidelines for enhancing the fire resistance of FRP-strengthened RC beams. These guidelines can be applied to undertake realistic fire assessment and also to achieve good fire resistance performance in FRP-strengthened RC beams.

CONCLUSIONS AND RECOMMENDATIONS

7.1 General

The experimental and numerical studies presented in this thesis examined the behavior of FRP-strengthened RC beams under realistic fire and loading conditions. A numerical model was developed to trace the response of FRP-strengthened RC beams under realistic fire, loading and restraint conditions. The model is based on a macroscopic finite element approach and uses time-dependent moment-curvature relationships to trace the response of the beam from pre-fire stage to failure under fire conditions. The critical factors, namely; high temperature material properties, fire induced bond degradation, axial restraint force, and different strain components having significant influence on the fire response of FRP-strengthened RC beams were incorporated in the model. For model validation, four FRP-strengthened RC beams were tested under non-standard fire, loading, and axially restraint conditions. Data from these tests was used to validate various response parameters which included cross sectional temperatures, debonding of FRP, mid-span deflections, and fire resistance. The validated model was used to conduct a set

of parametric studies to quantify the influence of various factors on the fire response of FRP-strengthened RC beams. Finally, results of parametric studies and fire resistance tests were utilized to recommend broad guidelines for enhancing the fire resistance of FRP-strengthened RC beams. These guidelines can be applied in design process to rationally evaluate fire resistance and ensure satisfactory fire endurance of FRP-strengthened RC beams.

7.2 Key Findings

Based on the information presented in this thesis, the following key conclusions are drawn:

- There is very little information on performance of FRP-strengthened RC beams under realistic fire and loading scenarios. Few available fire design guidelines for FRP-strengthened RC beams are based on limited fire tests conducted under "standard fire" exposure and are case specific. Therefore, these guidelines do not facilitate a rational approach in evaluating fire resistance of FRP-strengthened RC beams.
- The results of fire resistance experiments indicate that the fire performance of FRP-strengthened RC beams is enhanced when anchorage zone (terminating ends of FRP) is well protected against temperature rise. Presence of cooler anchorages enhances load carrying capacity of FRP-strengthened RC beams through *cable mechanism* which is provided by unbonded continuous fibers at the beam soffit. Also, presence of axial restraint conditions enhances the fire resistance of FRP-strengthened RC beams.
- The proposed macroscopic finite element model, based on moment-curvature relationships, is capable of predicting the response of FRP-strengthened RC beams in the entire range from the pre-fire stage to collapse under fire conditions. The model accounts

for high temperature material properties of constitutive materials (concrete, steel rebars, FRP and insulation), fire induced bond degradation, axial restraint force, and different strain components.

- Results from the parametric studies and fire resistance tests indicate that fire scenario, load level, fire induced bond degradation at FRP/concrete interface, magnitude and location of axial restraint force, thermal properties of insulation, insulation thickness and its geometric configuration are the key parameters that influence the fire resistance of FRP-strengthened RC beams, specifically:
 - The type of fire exposure has a significant effect on fire resistance of FRP-strengthened RC beams. Under most design fire scenarios, FRP-strengthened RC beams have higher fire resistance than under a standard fire exposure.
 - Higher load level leads to a lower fire resistance of FRP-strengthened RC beams.
 - The magnitude and location of fire induced axial restraint force significantly affect the fire resistance of FRP-strengthened RC beam. Fire resistance is higher when the axial restraint force is located below the centroidal axis of the beam.
 - The fire resistance of FRP-strengthened RC beams does not improve much by increasing the insulation thickness beyond an optimum thickness level.
- Data from fire tests clearly shows that FRP-strengthened RC beams, supplemented with 25 mm spray-applied Tyfo[®] WR Advanced Fire Protection system can survive failure under fire exposure comprising of 3 hours of ASTM E119 growth phase followed by a decay (cooling) phase.

- Reaching glass transition temperature (T_g) in CFRP does not lead to the strength failure in insulated CFRP-strengthened RC beams, thus, this is overly conservative failure criteria from structural point of view.
- Fire resistance in FRP-strengthened RC beams is not only influenced by the thickness of insulation, but also by insulation scheme. The proposed design guidelines for optimum insulation schemes and application of rational calculation methods will yield higher fire resistance for FRP-strengthened RC beams.

7.3 Recommendations for Future Research

Although a number of significant contributions have emerged from this study, further research is deemed necessary to fully characterize the complex behavior of FRP-strengthened RC members under fire. Some of the important recommendations for future research are:

- The proposed moment-curvature based macroscopic finite element numerical model can be extended to other concrete structures such as prestressed concrete beams strengthened with FRP and also to reinforced and pre-stressed concrete beam with near surface mounted (NSM) FRP reinforcement.
- More work is required to understand and accurately model the insulation behavior in terms of bond strength (mechanical properties) with concrete and FRP and possible mechanisms of delamination at elevated temperatures, crack formation and propagation. In addition, more investigation is needed to study the effect of charring as a result of pyrolysis process in thin FRP sheets.

- Further experimental data is needed to enhance the understanding on the behavior of FRP-strengthened members under other parameters such as fibers and matrix with different thermal and mechanical properties, and influence of different anchorage and insulation schemes. In addition, more work is needed to understand the relationship between T_g , heating rate, thermal and loading history on the beams for various currently available FRP and adhesives used in civil engineering applications.
- There is a need for characterizing high temperature constitutive relationships for thermal and mechanical (including bond) properties for wide variety of FRP and insulation materials available in the market. These high temperature material properties are essential to enhance the capability and confidence level in model predictions.
- Strain gage measurements can provide useful data for validation of the model under combined effect of applied load and fire, and to quantify different strain components under fire exposure. The high temperature strain gages currently available in the market do not provide reliable measurements at high temperatures (above 300°C) and thus there is a need for developing reliable high temperature strain gages.

7.4 Research Impact

Currently, there is very little guidance in codes and standards on the fire design FRP-strengthened RC beams under realistic fire and loading conditions. This is mainly because the response of FRP-strengthened RC beams under fire is not well understood and a number of phenomenons complicate fire resistance evaluation. Currently available FRP materials for civil engineering application experience significant loss of strength, stiffness and bond properties at elevated temperatures. A wide variety of FRP and adhesive (resins) systems are being used in

structural strengthening industry. Fire testing of full-scale FRP strengthened beams, with different combinations of FRP, insulation and RC beam parameters is expensive and time consuming. In recent years, the shift is towards rational design approaches and numerical fire modeling will become an important research tool for undertaking fire resistance analysis.

In lieu of full-scale fire testing of FRP-strength RC beams, the validated numerical model such as the one presented here, will provide a convenient way to evaluate fire resistance, and estimate optimum insulation thickness and its geometric configuration. Experimental studies, such as the one presented here, provide an insight to develop an understanding on the response of FRP-strengthened RC beams under realistic fire, loading, bond degradation and restraint support conditions. These fire tests and numerical studies have shown that FRP-strengthened RC beams with applied service loads and appropriate supplementary insulation can achieve fire endurance in excess of 3 hours under standard, as well as realistic (design) fire exposure. The proposed fire design guidelines, which have evolved from both experimental and numerical studies, will facilitate the wider use of FRP in strengthening of concrete members in buildings and other structures, where fire safety is one of the crucial issues.

APPENDIX A

Material Properties at Elevated Temperatures

This Appendix provides a summary of high temperatures material property relationships used in the numerical model and parametric studies. Information is presented for concrete, steel, FRP, and insulation, with respect to both thermal (specific heat, thermal conductivity) and mechanical (strength, stiffness) properties.

A.1 Concrete – ASCE Properties

These equations presented in this section have been reproduced after Lie (1992).

A.1.1 Thermal Capacity, $\rho_c, T c_{c,T}$

For siliceous aggregate concrete, with T_c in $^{\circ}\text{C}$ and $\rho_c, T c_{c,T}$ in $\text{J} / \text{m}^3 ^{\circ}\text{C}$

$$0 \leq T_c \leq 200: \quad \rho_c, T c_{c,T} = (0.005 T_c + 1.7) \times 10^6$$

$$200 \leq T_c \leq 400: \quad \rho_c, T c_{c,T} = 2.7 \times 10^6$$

$$400 \leq T_c \leq 500: \quad \rho_c, T c_{c,T} = (0.013 T_c - 2.5) \times 10^6$$

$$500 \leq T_c \leq 600: \quad \rho_c, T c_{c,T} = (-0.013 T_c + 10.5) \times 10^6$$

$$T_c \geq 3316: \quad \rho_c, T c_{c,T} = 2.7 \times 10^6$$

For carbonate aggregate concrete

$$\begin{aligned} 0 \leq T_c \leq 400: & \quad \rho_{c,T} c_{c,T} = 2.566 \times 10^6 \\ 400 \leq T_c \leq 410: & \quad \rho_{c,T} c_{c,T} = (0.1765T - 68.034) \times 10^6 \\ 410 \leq T_c \leq 445: & \quad \rho_{c,T} c_{c,T} = (-0.05043T + 25.00671) \times 10^6 \\ 445 \leq T_c \leq 500: & \quad \rho_{c,T} c_{c,T} = 2.566 \times 10^6 \\ 500 \leq T_c \leq 635: & \quad \rho_{c,T} c_{c,T} = (0.01603T - 5.44881) \times 10^6 \\ 635 \leq T_c \leq 715: & \quad \rho_{c,T} c_{c,T} = (0.005T - 100.90225) \times 10^6 \\ 715 \leq T_c \leq 785: & \quad \rho_{c,T} c_{c,T} = (-0.22103T + 176.07343) \times 10^6 \\ T_c \geq 785: & \quad \rho_{c,T} c_{c,T} = 2.566 \times 10^6 \end{aligned}$$

For lightweight aggregate concrete

$$\begin{aligned} 0 \leq T_c \leq 400: & \quad \rho_{c,T} c_{c,T} = 1.930 \times 10^6 \\ 400 \leq T_c \leq 420: & \quad \rho_{c,T} c_{c,T} = (0.0772T - 28.95) \times 10^6 \\ 420 \leq T_c \leq 435: & \quad \rho_{c,T} c_{c,T} = (-0.1029T + 46.706) \times 10^6 \\ 435 \leq T_c \leq 600: & \quad \rho_{c,T} c_{c,T} = 1.930 \times 10^6 \\ 600 \leq T_c \leq 700: & \quad \rho_{c,T} c_{c,T} = (0.03474T - 18.9140) \times 10^6 \\ 700 \leq T_c \leq 720: & \quad \rho_{c,T} c_{c,T} = (-0.1737T + 126.994) \times 10^6 \\ T_c \leq 720: & \quad \rho_{c,T} c_{c,T} = 1.930 \times 10^6 \end{aligned}$$

A.1.2 Thermal Conductivity, $k_{c,T}$

For siliceous aggregate concrete, with T_c in $^{\circ}C$ and $k_{c,T}$ in $W / m^{\circ}C$

$$0 \leq T_c \leq 800: \quad k_{c,T} = -0.000625T_c + 1.5$$

$$T_c \geq 800: \quad k_{c,T} = 1.0$$

For carbonate aggregate concrete

$$0 \leq T_c \leq 293: \quad k_{c,T} = 1.355$$

$$T_c \geq 293: \quad k_{c,T} = -0.001241T_c + 1.7162$$

For lightweight aggregate concrete

$$0 \leq T_c \leq 600: \quad k_{c,T} = -0.00039583T_c + 0.925$$

$$T_c \geq 600: \quad k_{c,T} = 0.6875$$

A.1.3 Thermal Strain (All Type)

$$\varepsilon_{th} = \left[0.004(T^2 - 400) + 6(T - 20) \right] \times 10^{-6}$$

A.1.4 Stress-Strain Relationships

$$\sigma_c = \begin{cases} f'_{c,T} \left[1 - \left(\frac{\varepsilon - \varepsilon_{\max,T}}{\varepsilon_{\max,T}} \right)^2 \right], & \varepsilon \leq \varepsilon_{\max,T} \\ f'_{c,T} \left[1 - \left(\frac{\varepsilon_{\max,T} - \varepsilon}{3\varepsilon_{\max,T}} \right)^2 \right], & \varepsilon > \varepsilon_{\max,T} \end{cases}$$

$$f'_{c,T} = \begin{cases} f'_c & , 20^\circ\text{C} \leq T \leq 450^\circ\text{C} \\ f'_c \left[2.011 - 2.353 \left(\frac{T-20}{1000} \right) \right] & , 450^\circ\text{C} < T \leq 874^\circ\text{C} \\ 0 & , 874^\circ\text{C} < T \end{cases}$$

$$\varepsilon_{\max,T} = 0.0025 + \left(6.0T + 0.04T^2 \right) \times 10^{-6}$$

A.2 Concrete – Eurocode Properties

These equations presented in this section have been reproduced after Eurocode 2 (2004)

A.2.1 Thermal Capacity

Specific Heat (J/kg-°C)

$$c = 900 \quad \text{for } 20^\circ\text{C} \leq T \leq 100^\circ\text{C}$$

$$c = 900 + (T - 100) \quad \text{for } 100^\circ\text{C} < T \leq 200^\circ\text{C}$$

$$c = 1000 + (T - 200)/2 \quad \text{for } 200^\circ\text{C} < T \leq 400^\circ\text{C}$$

$$c = 1100 \quad \text{for } 400^\circ\text{C} < T \leq 1200^\circ\text{C}$$

Density (kg/m³)

$$\rho = \rho(20^\circ\text{C}) \quad \text{for } 20^\circ\text{C} \leq T \leq 115^\circ\text{C}$$

$$\rho = \rho(20^\circ\text{C}) \left(1 - 0.02(T - 115)/85 \right) \quad \text{for } 115^\circ\text{C} < T \leq 200^\circ\text{C}$$

$$\rho = \rho(20^\circ\text{C}) \left(0.98 - 0.03(T - 200)/200 \right) \quad \text{for } 200^\circ\text{C} < T \leq 400^\circ\text{C}$$

$$\rho = \rho(20^\circ\text{C}) \left(0.95 - 0.07(T - 400)/800 \right) \quad \text{for } 400^\circ\text{C} < T \leq 1200^\circ\text{C}$$

A.2.2 Thermal Conductivity (All Type)

Upper Limit

$$k_c = 2 - 0.2451 (T / 100) + 0.0107 (T / 100)^2 \quad \text{for } 20^\circ\text{C} \leq T \leq 1200^\circ\text{C}$$

Lower Limit

$$k_c = 1.36 - 0.136 (T / 100) + 0.0057 (T / 100)^2 \text{ for } 20^\circ\text{C} \leq T \leq 1200^\circ\text{C}$$

A.2.3 Thermal Strain

Siliceous Aggregate

$$\varepsilon_{th} = -1.8 \times 10^{-4} + 9 \times 10^{-6} T + 2.3 \times 10^{-11} T^3 \text{ for } 20^\circ\text{C} \leq T \leq 700^\circ\text{C}$$

$$\varepsilon_{th} = 14 \times 10^{-3} \text{ for } 700^\circ\text{C} < T \leq 1200^\circ\text{C}$$

Carbonate Aggregate

$$\varepsilon_{th} = -1.2 \times 10^{-4} + 6 \times 10^{-6} T + 1.4 \times 10^{-11} T^3 \text{ for } 20^\circ\text{C} \leq T \leq 805^\circ\text{C}$$

$$\varepsilon_{th} = 12 \times 10^{-3} \text{ for } 805^\circ\text{C} < T \leq 1200^\circ\text{C}$$

A.2.4 Stress-Strain Relationship

$$\sigma_c = \frac{3 \varepsilon f'_{c,T}}{\varepsilon_{c1,T} \left(2 + \left(\frac{\varepsilon}{\varepsilon_{c1,T}} \right)^3 \right)}, \varepsilon \leq \varepsilon_{cu1,T}$$

For $\varepsilon_{c1(T)} < \varepsilon \leq \varepsilon_{cu1(T)}$, the Eurocode permits the use of linear as well as nonlinear descending branch in the numerical analysis. For the parameters in this equation refer to Table A.1.

Table A.1 Values for the Main Parameters of the Stress-strain Relationships of NSC at Elevated Temperatures (Eurocode 2)

T(°C)	Normal Strength Concrete					
	Siliceous Aggregate			Calcareous Aggregate		
	$\frac{f'_{c,T}}{f'_c(20^\circ C)}$	$\varepsilon_{c1,T}$	$\varepsilon_{cu1,T}$	$\frac{f'_{c,T}}{f'_c(20^\circ C)}$	$\varepsilon_{c1,T}$	$\varepsilon_{cu1,T}$
20	1	0.0025	0.02	1	0.0025	0.02
100	1	0.004	0.0225	1	0.004	0.023
200	0.95	0.0055	0.025	0.97	0.0055	0.025
300	0.85	0.007	0.0275	0.91	0.007	0.028
400	0.75	0.01	0.03	0.85	0.01	0.03
500	0.6	0.015	0.0325	0.74	0.015	0.033
600	0.45	0.025	0.035	0.6	0.025	0.035
700	0.3	0.025	0.0375	0.43	0.025	0.038
800	0.15	0.025	0.04	0.27	0.025	0.04
900	0.08	0.025	0.0425	0.15	0.025	0.043
1000	0.04	0.025	0.045	0.06	0.025	0.045
1100	0.01	0.025	0.0475	0.02	0.025	0.048
1200	0	-	-	0	-	-

A.3 Reinforcing Steel – ASCE Properties

A.3.1 Thermal Strain

$$\varepsilon_{ths} = \left[0.004(T^2 - 400) + 6(T - 20) \right] \times 10^{-6} \quad T < 1000^\circ\text{C}$$

A.3.2 Stress-strain Relationship

$$\sigma_s = \left\{ \begin{array}{ll} \frac{f(T, 0.001)}{0.001} \varepsilon_s & \varepsilon_s \leq \varepsilon_p \\ \frac{f(T, 0.001)}{0.001} \varepsilon_p + f(T, \varepsilon_s - \varepsilon_p + 0.001) - f(T, 0.001) & \varepsilon_s > \varepsilon_p \end{array} \right\}$$

$$f(T, x) = 6.9(50 - 0.04T) \left[1 - \exp((-30 + 0.03T)\sqrt{x}) \right]$$

$$\varepsilon_p = 4 \times 10^{-6} f_{y,20}$$

where: σ_s and ε_s = stress (MPa) and strain in steel reinforcement, respectively, and $f_{y,20}$ is the yield strength of reinforcing steel (MPa) at room temperature.

A.4 Reinforcing Steel – Eurocode Properties

A.4.1 Thermal Strain

$$\varepsilon_{ths} = \left\{ \begin{array}{ll} 1.2 \times 10^{-5} T + 0.4 \times 10^{-8} T^2 - 2.416 \times 10^{-4} & 20^\circ\text{C} \leq T < 750^\circ\text{C} \\ 1.1 \times 10^{-2} & 750^\circ\text{C} \leq T < 860^\circ\text{C} \\ 2 \times 10^{-5} T - 6.2 \times 10^{-3} & 20^\circ\text{C} \leq T < 750^\circ\text{C} \end{array} \right\}$$

A.4.2 Stress-strain Relationship

$$\sigma_s = \left\{ \begin{array}{ll} \varepsilon_s E_{s,T} & \varepsilon_s \leq \varepsilon_{sp,T} \\ f_{sp,T} - c + (b/a) \left(a^2 - (\varepsilon_{sy,T} - \varepsilon_s)^2 \right)^{0.5} & \varepsilon_{sp,T} < \varepsilon_s \leq \varepsilon_{sy,T} \\ f_{sy,T} & \varepsilon_{sy,T} < \varepsilon_s \leq \varepsilon_{st,T} \\ f_{sy,T} \left(1 - \frac{\varepsilon_s - \varepsilon_{st,T}}{\varepsilon_{su,T} - \varepsilon_{st,T}} \right) & \varepsilon_{st,T} < \varepsilon_s \leq \varepsilon_{su,T} \\ 0.0 & \varepsilon_s > \varepsilon_{su,T} \end{array} \right\}$$

Parameters

$$\varepsilon_{sp,T} = \frac{f_{sp,T}}{E_{s,T}} \quad \varepsilon_{sy,T} = 0.02 \quad \varepsilon_{st,T} = 0.15 \quad \varepsilon_{su,T} = 0.2$$

Functions

$$a^2 = (\varepsilon_{sy,T} - \varepsilon_{sp,T}) \left(\varepsilon_{sy,T} - \varepsilon_{sp,T} + \frac{c}{E_{s,T}} \right)$$

$$b^2 = c (\varepsilon_{sy,T} - \varepsilon_{sp,T}) E_{s,T} + c^2$$

$$c = \frac{(f_{sy,T} - f_{sp,T})^2}{(\varepsilon_{sy,T} - \varepsilon_{sp,T}) E_{s,T} - (f_{sy,T} - f_{sp,T})}$$

The values of $f_{sp,T}$, $f_{sy,T}$ and $E_{s,T}$ can be obtained from Table A.2

Table A.2 Values for the Main Parameters of the Stress-strain Relationships of Reinforcing Steel at Elevated Temperatures (Eurocode 2)

Steel Temperature T (°C)	f_{yT} / f_y	f_{sp} / f_y^*	E_{sT} / E_s^*
20	1	1	1
100	1	1	1
200	1	0.807	0.9
300	1	0.613	0.8
400	1	0.42	0.7
500	0.78	0.36	0.6
600	0.47	0.18	0.31
700	0.23	0.075	0.13
800	0.11	0.05	0.09
900	0.06	0.0375	0.0675
1000	0.04	0.025	0.045
1100	0.02	0.0125	0.0225
1200	0	0	0

* f_y and E_s are yield strength and modulus of elasticity at room temperature

A.5 Insulation - Tyfo ® Vermiculite-Gypsum (VG)

This insulation is manufactured by Fyfe Co. LLC as fire proofing system for FRP composites. These thermal properties relationships are based on Thermogravimetric Analysis (TGA) performed by Bisby (2003), as well as material property estimates from other sources:

A.5.1 Density

The VG insulation has two primary components, namely; gypsum and vermiculite. Based on typical densities of gypsum (865 kg/m³) and vermiculite (128 kg/m³) mixed in 2:1 ratio, the relationships obtained through TGA (Bisby 2003) are:

$$0 \leq T_{VG} \leq 100: \quad \rho_{VG,T} = 351$$

$$100 \leq T_{VG} \leq 200: \quad \rho_{VG,T} = 351 - \frac{351 - 287}{200 - 100} \cdot (T_{VG} - 100)$$

$$100 \leq T_{VG} \leq 200: \quad \rho_{VG,T} = 351 - \frac{351 - 287}{200 - 100} \cdot (T_{VG} - 100)$$

$$200 \leq T_{VG}: \quad \rho_{VG,T} = 287$$

where; ρ_{VG} is density in kg/m³ and temperature T_{VG} in °C

A.5.2 Specific Heat

The two components of insulation (vermiculite and gypsum) have different specific heat values with temperature variation. For specific heat relationships presented below, it has been assumed that specific heat of vermiculite remains constant whereas it changes with temperature for gypsum. The effect of dehydration has been included by artificially increasing the specific heat around 100°C.

$$0 \leq T_{VG} \leq 20: \quad c_{VG,T} = 1.1763$$

$$20 \leq T_{VG} \leq 78: \quad c_{VG,T} = 1.1763 + \frac{1.3058 - 1.1763}{78 - 20} \cdot (T_{VG} - 20)$$

$$78 \leq T_{VG} \leq 125: \quad c_{VG,T} = 1.3058 + \frac{6.9066 - 1.3058}{125 - 78} \cdot (T_{VG} - 78)$$

$$125 \leq T_{VG} \leq 137: \quad c_{VG,T} = 6.9066 + \frac{1.3722 - 1.1763}{137 - 125} \cdot (T_{VG} - 125)$$

$$137 \leq T_{VG} \leq 153: \quad c_{VG,T} = 1.3722 + \frac{1.3722 - 1.0136}{153 - 137} \cdot (T_{VG} - 137)$$

$$153 \leq T_{VG} \leq 610: \quad c_{VG,T} = 1.0136 + \frac{1.0136 - 0.8509}{610 - 153} \cdot (T_{VG} - 153)$$

$$610 \leq T_{VG} \leq 663: \quad c_{VG,T} = 0.8509 + \frac{1.6976 - 0.8509}{663 - 610} \cdot (T_{VG} - 610)$$

$$663 \leq T_{VG} \leq 690: \quad c_{VG,T} = 1.6976 + \frac{1.6976 - 0.9167}{690 - 663} \cdot (T_{VG} - 663)$$

$$690 \leq T_{VG}: \quad c_{VG,T} = 0.9167$$

where; c_{VG} is specific heat of VG insulation (J/kg-°C) and temperature in °C

A.5.3 Thermal Conductivity

The thermal conductivity of vermiculite is constant with temperature and that of gypsum varies with temperature. The variation of thermal conductivity (W/m-°C) with temperature (°C) is expressed by:

$$0 \leq T_{VG} \leq 100: \quad \kappa_{VG,T} = 0.1158$$

$$100 \leq T_{VG} \leq 101: \quad \kappa_{VG,T} = 0.1158 - \frac{0.1158 - 0.0726}{101 - 100} \cdot (T_{VG} - 100)$$

$$101 \leq T_{VG} \leq 400: \quad \kappa_{VG,T} = 0.0726$$

$$400 \leq T_{VG} \leq 800: \quad \kappa_{VG,T} = 0.0726 - \frac{0.1224 - 0.0726}{800 - 400} \cdot (T_{VG} - 400)$$

$$800 \leq T_{VG}: \quad \kappa_{VG,T} = 0.1224 - \frac{0.2087 - 0.1224}{1000 - 800} \cdot (T_{VG} - 800)$$

A.6 Insulation - Promatect Calcium-Silicate Boards

These boards are of calcium silicate insulating material manufactured by Promat.

A.6.1 Density

The density values (kg/m^3) are provided by Deuring (1994) and also Blontrock et al. (2000)

$$\text{Promatect-H} : \rho_i = 870$$

$$\text{Promatect-100} : \rho_i = 875$$

$$\text{Promatect-L} : \rho_i = 500$$

A.6.2 Specific Heat

The specific heat ($\text{J/kg}^\circ\text{C}$) for calcium silicate insulating slabs (obtained from website: www.nu-techresources.com/datasheet/PROMATECTH-eng.pdf) are:

$$\text{Promatect-H} : c_i = 0.92E3$$

$$\text{Promatect-100} : c_i = 0.84E3$$

$$\text{Promatect-L} : c_i = 0.95E3$$

A.6.3 Thermal Conductivity

The thermal conductivity for various types of insulation is expressed as:

$$\text{Promatect-H} : k_i = 1.833E - 4 \times T + 0.175 \quad \text{for } 0 \leq T \leq 390^\circ\text{C}$$

$$k_i = 0.25 \quad \text{for } T \geq 390^\circ\text{C}$$

$$\text{Promatect-100} : k_i = 0.285$$

Promatect-L : $k_i = 7.07E - 5 \times T + 0.083 \quad \text{for } 0 \leq T \leq 100^\circ C$

$$k_i = 4.0E - 5 \times T + 0.086 \quad \text{for } 100 \leq T \leq 200^\circ C$$

$$k_i = 6.0E - 5 \times T + 0.082 \quad \text{for } 200 \leq T \leq 400^\circ C$$

$$k_i = 8.0E - 5 \times T + 0.074 \quad \text{for } 400 \leq T \leq 500^\circ C$$

$$k_i = 0.144 \quad \text{for } T \geq 500^\circ C$$

where; k_i is thermal conductivity (W/m-°C) and T is temperature (°C)

A.7 FRP

A.7.1 Specific Heat, $c_{w,T}$

In the following equations, $c_{w,T}$ has units of (kJ/kg-°C) and T_w is in °C

$$0 \leq T_w \leq 325: \quad c_{w,T} = 1.25 + \frac{0.95}{325} \cdot (T_w)$$

$$325 \leq T_w \leq 343: \quad c_{w,T} = 2.2 + \frac{2.8}{18} \cdot (T_w - 325)$$

$$343 \leq T_w \leq 510: \quad c_{w,T} = 5.0 + \frac{-0.15}{167} \cdot (T_w - 343)$$

$$510 \leq T_w \leq 538: \quad c_{w,T} = 4.85 + \frac{-3.59}{28} \cdot (T_w - 510)$$

$$538 \leq T_w \leq 3316: \quad c_{w,T} = 1.265 + \frac{1.385}{2778} \cdot (T_w - 538)$$

$$T_w \geq 3316: \quad c_{w,T} = 0$$

A.7.2 Density, $\rho_{w,T}$

In the following equations, $\rho_{w,T}$ has units of (g/cm³) and T_w is in °C

$$0 \leq T_w \leq 510: \quad \rho_{w,T} = 1.6$$

$$510 \leq T_w \leq 538: \quad \rho_{w,T} = 1.6 + \frac{-0.35}{28} \cdot (T_w - 510)$$

$$538 \leq T_w \leq 1200: \quad \rho_{w,T} = 1.25$$

A.7.3 Thermal Conductivity, $k_{w,T}$

In the following equations, $k_{w,T}$ has units of (W/m-°C) and T_w is in °C

$$0 \leq T_w \leq 500: \quad K_{w,T} = 1.4 + \frac{-1.1}{500} \cdot T_w$$

$$500 \leq T_w \leq 650: \quad K_{w,T} = 1.4 + \frac{-0.1}{150} \cdot (T_w - 500)$$

$$T_w \geq 650: \quad K_{w,T} = 0.2$$

A.7.4 Strength, $f_{com,T}$ and Elastic Modulus, $E_{com,T}$

In the following equations the units of strength ($f_{com,T}$) and elastic modulus ($E_{com,T}$) are

MPa and for temperature (T_w) is °C

$$f_{com,T} = f_{com} \left[\frac{1-a_\sigma}{2} \tanh \left[-b_\sigma (T_w - c_\sigma) \right] + \frac{1+a_\sigma}{2} \right]$$

$$E_{com,T} = E_{com} \left[\frac{1-a_E}{2} \tanh \left[-b_E (T_w - c_E) \right] + \frac{1+a_E}{2} \right]$$

where for:

$$CFRP: a_{\sigma} = 0.1; b_{\sigma} = 5.83e-3; c_{\sigma} = 339.54; a_E = 0.05; b_E = 8.68e-3; c_E = 367.41$$

$$GFRP: a_{\sigma} = 0.1; b_{\sigma} = 8.10e-3; c_{\sigma} = 289.14; a_E = 0.05; b_E = 7.91e-3; c_E = 320.35$$

$$AFRP: a_{\sigma} = 0.1; b_{\sigma} = 8.48e-3; c_{\sigma} = 287.65; a_E = 0.05; b_E = 7.93e-3; c_E = 290.49$$

APPENDIX B

B.1 Design and Load Calculations of FRP-Strengthened RC Beam

This Appendix summarizes the design and load calculations using ACI 318 (2008) provisions reinforced concrete (RC) beam. The cross-section, shear force diagram, and bending moment diagram for the tested beams are shown in Figure B.1. The design calculations are presented in the following two sections.

B.1.1 Design of RC Beam

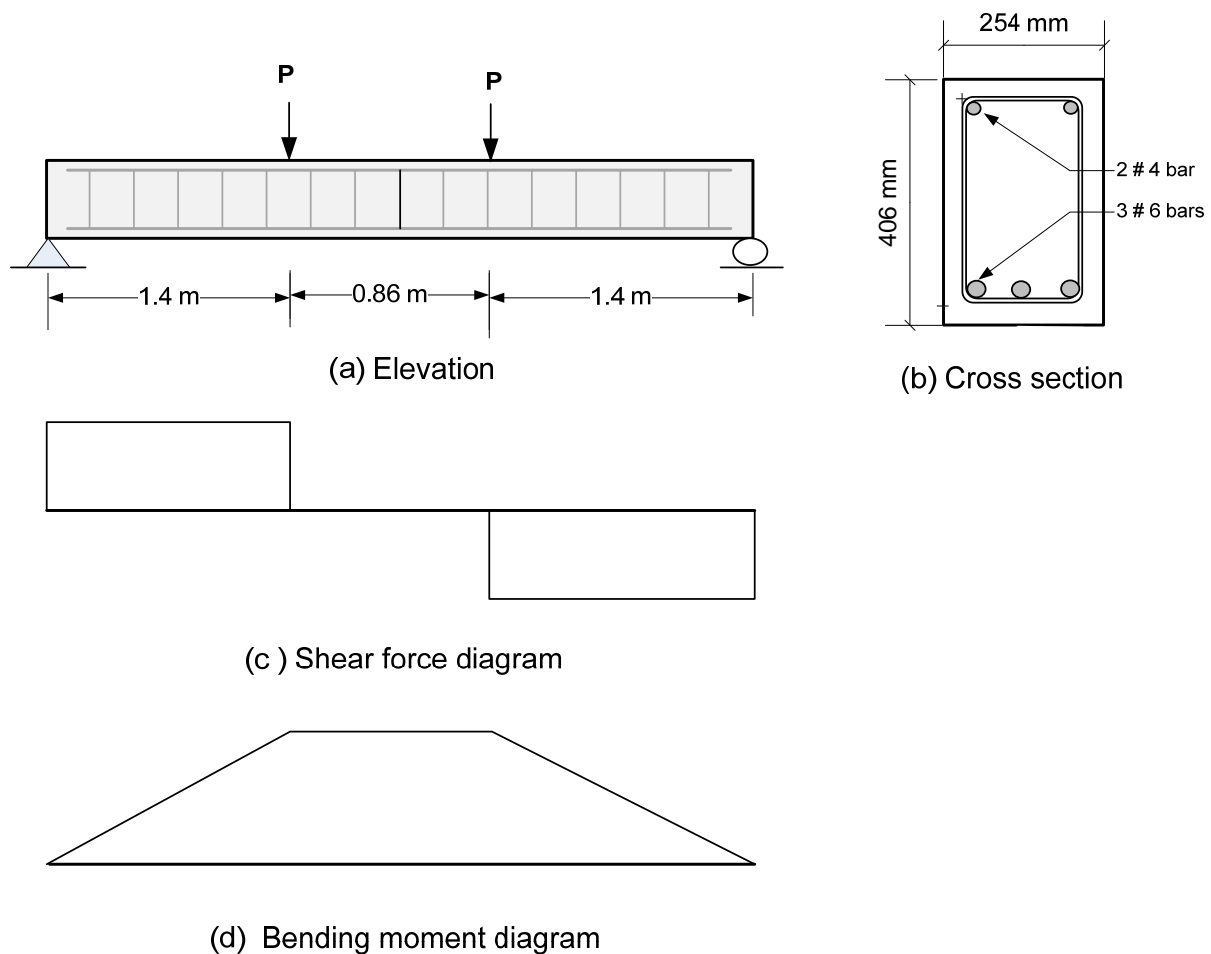


Figure B.1: Cross-section, Elevation, Shear Force Diagram, and Bending Moment Diagram for Tested Beams

$$f'_c = 41.3 \text{ MPa} \quad f_y = 413 \text{ MPa}$$

Neglecting the area of steel in the compression zone

The tensile area of steel $A_s = 855 \text{ mm}^2$

Clear concrete cover = 38 mm

$$h = 406 \text{ mm} \quad b = 254 \text{ mm}$$

$$d = 352.4 \text{ mm}$$

$$a = 39.6 \text{ mm}$$

$$a = \beta_1 c$$

Hence, $\beta_1 = 0.75$

$$\text{Therefore, } c = \frac{39.6}{0.75} = 52.8 \text{ mm}$$

Strain in tensile steel can be calculated by interpolation as follows:

$$\varepsilon_t = \frac{0.003}{c}(d - c) = \frac{0.003}{52.8}(352.4 - 52.8) = 0.017 > 0.005$$

$$\text{Therefore, } \phi = 0.9$$

Check minimum reinforcement

$$\rho_{\min} = 0.0039$$

$$\rho = \frac{A_s}{bd} = 0.00955 > \rho_{\min}$$

The moment capacity of the beam is

$$M_n = A_s f_y \left(d - \frac{a}{2} \right) = \frac{855 \times 413 \times \left(352.4 - \frac{39.6}{2} \right)}{10^6} = 117 \text{ kN.m}$$

$$M_n = 1.4 P_n$$

$$P_n = 83.9 \text{ kN} \quad \text{and} \quad P_u = 75.5 \text{ kN}$$

Design for shear

The ultimate shear force is at distance d from the face of the support:

$$V_u = P_u = 75.5 \text{ kN}$$

Required nominal shear strength:

$$\phi = 0.75$$

$$V_n = \frac{V_u}{\phi} = \frac{75.5}{0.75} = 100.7 \text{ kN}$$

The concrete shear strength is:

$$V_c = 0.16\sqrt{f'_c}b_wd = \frac{0.16\sqrt{41.3} * 254 * 352.4}{1000} = 92 \text{ kN}$$

The required shear strength obtained by shear reinforcement must be:

$$V_n > V_c$$

$$V_s = V_n - V_c = 100.7 - 92 = 8.7 \text{ kN}$$

$$V_{s \text{ min}} = \max \left\{ \begin{array}{l} 0.344b_wd \\ 0.06\sqrt{f'_c}b_wd \end{array} \right\} = 35 \text{ kN}$$

Use minimum shear reinforcement

The required shear reinforcement will be found to be

$$\frac{A_v}{s} = 0.237 \text{ mm}$$

Using #2 stirrups

The area of each leg is 31.6 mm^2

Hence, $A_v = 2 \times 31.6 = 63.2 \text{ mm}^2$

The required spacing will be:

$$s = \frac{63.2}{0.237} = 267 \text{ mm} \leq \frac{d}{2} = \frac{352.4}{2} = 176.2 \text{ mm} \quad (\text{ACI 318 11.5.4.1})$$

Hence, use #2 stirrups 150 mm c/c

Check Deflection

The gross moment of inertia (neglecting the compressive and tensile steel) can be calculated as:

$$I_g = \frac{bh^3}{12} = 1.416 \times 10^9 \text{ mm}^4$$

The cracked moment of inertia (neglecting the compressive steel) can be calculated as follows:

$$E_s = 210 \text{ GPa}$$

$$E_c = 4730\sqrt{f'_c} = 30.4 \text{ GPa}$$

$$n = \frac{E_s}{E_c} = 6.9$$

$$x = \frac{\sqrt{(nA_s)^2 + 2bdnA_s} - nA_s}{b} = 106.9 \text{ mm}$$

$$I_{cr} = \frac{bx^3}{3} + nA_s(d-x)^2$$

$$I_{cr} = 0.459 \times 10^9 \text{ mm}^4$$

The modulus of rupture is:

$$f_r = 0.6\sqrt{f'_c} = 3.86 \text{ MPa}$$

The cracking moment is

$$M_{cr} = \frac{f_r I_g}{y_t} = 26.9 \text{ kN.m}$$

The effective moment of inertia will be:

Assume M_a to be $0.7M_u$, then

$$M_a = 0.7 \times 117 \times 0.9 = 73.71 \text{ kN.m}$$

$$I_e = \left(\frac{M_{cr}}{M_a} \right)^3 I_g + \left[1 - \left(\frac{M_{cr}}{M_a} \right)^3 \right] I_{cr} \leq I_g$$

$$I_e = 0.506 \times 10^9 \text{ mm}^4$$

Hence, the deflection of the beam will be:

$$\delta = \frac{M}{2E_c I_e} \left(\frac{L^2}{4} - \frac{a^2}{3} \right) = 6.5 \text{ mm}$$

Load Calculations

$$f'_c = 58.2 \text{ MPa} \quad f_y = 450 \text{ MPa}$$

Neglecting the area of steel in the compression zone

The tensile area of steel $A_s = 855 \text{ mm}^2$

Clear concrete cover = 38 mm

$$h = 406 \text{ mm} \quad b = 254 \text{ mm}$$

$$d = 352.4 \text{ mm}$$

$$a = 30.62 \text{ mm}$$

$$a = \beta_1 c$$

Hence, $\beta_1 = 0.624$

$$\text{Therefore, } c = \frac{30.62}{0.624} = 49.07 \text{ mm}$$

Strain in tensile steel can be calculated by interpolation as follows:

$$\varepsilon_t = \frac{0.003}{c} (d - c) = \frac{0.003}{49.07} (352.4 - 49.07) = 0.0185 > 0.005$$

Hence, $\phi = 0.9$

Check minimum reinforcement:

$$\rho_{\min} = 0.0039$$

$$\rho = \frac{A_s}{bd} = 0.00955 > \rho_{\min}$$

The moment capacity of the beam is:

$$M_n = A_s f_y \left(d - \frac{a}{2} \right) = \frac{855 \times 450 \times \left(352.4 - \frac{30.62}{2} \right)}{10^6} = 129.7 \text{ kN.m}$$

$$M_n = 1.4 P_n \quad ; \quad P_n = 92.64 \text{ kN} \quad \text{and} \quad P_u = 83.5 \text{ kN}$$

The load ratio is defined as the ratio of applied load under fire conditions to the capacity of the section at room temperature (Buchanan 2002). Accordingly, the load ratio is given as:

$$LR = \frac{50}{92.7} \times 100 \% = 54\%$$

B.2.1 FRP Strengthening of RC Beam

All calculations have been performed in SI units. The design equations from American codes (ACI 318 and ACI 440.2R-08) have been used. The RC beam is required to be strengthened to increase the moment capacity by about 50%. Two unidirectional CFRP sheets of 203 mm width are used to strengthen the beam. The detailed calculations are as follows:

Material properties

$$h = 406 \text{ mm}$$

$$b = 254 \text{ mm}$$

$$d = 352.4 \text{ mm}$$

$$A_s = 855 \text{ mm}^2$$

$$f'_c = 58.2 \text{ MPa}$$

$$f_y = 450 \text{ MPa}$$

$$E_s = 210000 \text{ MPa}$$

$$E_c = 36000 \text{ MPa}$$

$$E_{frp} = 52000 \text{ MPa}$$

$$f_{fu} = 634 \text{ MPa (assuming } C_E = 0.85)$$

FRP Area Calculations

The properties of existing steel reinforcement:

$$A_s = 855 \text{ mm}^2$$

$$\rho_s = \frac{A_s}{b \times d} = 9.552 \times 10^{-3}$$

$$\text{Modular ratio: } n_s = \frac{E_s}{E_c} = 5.8$$

The properties of externally bonded CFRP reinforcement:

Number of CFRP sheets

$$n = 2$$

Width of each sheet

$$b_{frp} = 203 \text{ mm}$$

Hence, the area of externally bonded CFRP is:

$$A_{frp} = n \times t_{frp} \times b_{frp} = 406 \text{ mm}^2$$

$$\rho_s = \frac{A_{frp}}{b \times d} = 4.536 \times 10^{-3}$$

$$\text{Modular ratio: } n_{frp} = \frac{E_{frp}}{E_c} = 1.4$$

Since the beams are strengthened in the laboratory, therefore it is assumed that the initial strains at the beam soffit at the time retrofitting is zero ($\varepsilon_{bi} = 0$)

Determining the bond-dependant coefficient of FRP system:

$$\kappa_m = \frac{1}{60\varepsilon_{fu}} \left(1 - \frac{nE_t t f}{360000} \right) \leq 0.90$$

$$\text{where: } \varepsilon_{fu} = C_E \times \varepsilon_{frp} = 0.1$$

$$\kappa_m = 1.14$$

Since computed coefficient is greater than 0.9, therefore, $\kappa_m = 0.9$

Computing the depth of the neutral axis:

$$0.85f'_c b a^2 + [A_{frp} E_{frp} (\varepsilon_{cu} + \varepsilon_{bi}) - A_s f_y] a - \beta_1 A_{frp} E_{frp} \varepsilon_{cu} h = 0$$

$$a = 50.75 \text{ mm}$$

$$c = 81.28 \text{ mm}$$

Effective strain in CFRP reinforcement

$$\varepsilon_{fe} = 0.003 \left(\frac{h-c}{c} \right) - \varepsilon_{bi} \leq \kappa_m \varepsilon_{fu}$$

$$0.012 \leq 0.009$$

Therefore, strain in CFRP is $\varepsilon_{fe} = 0.009$ and $f_{fe} = E_{frp} \times \varepsilon_{fe} = 468 \text{ MPa}$

Calculating new depth of neutral axis

$$a = \frac{(A_{frp} E_{frp} \varepsilon_{fe}) + A_s f_y}{0.85 f_c b} = 45.74 \text{ mm}$$

$$c = 73.25 \text{ mm}$$

The moment capacity of CFRP strengthened RC beam is:

$$M_n = A_s f_y \left(d - \frac{a}{2} \right) + A_{frp} f_{fe} \left(h - \frac{a}{2} \right) = 199.58 \text{ kN-m}$$

The increase in moment capacity is **53.88%**

Calculations of Load

$$M = 1.4P ; P = \frac{200}{1.4} = 142.9 \text{ kN}$$

The load ratio given as:

$$LR = \frac{70}{142.9} \times 100 = 49\%$$

APPENDIX C

C.1 Finite Element Formulation

To solve the heat and mass transfer problems, the cross-section of the beam segment is divided into rectangular elements as shown in Figure 4.1. Since the dependent variable (the variable to be computed) in the two problems is scalar, Q4 (four node) element is used in the analysis. Due to the nonlinearity of both the problems, integrations in Eqs. (4.11) through (4.13) are evaluated numerically using Gaussian quadrature integration technique. The vector of shape functions for Q4 element can be written as:

$$N = \begin{bmatrix} \frac{(1-s)(1-t)}{4} \\ \frac{(1+s)(1-t)}{4} \\ \frac{(1+s)(1+t)}{4} \\ \frac{(1-s)(1+t)}{4} \end{bmatrix}$$

where: s and t = transformed coordinates as shown in Figure C.1.

The analysis is generally carried out using four Gauss points and the element stiffness matrix (K_e), mass matrix (M_e) and nodal heat or mass flux (F_e) are evaluated at every Gauss

point. Those values of the element matrices at the four Gauss points are summed to form the element material property matrices which are used for the subsequent steps in the analysis.

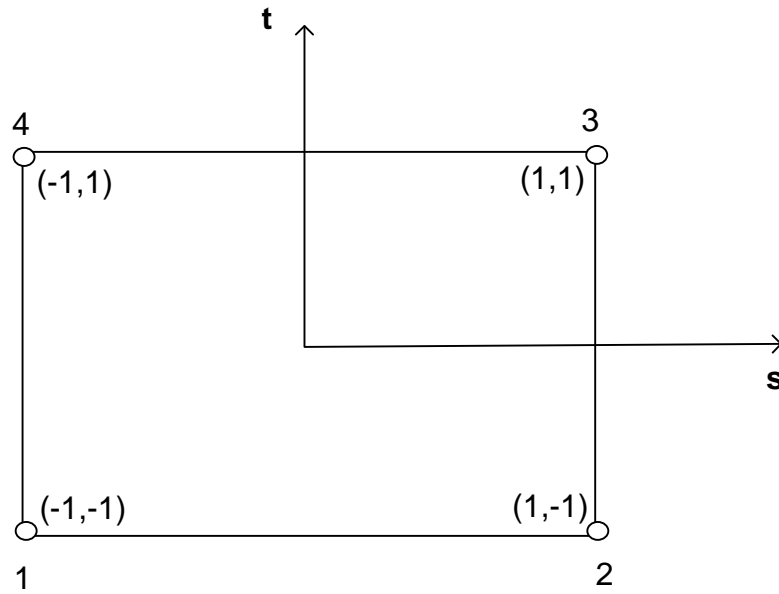


Figure C.1: Q4 elements in transformed coordinates

REFERENCES

- ACI 318-08. (2008). "Building Code Requirements for Reinforced Concrete and Commentary." American Concrete Institute, Farmington Hills, MI.
- Ahmed, A., and Kodur, V. K. R. (2010). "Factors Governing Fire Resistance of FRP-Strengthened Reinforced Concrete Beams." *Composite & Polycon, American Composites Manufacturers Association (ACMA)*, Las Vegas, Nevada.
- Al-Homoud, D., and Mohammad, S. (2005). "Performance characteristics and practical applications of common building thermal insulation materials." *Building and Environment*, 40(3), 353-366.
- American Concrete Institute (ACI). (2006). "Guide for the design and construction of structural concrete reinforced with FRP bars." ACI 440.1R-06, ACI Committee 440, Farmington Hills, MI.
- American Concrete Institute (ACI). (2008). "Guide for the design and construction of externally bonded FRP systems for strengthening concrete structures ", ACI 440.2R-08, ACI Committee 440, Farmington Hills, MI.
- American Society for Testing and Materials (ASTM). (1993). "Standard test methods for determining glass transition temperature." ASTM E1545
- American Society for Testing and Materials (ASTM). (2007). " Standard test methods for fire tests of building construction and materials." ASTM E119, West Conshohocken, PA.
- American Society of Civil Engineers (ASCE). (2009). "Report Card for America's Infrastructure." Reston, Virginia.
- Anderberg, Y., and Thelandersson, S. (1976). Stress and deformation characteristics of concrete at high temperatures, 2-Experimental investigation and material behaviour model, Bulletin 54, Lund Institute of Technology, Lund, Sweden
- Apicella, F., and Imbrogno, M. (1999a). "Fire Performance of CFRP-Composites Used for Repairing and Strengthening." *Proceedings of Fifth ASCE materials Engineering Conference*, Cincinnati, Ohio, 266.
- Arduini, M., and Nanni, A. (1997). " Behavior of pre-cracked RC beams strengthened with carbon FRP sheets " *Journal of Composites for Construction*, 1(2), 63-70.
- ASCE Manuals and Reports on Engineering Practice No. 78. (1992). "Structural Fire Protection." New York: American Society of Civil Engineers.

- Ashour, A. F., El-Refaie, S. A., and Garrity, S. W. (2004). "Flexural strengthening of RC continuous beams using CFRP laminates." *Cement and concrete composites*, 26(7), 765-775.
- Bakis, C. E. (1993). *FRP reinforcement: materials and manufacturing*, Elsevier Science Publisher.
- Bakis, C. E., Cosenza, E., Lesko, J. J., and Machida, A. (2002). "Fiber-reinforced polymer composites for construction—state-of-the-art review." *Journal of Composites for Construction*, 6, 73.
- Balaguru, P., Nanni, A., and Giancaspro, J. (2008). *FRP composites for reinforced and prestressed concrete structures: a guide to fundamentals and design for repair and retrofit*, Taylor & Francis Group.
- Ballinger, C., Maeda, T., and Hoshijima, T. "Strengthening of reinforced concrete chimneys, columns and beams with carbon fiber reinforced plastics." *Fiber-Reinforced-Plastic (FRP) Reinforcement for Concrete Structures: Properties and Applications*, 233–247.
- Bank, L. C., Gentry, T. R., and Barkatt, A. (1995). "Accelerated test methods to determine the long-term behavior of FRP composite structures: environmental effects." *Journal of Reinforced Plastics and Composites*, 14(6), 559.
- Barnes, R., and Fidell, J. (2006). "Performance in fire of small-scale CFRP strengthened concrete beams." *Journal of Composites for Construction*, 10, 503-508.
- Bisby, L. A. (2003). "Fire behavior of fibre-reinforced polymer (FRP) reinforced or confined concrete," Doctoral Thesis, Queen's University, Kingston, Canada.
- Blaschko, M., Niedermeier, R., and Zilch, K. (1998). "Bond failure modes of flexural members strengthened with FRP." *Fiber Composites in Infrastructure*, 315-327.
- Blontrock, H., Taerwe, L., and Matthys, S. (1999). "Properties of fiber reinforced plastics at elevated temperatures with regard to fire resistance of reinforced concrete members." 188, 43-54.
- Blontrock, H., Taerwe, L., and Vandeveld, P. (2000). "Fire tests on concrete beams strengthened with fibre composite laminates." *Third PhD Symposium*, Vienna, Austria.
- Blontrock, H., Taerwe, L., and Vanwalleghem, H. (2002). "Bond testing of externally glued FRP laminates at elevated temperature." *Proceeding of the International*

Conference Bond in Concrete – from research to standards, Budapest, Hungary, 648-654.

Bourbigot, S., and Flambard, X. (2002). "Heat resistance and flammability of high performance fibres: A review." *Fire and Materials*, 26(4-5), 155-168.

British Standard Institute (BSI). (1987). "Fire test on building materials and structures - Part 20: Method for determination of fire resistance of elements of construction (General principles)." BS476-20, London, UK.

British Standards Institute (BSI). (2009). "Fire tests on building materials and structures. Guide to the principles, selection, role and application of fire testing and their outputs." BS 476-10, Bristol, UK.

Buchanan, A. H. (2002). *Structural design for fire safety*, Wiley Chichester, UK.

Camata, G., Pasquini, F., and Spacone, E. (2007). "High temperature flexural strengthening with externally bonded FRP reinforcement." *Proceedings of 8th International Symposium on Fiber Reinforced Polymer (FRP) Reinforcement for Concrete Structures (FRP8RCS)*, Patras, Greece, 1-10.

Campbell, T. I., and Kodur, V. K. R. (1990). "Deformation controlled nonlinear analysis of prestressed concrete continuous beams." *PCI Journal*, 35(5), 42-90.

Canadian Standards Association (CSA) S806-02. (2002). "Design and construction of building components with fibre-reinforced polymers." CAN/CSA S806-02, Rexdale, Canada.

Chaallal, O., Nollet, M. J., and Perraton, D. (1998). "Strengthening of reinforced concrete beams with externally bonded fiber-reinforced-plastic plates: design guidelines for shear and flexure." *Canadian Journal of Civil Engineering*, 25(4), 692-704.

Chen, J. F., and Teng, J. G. (2003). "Shear capacity of FRP-strengthened RC beams: FRP debonding." *Construction and Building Materials*, 17(1), 27-41.

Cook, R. D., Malkus, D. S., Plesha, M. E., and Witt, R. J. (2007). *Concepts and applications of finite element*, John Wiley & Sons, INC., NY, USA.

Darwish, M. N. (2000). "Upgrading Reinforced Concrete Columns by Jacketing with Carbon Fiber-Reinforced Plastic (CFRP) Sheets." *Special Publication*, 193, 488-502.

- Davies, J. M., Wang, Y. C., and Wong, F. M. H. (2004). "Polymer composites in fire." *Proceedings of Advanced Composites for Structural Applications in Construction*, Guildford, Surrey, UK, 3-17.
- Denton, S. R. (2001). "Analysis of stresses developed in FRP plated beams due to thermal effects." *FRP Composites in Civil Engineering*, 1, 527-536.
- Deuring, M. (1994). "Brandversuche an nachtraglich verstärkten tragern aus beton." Swiss Federal Laboratories for Materials Testing and Research, Dubendorf, Switzerland.
- Di Tommaso, A., Neubauer, U., Pantuso, A., and Rostasy, F. S. (2001). "Behaviour of Adhesively Bonded Concrete-CFRP Joints at Low and High Temperatures." *Mechanics of Composite Materials*, 37(4), 327-338.
- Dodds, N., Gibson, A. G., Dewhurst, D., and Davies, J. M. (2000). "Fire behaviour of composite laminates." *Composites Part A: Applied Science and Manufacturing*, 31(7), 689-702.
- Dortzbach, J. (1999). "Carbon Fiber Reinforcing Polymers as Negative Moment Reinforcing in Repair of Composite Steel Parking Deck." Special Publication 188, American Concrete Institute, Detroit, Michigan.
- Dwaikat, M. B. (2009). "Flexural response of reinforced concrete beams exposed to fire," Doctoral Thesis, Michigan State University, East Lansing, Michigan, USA.
- Dwaikat, M. B., and Kodur, V. K. R. (2008). "A numerical approach for modeling the fire induced restraint effects in reinforced concrete beams." *Fire Safety Journal*, 43(4), 291-307.
- El-Hacha, R., Wight, R. G., and Green, M. F. (2001). "Prestressed fibre-reinforced polymer laminates for strengthening structures." *Progress in Structural Engineering and Materials*, 3(2), 111-121.
- Ellingwood, B. R., and Corotis, R. B. (1991). "Load combinations for buildings exposed to fires." *Engineering Journal*, 28(1), 37-44.
- Eurocode 1. (2002). "EN 1991-1-2: Actions on structures. Part 1-2: General actions - Actions on structures exposed to fire." European Committee for Standardization, Brussels, Belgium.

- Eurocode 2. (2004). "EN 1992-1-2: Design of concrete structures. Part 1-2: General rules - Structural fire design." European Committee for Standardization, Brussels, Belgium.
- Eurocode 3. (1995). "Eurocode 3: Design of Steel Structures. Part 1-2: General Rules - Structural Fire Design." European Committee for Standardization, Brussels, Belgium.
- Fédération Internationale du Béton (FIB). (2001). "Design and use of externally bonded FRP reinforcement for RC structures." Bulletin 14, Lausanne, Switzerland.
- Ferrillo, R. G., and Achorn, P. J. (1997). "Comparison of thermal techniques for glass transition assignment. II. Commercial polymers." *Journal of Applied Polymer Science*, 64(1), 191-195.
- Gamage, J., Al-Mahaidi, R., and Wong, M. B. (2006). "Bond characteristics of CFRP plated concrete members under elevated temperatures." *Composite Structures*, 75(1-4), 199-205.
- Gao, B., Leung, C. K. Y., and Kim, J. K. (2005). "Prediction of concrete cover separation failure for RC beams strengthened with CFRP strips." *Engineering Structures*, 27(2), 177-189.
- Garden, H. N., and Hollaway, L. C. (1998). "An experimental study of the influence of plate end anchorage of carbon fibre composite plates used to strengthen reinforced concrete beams." *Composite Structures*, 42(2), 175-188.
- Gates, T. S. (1991). "Effects of Elevated Temperature on the Viscoelastic Modeling of Graphite/Polymeric Composites." NASA Technical Memorandum 104160, National Aeronautics and Space Administration, Langley, USA.
- Ghobarah, A. (2001). "Seismic rehabilitation of beam-column joints using FRP laminates." *Journal of earthquake engineering*, 5(1), 113-129.
- Grace, N. F. (2001). "Strengthening of negative moment region of reinforced concrete beams using carbon fiber-reinforced polymer strips." *ACI Structural Journal*, 98(3), 347-358.
- Grace, N. F., Sayed, G. A., Soliman, A. K., and Saleh, K. R. (1999). "Strengthening reinforced concrete beams using fiber reinforced polymer (FRP) laminates." *ACI structural Journal*, 96(5), 865-874.

- Green, M. F., Bisby, L. A., Beaudoin, Y., and Labossière, P. (2000). "Effect of freeze-thaw cycles on the bond durability between fibre reinforced polymer plate reinforcement and concrete." *Canadian Journal of Civil Engineering*, 27(5), 949-959.
- Green, M. F., Dent, A. J. S., and Bisby, L. A. (2003). "Effect of freeze-thaw cycling on the behaviour of reinforced concrete beams strengthened in flexure with fibre reinforced polymer sheets." *Canadian Journal of Civil Engineering*, 30(6), 1081-1088.
- Griffis, C. A., Masumura, R. A., and Chang, C. I. (1981). "Thermal response of graphite epoxy composite subjected to rapid heating." *Journal of Composite Materials*, 15(5), 427.
- Harmathy, T. Z. (1967). "A comprehensive creep model." *J. Basic Eng.*, 89(3), 496-502.
- Harmathy, T. Z. (1993). *Fire safety design and concrete*, John Wiley & Sons, Inc., New York, NY.
- Hawileh, R. A., Naser, M., Zaidan, W., and Rasheed, H. A. (2009). "Modeling of insulated CFRP-strengthened reinforced concrete T-beam exposed to fire." *Engineering Structures (In Press)*, doi:10.1016/j.engstruct.2009.08.008
- Hiroyuki, Y., and Wu, Z. (1997). "Analysis of debonding fracture properties of CFS strengthened member subject to tension." *Proceedings of 3rd International Symposium Sapporo, Japan*, 287-294.
- Institute of Structural Engineering (ISE). (1999). "Interim guidance on the design of reinforced concrete structures using fiber composites reinforcement." Reference No 319, London, UK.
- Intelligent Sensing for Innovative Structures (ISIS) (2001). "Strengthening reinforced concrete structures with externally-bonded fibre reinforced polymers." Design Manual No. 4, Winnipeg, Canada.
- Intelligent Sensing for Innovative Structures (ISIS) (2006). "Monograph on durability of fiber reinforced polymers in civil infrastructure." Winnipeg, Canada.
- Kachlakev, D., and McCurry, D. D. (2000). "Behavior of full-scale reinforced concrete beams retrofitted for shear and flexural with FRP laminates." *Composites Part B: Engineering*, 31(6-7), 445-452.

- Khalifa, A., Gold, W. J., Nanni, A., and Aziz, A. (1998). "Contribution of externally bonded FRP to shear capacity of flexural members." *ASCE Journal of Composites for Construction*, 2(4), 195-203.
- Khoury, G. A. (2000). "Effect of fire on concrete and concrete structures." *Progress in Structural Engineering and Materials*, 2(4), 429-447.
- Klamer, E. L., Hordijk, D. A., and Hermes, M. C. J. (2008). "The influence of temperature on RC beams strengthened with externally bonded CFRP reinforcement." *Heron*, 53(3), 157-185.
- Klamer, E. L., Hordijk, D. A., and Janssen, H. J. M. (2005a). "The influence of temperature on debonding of externally bonded CFRP." *Special Publication*, 230, 1551-1570.
- Klamer, E. L., Hordijk, D. A., and Janssen, H. J. M. (2005b). "The influence of temperature on the debonding of externally bonded CFRP." *Proceedings of 7th International Symposium on Fiber Reinforced Polymer (FRP) Reinforcement for Concrete Structures (FRP7RCS)*, Kansas City, 1551-1592.
- Kodur, V. K. R. (1999). "Fire resistance requirements for FRP structural members." *Annual Conference of the Canadian Society for Civil Engineering*, Saskatoon, Canada, 83-95.
- Kodur, V. K. R., Ahmed, A., and Dwaikat, M. B. (2009). "Modeling the fire performance of FRP-strengthened reinforced concrete beams." *Composite & Polycon*, American Composites Manufacturers Association (ACMA), Tampa, Florida.
- Kodur, V. K. R., and Ahmed, A. (2010). "A numerical model for tracing the response of FRP-strengthened reinforced concrete beams exposed to fire." *in Press: ASCE Journal of Composites*.
- Kodur, V. K. R., and Baingo, D. (1998). "Fire resistance of FRP reinforced concrete slabs." IRC Internal Report No. 758, Institute for Research in Construction, National Research Council of Canada, Ottawa, ON, Canada.
- Kodur, V. K. R., and Dwaikat, M. (2008). "A numerical model for predicting the fire resistance of reinforced concrete beams." *Cement and concrete composites*, 30(5), 431-443.
- Kodur, V. K. R., and Harmathy, T. Z. (2008). *Properties of building materials*, National Fire Protection Association, Quincy, MA.

- Kodur, V. K. R., and Sultan, M. A. (2003). "Effect of temperature on thermal properties of high-strength concrete." *Journal of Materials in Civil Engineering*, 15(2), 101-107.
- Kodur, V. K. R., Bisby, L. A., and Green, M. F. (2006). "FRP retrofitted concrete under fire conditions." *Concrete International*, 28(12), 37-44.
- Kodur, V. K. R., Wang, T. C., and Cheng, F. P. (2004). "Predicting the fire resistance behaviour of high strength concrete columns." *Cement and concrete composites*, 26(2), 141-153.
- Kumar, A. (2003). "Behavior of RCC Beams after Exposure to Elevated Temperatures." *Journal of the Institute of Engineers (India) : Civil Engineering Division*, 84(3), 165-170.
- Lan, Y. M., Sotelino, E. D., and Chen, W. F. (1998). "State-of-the-art Review of Highway Bridge Columns Retrofitted with FRP Jackets." *Structural Engineering Rep. No. CE-STR-98-5, School of Civil Engineering, Purdue Univ., West Lafayette, Ind.*
- Leone, M., Matthys, S., and Aiello, M. A. (2009). "Effect of elevated service temperature on bond between FRP EBR systems and concrete." *Composites Part B*, 40(1), 85-93.
- Lie, T. T. (1992). "Structural fire protection." ASCE Committee on Fire Protection, Structural Division, American Society of Civil Engineers, New York, NY, 225-229.
- Lie, T. T., and Irwin, R. J. (1993). "Method to calculate the fire resistance of reinforced concrete columns with rectangular cross section." *ACI structural Journal*, 90(1), 52-60.
- Lie, T. T., and Kodur, V. K. R. (1995). "Thermal properties of fibre-reinforced concrete at elevated temperatures." *Institute for Research in Construction, National Research Council of Canada, Ottawa, Ont., Internal Report*, 683.
- Lie, T. T., and Kodur, V. K. R. (1996). "Thermal and mechanical properties of steel-fibre-reinforced concrete at elevated temperatures." *Canadian Journal of Civil Engineering*, 23(2), 511-517.
- Maeda, T., Asano, Y., Sato, Y., Ueda, T., and Kakuta, Y. (1997). "A study on bond mechanism of carbon fiber sheet." *Proceedings of 3rd International Symposium*, Sapporo, Japan, 279-286.

- Mallick, P. K. (1993). Fiber-reinforced composites: Materials, manufacturing, and design, Marcel Dekker, New York, NY.
- Mallik, P. K. (1988). Fiber reinforced composites: Materials, manufacturing and design, Marcel Dekker Inc., New York.
- Mayo, R., Nanni, A., Gold, W., Barker, M., and Rolla, M. O. (1999). "Strengthening of Bridge G270 with externally-bonded CFRP reinforcement." SP-188, American Concrete Institute, Proc., 4th International Symposium on FRP for Reinforcement of Concrete Structures(FRPRCS4), Baltimore, MD.
- Meier, U. (1995). "Strengthening of structures using carbon fibre/epoxy composites." *Construction and Building Materials*, 9(6), 341-351.
- Meier, U., and Kaiser, H. (1991). "Strengthening of structures with CFRP laminates." Advanced Composite Materials in Civil Engineering Structures – ASCE Specialty Conference, Las Vegas, Nevada, 224–232.
- Mouritz, A. P. (2002). "Post-fire flexural properties of fibre-reinforced polyester, epoxy and phenolic composites." *Journal of Materials Science*, 37(7), 1377-1386.
- Neale, K. (2001). "Strengthening Reinforced Concrete Structures with Externally Bonded Fibre Reinforced Polymers. Design Manual No. 4." *ISIS Canada, Winnipeg, Man.*
- Nelson, G. L. (1995). "Fire and polymers: an overview." *Proceedings Fire and Polymers II, ASC Symposium Series 599*, Washington DC, 1-26.
- Neves, I. C., Rodrigues, J. P. C., and Loureiro, A. D. P. (1996). "Mechanical properties of reinforcing and prestressing steels after heating." *Journal of Materials in Civil Engineering*, 8(4), 189-194.
- Papadopoulos, A. M. (2005). "State of the art in thermal insulation materials and aims for future developments." *Energy and Buildings*, 37(1), 77-86.
- Pei, N., and Pilakoutas, K. (2003). "Concrete beams with externally bonded flexural FRP-reinforcement: analytical investigation of debonding failure." *Composites Part B: Engineering*, 34(4), 327-338.
- Pellegrino, C., and Modena, C. (2002). "Fiber reinforced polymer shear strengthening of reinforced concrete beams with transverse steel reinforcement." *Journal of Composites for Construction*, 6, 104.

- Purkiss, J. A. (2007). *Fire safety engineering design of structures*, Butterworth-Heinemann, UK.
- Purser, D. A. (2000). "Toxic product yields and hazard assessment for fully enclosed design fires." *Polymer International*, 49(10), 1232-1255.
- Rahman, A. H., Taylor, D. A., and Kingsley, C. Y. (1993). "Evaluation of FRP as reinforcement for concrete bridges." *ACI, Special Publication*, 138, 71-86.
- Ritchie, P. A., Thomas, D. A., Lu, L. W., and Conelly, G. M. (1991). "External reinforcement of concrete beams using fiber reinforced plastics." *ACI structural Journal*, 88(4).
- Saad, M., Abo-El-Enein, S. A., Hanna, G. B., and Kotkata, M. F. (1996). "Effect of temperature on physical and mechanical properties of concrete containing silica fume." *Cement and Concrete Research*, 26(5), 669-675.
- Saadatmanesh, H., and Ehsani, M. R. (1991). "RC beams strengthened with GFRP plates. I: Experimental study." *Journal of Structural Engineering*, 117(11), 3417-3433.
- Sato, Y., Kimura, K., and Kobatake, Y. (1997). "Bond behavior between CFRP sheet and concrete (Part 1)." *Journal of Structural and Construction Engineering*, 500, 75-82.
- Schneider, U. (1988). "Concrete at high temperatures--A general review." *Fire Safety Journal*, 13(1), 55-68.
- Scott, D. W., Lai, J. S., and Zureick, A. H. (1995). "Creep behavior of fiber-reinforced polymeric composites: a review of the technical literature." *Journal of Reinforced Plastics and Composites*, 14(6), 588-617.
- Shahrooz, B. M., and Boy, S. (2004). "Retrofit of a Three-Span Slab Bridge with Fiber Reinforced Polymer Systems—Testing and Rating." *Journal of Composites for Construction*, 8, 241-247.
- Shahrooz, B. M., Boy, S., and Baseheart, T. M. (2002). "Flexural Strengthening of Four 76-Year-Old T-Beams with Various Fiber-Reinforced Polymer Systems: Testing and Analysis." *ACI*, 681-691.
- Shin, K. Y., Kim, S. B., Kim, J. H., Chung, M., and Jung, P. S. (2002). "Thermo-physical properties and transient heat transfer of concrete at elevated temperatures." *Nuclear Engineering and Design*, 212(1-3), 233-241.

- Sorathia, U., Dapp, T., and Beck, C. (1992). "Fire performance of composites." *Material Engineering*, 109(9), 10-12.
- Tadeu, A. J. B., and Branco, F. J. F. G. (2000). "Shear Test of Steel Plates Epoxy-Bonded to Concrete Under Temperatures." *Journal of Materials in Civil Engineering*, 12(1), 74-80.
- Takeda, K., Mitsui, Y., Murakami, K., Sakai, H., and Nakamura, M. (1996). "Flexural behaviour of Reinforced Concrete Beams Strengthened with Carbon Fiber Sheets." *Composites Part (A)*, 27 A, 981-987.
- Tanaka, T. (1996). "Shear resisting mechanism of reinforced concrete beams with CFS as shear reinforcement." *Graduation Thesis, Hokkaido University, Japan*.
- Teng, J. G., Chen, J. F., Smith, S. T., and Lam, L. (2002). *FRP-strengthened RC structures*, John Wiley & Sons Inc.
- Teng, J. G., Lam, L., and Chen, J. F. (2004). "Shear strengthening of RC beams with FRP composites." *Progress in Structural Engineering and Materials*, 6(3), 173-184.
- Toutanji, H. A., and Gomez, W. (1997). "Durability characteristics of concrete beams externally bonded with FRP composite sheets." *Cement and Concrete Composites*, 19(4), 351-358.
- Toutanji, H. A., and Gomez, W. (1997). "Durability characteristics of concrete beams externally bonded with FRP composite sheets." *Cement and Concrete Composites*, 19(4), 351-358.
- Triantafillou, T. C. (1998). "Strengthening of structures with advanced FRPs." *Progress in Structural Engineering and Materials*, 1(2), 126-134.
- Uomoto, T., Mutsuyoshi, H., Katsuki, F., and Misra, S. (2002). "Use of fiber reinforced polymer composites as reinforcing material for concrete." *Journal of Materials in Civil Engineering*, 14, 191.
- Van Geem, M. G., Gajda, J., and Dombrowski, K. (1997). "Thermal Properties of Commercially Available High-Strength Concretes." *Cement Concrete and Aggregates*, 19, 38-54.
- Waldron, P., Byars, E. A., and Dejke, V. (2001). "Durability of FRP in Concrete: A State of the Art." *Proceedings of the International Workshop on Composites in Construction: A Reality*, 92-101.

- Wang, Y. C., and Hsu, K. (2009). "Design recommendations for the strengthening of reinforced concrete beams with externally bonded composite plates." *Composite Structures*, 88(2), 323-332.
- William, B., and Richard, D. (1990). A first course in the finite element method, Irwin, Inc., Boston, MA.
- Williams, B. K. (2004). "Fire performance of FRP-strengthened reinforced concrete flexural members," Doctoral Thesis, Queen's University, Kingston, Canada.
- Williams, B., Bisby, L., Kodur, V. K. R., Green, M., and Chowdhury, E. (2006). "Fire insulation schemes for FRP-strengthened concrete slabs." *Composites Part A*, 37(8), 1151-1160.
- Williams, B., Kodur, V. K. R., Green, M. F., and Bisby, L. (2008). "Fire endurance of fiber-reinforced polymer strengthened concrete T-Beams." *ACI Structural Journal*, 105(1), 60-67.
- Wu, Z. S., Iwashita, K., Yagashiro, S., Ishikawa, T., and Hamaguchi, Y. (2004). "Temperature Effect on Bonding and debonding Behaviour Between FRP sheets and Concrete." *FRP Composites in Civil Engineering (CICE)*, 905-912.
- Yang, X., and Nanni, A. (2002). "Lap Splice Length and Fatigue Performance of FRP Laminates." *ACI Materials Journal*, 99(4), 386-392.
- Yuan, H., and Wu, Z. (1999). "Interfacial fracture theory in structures strengthened with composite of continuous fiber." *Proceedings of the Symposium of China and Japan, Science and Technology of the 21st Century*, Tokyo, Japan, 142-155.
- Yuan, H., Wu, Z., and Yoshizawa, H. (2001). "Theoretical solutions on interfacial stress transfer of externally bonded steel/composite laminates." *Structural Earthquake Engineering*, 18(1), 27-40.
- Zhang, Z., Hsu, C. T. T., and Moren, J. (2004). "Shear strengthening of reinforced concrete deep beams using carbon fiber reinforced polymer laminates." *Journal of Composites for Construction*, 8, 403.